論文 / 著書情報
Article / Book Information

題目(和文)	飽和砂質土の内部浸食とそれに伴う力学特性の変化に関する研究
Title(English)	Investigation on internal erosion characteristics and its mechanical consequences for saturated non-cohesive soil
著者(和文)	柯琳
Author(English)	Lin Ke
出典(和文)	学位:博士(学術), 学位授与機関:東京工業大学, 報告番号:甲第9572号, 授与年月日:2014年3月26日, 学位の種別:課程博士, 審査員:高橋　章浩,北詰　昌樹,竹村　次朗,鼎　信次郎,ﾋﾟﾊﾟｯﾄﾎﾟﾝ　ﾃｨﾗﾎﾟﾝ
Citation(English)	Degree:Doctor (Academic), Conferring organization: Tokyo Institute of Technology, Report number:甲第9572号, Conferred date:2014/3/26, Degree Type:Course doctor, Examiner:,,,,
学位種別(和文)	博士論文
Type(English)	Doctoral Thesis

Investigation on internal erosion characteristics and its mechanical consequences for saturated non-cohesive soil

Lin KE

February 2014

A Dissertation Submitted to

Faculty of Graduate School of Engineering at

Tokyo Institute of Technology

In Partial Fulfilment of the Requirements for the Degree of

Doctor of Philosophy

Department of Civil Engineering

DEDICATION

To

my beloved Mother (Ziufang Yu)

ABSTRACT

The phenomenon of internal erosion in cohesionless soils exhibits itself as the gradual migration of fine grains through the voids of the coarse matrix transported by volumes of seepage water. With the erosion of soils, it may cause a loose soil packing and consequently, a reduction in soil strength. This dissertation mainly reveals the mechanical consequences of internal erosion.

To preliminarily understand the mechanism of erosion, seepage tests are conducted in a commonly-used fixed-wall permeameter. A multi-stage test procedure is followed to assess the hydraulic conditions necessary to trigger the internal erosion. Parametric study is conducted to examine the effects of soil properties (i.e., relative density, initial fines content) and hydraulic conditions on the erosion mechanism. The soil strength reduction after erosion in the fixed-wall seepage test is elaborated by interpreting the cone tip resistance profile of the eroded specimens. It is found that internal erosion initiates at a hydraulic gradient much lower than the Terzaghi's critical hydraulic gradient. With the progress of erosion, large amounts of fines would be eroded away and the hydraulic conductivity increases. Erosion of fines would cause the contractive deformation. The specimens with larger initial fines content and looser state would be more vulnerable to erosion. The internal erosion causes a reduction in cone tip resistance, the extent of which may be related to the imposed hydraulic gradient.

A new triaxial permeameter, capable of directly investigating not only the hydraulic characteristics of soils at the onset and the progress of internal erosion under preferred stress state but also the mechanical behaviors of those internally eroded soils, is developed. By installing a sedimentation tank, back pressure could be maintained in the tested specimens during erosion test to ensure a relatively high saturation degree. A system of measuring the cumulative eroded soil mass is installed in the tank to continuously record the eroded soil mass. Erosion tests are performed by constant-flow-rate control with the measurement of the induced pressure difference between the top and the bottom of the tested specimens.

By conducting seepage test in a triaxial condition, the hydromechanical behaviors of tested specimen during the progress of internal erosion are studied by assessing the changes of the key parameters, such as hydraulic gradient, hydraulic conductivity, soil deformation and cumulative eroded soil mass. The effects of effective confining pressure and initial fines content are experimentally investigated. The influence of erosion on the stress ~ strain relationship is directly indicated by conducting undrained & drained monotonic compression test on the internally eroded soil specimen. The influence of effective confining pressure and initial fines content are considered. Influence of internal erosion on the cyclic resistance of tested specimens is studied by performing undrained cyclic test on the eroded soil specimens and companion specimens without erosion, respectively, under the same effective confining pressure.

Test results indicate that under the constant-rate-flow, the hydraulic gradient changes with the progress of internal erosion accompanying with the dislodgement of large

amounts of fines. Assigned the seepage flow with the same velocity, the specimens with the larger effective confining pressure show less increments in hydraulic conductivity within the test range. A larger effective confining pressure would cause a less percentage of cumulative fines loss and volumetric strain induced by internal erosion. In terms of initial fines content, a larger fines loss and volumetric strain is observed at the specimens with larger initial fines content. In this series of seepage tests, the tested specimens show contractive behavior and the post-erosion void ratio increases.

Departing from clean sand, an exceptional mechanical behavior of eroded soil is observed. The volumetric strain at failure derived from drained tests reduces with the increasing of effective confining pressure. A temporary drop in soil stiffness at the initial stage of shearing with respect to the axial strain ranging from 0% ~ 1% is observed. In terms of undrained tests, generally, the mobilized friction angle at peak shows trend of increasing with the increasing of effective confining pressure. Compression test results have revealed the probable existence of a reinforced packing of soil grains after internal erosion. The reinforced post-erosion soil packing renders the eroded specimen much stiffer and less compressible. The changes in soil strength after internal erosion are assessed by various criteria. In terms of ASTM criterion, the drained strength of eroded specimens is less than that of original specimens by 20% in average, irrespective of effective confining pressure. The variations in undrained strength appear to be influenced by the effective confining pressure. Mostly, the soil strength decreases after erosion. The critical friction angle of eroded specimen and original specimen, derived from drained monotonic tests, is 35.27° and 36.87°, respectively. At the same normal stress, the shear strength decreases by 5.7% after internal erosion. A larger instability region is observed for the eroded specimens. The cyclic strength increases by two times after internal erosion.

ACKNOWLEDGEMENTS

"To accomplish great things we must not only act, but also dream, not only plan, but also believe and the belief in a thing makes it happen" (Anatole France)

I am grateful to my academic advisor, Associate Professor Akihiro Takahashi for this consistent support, encouragement and guidance throughout my research. He is an ambitious and vibrant researcher with several novel research ideas. Thanks to him, I begin the frontier research on the mechanical consequence of erosion. Being creative in the research means difficulty and even torture because of no established paths. Whenever I came across the obstacles in the study, his firm support and confidence has motivated me towards my research goals. Whenever I felt confused and doubtful about the study, his kind guidance has corrected my understanding and broadened my academic view.

I am thankful to Associate Professor Jiro Takemura for valuable comments and suggestions on my research. He always wears kind smile and patiently discusses with me for the academic problems I encountered. He is experienced researcher, especially at the area of seepage flow in a porous media. His suggestions always enlighten me.

I wish to express my sincere gratitude to Professor Masaki Kitazume, Associate Professor Thirapong Pipatpongsa and Assistant Professor Tomohide Takeyama. I learned how to carefully and logically analyze my research results. Open discussions with them have improved my comprehension towards my research.

I appreciate the help of Professor Shinjiro Kanae, for taking the time to serve on my committee and his review of this dissertation.

I would like to thank Mr. Sakae Seki who serves as the technician of the Geotechnical group. Without his help, I may not develop the new apparatus successfully.

Thanks are extended to all my dear friends in the laboratory. Mao Ouyang has supported and assisted my laboratory testing for several days and nights, which makes the testing less exhausting. Monika Maharjan, my junior in the lab, encourages me with the research. Ittichai Boonsiri is my classmate since the first day I came Japan. We encourage each other during our study. So many thanks to all the members in the Geotechnical group. They make it a pleasant group to conducted study with.

I acknowledge the scholarship provided by the Ministry of Education, Culture, Sports, Science and Technology, Japan. With this support, I could conduct this research.

Special thanks are due to my beloved mother. Since eleven years ago I left home for study, she has been supporting me to pursue my goal. I am sincerely grateful for her love, patience and sacrifice. This work could be completed without her support.

CONTENTS

LISTS OF FIGURES

Chapter 1

Chapter 2

Chapter 3

Chapter 4

Chapter 5

Chapter 6

LISTS OF TABLES

NOTATIONS

A: cross sectional area of a soil specimen (cm^2);

C_c: Curvature coefficient;

C_u: uniformity coefficient;

d_{50}: median grain size (mm);

d_{10}: effective grain size (mm);

D_{xc}: grain size for which x% mass passing is finer of the coarse fractions of a grading curve (mm);

d_{xf}: grain size for which x% mass passing is finer of the fines fractions of a grading curve (mm);

D_{xF}: grain size for which x% mass passing is finer of the filter (mm);

d_{xB}: grain size for which x% mass passing is finer of the base soil (mm);

d_x: grain size for which x% mass passing is finer of a soil (mm);

d: representative grain diameter of a soil specimen (mm);

d_0: average diameter of the assumed capillary tubes, proposed by Kovacs (1981) (mm);

D_r: relative density (%);

D_h^c: average diameter of an interval of grain distribution of the coarse fraction (mm);

e: soil void ratio;

e_0: postulated void ratio of eroded soil assuming that no volumetric deformation occurs during internal erosion;

e_c: void ratio after consolidation;

e_e: post-erosion void ratio;

e_i: initial void ratio, referring to the void ratio after saturation in this study;

e_{max}: maximum void ratio;

e_{min}: minimum void ratio;

e_s: void ratio of coarse grains in a binary mixture (fines are regarded as voids) (intergranular void ratio);

e_s^*: equivalent intergranular void ratio;

e_f: void ratio of fines in a binary mixture;

e_{c_max}: maximum void ratio of the coarse fractions in a binary soil;

e_{c_min}: minimum void ratio of the coarse fractions in a binary soil;

e_{f_max}: maximum void ratio of the fine fractions in a binary soil;

e_{f_min}: minimum void ratio of the fine fractions in a binary soil;

FC: percentage of fines content by volume (%);

FC_{th}: threshold fines content denoting the soil fabric transform (%);

f_s: mass ratio of coarse grains;

f_f : mass ratio of fines;

G_s: specific gravity of soil grain;

h: water head difference in the fixed-wall seepage test (cm);

h_0: total water head difference in the fixed-wall seepage test (cm);

h_n: local water head difference in the fixed-wall seepage test (cm)

I_r: instability degree;

i: hydraulic gradient;

i_0: average hydraulic gradient in the fixed-wall seepage test;

i_n: local hydraulic gradient in the fixed-wall seepage test;

i_c: critical hydraulic gradient for soil stability;

i_s: critical hydraulic gradient for internal erosion;

k_0: average hydraulic conductivity of tested specimens in the fixed-wall seepage test (cm/s);

k_n: local hydraulic conductivity in the fixed-wall seepage test (cm/s);

K: intrinsic permeability (m^2);

L_0: length of tested soil specimen for the fixed-wall seepage test (cm);

L_n: length of seepage flow at different layers for the fixed-wall seepage test (cm);

n: soil porosity;

n_c: porosity of the coarse fraction in a soil;

N_q: bearing capacity number;

p': mean effective stress at Cambridge stress field (kPa);

p_0': initial mean effective stress (kPa);

Q: flow rate (volume of fluid in unit time) (cm^3/s);

v: Darcy velocity (cm/s);

q: deviator stress at Cambridge stress field (kPa);

q_{peak}: deviator stress at peak (kPa);

q_{ss}: local minimum deviator stress after initial peak at quasi-steady state (kPa);

Re: Reynolds number;

S: cross-section area of pipette in the fixed-wall seepage test (cm^2);

U_n: Degree of undercompaction (%);

V: Average velocity (interstitial velocity) (cm/s);

V_s: Volume of coarse grains forming the primary fabric of soil;

V_f: Volume of erodible fines filling in the voids between coarse grains;

V_w: Volume of water (void volume for fully saturated soil);

W_s: Weight of coarse grains;

W_f: Weight of erodible fines;

v: specific volume, equals to $1+e$;

γ_w: unit weight of water (kN/m^3);

v: kinematic viscosity of fluid (cm^2/s);

ΔV: water volume difference between pipettes (ml);

ΔV_f: soil volume change caused by fines loss;

ΔV_w: void volume change due to the rearrangement of coarse grains;

Δq_c: increment of cone resistance (kPa);

$\Delta \sigma'_v$: vertical effective stress (kPa);

ϕ': drained angle of shearing resistance (degree);

ΔR: strength reduction by ratio after erosion;

$\phi'_{post-erosion}$: angle of shearing resistance after internal erosion (degree);

$\phi'_{before-erosion}$: angle of shearing resistance before internal erosion (degree);

τ_c: critical shear stress (Pa);

α_D: shape coefficient;

σ_1': major principle stress, corresponding to axial stress in a triaxial test (kPa);

σ_3': minor principle stress, corresponding to radial stress in a triaxial test (kPa);

σ_{cycd}: cyclic stress difference applied to a specimen (kPa);

σ_r': initial effective confining pressure (kPa);

ε_a: axial strain (%);

ε_r: radial strain (%);

ε_v: volumetric strain, equals to $\varepsilon_a+2\varepsilon_r$ (%);

ε_s: shear strain, equals to $2(\varepsilon_a-\varepsilon_r)/3$(%);

ϕ_{ss}: slop angle of the phase transformation line at QSS (°);

Λ: Ratio of the increments of void volume to that of solid volume due to particle removal

(McDougall *et al.*, 2004, 2013)

CSL: critical state line;

NCL: normal compression line;

QSSL: quasi-steady state line;

CHAPTER 1

INTRODUCTION

1.1 Problem Statement

Phenomenon of seepage-induced transfer of soil grains is observed widely both in natural soil deposits and in earth structures. This process is generally known as "erosion". Jones (1981) comprehensively illustrated the factors governing seepage-induced erosion in natural deposits from the hydrological perspective, as is shown in Fig.1.1. Flow of water rushes into downstream river through the "pipes" or conduits, which are called "macropores" in hydrology literature, triggers erosion of soil grains. The hydraulic conductivity of those regions is substantially higher than adjacent areas. Climatic factors, human activities, soil morphology, composition and physical-chemical properties primarily initiate and accelerate soil erosion.

Significant damage to potentially eroded high embankments of mountainside roads during Noto Peninsula Earthquake of Japan in 2007 stimulates the research interests on the effects of internal erosion on soil strength change. Sugita *et al.* (2008) discovered that the road facilities in approximate 80 places had been devastated. A number of the damage was the flow slide of embankments constructed on catchment topography such as swamps and valleys which usually accompanied by a large volume of fresh water. It is possible that those earth structures have suffered from years of erosion, which chronically turned the soil packing becoming loose, and consequently was vulnerable to seismic shaking. Similarly, numerous soil structure failure reported in literature was attributed to soil erosion. Crosta and Prisco (1999) presented a slope failure along an old fluvial terrace in Italy. By site investigation and numerical analysis, authors concluded that seepage erosion and tunnel scouring in the superficial layers, and seepage erosion at the slop toe would be the vital factors triggering the failure. Muir Wood (2007) reported two large sinkholes, formed by internal erosion, were observed at the crest of the W.A.C Bennett Dam in Canada, which would be huge threats for dam safety. The most critical influence of soil erosion is on earth structure, the failure of which would have catastrophic consequence. By literature review of the recent dam failures, Richards and Reddy (2007) concluded that nearly half of the world's dam failure was triggered by internal erosion. Although the statistics was rough and based on the engineering judgment, it was specific that the main reason of soil dam failure might be attributed to soil erosion. In Hagi city of Yamaguchi Prefecture of Japan, the ground was suddenly subsided, forming a 5-meter-in-length sinkhole in December of 2009 because of intense soil erosion by a large amount of underground water which was resulted from the pipeline breakage (Nikkei Construction, 2009).

However, hitherto, the mechanism of erosion triggered soil strength change is not fully understood. A clear and explicit explanation of soil fabric and strength change induced by internal erosion is necessary for engineering practice.

1.2 Terminology

A number of technical terms are used in literature regarding different types of internal erosion phenomena such as piping, backwards erosion, suffusion, tunneling and heave etc. There is no universally accepted definition of these terms. Under most circumstance, seepage-induced soil erosion is simply regarded as piping. For clarity, it is necessary to specifically define those commonly used terms.

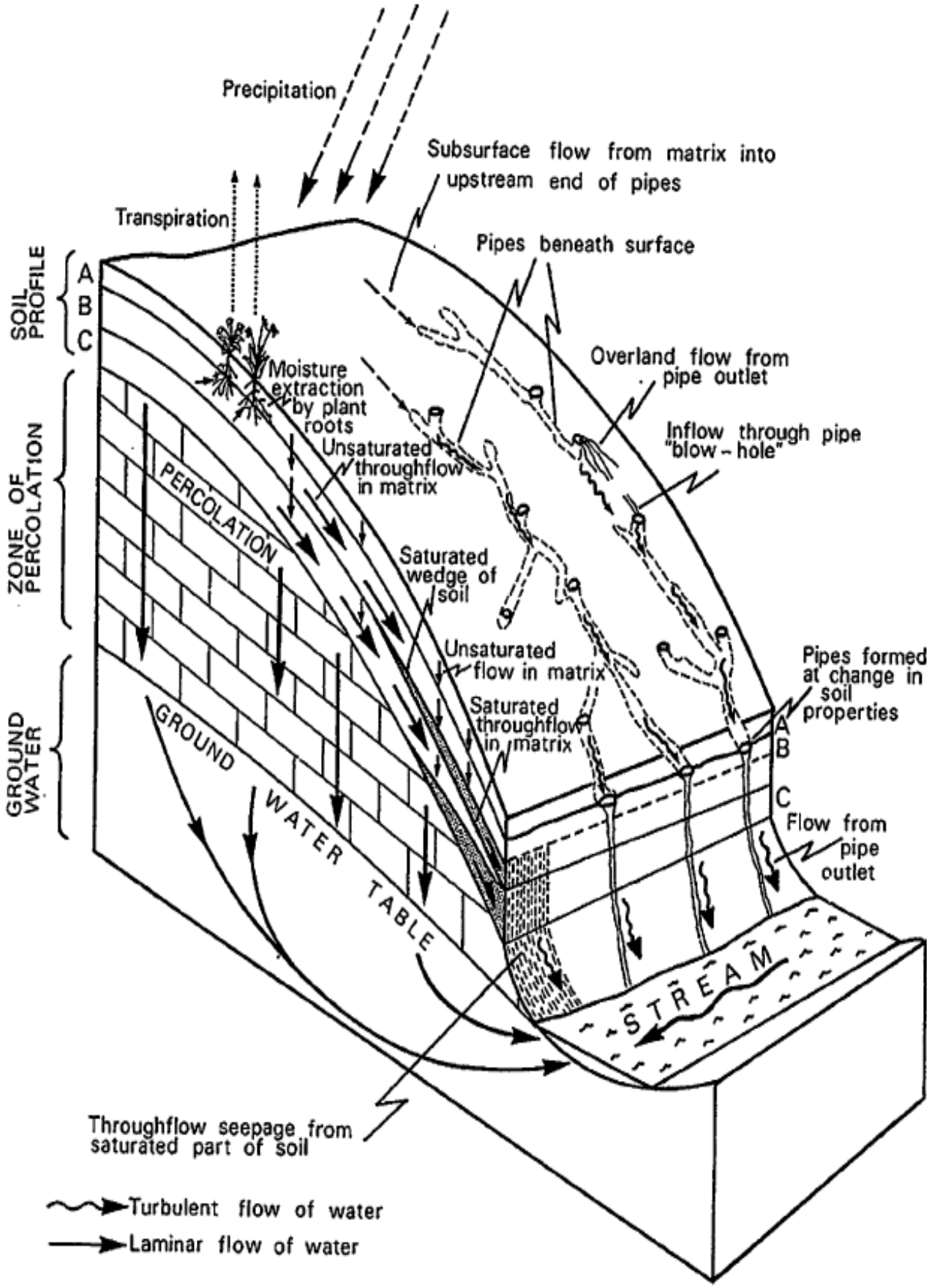

Figure 1.1 Hydrological view of soil erosion (after Jones, 1981)

1.2.1 Internal erosion

In the present study, internal erosion is a versatile term to describe the phenomenon that the soil grains within the body of natural deposit or earth structure are carried away by the seepage flow generated by the reservoir or groundwater. It includes two fundamental types: suffusion and piping, which differs in how the soil grains are eroded away from soil body.

1.2.2 Suffusion

As early as the beginning of 20 century, Russian researcher has published a comprehensive study about the phenomenon of the selective erosion of fine grains through a coarse matrix (coarse grains are not floating on the fines) leaving the coarse skeleton (Goldin and Rumyantsev, 2009). The fine grains are transported through the voids among the larger grains by seepage flow. Now this phenomenon is named as “suffusion”, which comes from the Latin “suffossio, onis”, meaning digging under or up, undermining. Another frequently used term “percolation” in power industry refers to the same phenomenon as well.

A schematic diagram showing the suffusion process is presented in Fig.1.2. In the non-cohesive materials, suffusion leads to great changes of porosity and significant increase of hydraulic conductivity. Gap-graded soils, like sandy gravels, are more prone to suffusion due to its deficiency in certain grain size. Soils that are vulnerable to suffusion are often thought of internally unstable. Recently, a greater refinement of the definition is presented. Moffat and Fannin (2006) separated the phenomenon as “suffusion” and “suffosion”. They defined “Internal instability describes the migration of a portion of the finer faction of a soil through its coarser fraction. Redistribution of the finer fraction, termed suffusion, may yield a loss of grain and instigate a process of undermining, termed suffosion.” Richards and Reddy (2007) clearly defined suffusion as “the phenomenon that the finer fraction of an internally unstable soil moves within the coarser fraction without any loss of matrix integrity or change in total volume”, whereas suffosion, “on the other hand, means the erosion of grains would yields a reduction in total volume and a consequent potential for collapse of the soil matrix”.

Another commonly accepted category is proposed by Kovacs (1981). He divided the suffusion into two subcategories: Internal suffusion and external suffusion. “Internal suffusion” occurs when the hydrodynamic forces are large enough to move fine grains from soils, affecting only the local hydraulic conductivity. In contrast, the “external suffusion” occurs at the surface of a soil layer, which is “when volume of the solid matrix is reduced, accompanied by an increase in permeability, but the stability of the skeleton composed by the coarse grains is unaffected”.

Suffusion is a comparatively slow seepage process. Therefore, it is a chronic problem which accompanies with the constant quantities of seepage flow over a period of years.

1.2.3 Piping

Piping describes the phenomenon that underground water flows along a continuous opening, such as crack and simultaneously soil erosion takes place along the wall of a “pipe”. Different from backwards erosion which is initiated by Darcy flow at an exit point, piping is triggered by erosive forces of water along a “pipe”. Therefore, it can be expected that piping erosion would initiate in accordance with the cubic law of flow for planar openings (Richards and Reddy, 2007). Fig. 1.3 shows the schematic diagram of piping process.

Strong piping may also be found at a soil-structure contact where the flow velocity is higher. Erosive force would be much larger for a given hydraulic gradient. Also, as the hydraulic conductivity tends to be slightly greater at soil-structure contact, this is often the first place that increasing hydraulic gradients may express themselves through erosion.

1.2.4 Backward erosion

Backward erosion indicates the erosion of soil grains at the exit of a seepage path due to a high exit velocity (Wan, 2006). The exit of the seepage path is usually a free surface, such as the ground surface downstream of a soil foundation or the downstream face of a homogeneous embankment. In the case of backward erosion, resistance to the removal of soil grains is dependent on the hydraulic gradient through the soil (which is necessary to overcome soil resistance) and the stress state of the soil around exit.

This type of erosion is produced by the tractive forces of intergranular seepage water. The mobilizing tractive forces are balanced by the shear resistance of grains, soil grains weight and filtration. The erosive forces are greatest where flow concentrates at a point of exit and as long as soil grains are transported by erosion the magnitude of the erosive forces increases due to the increased concentration of flow. The tractive forces are directly proportional to the velocity of intergranular flow.

1.2.5 Tunnelling or jugging

This occurs within the vadose zone and results from chemical dispersion of clay soils induced by rainwater passing through open cracks or natural conduits. It is usually observed in dispersive soils caused by rainfall erosion and is discussed by a number of Australian and New Zealand scholars (Jones, 1981).

1.2.6 Heaving, boiling or blowout

This seems to be an engineering term rather than a hydraulic term. Terzaghi (1943) reported this phenomenon when assessing a sheet pile cofferdams. According to him, heaving or boiling happens when a semi-permeable barrier overlies a pervious zone under relatively high fluid pressures. Different from the failure mode of suffusion or piping, it requires a high enough seepage velocity to move individual soil grains causing a “zero” effective stress of the soils.

From the above definitions, it can be noted that wholly different mechanisms dominate various modes of soil erosion. Meanwhile, it also shows that those types of erosion are internally related. Heaving initiates suffusion as well as backward erosion (Skempton and Brogan, 1994). From micro perspective, suffusion is caused by a number of piping erosion. Also, the piping erosion will greatly accelerate the extent of suffusional erosion. Suffusion and piping are always coupled phenomenon. Hence, it is impossible to exactly simulate one type of soil erosion without the occurrence of other types. To avoid the dilemma, the common term “internal erosion” is used in this dissertation to describe the target phenomenon that small grains are washed out through the voids between the coarser grains by seepage flow.

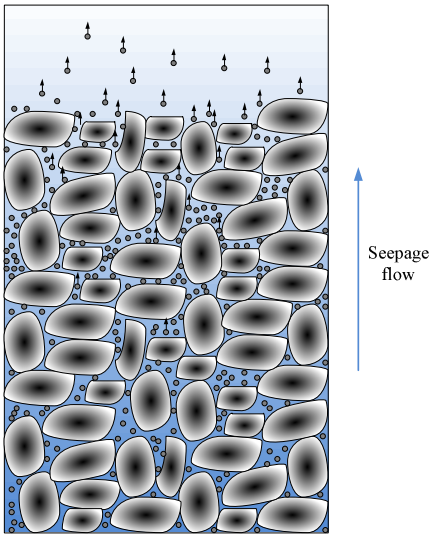

Figure 1.2 Process of suffusion

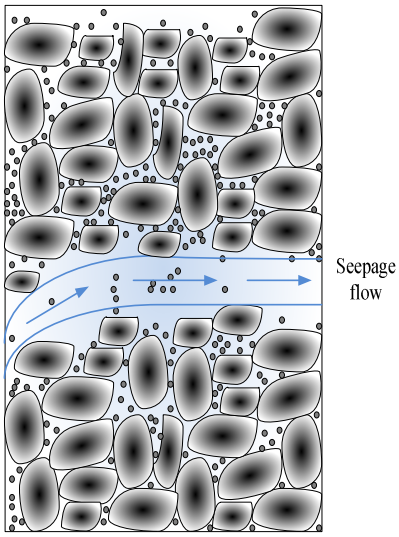

Figure 1.3 Process of piping

1.3 Phenomena description

The nature deposits are usually comprised of, respectively, a “fine fraction” and a “coarse fraction”. When underground water flows through the deposit, the tractive force of seepage water, theoretically given by “$i\gamma_w$”, is capable of dislodging fine grains from the matrix of the coarser fraction, triggering the soil instability. This phenomenon would be understood from two perspectives: hydraulic mechanism and soil mechanics.

From hydraulic point of view, it is of significance to understand that (I) the factors governing the onset of internal erosion, (II) the amount of soil grains passing through the soil matrix and, correspondingly, (III) the variation of hydraulic parameters during the progress of internal erosion. The onset of internal erosion is governed by two constrains, geometrical constraint and hydro-mechanical constraint. Instinctively, geometrical constraint refers to the size of fines should be smaller than the size of voids in soil. Following the basic idea, many empirical criteria have been proposed to assess the internal stability of soil based on the grain size distribution (US Army Corps of Engineers, 1953; Istomina, 1957; Lubochkov, 1962, 1965; Kezdi, 1979; Kenney and Lau, 1985, 1986; Burenkova, 1993; Skempton and Brogan, 1994; among others), which will be delivered in detail in Chapter 2. Kovacs (1981) defined the hydro-mechanical constraint as “the critical velocity or hydraulic gradient, above which the fine grains start to move”, which is found closely related with the effective stress level in soil. Skempton and Brogan (1994) firstly analyzed the influence of effective stress level on soil internal stability. A reduction factor was proposed to note that the soil internal stability will be triggered at a hydraulic gradient significantly lower than the anticipated from theory. Based on the results of series of permeameter tests, Moffat and Fannin (2011) demonstrated the effective stress level dependent hydraulic gradient characteristics and proposed the concept of a hydromechanical path in stress ~ gradient space. Li and Fannin (2012) proposed a linear hydromechanical envelope in stress ~ gradient space. The envelope is governed by the proportion of effective stress in fines.

For the potentially unstable soils, the fine grains could be freely dislodged from the soil skeleton, leading to certain amounts of soil loss. The amount of cumulative eroded soil mass is the vital parameter because the derived erosion rate is necessary in assessing the soil erosion condition. Also, erosion of soil grains would induce the soil microstructure rearrangement, leading to the changes of hydraulic conductivity, volumetric deformation and soil mechanical behaviors.

There are other influential factors, such as vibration (e.g., earthquake induced or mechanical tamping), saturation degree and temperature etc. Those factors are neglected in this research.

From soil mechanics point of view, the sand behavior is largely dependent on the friction along grain contacts. With the progress of soil erosion, the original sand microstructure may be fully deteriorated and lose the strength at certain hydraulic gradient, which is called "hydraulic gradient at failure" (Chang and Zhang, 2011a). Correspondingly, the mechanical behavior of soil may vary with the development of internal erosion. The study of the erosion dependent soil behavior is still on progress in literature. Muir Wood *et al.* (2010) attempted to model the mechanical consequences of internal erosion by two-dimensional discrete element analysis. The simulation indicated that the erosion could trigger the soil state change, from "dense" (below the critical state line) to "loose" (above the critical state line), with corresponding available strength lower than the critical state strength. Scholtès *et al.* (2010) considered the internal erosion as the progressive removal of the finest grains and concluded that the soil strength was strongly influenced by the erosion: the soil behavior changed from a dilatant to a contractant when extracting the fine grains. Those zones in the soil structure where internal erosion occurs would be more prone to fail. By the seepage tests in newly developed triaxial apparatus, Chang and Zhang (2011b) proved that the originally dilative tested specimens became contractive after the loss of a significant amount of fine grains due to internal erosion.

1.4 Purpose and scope of the study

Gap-graded soils are frequently presented both in nature and construction practice, for example at the River Indus at Tarbela in Pakistan mentioned by Skempton and Brogan (1994) (Fig.1.4). This kind of material has played a significant role in the potential for seepage induced internal erosion. Extensive studies, focusing on the filter mechanism and soil internal stability from soil microstructure geometrics, have been published. The main concern is to develop a reliable procedure for evaluating internal erosion potentials, proper filter design criteria, and assess the hydraulic gradient which triggers internal erosion. However, it is significant to note that the failure of soil structure due to internal erosion is not only produced by hydraulic erosion but also mechanical failure. The mechanical failure and hydraulic erosion is couple to one another because washing-out of soil grains increases soil porosity and causes readjustment of intergranular forces leading to further strength decrease and damage of soil structure. On the other hand, strength reduction leads to smaller intergranular forces, which in turn increases the amount of fine grains potentially being able to leave

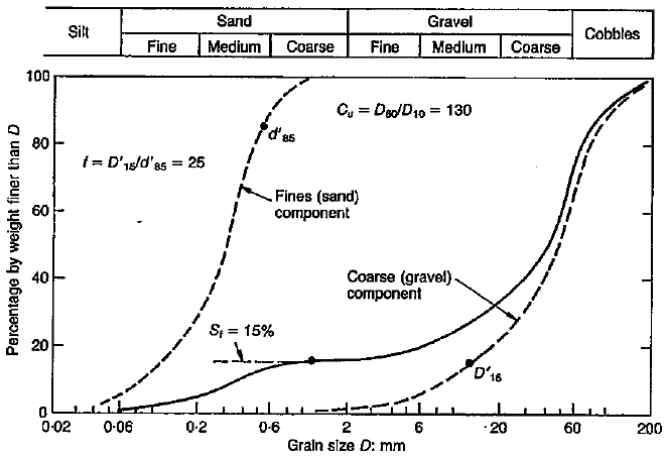

Figure 1.4 Grain size distribution of Indus alluvium at Tarbela (after Skempton and Brogan, 1994)

the coarse matrix and transport. Therefore the influence of both soil mechanics and hydraulic erosion must be considered to properly account for soil failure induced by internal erosion. A clear and explicit understanding of this coupled process is helpful for both engineering design and construction.

The primary objective of this research is to demonstrate the soil mechanical behavior change after internal erosion. Specifically,

(1) Develop a triaxial permeameter capable of directly investigating the erosion mechanism of tested soil at the onset and the progress of internal erosion and the changes in soil mechanical behaviors induced by internal erosion.

(2) Illustrate the soil behavior during the erosion test. Special attentions are given to the vulnerability of the tested specimen to internal erosion and the variation of the key parameters at the development of erosion, such as hydraulic gradient, hydraulic conductivity, soil deformation and cumulative eroded soil mass.

(3) Study the mechanical consequences of internal erosion in terms of the changes in soil strength parameters.

To fulfill the objectives, the following work has been performed:

(1) Common fixed wall seepage test has been conducted to preliminarily understand the erosion mechanism of the tested soil specimen. A multi-stage test procedure is followed to assess the hydraulic conditions necessary to trigger the internal erosion. Parametric study is conducted to examine the effects of soil properties (i.e., relative density, initial fines content) and hydraulic conditions on the erosion mechanism.

(2) Several new components have been installed to an automated triaxial testing system to accommodate the seepage test in a triaxial condition, including a flow pump, a sedimentation tank and a revised pedestal.

(3) The hydromechanical behavior of tested specimen during the progress of internal erosion are studied by assessing the changes of the key parameters, such as hydraulic gradient, hydraulic conductivity, soil deformation and cumulative eroded soil mass in the new triaxial system. The effects of stress state and initial fines content are experimentally investigated.

(4) The soil strength reduction after erosion in the fixed-wall seepage test is elaborated by interpreting the cone tip resistance profile of the tested specimens after erosion. For the flexible-wall permeameter, the stress ~ strain relationship is directly indicated by conducting undrained & drained monotonic compression test on the internally eroded soil specimen. The influence of stress state and initial fines content are considered.

(5) Influence of internal erosion on the cyclic resistance of tested specimens is studied by performing undrained cyclic test on the eroded soil specimens and companion specimens without erosion, respectively, at the same effective confining pressure.

1.5 Organization of the dissertation

There are a total of 7 Chapters in the dissertation. Chapter 1 is the current chapter which introduces the background of the research, the frequently used terms and the objectives of the research.

Chapter 2 describes the review of literature related with internal erosion (suffusion) from four perspectives: current soil erosion testing technique, mechanisms of internal erosion, analytical models for internal erosion assessment and mechanical consequences of internal erosion. The criteria for soil internal stability assessment are provided, namely, geometrical and hydraulic criteria. The soil behavior at the progress of internal erosion is summarized. The studied until now on mechanical behavior of eroded soil are stated and in addition, effects of fines content on soil mechanical property is discussed to seek for the full understanding of the mechanical influence of fine loss which is induced by internal erosion.

Chapter 3 illustrates the details of the seepage test in the fixed-wall permeameter, including the test apparatus, multi-steps test procedure and the primary properties of the tested soil. The soil behavior at the onset and progress of internal erosion is demonstrated by the changes of hydraulic conductivity, fine loss and soil deformation. By interpreting the cone tip resistance profiles, the soil strength reduction after internal erosion is discussed.

Chapter 4 presents the details of the newly developed flexible-wall permeameter. The main components, including constant flow rate control unit, automated triaxial system and eroded soil collection unit are elaborated.

Chapter 5 mainly focuses on the soil hydromechanical behavior at the seepage test conducted with the flexible-wall permeameter. The seepage tests are conducted at the constant flow rate. Changes of hydraulic gradient, hydraulic conductivity, cumulative eroded soil mass and soil deformation are presented. The influence of effective confining pressure and initial fines content is demonstrated as well.

Chapter 6 examines the mechanical consequences of internal erosion on the tested specimens. Undrained monotonic test, drained monotonic test and undrained cyclic tests are performed on the eroded specimens and the companion specimens. By comparison, the changes of soil mechanical response induced by internal erosion might be fully discussed. Additionally, the effects of soil erosion on the cyclic resistance of soil are illustrated.

Chapter 7 gives the conclusions drawn from the research and recommendations for future study.

CHAPTER 2

LITERATURE REVIEW FOR INTERNAL EROSION RELATED STUDY

The phenomenon of internal erosion in cohesionless soils exhibits itself as the gradual migration of fine grains through a coarse matrix leaving the coarse skeleton. It is accompanied by great changes in porosity, significant increase of hydraulic conductivity, and potential changes of soil fabric. This phenomenon was firstly observed in the experimental investigations of filter and base soil compatibility. Thereafter, many empirical methods were proposed by a number of investigators to evaluate the soil instability by analyzing the geometrical size of the soil (US Army Corps of Engineers, 1953; Istomina, 1957; Lubochkov, 1962, 1965; Kezdi, 1979; Kenney and Lau, 1985, 1986; Burenkova, 1993; Skempton and Brogan, 1994; among others). The hydraulic gradient at which internal erosion initiates, named "critical hydraulic gradient", had been fully studied to understand the hydraulic conditions for the onset of soil erosion. In addition, the possible influence of the difference in soil properties (i.e., cohesion, fines content, etc.) on soil erosion was elaborated. The recent research showed that the stress level exerted great influences on the onset of internal erosion in terms of the critical hydraulic gradient (Moffat and Fannin, 2011; Li and Fannin, 2012; Chang and Zhang, 2012). A few physical models had been proposed to identify the hydro-mechanical influence on the onset of soil internal stability. (Indraratna and Vafai, 2002; Bonelli and Marot, 2008; Fujisawa *et al.*, 2010; among others). The mechanical consequences of internal erosion were experimentally and numerically investigated (Muir Wood *et al.*, 2010, Scholtès *et al.*, 2010, Xiao and Shwiyhat, 2012), which proved that the soil erosion would cause the soil strength reduction to some extent.

The critical review of the current knowledge about internal erosion is presented with reference to experimental investigations, empirical criteria for internal erosion assessment, analytical models and mechanical influences of internal erosion.

2.1 Review of current soil erosion testing technique

Experimental studies of soil grain migration began from filter design in Dam Engineering. The phenomenon that the base soil that satisfies the geometrical criteria may fail due to erosion of fine grains, discovered in the base soil and filter compatibility studies inspired the laboratory test on those "poor graded" soils, such as gap-graded or coarse widely graded soils. In those experimental investigations, not only the soil geometric characteristics, but also the influence of flow velocity, flow direction, hydraulic gradient and possible chemical reaction was taken into consideration.

2.1.1 Standard soil erosion test

The well-known standardize laboratory tests for soil erosion are pinhole test (ASTM D4647-06e1) and the double hydrometer test (ASTM D4221-11), developed by Sherard *et al.* and Decker *et al.* respectively in the 1970s. The purpose of those tests is to

identify the dispersive clay in soils, which are highly prone to internal erosion. For pinhole test, the equipment of the tests includes a cylinder and two steel or aluminum plates with o-rings for sealing the tube at both ends. The clay is compacted into the cylinder by tampers. A plastic nipple is pushed into the top of the specimen and a hole is punched through the nipple along the cylinder axis to accelerate the erosion. Soil would be categorized into five classifications according to the hydraulic gradient at which the erosion begins, the visual estimate of clarity, and the size of the eroded hole after the test. The recently developed standard laboratory tests to study the soil erosion of cracks include slot erosion test (SET) and hole erosion test (HET) (Wan and Fell, 2004a, 2004b; Bonelli *et al.*, 2006; Haghighi *et al.*, 2013), which could determine the erosion rate, the minimum hydraulic shear stresses to initiate piping erosion, and their relationships to the soil properties. SET and HET are mainly served for the dam risk assessment. Indraratna *et al.* (2013) developed the Process Simulation Apparatus for Internal Crack Erosion (PSAICE) to assess the erosion rate of a sandy soil with cracks at different hydraulic gradients.

2.1.2 Base soil and filter compatibility test

Extensive laboratory tests on filtration mechanism were firstly performed by Bertram in 1940s under the direction of Terzaghi and Casagrande (Fell *et al.*, 2005). Since then, seepage tests on the various filters/base soil combinations probably encountered in practice had been conducted to validate the effectiveness of filtration (U.S. Army Corps of Engineers, 1941; Pare *et al.*, 1982; Sherard *et al.*, 1984; Lafleur, 1984; Lafleur *et al.*, 1989; Tomlinson and Vaid, 2000; among others). The typical permeameters used are stated in Figs.2.1~2.5. The main apparatus comprises a fixed-wall permeameter cell together with the transducers for the measurement of pore water pressure spatial variations and effective stress distribution along the specimen. To prevent the formation of large seepage channels along the fixed-wall, an extra layer, such as a compressive rubber layer or a silicon grease layer against the inside wall may be necessary. The permeameter cell is usually transparent with opening on the top or bottom in order to record the process of internal erosion by either microscopic or visual observation. For those cases conducted with external loading, the permeameter cell is mounted into a reaction frame to accommodate an axial loading system. Vertical effective stress on the top surface is calculated from axial force of the loading rod. A displacement transducer mounted on the loading rod monitors the axial displacement. The base soil could be either cohesive soil or cohesionless soil while the filters are usually composed of gravels with well grading. The reconstituted base soils could be either above one filter layer or sandwiched between two filter layers.

Controlled seepage flow is necessary for internal erosion test. Occasionally, a light vibration is also applied on soil sample to ensure full erosion. The seepage flow is usually unidirectional, either upward or downward, which is generated by the hydraulic pressure difference between the top and bottom of a specimen. In some studies, horizontal flows are assigned to investigate the effects of flow directions on erosion mechanism (Pare *et al.*, 1982). Deaerated water is recommended as seepage fluid to prevent the possible decrease in measured hydraulic conductivity. The given hydraulic conditions are usually the hydraulic gradient imposed on the filter/base soil. Therefore,

it is critical to produce a stable hydraulic head (pressure) in the testing system. In the earlier experiments, the inlet hydraulic pressure is maintained by a constant-water-head tank while the outlet is open to atmosphere or connected to another constant-water-head tank. The tank could be raised or lowered to control the hydraulic gradient along the soil. The flow rate is estimated by measuring the volume of discharge effluent per minute by a cylinder. To overcome the possible errors in the constant head control system, several improvements have been applied. For instance, one stabilization tube and one overflow tube could be installed to maintain the constant upstream water head. Tomlinson and Vaid (2000) kept the hydraulic head at the inlet by throttling a valve open to the water supply pressure while that at the outlet is maintained by submerging the permeameter into a large water bath with a constant water head. Flow rate is monitored by the volume of effluent out of the water bath. The water circulation system is usually adopted in experiments as well. Lafleur (1984) recirculated the water by means of a system of solenoid valves that ensured refilling of the upstream tank when it was empty. Kenney and Lau (1985, 1986) pumped the water in the effluent tank back to upper water tank to fulfill the circulation of seepage water. However, those systems could not reach the comparatively high hydraulic gradient that is usually necessary to initiate internal erosion in soils subjected to surcharge. Two pressurized storage reservoirs, namely influent and effluent reservoirs, are introduced as inflow and outflow tank to obtain the larger hydraulic gradient. To prevent the dissolution of air into water, which might lead to great errors in erosion test, each tank has an internal membrane acting as an air-over-water interface. The water temperature in the storage reservoir and inlet/outlet tanks keeps at constant temperature (20±1°C).

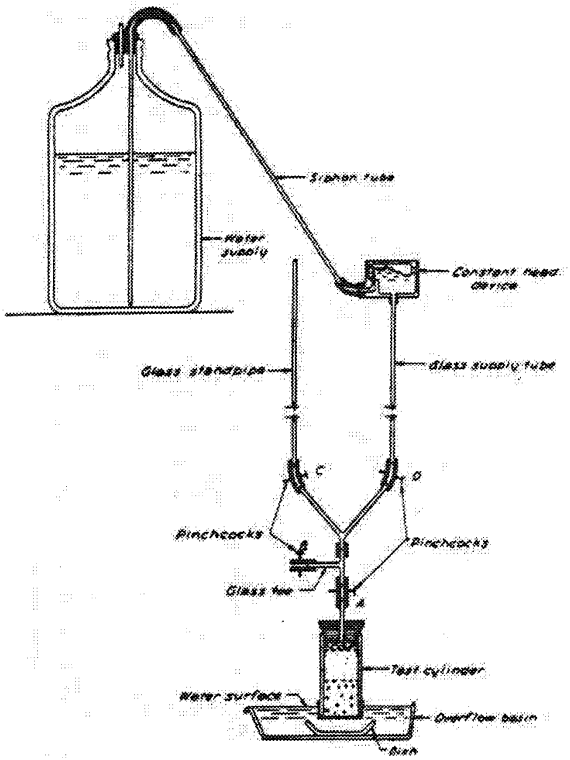

Figure 2.1 Test apparatus details (after Bertram, 1940 [Fell *et al.*, 2005])

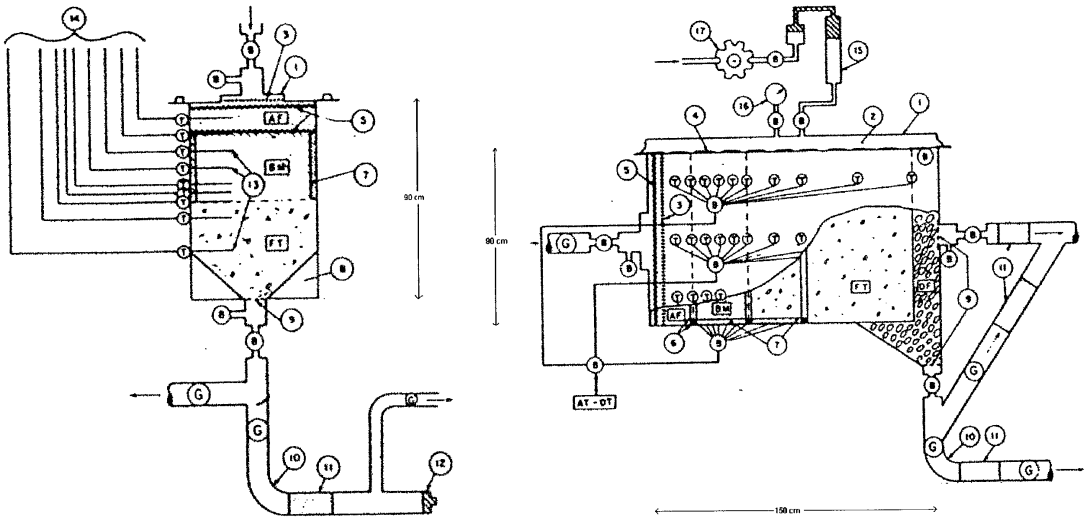

(a) (b)

Figure 2.2 Permeameters details: (a) vertical direction (b) horizontal direction (after Pare *et al.*, 1982)

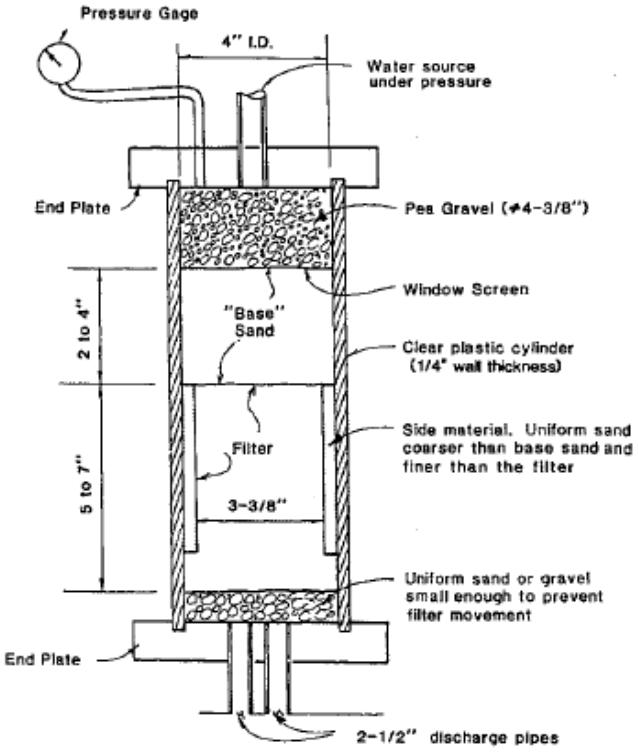

Figure 2.3 Filter test apparatus details (after Sherard *et al.*, 1984)

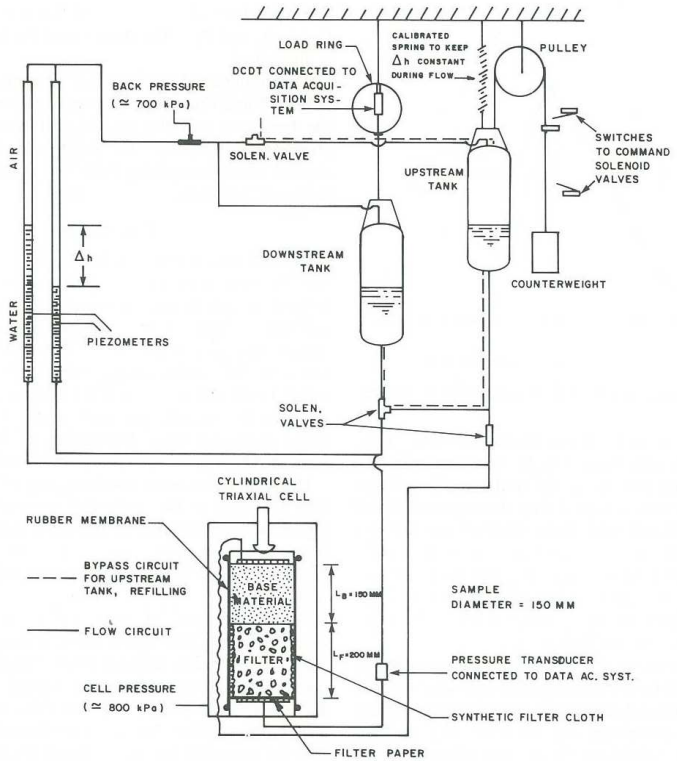

Figure 2.4 Test apparatus details (after Lafleur, 1984)

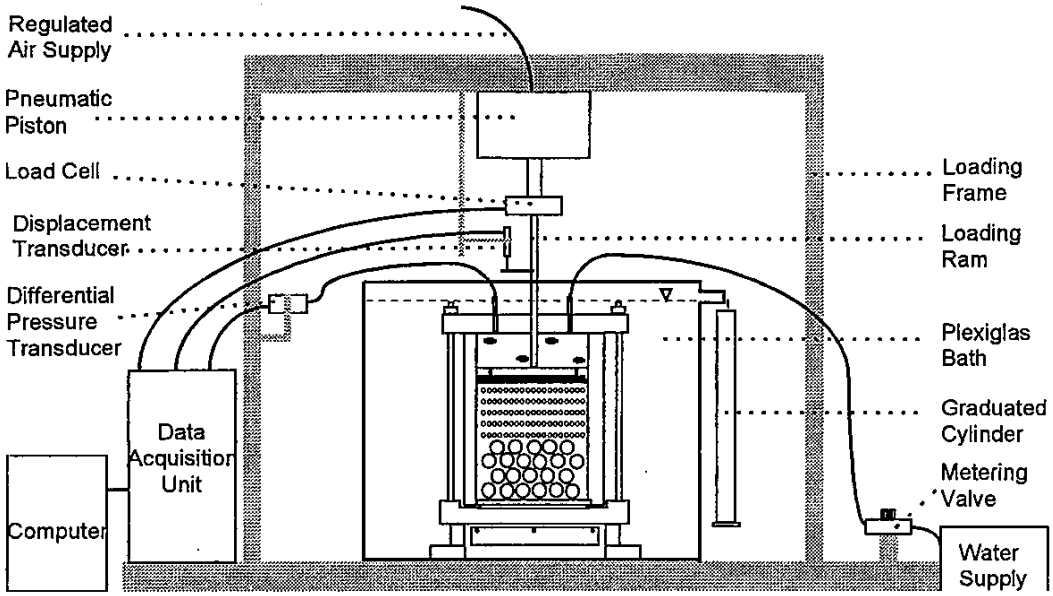

Figure 2.5 Apparatus details (after Tomlinson and Vaid, 2000)

Depending on the test cases, the duration of one case might be minutes or even up to days. Since internal erosion is chronic phenomenon, long duration is predominantly preferred. The test procedures are usually multi-steps, except for some studies which underline the effects of rate of gradient increase. The maximum imposed hydraulic gradient through the base soil varies with cases, from 1 up to 30. Commonly, it

demands larger hydraulic gradient to initiate internal erosion for cohesive clay than non-cohesive sand.

2.1.3 Soil internal stability test

The phenomenon that base soil or filter, that satisfies the Terzaghi's retention criteria, may fail because of internal erosion of fine fractions itself led to the soil internal instability studies (Kenney and Lau, 1985, 1986; Tanaka and Toyokuni, 1991; Skempton and Brogan, 1994; Chapuis *et al.*, 1996; Honjo *et al.*, 1996; Moffat and Fannin, 2006; Wan and Fell, 2008; Anisimov and Ter-Martirosyan, 2009; among others). The main apparatus, measurements, control of hydraulic condition and test procedures are similar to that of the filter/base soil study. A summary of the test equipment is shown in Figs. 2.6~2.13. Extensive efforts are exerted on the eroded soil collection and weighing system because mass of soil loss is considered as the key parameter to comprehend the onset and progression of internal erosion. Tested soil deformation and changes of fabric are closely related with the soil loss. In case of non-cohesive soil, for the downward flow test, the eroded soil is collected at the base of a permeameter. A drainage system, such as a silicon hose directed by a conical trough, is better to be included to prevent the possible clogging. For upward flow test, a gentle air flow through a thin tube at the top of the sample could be applied to avoid the sedimentation of the eroded grains (Sterpi, 2003). With regard to those cases with difficulties in installing the soil collection system, especially for the upward flow test, a graphical method proposed by Kenney and Lau (1985) could be used to approximately assess the fraction of eroded fine grains as well as the largest eroded fine grains based on the amounts of movements of grading curves after erosion from the original position. In case of cohesive soil, a flow-through turbidimeter could be connected to the outlet pipe to assess the eroded soil mass (Bendahmane *et al.*, 2008; Marot *et al.*, 2011).

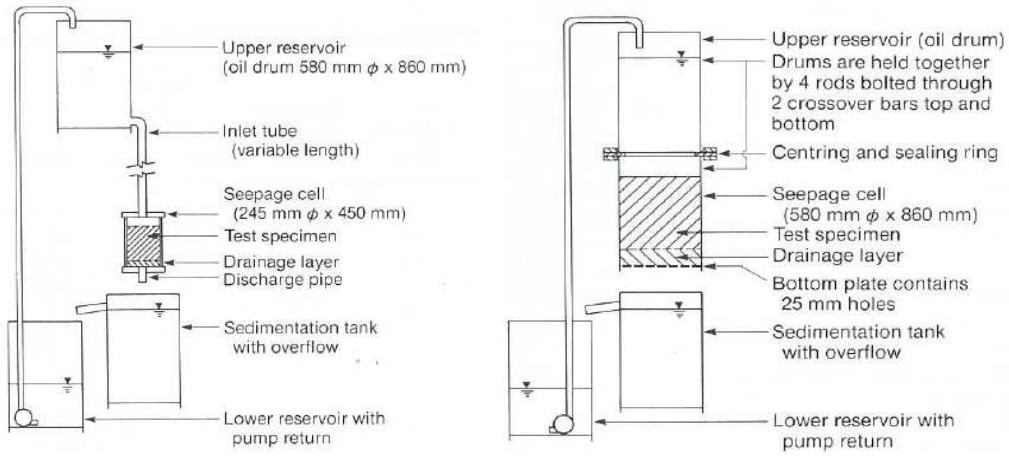

Figure 2.6 Test Permeameters (after Kenney and Lau, 1985)

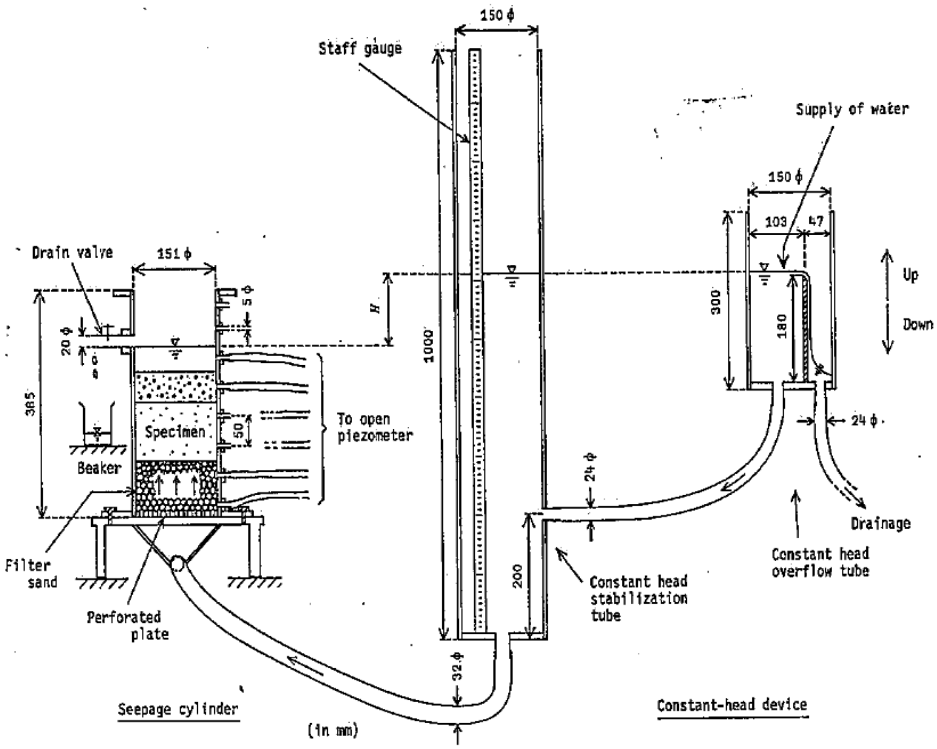

Figure 2.7 Test Apparatus (after Tanaka and Toyokuni, 1991)

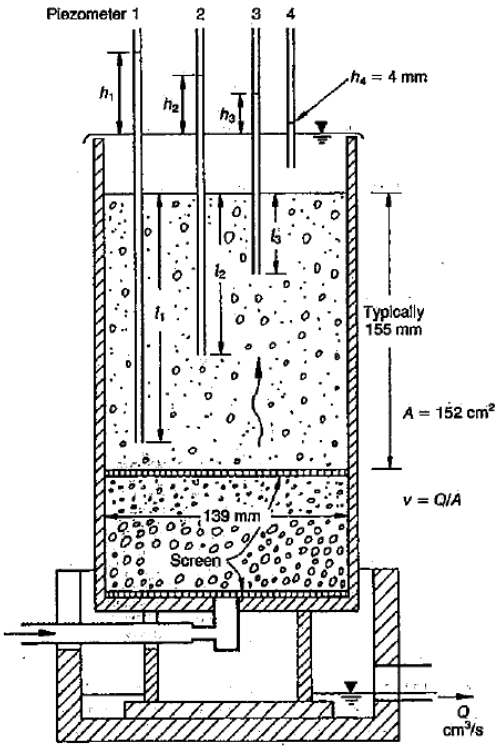

Figure 2.8 Test Apparatus (after Skempton and Brogan, 1994)

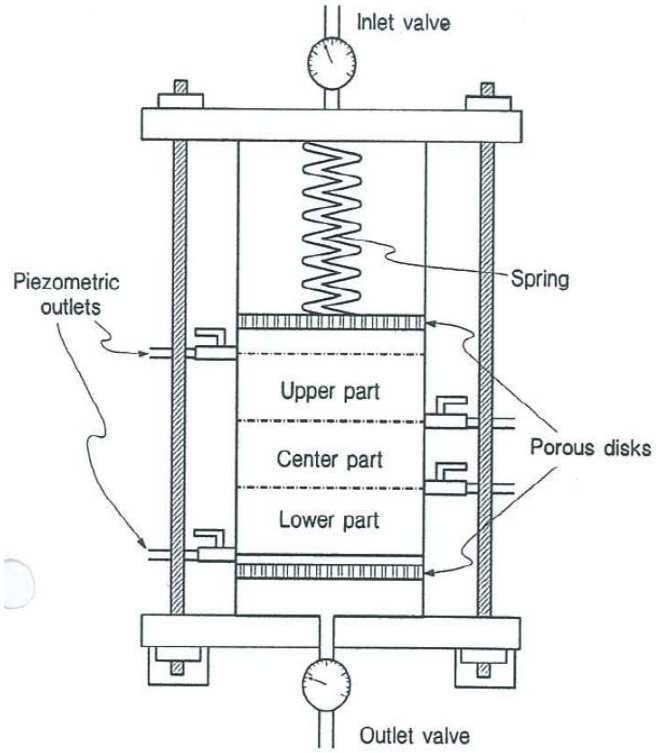

Figure 2.9 Test Apparatus (after Chapuis *et al.*, 1996)

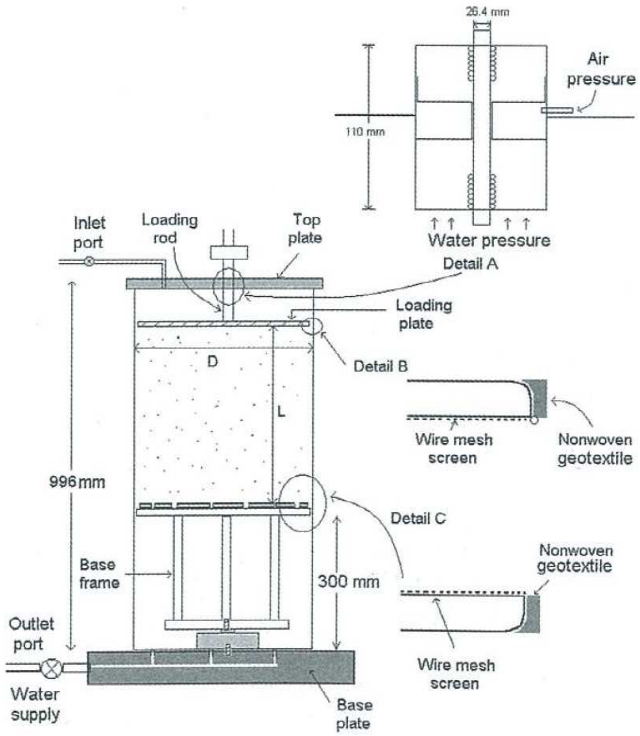

Figure 2.10 Permeameter details (after Moffat and Fannin, 2006)

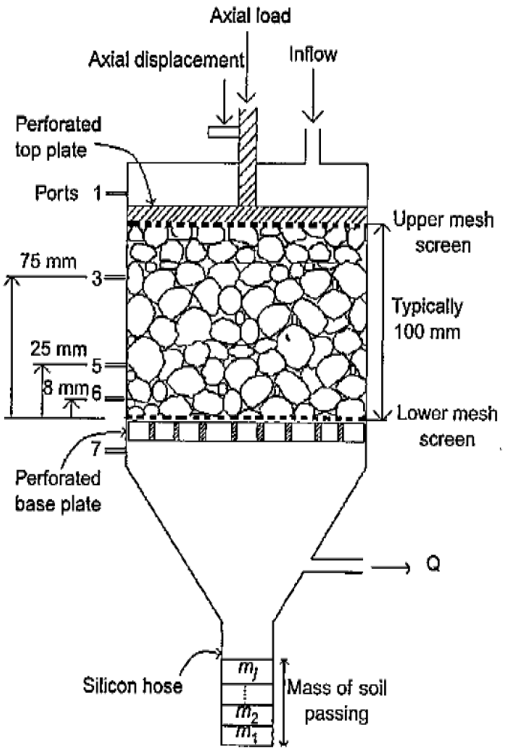

Figure 2.11 Permeameter apparatus (after Fannin and Moffat, 2006)

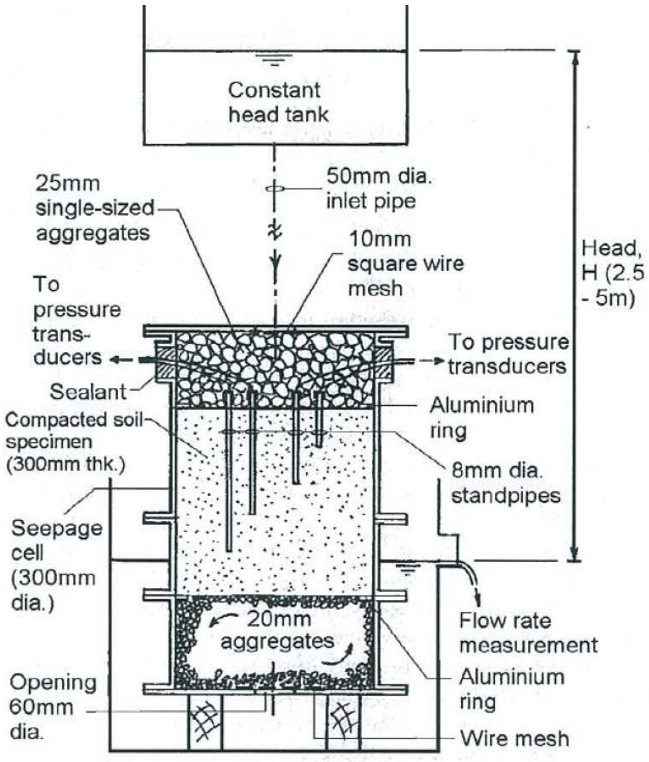

Figure 2.12 Downward seepage test (after Wan and Fell, 2008)

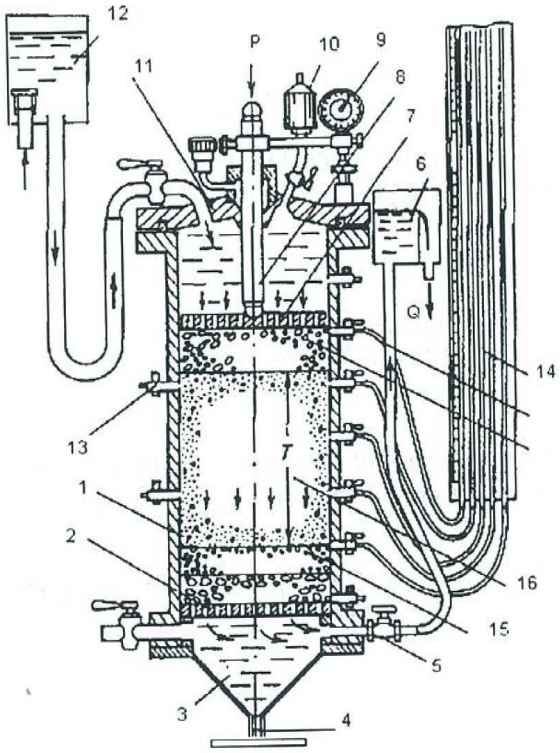

Figure 2.13 Permeameter details (after Anisimov and Ter-Martirosyan, 2009)

The weakness of the commonly utilized fixed-wall permeameters in the laboratory investigations is the sidewall leakage, which would be more serious when testing stiff soils or permeating soils at a very low compression stress (Daniel *et al.*, 1984). The flexible-wall permeameters, on the other hand, could minimize the leakage and permit applying back pressure to improve the saturation degree of tested specimens. By controlling the vertical and confining pressure, the vulnerability of soils to internal erosion could be tested under various stress states. Those merits motivate the trials of adopting a flexible wall permeameter, which is a revised triaxial apparatus, in laboratory testing. The first experimental investigations of soil erosion potential by modified triaxial cell were fulfilled by Sanchez *et al.* (1983). The confining pressure was applied during erosion test to consider the real stress environment in the embankment. Several sophisticated triaxial erosion tests have been successfully performed recently. Bendahmane *et al.* (2008) and Marot *et al.* (2009) studied the influence of hydraulic and mechanical characteristics of cohesive soils on internal erosion in a developed triaxial apparatus, which allowed for saturation, consolidation and measurement of volumetric change (Fig.2.14 & Fig.2.15). A drainage system was added at the bottom of the cell. The eroded soil in the effluent was detected by a developed photo sensor, which was explicitly explained in Marot *et al.* (2011).

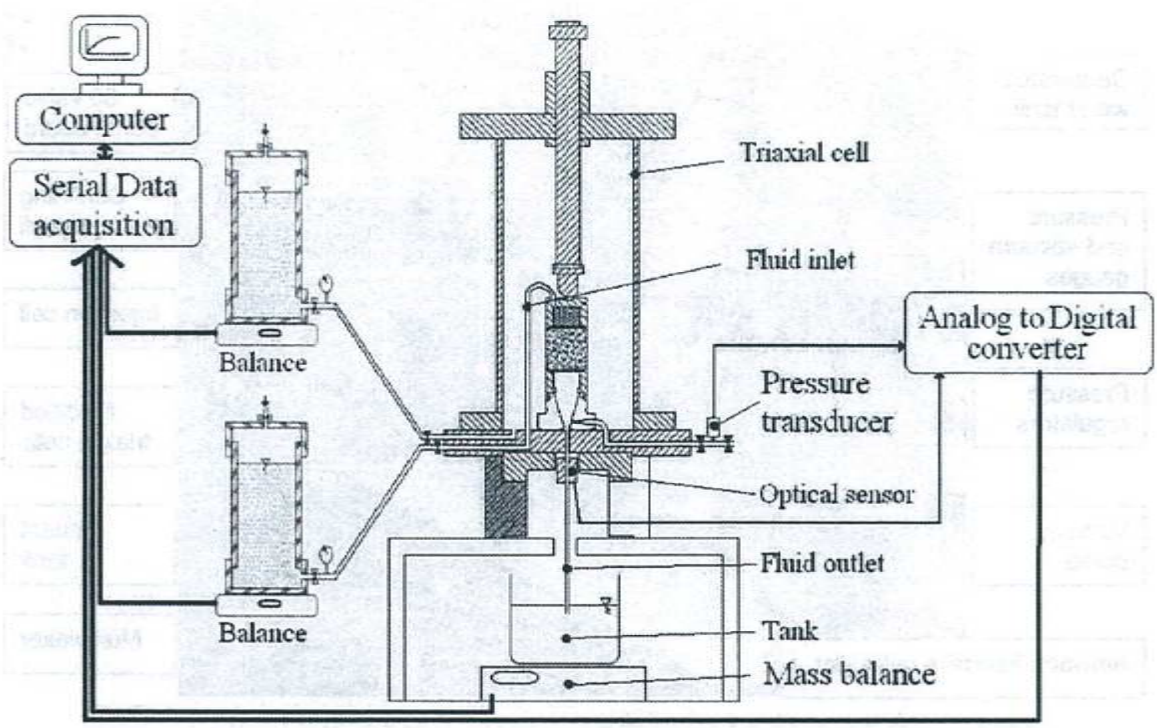

Figure 2.14 Triaxial apparatus (after Bendahmane *et al.* 2008)

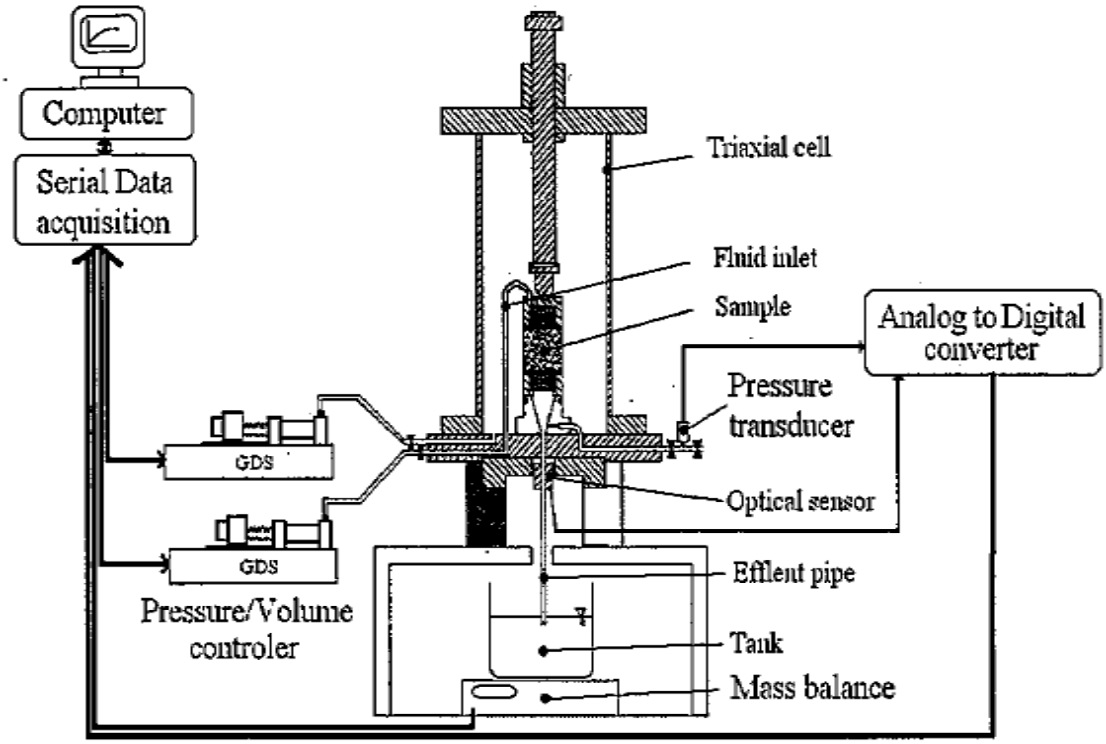

Figure 2.15 Triaxial apparatus (after Marot *et al.* 2009)

Richards and Reddy (2010) developed a true triaxial piping test apparatus to assess the backwards erosion potential of a wide range of soils, particularly non-cohesive soils, at

various stress states (Fig.2.16). The apparatus mainly consisted of the true triaxial load cell, capable of applying a range of mutually perpendicular pressures, inlet-outlet pressure control panel, an inlet-flow control panel, trubidimeter and several pressurized vessels. It is worth stressing that the key component of erosion triaxial test is the eroded soil collection system, the design of which should ensure the eroded soil grains are perfectly collected. Shwiyhat and Xiao (2010), Xiao and Shwiyhat (2012) studied the changes in soil hydraulic conductivity and soil volume induced by internal erosion, and the stress ~ strain relation of internally eroded soil. The base pedestal of the triaxial apparatus was modified to allow for collection of discharge effluent and the weight of eroded grains were determined by oven dry of the effluent (Fig.2.17). Similarly, Chang and Zhang (2011b, 2012) investigated the internal erosion potential of gap-graded sands subjected to multi-step seepage flow at complex stress state by a triaxial permeameter cell (Fig.2.18). The eroded soil grains were collected by a detachable container at regular intervals. Luo *et al.* (2013) implemented a revised system to conduct the seepage test under complex stress state. A low-angle and funnel-shaped screen was installed for smooth erosion of fines (Fig.2.19).

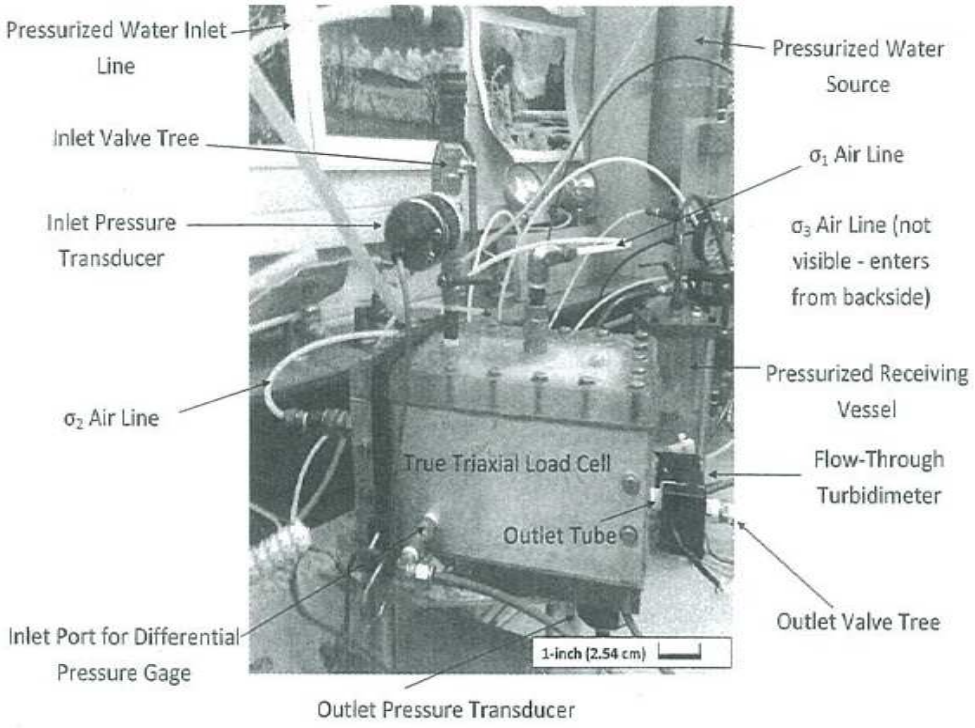

Figure 2.16 True triaxial cell (after Richards and Reddy, 2010)

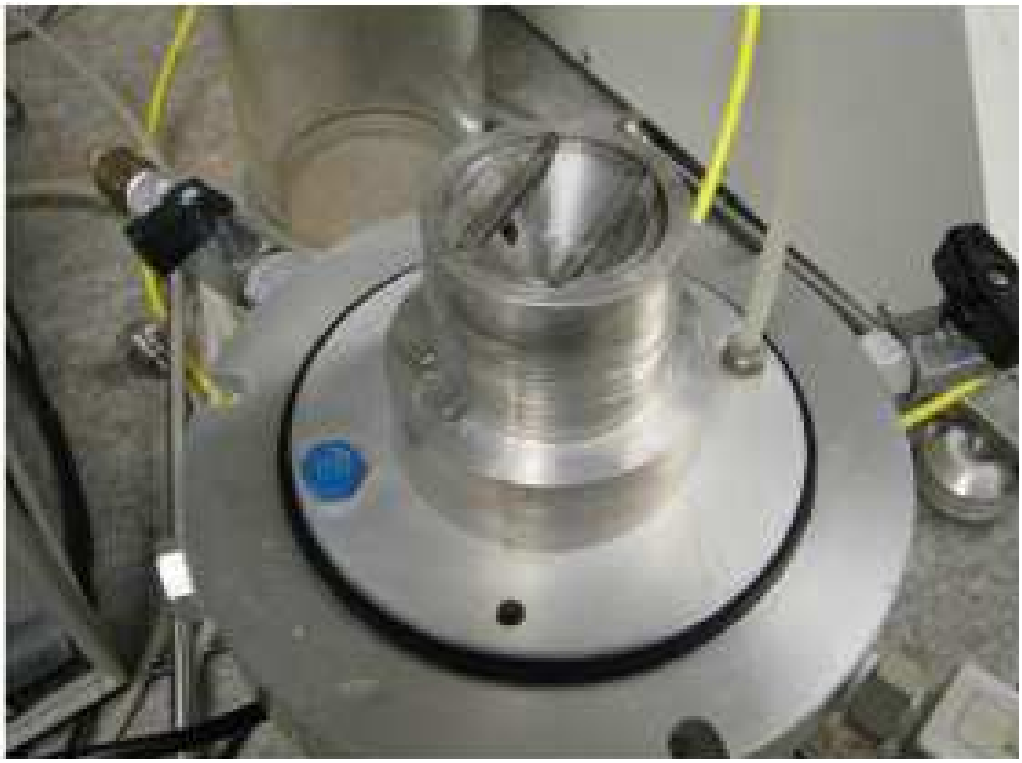

Figure 2.17 Photography of revised base pedestal (after Xiao and Shwiyhat, 2012)

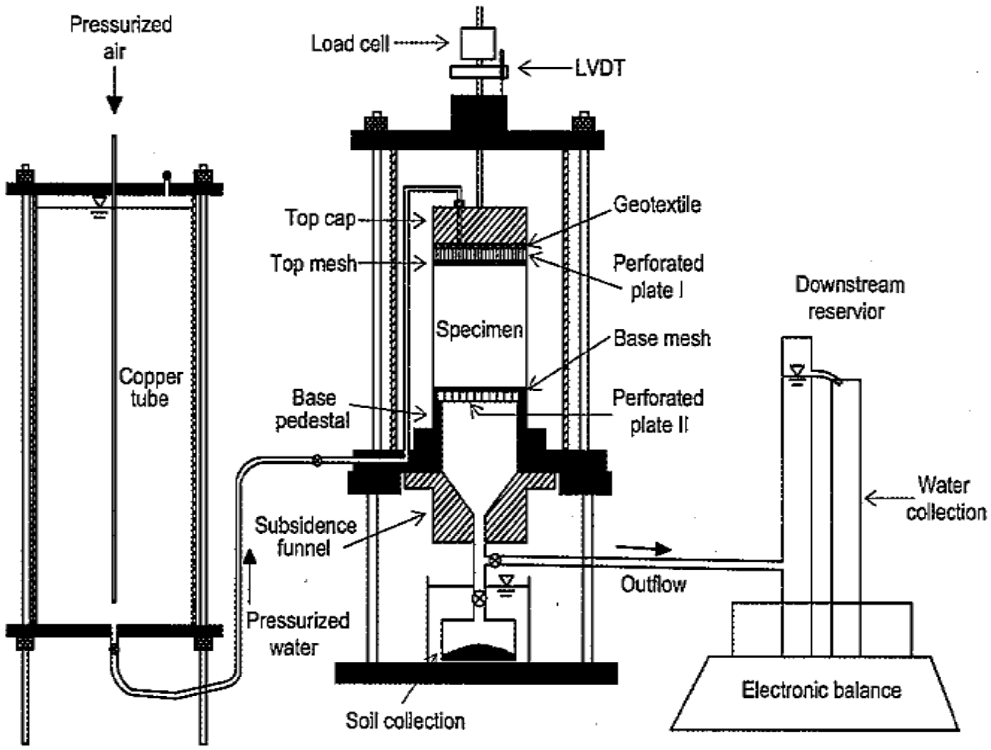

Figure 2.18 Apparatus details (after Chang and Zhang, 2011)

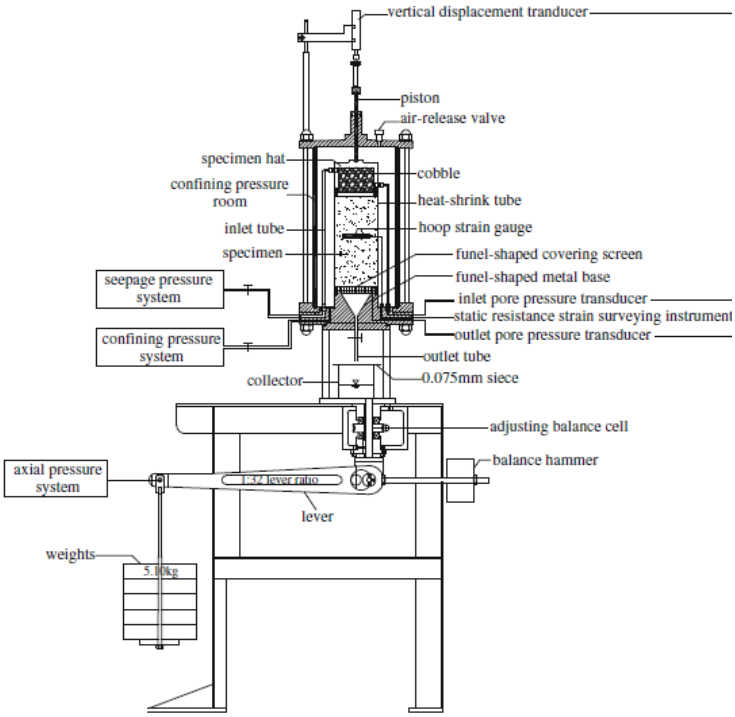

Figure 2.19 Schematic diagram of the apparatus (after Luo *et al.*, 2013)

2.1.4 Other internal erosion tests

For practical purpose, several other test methods had been proposed to assess the soil erosion potential. To measure erosion of soils in channels/canals, flume tests were developed (Arulanandan and Peery, 1983). Moore and Masch (1962) proposed Jet erosion test to evaluate erosion of soils in spillways for small dams and simulates back-cutting erosion with water plunging over a vertical face. Meanwhile, they studied the relationship between erosion rate and hydraulic shear stress and determined the critical shear stress at which erosion initiates by Rotating cylinder test. Briaud *et al.* (2001) predicted the scour rate in the tested soil by Erosion function apparatus. Emerson (1964) utilized soil dispersivity tests, *e.g.*, Pinhole, Emerson Crumb, Double hydrometer to measure dispersivity as a possible index to initiate erosion.

2.2 Mechanisms of internal erosion

The Initial foci of the internal erosion mechanism studies were to determine the characteristic size of the coarse grains and the fines, which would influence the constriction size, and hence the capacity for retention of base soil. The afterward experimental investigations introduced the “filter” concept for soil internal stability assessment and pinpointed the importance of optimizing the gain size distribution curve. Interpretation of laboratory seepage tests gave the threshold for the onset of soil internal instability at certain hydraulic conditions. Schuler (1995) concluded that the susceptibility of a soil to internal erosion (suffusion) greatly depends on the geometric of soil structure (e.g., soil grain size and distribution, pore size and distribution, grain shape and pore shape), hydraulic conditions (e.g., imposed hydraulic gradient, direction

of seepage flow, pore flow velocity and chemicals in the fluid) and mechanical properties of a soil (e.g., compaction degree, cohesion and effective stress). Following this summary, a critical review of the internal erosion mechanism will be presented here from the perspectives of geometric constraint, hydraulic constraint, progression of internal erosion, influence of soil properties and effects of stress state.

2.2.1 Geometric criteria

Terzaghi (1939) proposed the well-known retention criterion of $D_{15F} / d_{85B} \leq 4$ for Filter design, shown in Fig. 2.20. He assumed that D_{15F} characterized the pore size constriction of the filter while d_{85B} was the representative grain size of base soil. This criterion is the fundamentals for further geometric criteria research on soil internal stability. The "filter" concept was introduced whereby coarser fractions serve as a filter if water flows through. Whether or not the finer fractions would be potentially flushed off depends on the effective grain size ratio between the filter and fines. The ratio should not exceed an empirically derived threshold. The frequently used representative grain sizes are D_{15c}, D_{85c} of the coarse fraction, and d_{15f}, d_{85f} of the fines fraction in which migration of soil may occur. By extensive of experimental investigations, Kezdi (1969) confirmed the effectiveness of Terzaghi's retention criteria for soil internal stability assessment. A soil would be stable if the following equation is satisfied:

$$\frac{D_{15c}}{d_{85f}} < 4 < \frac{D_{15c}}{d_{15f}} \quad \text{……. (2.1)}$$

de Mello (1975) proposed similar soil internal stability criteria for gap-graded soil. Sherard *et al.* (1979) argued that sinkholes always occur at those dams consisting of cohesionless broadly graded soils and to avoid internal instability, the instability degree I_r ($I_r = D_{15c} / d_{85f}$) should be less than 5. The effective grain size ratio virtually represents the slope of a gradation curve which highlights the variation in grain size over a designated interval of the curve. Chapuis (1992) summarized the Sherard and Kezdi criteria for internal stability assessment of granular soils and unified the criteria to one parameter which is the grading curve slope value. Different methods propose different curve slope values. Similarly, after critically reviews, Schuler and Brauns (1993) concluded that the adaptation of those criteria should be based on the size

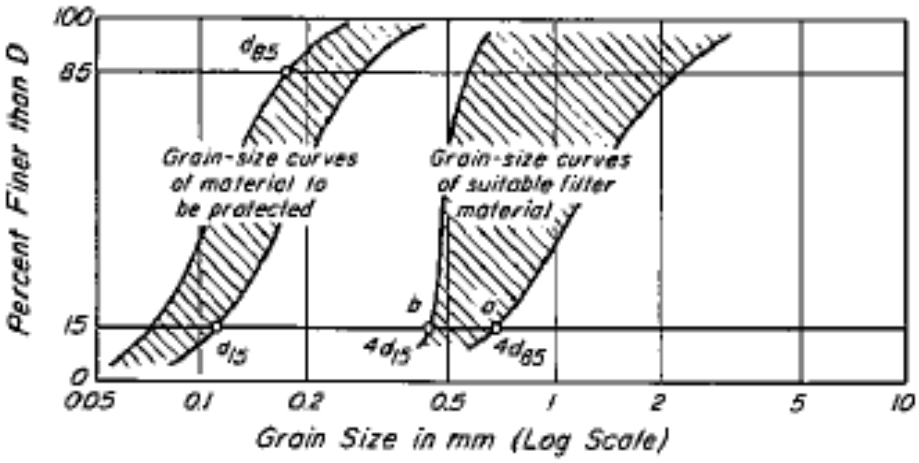

Figure 2.20 Retention criteria (after Terzaghi, 1939)

distribution curve characteristics. On the other hand, from the perspective of micromechanics, the effective grain size of coarse fractions acclaimed in those methods may represent the constriction size in soil. Terzaghi and Peck (1948) proposed $D_{15F}/4$ to quantify the constriction size in filter from which the soil retention criterion $D_{15F}/4<d_{85B}$ is derived. Similarly, Kezdi (1979) noted the value of $D_{15c}/4\sim D_{15c}/5$ can approximate the constriction size in the coarse fraction by assuming a contacting spheres packing of soil. Kenney and Lau (1985) inferred the predominant constriction size in the voids of a filter is approximately equal to the grain size of the soil making up the filter for which 25% by weight is finer.

U.S. Army Corps of Engineers (1953) and Istomina (1957) [ref. Kovacs (1981)] judged the soil erosion potential by soil uniformity coefficient (C_u). A value of 20 was designated as the threshold. Soil would be vulnerable to erosion if C_u is less than 20. Lubochkov (1962, 1965) argued that not all soil specimens satisfying $C_u \geq 20$ were vulnerable to erosion and inferred that a soil would not be susceptible to erosion if the slope of the grain size distribution curve was equal to or smaller than a given limit in each grain size interval.

Besides the assessment by single parameter, several empirical methods adopted multi-parameters to consider the influence of other factors. Kenney and Lau (1985) postulated that those soil grains finer than size d (having a weight fraction by percentage, F) will likely be eroded if there is not enough soil grains in the size range d to $4d$ (having a weight fraction by percentage, H). The narrowly-graded and widely-graded soils were evaluated separately. Burenkova (1993) reckoned that the internal stability of a soil depends on the conditional factors of uniformity, h' and h'' defined as: $h'' = d_{90} / d_{15}$, $h' = d_{90} / d_{60}$. On a plot of h' against $log\ (h'')$, the "suffusive soils" could be separated from "Non-suffusive soils" by defined boundaries. Mao (2005) introduced void ratio into the retention criteria for gap-graded soil and assumed that internal erosion would not occur if the fines are fully filled with the voids between coarse grains. For the broad-graded soil specimen, author recommended splitting the grading curve into two fractions: the coarse fraction and fine fraction. The splitting point corresponds to the characteristic grain size, (i.e., $1.3\sqrt{d_{15}d_{85}}$).

Recent efforts have been exerted to unify the various criteria to a simply comprehensive criterion. Schuler and Brauns (1993) critically assessed several available geometric criteria and concluded that de Mello (1975) and Sherard (1979) methods are suitable for gap-graded soils, whereas Kenney and Lau (1985, 1986) and Burenkova (1993) method worked appropriately for broadly-graded soils. Li and Fannin (2008) compared Kezdi and Kenney criteria and concluded that the two criteria are similar in terms of quantifying the slope of grain size distribution curve over a defined interval, but different in the determination of the interval. Both criteria converge to give the same index value at $F=15\%$. Kezdi criterion is proved to be effective in predicting gap-graded soils while Kenney criterion is more successful in the evaluation of widely graded soils. On the basis of Istomina's criteria, Kezdi's criteria, and Kenney and Lau's criteria, Chang and Zhang (2013) comprehensively investigated the internal stability of soils with fines content and proposed a new combined method for assessment purpose.

Most of these proposed criteria are based on the analysis of the grain size distributions. Although validated by experimental tests, they were empirical criteria: confidence in their applicability to other soils depends on the similarity of those soils with the ones used in those tests. A detailed summary of the selected geometric criteria is shown in Table 2.1.

2.2.2 Hydraulic constraint

The onset of internal erosion is generally described by three distinct approaches: critical hydraulic gradient, critical flow velocity and critical hydraulic shear stress.

Initially, it is believed that the onset of internal erosion would occur as long as the critical hydraulic gradient is reached. Terzaghi (1943) initially reported the influence of effective stress on seepage failure. By assigning upward seepage flow on a sand column, the phenomenon of "heaving" was observed when certain critical hydraulic gradient was reached, at which the effective stress diminished into zero. A well-known equation of evaluating the critical hydraulic gradient i_c is proposed:

$$i_c = (G_s - 1)/(1 + e) \quad \ldots\ldots\ldots \quad (2.2)$$

However, this critical hydraulic gradient does not always coincide with experimental research. Tanaka and Toyokuni (1991) conducted seepage tests in a sand column, which showed that the critical hydraulic gradient may be different from the above theoretical value depending on the soil geometric properties (i.e., grain size distribution) and stress level. In terms of internal erosion, Skempton and Brogan (1994) argued that the "segregation piping" occurs at the hydraulic gradient about one-third to one-fifth of the Terzaghi's critical gradient for a homogeneous granular soil and attributed the reason to the uneven distribution of effective stress in the coarse grains and fines. They assumed that in an internally unstable soil, the primary fabric probably carried most of the stress while the fines were relatively free. A reduction factor had been inserted into Equation (2.2) for correction. Monnet (1998) [ref. Bonelli (2012)] explored the critical hydraulic gradient for internal erosion by the representative grain size and suggested that the reduction factor depended on grain size and hydraulic conductivity. Recently, the significance of stress state on the critical hydraulic gradient has been discussed. Moffat and Fannin (2011) postulated that there was a hydromechanical path in stress and hydraulic gradient space. The curve begins from origin and terminates at the critical hydraulic gradient given by Terzaghi. It is regarded as the hydromechanical boundary governing the onset of seepage-induced internal instability. Li and Fannin (2012) further elaborated the theoretical hydromechanical envelope in effective stress and hydraulic gradient space for upward seepage tests. In their approach, the envelope considered both the critical hydraulic gradient of intriguing internal erosion and stability. The two critical lines are defined correspondingly, which are critical line for internal erosion and critical line for stability. The selected equations for critical hydraulic gradient assessment are summarized in Table 2.2.

Table 2.1 Selected geometric criteria for soil stability assessment

Criteria	Applicable soil	The mixture is internally stable if	Comment
U.S. Army (1953)	Gravels	$C_u < 20$	
Lubochkov (1965) [refer Kovacs (1981)]	All soils	$(\Delta S_1/\Delta S_2)/4 \le 1$ [(1)] ($d_{n-1}/d_n = d_n/d_{n+1} = 10$); $(\Delta S_1/\Delta S_2)/2.6 \le 1$ ($d_{n-1}/d_n = d_n/d_{n+1} = 5$); $(\Delta S_1/\Delta S_2)/1.7 \le 1$ ($d_{n-1}/d_n = d_n/d_{n+1} = 2.5$);	
Istomina (1957) [refer Kovacs (1981)]	Sand-gravels	$C_u \le 20$	
de Mello (1975)	Gap-graded soils	$(D_{15c}/d_{85f})_{\text{at gap}} < 5$	
Kezdi (1979)	All soils	$(D_{15c}/d_{85f})_{\max} \le 4$	
Sherard (1979)	Broadly graded soils	$(D_{15c}/d_{85f})_{\text{at gap}} < 5$	
Kenney and Lau (1985, 1986)	Gravels	$(H/F)_{\min} \ge 1$ ($0 < F < 0.2$)[(2)]	Medium to dense soils
Burenkova (1993)	Sand-gravels	$0.76log(h'')+1<h'<1.86log(h'')+1$[(3)]	
Schuler and Brauns (1993)	All soils	$(D_{15c}/d_{85f})_{\text{at gap}} < 5$ (Gap-graded soils); Kenney and Lau (1985, 1986) or Burenkova (1993) method (broadly-graded soils with a tail of fines)	Combined method
Mao (2005)	Gravels	$4P_f(1-n) \ge 1$[(4)]	Soil porosity is considered
Wan and Fell (2008)	Broadly-graded soils	$30/\log(d_{90}/d_{60}) < 80$ and $15/\log(d_{20}/d_5) > 22$	
Li and Fannin (2008)	Granular soils	$(H/F)_{min} \ge 1$ ($F < 15$) $H \ge 15$ ($F > 15$)	Combined method
Chang and Zhang (2013)	Well-graded soils	$(H/F)_{min} > 10$ ($FC < 5$); $(H/F)_{min} > -(1/15)FC + 4/3$ ($5 \leqq FC \leqq 20$)*; or $FC > 20$	*for low plastic soils
Chang and Zhang (2013)	Gap-graded soils	$G_r < 3$ ($FC < 10$)[(5)]; $G_r < 0.3FC$ ($10 \leqq FC \leqq 35$)*; or $FC > 35$	*for medium plastic soils

Note:

(1) $\Delta S_1 = S_{n-1} - S_n$ is the percentage in weight for the soil with grain size between d_{n-1} and d_n; $\Delta S_2 = S_n - S_{n+1}$ is the percentage in weight for the soil with grain size

between d_n and d_{n+1};

(2) F is the weight fraction of the soil finer than size d; H is the weight fraction of the soil in the size ranging from d to $4d$;

(3) $h'=d_{90}/d_{60}$, $h''=d_{90}/d_{15}$;

(4) P_f is the fines content by weight in soil (for gap-graded soils, P_f =percentage of mass passing at gap; for well-graded soils, P_f =percentage of mass passing at a division diameter of $d_f = 1.3\sqrt{d_{15}d_{85}}$), n is the porosity;

(5) G_r is the gap ratio, defined as the ratio of d_{max} to d_{min}.

Table 2.2 Selected assessment of critical hydraulic gradient

Assessment criteria	Expressions
Terzaghi (1943)	$i_c = \frac{G_s - 1}{1+e}$
Skempton and Brogan (1994)	$i_s = \alpha \frac{G_s - 1}{1+e}$ (1)
Monnet (1998) [refer Bonelli (2012)]	$i_s = 0.01 \frac{(d_{15})^2}{k} i_c$
Li and Fannin (2012)	$i_s = \frac{\alpha}{1-0.5\alpha}[\overline{\sigma'}_{vm} + \frac{0.5(G_s-1)}{1+e}]$ (2)

Note:

(1) α is the stress reduction factor, indicating the stress distribution between coarse grains and fines;

(2) $\overline{\sigma'}_{vm}$ indicates the initial effective axial stress.

The coupling phenomenon that the porosity of soils changes if seepage flow is imposed to flow through, which again influences the critical hydraulic gradient, triggered the studies on the alternative parameters to describe the onset of internal erosion. Daniel (1994) summarized that the seepage test by constant-flow-rate control had several advantages comparing to the test by constant-head. Richards and Reddy (2010, 2012) concluded that outweighing the hydraulic gradient, seepage velocity is a better indicative parameter for the onset of internal erosion, termed “critical seepage velocity”. Laboratory tests on several soil mixtures have confirmed that the critical seepage velocity is constantly within the range of 0.6 ~ 1.2cm/s. From element level, Perzlmaier (2007) recommended the usage of average pore velocity, which is the ratio of the Darcy velocity to the porosity corrected by the tortuosity. As a consequence, the critical pore velocity is closely related with the grain size. He predicted a critical velocity of approximate 0.1 cm/s for the size of soil grains less than 0.1mm.

Mainly for cohesive soils, a concept of “critical shear stress, τ_c”, defined as the stress required to initiate erosion by seepage flow, is proposed. Several experimental investigations have been performed to empirically estimate the critical shear stress by several parameters, such as plasticity index, dispersion ratio (ratio of the total mass of silt and clay sized aggregates to the total mass of silt and clay sized grains), grain size and percentage of clay content (Smerdon and Beaseley, 1961; Arulanandan and Perry, 1983; Mitchener and Torfs, 1996; Julian and Torres, 2006; Thoman and Niezgoda, 2008;

among others). The implementation of the "critical shear stress" in the internal erosion study is realized by assuming that the internal structure of a soil is comparable to a network of parallel capillary tubes with constant radius (Khilar *et al.*, 1985). Reddi *et al.* (2000) developed an expression of the hydraulic shear stress:

$$\tau = 1.414\left(\frac{\Delta P}{\Delta L}\right)\sqrt{\frac{K}{n}} \quad \text{..... (2.3)}$$

Where $\Delta P/\Delta L$ is the average pressure gradient (kN/m^3). As long as the hydraulic shear stress reaches the critical shear stress, internal erosion initiates. This evaluation process is mostly used in the surface erosion study (e.g., Hanson and Simon, 2001).

Attractive though those approaches are, difficulties still exist when it comes to identify the onset of internal erosion in experiment. No widely recognized rules have been established. Hitherto, mainly three criteria are implemented. By intuition, the direct way is the detection of fines loss during soil erosion test (Lafleur, 1984; Kenney and Lau, 1985; Moffat and Fannin, 2006; Bendahmane *et al.*, 2008; Xiao and Shwiyhat, 2012; among others). The seepage flow is usually in the downward direction, convenient for the collection of eroded fines. Some other researches adopt the criteria of visual observation, especially for upward seepage flow test (Sterpi, 2003; Wan, 2006). They regard the observed movement of fines as the indication of the initiation of internal erosion. Also, onset of internal erosion could be recognized by the changes in hydraulic properties (i.e., hydraulic gradient or hydraulic conductivity) during seepage test. Due to the erosion of fines, the hydraulic properties of a soil would alter correspondingly, which might be a reliable indicator. This criterion has been adopted by several researches (Sun, 1989; Skempton and Brogan, 1994; Tomlinson and Vaid, 2000; Cividini *et al.*, 2009; Luo *et al.*, 2013; among others).

2.2.3 Progression of internal erosion

As long as internal erosion initiates, the hydraulic properties of soils (such as hydraulic gradient, hydraulic conductivity) will alter accordingly. Typical hydraulic gradient and Darcy velocity relation during seepage test for internally unstable soil is shown in Fig. 2.21 together with that relation for pure sand (Skempton and Brogan, 1994). Both of the soils will reach the state of zero effective stress indicated by the occurrence of the "heaving" phenomenon when the imposed hydraulic gradient is large enough to be equal to or higher than Terzaghi's critical hydraulic gradient. However, significance difference could be observed before the "heaving". For pure sand, there is an approximate linear relationship between the hydraulic gradient and the Darcy velocity, in accordance with Darcy's law, which indicates no occurrence of internal erosion. The effective porosity, representing the porosity available for contribution to the fluid flowing through the specimens, stays basically the same irrespective of the hydraulic gradient. Contrastively, the internal unstable soil shows a non-linear relation between hydraulic gradient and Darcy velocity as soon as the critical hydraulic gradient for internal erosion is reached, which triggers the onset of internal erosion. Since fines are constantly dislodged by the seepage flow, leading to the increase in effective porosity, and thus, Darcy velocity, the increment of the Darcy velocity is greatly accelerated with the progress of internal erosion. The hydraulic conductivity is increasing all the way until "heaving" occurs. Similar behavior could be observed at the erosion test controlled

by the constant flow rate, shown in Fig.2.22 (Richards and Reddy, 2012). The dark solid line indicates the inlet pressure while the dark dash line stands for the outlet pressure. The backwards erosion in their research indicates the movement of sand grains, which is similar to the "heaving" phenomenon while suffusion means the erosion of fines. As is observed, for the uniform sand, the water pressure keeps approximately constant before the onset of backwards erosion (piping of sand grains), after which water pressure suddenly drop to a minimum value of 5kPa, indicating the complete destroy of the soil specimen. However, the internally unstable soil mixtures experience a gradual drop in water pressure before backwards erosion, which indicates a gradual decrease in hydraulic gradient with the progress of internal erosion. By Darcy's law, the hydraulic conductivity increases as a consequence of soil internal erosion (suffusion). Further division of the erosion stage has been proposed by Chang and Zhang (2012). They argued that no critical changes in soil properties as soon as internal erosion initiates and a hydraulic gradient, named "skeleton-deformation hydraulic gradient", exists, which is indicated by the sudden increases in hydraulic conductivity and soil deformation.

The direct consequence of internal erosion is the erosion of fines with time, which is regarded as the most significant parameter in soil erosion study, which is commonly termed as "Erosion law". In literature, this law greatly depends on the imposed hydraulic boundary conditions (i.e., constant hydraulic gradient, incremental hydraulic gradient or constant flow rate). Therefore, in practice, the feasibility of the laboratory results depends on the similarity of the hydraulic boundary conditions applied. A representative evolution of cumulative eroded soil mass with time during erosion test by constant hydraulic gradient control is shown in Fig. 2.23 (Sterpi, 2003). The cumulative eroded soil mass will increase with the progress of erosion till a constant value is reached finally. The erosion rate is the largest at the initial and then gradually decreases with time. Larger imposed hydraulic gradient would cause more erosion of soil grains.

Due to the erosion of fines, soil would deform correspondingly. Due to the nature of upward flow seepage test, an accurate measurement of soil deformation is difficult to achieve. Most of the available results are obtained from the downwards flow seepage test, in terms of surface displacement (Tomlinson and Vaid, 2000; Moffat *et al.*, 2011) or volumetric strain (Shwiyhat and Xiao, 2010; Xiao and Shwiyhat, 2012; Chang and Zhang, 2011b). Those researches mostly indicate a contractive soil behavior during erosion test because of the loss of soil grains. A typical deformation pattern is shown in Fig. 2.24, which shows that the erosion induced deformation seems to be sudden and rapid. Meanwhile, the void ratio of the tested specimen might change as a consequence. To quantitatively assess the evolution of void ratio during erosion, Scholtès *et al.* (2010) assumed that void ratio changes following a two-stage pattern. The void ratio is firstly derived solely by the loss of fines and then corrected by the volumetric deformation. They argued that the contraction of soil during erosion test may delay the increase of void ratio while dilation will accelerate it.

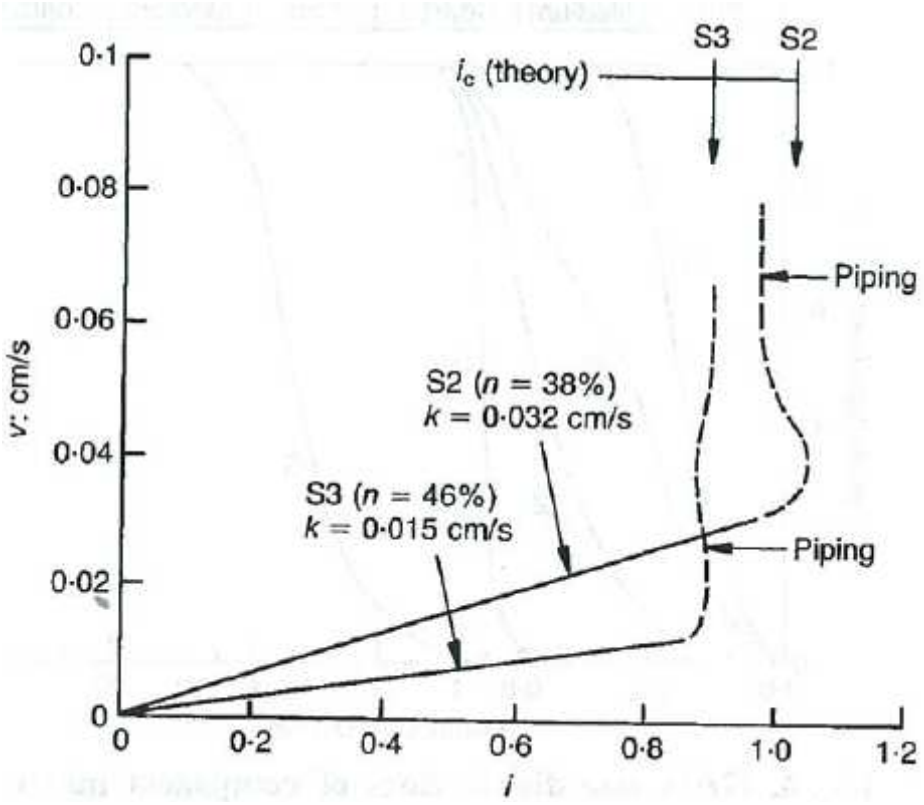

(a) Piping test on pure sand

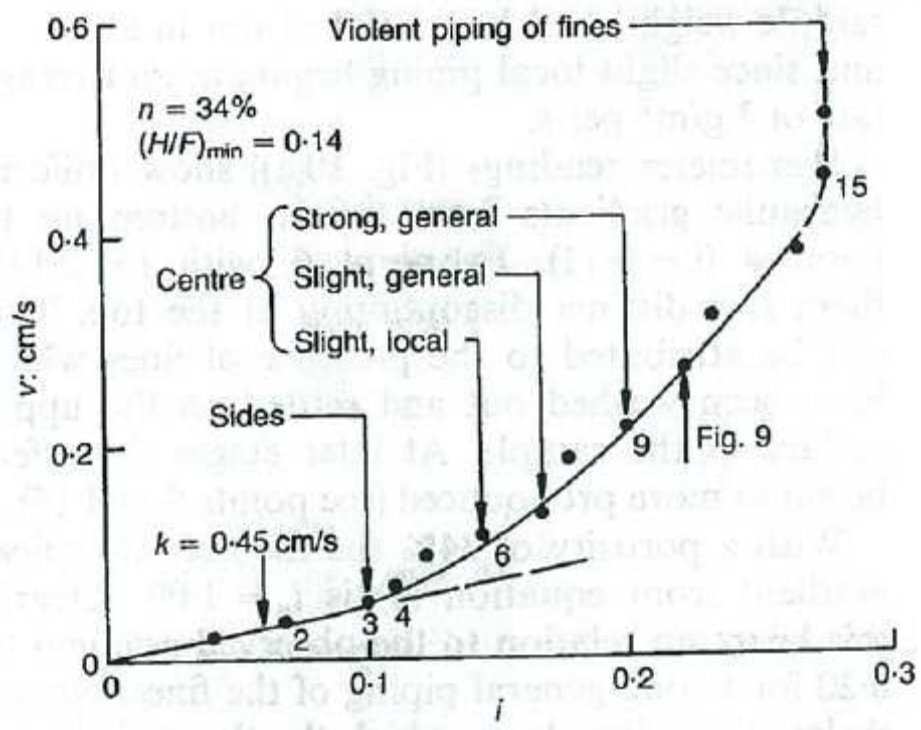

(b) Piping test on internally unstable soil

Figure 2.21 Typical hydraulic gradient and Darcy velocity relation for (a) pure sands and (b) internally unstable soil (after Skempton and Brogan, 1994)

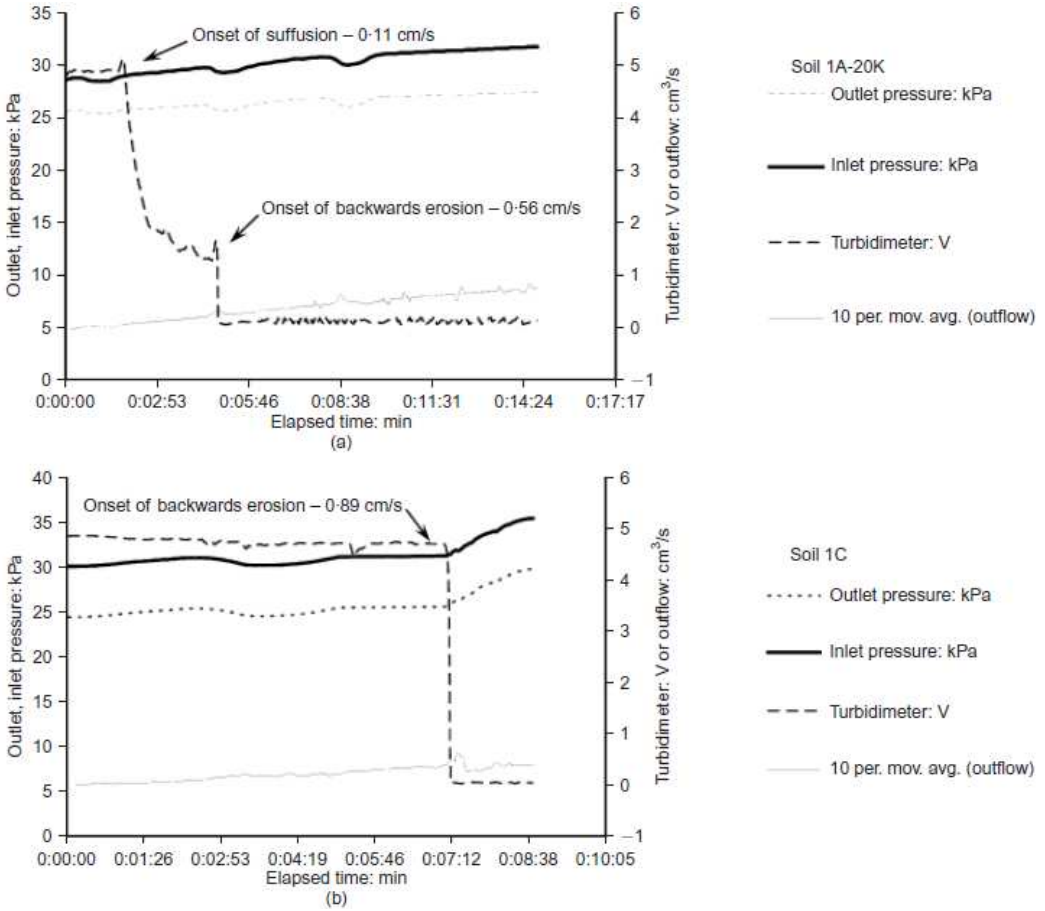

Figure 2.22 Evolution of outlet, inlet pressure during erosion: (a) internally unstable soil mixtures; (b) uniform sand (after Richards and Reddy, 2012)

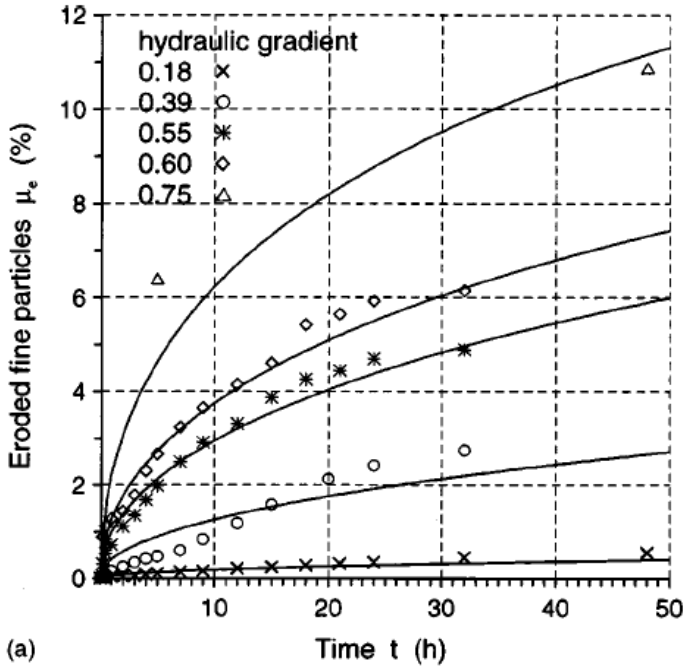

Figure 2.23 Evolution of cumulative eroded soil mass with time (after Sterpi, 2003)

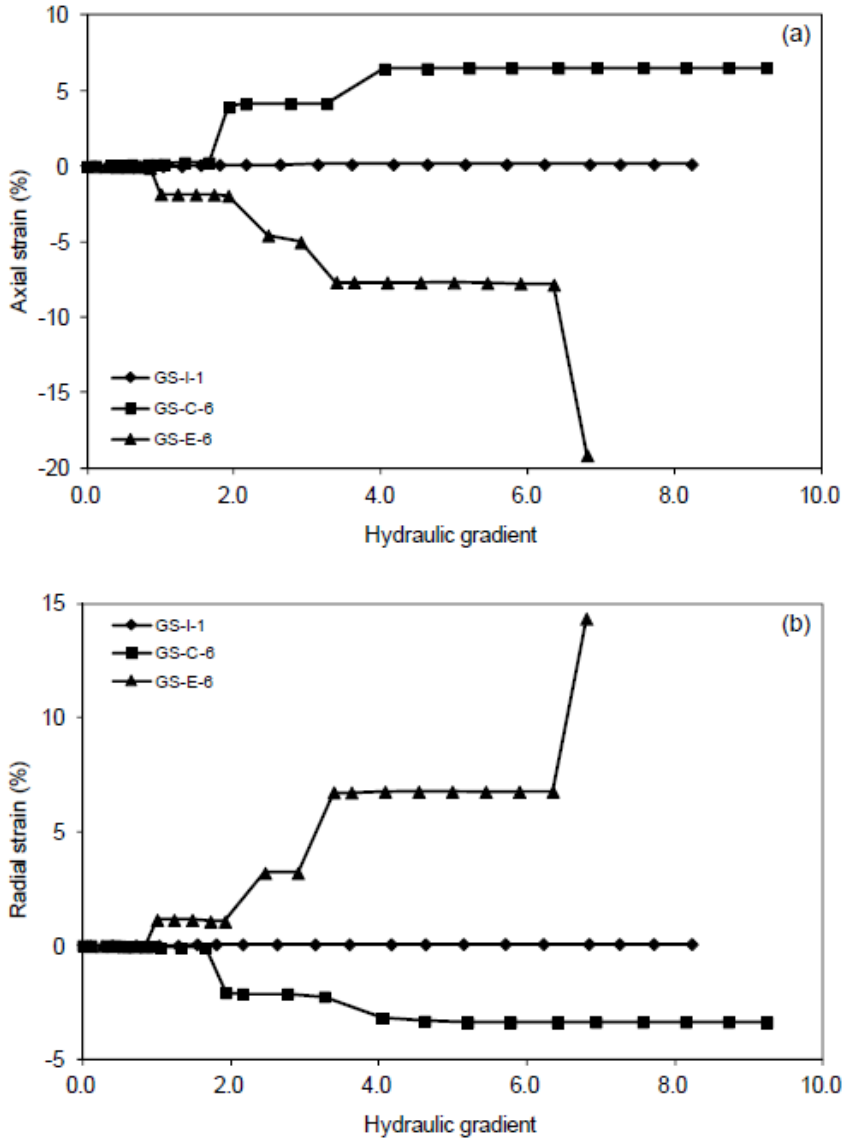

Figure 2.24 Internal erosion induced soil deformation (after Chang and Zhang, 2012)

As a consequence of internal erosion, the post-erosion grain size distribution curve would move downward from the original position due to the loss of fines. The standard assessment of the grain grading curves of different layers of soil is usually conducted. Kenney and Lau (1985) proposed a graphical method for approximate assessment of the fraction of eroded fine grains, as well as the largest eroded fine grains, based on the changes in the grain grading curve. The main idea is to extend the initial grain size distribution curve to match the curve after internal erosion. Since the coarse grains stay the same irrespective of internal erosion, by extending the vertical scale of the initial grain size distribution curve, the coarse part of the initial curve should match that of the post-erosion grain size distribution curve. The fraction of eroded fines can be calculated from the amount of movement of the initial grain size distribution curve. This method has been proven to be effective (Wan, 2006; Zhang, 2007).

2.2.4 Influence of soil properties

Internal erosion is the consequence of seepage fluid flowing through the pores of soils. Therefore, those characteristic parameters affecting the fluid and solid phase (i.e., chemicals of fluid, soil geometry) determine the initiation and development of internal erosion. This session will mainly discuss the influential factors related with soil geometry, including grain size distribution and grain shape. The dislodgement of fines through the pore network of a soil requires a sufficient pore size, which is commonly derived by the grain size distribution curve. Terzaghi (1943) proposed the use of $D_{15}/4$ to quantify the opening voids size which leads to the empirical-based filter design criterion. Effects also have been taken to detect the susceptibility of a soil to erosion by the classification of grain size distribution curves. Lafleur (1984) designated an acceptable range for the grading curves of filters. Test results of Lafleur *et al.* (1989) and, Foster and Fell (2001) suggested that among the soil specimens with various grading curves tested, widely-graded soils with tailing of fines and gap-graded soil might be susceptible to internal erosion.

The influence of grain shape on internal erosion is through its effect on pore size. The classic capillary tube soil model proposed by Kovacs (1981) includes a shape coefficient to calculate the tube diameter. This coefficient of angular soil grains is larger than that of spherical grains, which results in a smaller size of pore diameter and consequently, inhibits the soil erosion. Experimental investigations by Marot *et al.* (2012) proved this tendency: loss of fines is larger for the soil mixtures with round grains, such as glass beads.

2.2.5 Effects of stress state

Here the significance of stress state should be stressed. As is universally recognized, the behavior of soil is highly influenced by its stress state. However, hitherto, the effect of stress state on erosion mechanism is obscure and controversial. Sanchez *et al.* (1983) concluded that varying compacted density had little influence on erosion potential for silty materials. Whereas erosion rate of clay mixture would increase as the compacted density decreased. Wan and Fell (2004b) noted that the degree of compaction had a minor effect on the erosion rate of silty and cohesive natural soils comparing to the water content and hence, degree of saturation. Some researchers reckon that, oppositely, stress state exerts large influence on properties of internal erosion. Chang and Zhang (2012) conducted seepage tests at isotropic stress state, compression stress state and extension stress state to simulate the soil state at various locations of a dam. The maximum erosion of fines was detected in the extension stress state. Richards and Reddy (2010) found the major principal stress exerts more influence on the piping potential than the minor principal stress.

The magnitude of confining pressure shall affect the soil hydraulic behavior as well. At the higher confining pressure, the fines are expected to be densely packed among coarse grains and the interstitial spaces may be narrower. In the soil specimens with the higher confining pressure, the seepage flow might dislodge fewer fines. However, the force

transfer mechanism of granular material is much more complex. Due to the boundary frictions, force-arching may develop at the intersections of the bottom boundary, which may hold the fines from erosion. At the higher confining pressure, it is possible that the force-arching is failed, which, instead, might cause further erosion of fines (Tomlinson and Vaid, 2000). This tendency is especially obvious for the soil specimen with small grain size ratio (D'_{15}/ d'_{85}). Bendahmane *et al.* (2008) showed that for cohesiveless soil, the erosion rate tends to increase with the rising of confining pressure. They assumed the existence of a secondary critical gradient. If the assigned hydraulic gradient is below this value, the confining pressure tends to increase the soil resistance to suffusion while larger than this value, backward erosion begins. Moffat *et al.* (2011) and, Moffat and Fannin (2011) noted that an increase in effective confining pressure would cause an increase in the critical hydraulic gradient for erosion. Correspondingly, Li and Fannin (2011) proposed a failure envelope in stress ~ hydraulic gradient space, indicating that a decrease in effective confining pressure may result in a lower critical hydraulic gradient.

2.3 Analytical models for internal erosion assessment

Great efforts have been exerted to develop mathematical models to predict the hydro-behavior of internally unstable soils under seepage flow. Generally, the models could be classified into two categories: the limit equilibrium analysis of individual grains in a pore channel at element level and soil/fluid transportation in continuum media.

2.3.1 Limit equilibrium analysis

The approach of limit equilibrium analysis is to establish the force equilibrium relation of a movable soil grain by considering the hydraulic conditions. The fundamental approach assumes that the pores among coarse fractions are interconnected and develop into an array of parallel capillary tubes with identical diameter, as is shown in Fig. 2.25. This diameter represents the constriction size of a soil specimen. Kovacs (1981) gave the following expression to calculate the diameter:

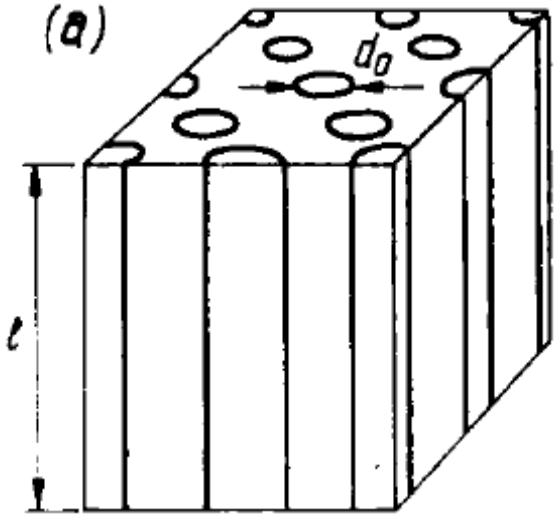

Figure 2.25 Assumed capillary tubes (after Kovacs, 1981)

$$d_0 = 4\frac{n_c}{1-n_c}\cdot\frac{D_h^c}{\alpha_D} \quad \text{……. (2.4)}$$

In this approach, the diameter of the tubes is the key parameter governing the filtration mechanism. If an erodible soil grain would pass through a filter, the size of the grain should be smaller than that of the tube. The accuracy of the calculation depends on the details of force equilibrium analysis of an individual grain. Usually, the hydrodynamic forces are generated by the imposed hydraulic gradient and resistance force is produced by contact friction between soil grains (Wu, 1980; Indraratna and Vafai, 1997; Indraratna and Radampola, 2002; Liu, 2003; Srivastava and Sivakumar Babu, 2011). Mainly an expression of critical hydraulic gradient would be derived.

Thanks to the advances in computer science, theoretical assessment of constriction size could be approached in detail. Reboul *et al.* (2010) summarized the method of evaluating the constriction size distributions of a numerical assembly of spheres which were generated by Discrete Element Method (DEM). The measurement of the void geometry was fulfilled by a radical Delaunay tessellation. Since high computational expense is necessary for such evaluation, a simple probabilistic based alternative is commonly used. Silveira (1965) assessed the soil filtration/retention by analyzing cumulative constriction size distribution (CSD) which was derived from grain size distribution with assumptions of geometric packing. It examines the probability of a soil grain with equivalent size could would go through a probable path in a granular medium, which depends on the constriction sizes of the voids and their occurrences within the filter. This concept has been widely applied in the filtration study (Locke *et al.*, 2001, 2002; Indraratna *et al.*, 2006, 2007; Scheuermann *et al.*, 2010; Sjan and Vincens, 2012; Moraci *et al.*, 2012; among others). In this approach, the possibilities of soil transportation in a granular medium depend both on the constriction size and the positions of the openings in filter. Accordingly, cumulative Void Size Distribution (VSD) was proposed to characterize the possibility of the occurrence of certain opening sizes. It is obtained by enumerating all possible combinations of soil grains with various equivalent diameters, which is derived from the discretized Grain Size Distribution in a regular interval. Then, the movement of the fines through a series of soil layers could be simulated by estimating the probability that a fine grain transverse *m* unit soil layers or by directly comparing the size of each fine grain in the *i* layer with that of constrictions of the next *i+1* layer.

2.3.2 Soil/fluid transportation in continuous media

The soil/fluid transportation in continuous media rest upon a three-phase mixture theory: skeleton solids, fluidized solids and fluid. For each phase, mass balance equations are formulated, complemented by an expression for the rate of soil erosion, namely, “erosion law” or “constitutive law of erosion”.

Intuitively, the direct way is to derive the erosion law from erosion test. Sterpi (2003) obtained an empirical law by conducting an upward seepage flow test. The percentage of cumulative eroded soil mass is expressed as a function of time and imposed hydraulic gradient. By curve-fitting, the parameters in the expressions could be determined. One

advantage of this method is that it is not necessary to consider the phenomena of clogging and grain redeposition, which has already accounted for in the experimental results. Afterwards, Cividini and Gioda (2004), and Cividini *et al.* (2009) adopted this erosion law to analyze the ground settlement in Milan City induced by underground erosion. Ichiyama (2011) studied the influence of internal erosion on the stability of earthen dam using this erosion law.

Vardoulakis *et al.* (1996, 2001, 2004a, 2004b) proposed three theoretical constitutive laws: fluidized grains model, filtration law and porosity diffusion model. The first model is empirically derived from extensive experimental tests of filtration. This law considered that the rate of eroded mass is proportional to discharge mass of fluidized grains by a coefficient. The filtration law is developed based on the assumption that the gradient of solid concentration is proportional to the concentration. The porosity diffusion model considered that the erosion of solids would cause the increase of porosity and therefore, the discharge rate is proportional to the porosity gradient. A potential assumption of those approaches is that the hydrodynamic forces generated by seepage flow are large enough to be able to fully dislodge all the free fines that are likely to be transported. That is to say, clogging or grain redeposition is not taken into consideration. Those laws have been adopted by others to study the problem of sand production from wells in the oil industry as an erosion phenomenon (Stavropoulou *et al.*, 1998; Papamichos *et al.*, 2001, 2005; Wan and Wang, 2004; Wang and Wan, 2004).

The concept of “critical shear stress”, which is commonly used in surface erosion, has been adopted by some researchers as the erosion law to study the internal erosion (Bonelli *et al.*, 2006, 2008; Fujisawa *et al.*, 2010). Those studies potentially postulate that the constrictions among coarse grains form an array of parallel capillary tubes along the direction of seepage flow and soil aggregate with unit mass will be dislodged from the internal surface of the tubes if the hydraulic shear stress is large enough. The hydraulic shear stress is obtained by Reddi’s expression. As long as the hydraulic shear stress reaches the critical shear stress, internal erosion initiates. This erosion law is commonly applicable to clay mixtures.

2.4 Mechanical consequences of internal erosion

For the non-cohesive soils, due to the large amounts of loss in fines, internal erosion may render a loose soil structure with increased porosity and hydraulic conductivity. The coarse grain may rearrange their inter-position into a new equilibrium and consequently, soil fabric might be altered. The stress ~ strain relationship of the internally eroded soil might be greatly changed comparing to the original soil specimen. There is a high possibility that the strength of the post-erosion soil may decrease due to the destructive function of erosion. It would be a huge threat for the existing earthen structure which has been suffering from years of internal erosion. But, unfortunately, few studies could deliver comprehensive investigations about the consequences of erosion from the perspective of soil mechanics in the literature. The mechanical consequences of internal erosion will be summarized from the perspective of experimental investigations and theoretical approaches.

2.4.1 Experimental investigations

Chang and Zhang (2011b) conducted drained monotonic compression test on a series of eroded soil specimens, on which seepage tests at various stress state have been performed. It is found that the stress ~ strain relationship of the tested soil specimen will alter from dilative behavior to contractive behavior after the loss of a significant amounts of fines. The drained soil strength decreases after the erosion. Undrained monotonic compression tests on internally eroded soil have been conducted by Xiao and Shwiyhat (2012). They found that the peak deviator stress of eroded soil is larger than the soil without erosion, which may be attributed to the low degree of saturation. However, Chang and Meidani (2012) performed undrained monotonic compression tests on internally eroded soil specimens and detected a distinct mechanical response of the eroded soil specimens from Xiao and Shwiyhat (2012). They classified the eroded soil behavior into two categories according to the confining pressure when erosion tests are conducted. For the soil specimens suffered erosion under low confining pressure, the post-erosion void ratio is on the dense side of the CSL (Critical State Line), indicating a dilative response. By contrast, those specimens which are eroded under high confining pressure show much contractive response with a lower undrained strength.

In sum, the quality of those strength tests on the eroded soil specimen might be not so high because of the low saturation degree. Xiao and Shwiyhat (2012) found that the B-value of the eroded soil specimen immediately after the erosion test is approximately 0.86. Since undrained response of soil specimens is quite sensitive to saturation degree, the undrained stress ~ strain relationship might not reflect the true the soil mechanical response, which might be an explanation of the conflicting test results. Therefore, a higher saturation degree is necessary to guarantee the quality of compression test on those eroded soil specimens. Also, the mechanical properties of the mixtures should be stressed including the mechanical behavior of the coarse fraction and fine fraction. Since a direct consequence of soil erosion is the loss of fines, therefore, an investigation of the mechanical influence of fines might be helpful to understand the response of the internally eroded soil specimens.

2.4.2 Theoretical approach

The occurrence of sinkholes in the WAC Bennett Dam in British Columbia in 1996 led Muir Wood (2006, 2007) to investigate the mechanical consequence of fine particle erosion. Based on a new parameter, namely “grading state index”, Muir Wood *et al.* (2008, 2010) modelled the mechanical consequences of internal erosion by two-dimensional discrete element analysis. In their approach, the progress of erosion was approximated by progressively removing grains from assemblies of circular discs at different stages of shearing. Several assumptions of post-erosion void ratio, changes of positions of CSL in the $e \sim logp'$ space have been proposed. The modelling indicated that the erosion could trigger the soil state change from “dense” (below CSL) to “loose” (above CSL). Similarly, Scholtès *et al.* (2010) adopted a discrete element model and an analytical micromechanical model to simulate the mechanical response of eroded soil. They noticed that the soil behaviour changed from a dilatant to a contractant when extracting the fine grains. Those zones in the soil structure where internal erosion occurs

would be more prone to fail. Hicher (2013) modelled the effects of particle removal on the behavior of granular materials and concluded that removal of soil particles may cause diffuse failure in eroded soil mass.

2.5 Summary

The phenomenon of internal erosion could be understood from four aspects: experimental investigation, mechanisms of internal erosion, analytical models and mechanical consequences.

Mainly, the experimental investigations are performed to evaluate the soil stability. Specific permeameters are designed for various purposes. The flow rate, percentage of fines loss, hydraulic conductivity change and volumetric deformation are the prime concern. Through those experiments, a series of empirical criteria for internal stability assessment had been proposed. Effective though those empirical criteria are in the experimental validation, those empirical criteria might be not applicable to the common cases. The reliability of the criteria depends on the similarity of the soil to the one tested in the laboratory. Due to the differences in the hydraulic boundary conditions, there is no universally accepted summary to describe the mechanisms of internal erosion. Understanding of the hydraulic behavior of tested soil should take the imposed hydraulic conditions into consideration.

Analytical models, derived from limit equilibrium analysis of movable fine grains or soil/fluid transportation in continuous media, have been extensively performed to simulate the process of erosion. However, due to limited comparison with experimental data, those theories are not totally accepted.

Results from experimental investigations on the mechanical consequences of internal erosion are somehow contradictive, especially for the undrained test. One potential reason might be attributed to the relatively low saturation degree of the tested specimen after internal erosion. Also, without a detailed description of the mechanical properties of the soil mixtures, including the mechanical behavior of the coarse fraction and fine fraction, it might be difficult to logically understand the response of the internally eroded soil specimens.

2.6 Further improvement

Since internal erosion is a chronic phenomenon (it usually takes years in nature), a continuous constant seepage flow sustaining for a relatively long time in the test apparatus is necessary. Another improvement is related with the saturation degree. Since a low saturation degree in tested specimens may consequently lead to a not well performed undrained compression test. Therefore, it is better to apply back pressure during seepage test. The above two issues will be addressed in this dissertation.

CHAPTER 3

SOIL BEHAVIOR IN FIXED-WALL SEEPAGE TEST

3.1 Introduction

The seepage tests by fixed-wall permeameter are conducted under low confining pressure. The tests results could be helpful for the design of flexible-wall permeameter. In this series of tests, the soil specimens experience seepage-induced migration of soil grains. This principle governs the design of the main feature of the test assembly. Following soil preparation by moist tamping techniques in the permeameter, the specimens are subjected to upward seepage flow. The average flow rate is measured by cylinder at the outlet. Hydraulic gradient is derived from the spatial variation of water table along the specimen. Other variables such as temperature are also recorded to correct the hydraulic conductivity. Soil grain loss is estimated by analyzing the post-test grain size distribution curves. In this chapter, a comprehensive description of the test apparatus and the selected material are illustrated. The soil strength reduction induced by internal erosion is discussed in terms of the interpretation of CPT results.

3.2 Upward seepage test

3.2.1 Experiment apparatus

Constant head seepage tests with upward water flow are performed to cause internal erosion. A schematic diagram of the seepage test apparatus is shown in Fig. 3.1. The cylindrical seepage cell is 100 mm in internal diameter and 300 mm in height (Fig. 3.2). The transparent seepage cell allows for the observation of the internal erosion from the side. The upper end of the seepage cell is left open so that the erosion process can be observed from the top. An overflow pipe is fitted at the top portion of the seepage cell to manually measure the flow rate by a cylinder. Two 10-mm-thick plastic rings with waterproof tape are set separately on the top and the bottom of the specimen to prevent the formation of large seepage channels between the soil and the side wall. The layer consisting of 2-mm single-sized glass balls underneath the 170-mm-thick specimen serves to break up the incoming flow to ensure a uniform water flow on the specimen. Nonwoven textile is placed at the bottom of the specimen to prevent downward fine particle loss. The variation in water head within the specimen is measured by four stand pipes at four different depths, namely, 20 mm, 50 mm, 105 mm and 165 mm. The inlet is connected to a constant water head tank, which can be raised or lowered to control the hydraulic gradient across the specimen, while the outlet is open to the atmosphere. Higher seepage gradient can be achieved by raising the constant head water supply tank to a higher level.

3.2.2 Multi-stage test procedures

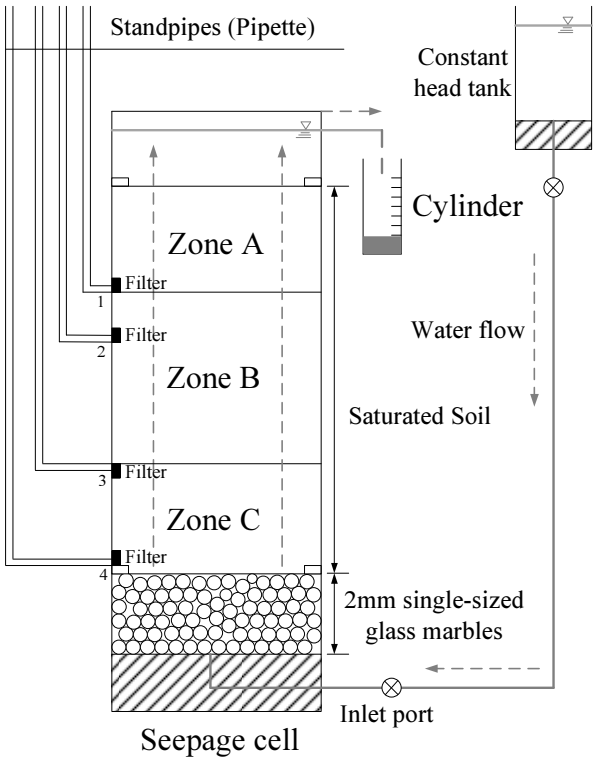

Figure 3.1 Schematic diagram of seepage test assembly

Figure 3.2 Photography of seepage test cell

A series of tests is conducted following the multi-stage procedure. Each test usually takes 5 ~ 6 hours depending on the imposed hydraulic gradient. The detailed test procedure is as follows:

(1) Before the test, check the position of the water level of the four standpipes to make sure the initial water head of all four is the same. Adjust the level of the constant water head tank to ensure that its water table is the same as that of the seepage cell.

(2) The initially imposed hydraulic gradient is usually in the range of 0.05~0.1. Increase the hydraulic gradient at approximately the same increments. When the hydraulic gradient reaches around the value required to cause initial internal erosion, the increment could be relatively smaller.

(3) For each step, allow 30 minutes to ensure the completion of the internal erosion, i.e., the discharge rate is stable and the effluent color becomes clear. Record the water head distribution from the stand pipes. Estimate the discharge rate by measuring the volume of discharge effluent per minute three times. Record the water temperature. Carefully observe the phenomena occurring during the test, such as the flow turbidity, the jumping, the piping or the transportation of the fine particles, and record them with a camera.

(4) Repeat (2) and (3) until the soil becomes unstable, e.g., the specimen shows “boiling”, or until the largest achievable hydraulic gradient is imposed if instability does not occur.

3.2.3 Measurements and calculation

The directly measured variables in the test are discharge rate, volume of water in the pipette and the specimen length. Correspondingly, the total and local hydraulic gradient, hydraulic conductivity and average flow velocity could be derived. The schematic diagram of the key variables is indicated in Fig. 3.3 and equations for calculation are summarized in Table 3.1.

The fundamental assumption is that the seepage flow follows Darcy’s law. Special attentions are given to validate the laminar flow condition, by satisfying which the Darcy’s law is applicable. Reynolds number (*Re*), usually used as a criterion to distinguish between laminar flow occurring at low velocities and turbulent flow, needs to be defined. Bear (1972) illustrated that for flow through porous media a Reynolds number is given by: $Re = vd/\upsilon$, where υ is the kinematic viscosity of the fluid ($0.0114 cm^2/s$ for water at the standard temperature of 15°C). d indicates a length dimension representing the elementary channels of the porous medium. Usually, the representative grain diameter may be regarded as the length dimension for soil. Since the fluid with fluidized fines would be dislodged through the constrictions among coarse grains, the d_{50} of the coarse soil is therefore considered as a representative grain diameter, which might be determined by the grain size distribution curve. If the viscosity of the flow discharge with fluidized fines would be the similar to water, then the Reynolds number could be confirmed. Darcy’ law is valid as long as the Reynolds

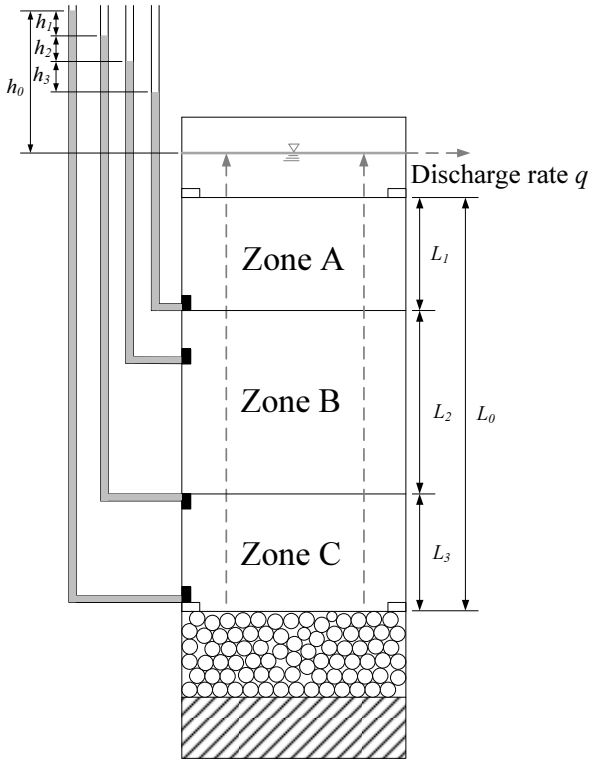

Figure 3.3 Key parameters for calculation

Table 3.1 A summary of the equations for calculating key variables

Variables	Expression	Notes
Water head difference (cm)	$h = \frac{\Delta V}{S}$	ΔV: water volume difference (ml) S: cross-section area of pipette (cm^2, the diameter of pipette is 0.87cm)
Average hydraulic gradient	$i_0 = \frac{h_0}{L_0}$	h_0: total water head difference (cm) L_0: specimen length (17cm)
Local hydraulic gradient	$i_n = \frac{h_n}{L_n}$ (n=1, 2, 3)	h_n: local water head difference (cm) L_n: corresponding seepage length (L_1=6cm, L_2=5.5cm, L_3=3cm)
Darcy velocity (cm/s)	$v = \frac{Q}{A}$	Q: discharge rate (cm^3/s); A: specimen cross sectional area (cm^2)
Average velocity of fluid flow (interstitial velocity) (cm/s)	$V = \frac{v}{n}$	n: soil porosity
Average hydraulic conductivity (cm/s)	$k_0 = \frac{q}{i_0}$	At standard water temperature (15°C)
Local hydraulic conductivity (cm/s)	$k_n = \frac{q}{i_n}$ (n=1, 2, 3)	At standard water temperature (15°C)

number based on average grain diameter is not greater than 10. Reddi and Inyang (2000) concluded that for majority cases of importance in groundwater flow, Darcy's law is generally applicable to soil. During the test, the discharge rate is monitored all the time to ensure the laminar flow condition.

3.2.4 Specification

During the seepage test, the temperature of water should not lower than that of specimen. The water flow used in those tests is Tokyo tap water without de-aired. If the water temperature is comparatively lower, the air inside the water will be released out, resulting in a lower saturation degree of the tested specimens.

Due to the tested grains are large in size, the sidewall leakage might occur. That is to say, the seepage flow might run through the channel between the wall and large grains, where the porosity is larger. To avoid this negative effect, 1cm-thickness plastic ring with waterproof tape is installed around the bottom of soil specimen. However, the subsequent tests still show amounts of fines dislodged from the sidewall, which might influence the hydraulic conductivity.

3.3 Soil specimens

Those soils with, namely “finer fraction” and “coarser fraction”, is vulnerable to internal erosion. The mixtures of two different types of silica sand, namely, No.3 and No.8 are used. To verify the characteristics of the materials, soil property tests including, grain size distribution, specific gravity, maximum and minimum void ratio, and permeability tests are conducted following the related requirements of Japanese Industry Standard (JIS) and Japanese Geotechnical Society Standard (JGS). Results are summarized as following:

3.3.1 Soil property

The binary mixtures in this study consist of two silica sands (silica No. 3 and No. 8) having different dominant particle sizes. With a larger particle size, the silica No. 3 works as the coarse particles, while the fine silica No. 8 is the erodible fine particles. The siliceous sand used here is mainly composed of quartz, categorized as an angular to sub-angular material. Grain size distribution, specific gravity, maximum and minimum void ratios, and hydraulic conductivity is summarized in Fig. 3.4, Table 3.2 and Table 3.3.

3.3.2 Tested soil mixtures

The primary target of the seepage tests is to create internally eroded saturated soil specimens. To this end, the initial conditions of those test specimens have to meet the criteria for the above-mentioned onset of internal erosion. The geometrical criteria can be satisfied if the phase relationship between the coarse grains and the fines, shown in Fig. 3.5, are considered.

The mass balance of the soil can be expressed as

$$f_s + f_f = 1 \quad \text{……. (3.1)}$$

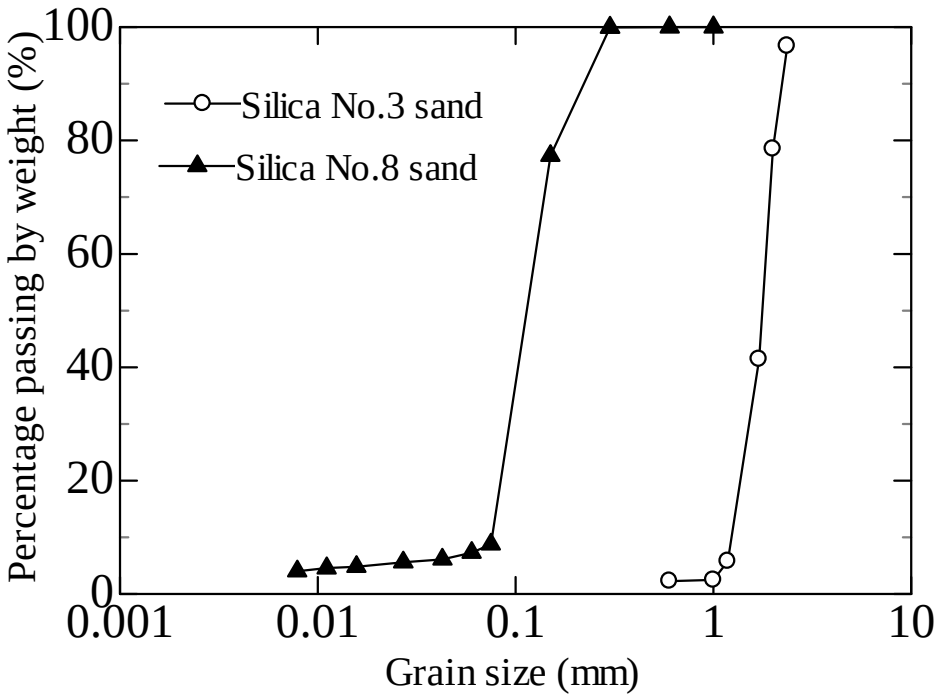

Figure 3.4 Grain size distribution curves for silica Nos. 3 and 8

Table 3.2 Sand grain size distribution parameters

Property	Silica No. 3	Silica No. 8
Median grain size d_{50} (mm)	1.72	0.16
Effective grain size d_{10} (mm)	1.37	0.087
Uniformity coefficient C_u	1.29	2.09
Curvature coefficient C_c	0.99	2.34

Table 3.3 Properties of silica sand

		Silica No. 3	Silica No. 8
Specific gravity		2.63	2.63
Maximum void ratio		1.009	1.333
Minimum void ratio		0.697	0.703
Hydraulic conductivity (m/s)	30%(1)	6.6×10^{-3}	3.4×10^{-5}
	60%(1)	5.6×10^{-3}	2.6×10^{-5}
	80%(1)	4.9×10^{-3}	2.1×10^{-5}

Note:
(1) Relative density

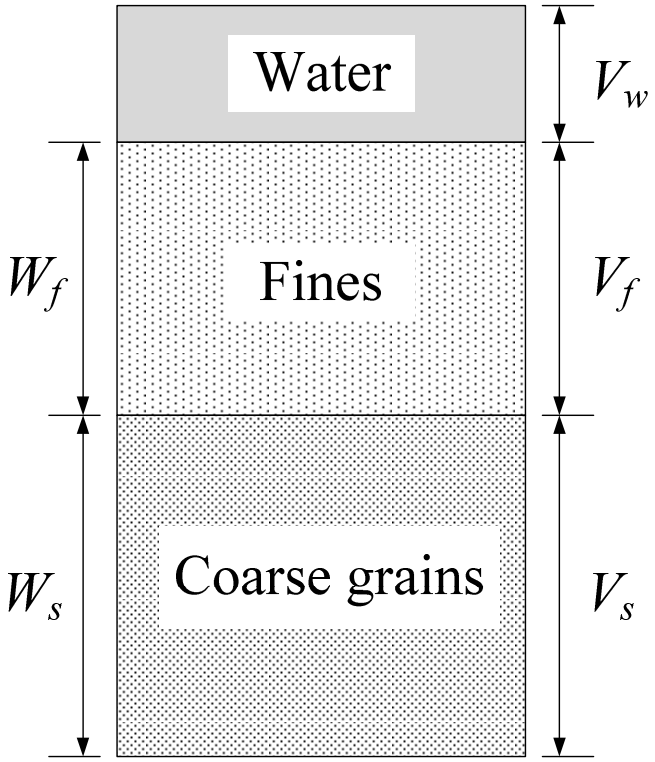

Figure 3.5 Schematic phase diagram of saturated binary soil

where f_s is the mass ratio of the coarse grains, equaling $W_s/(W_s+W_f)$, and f_f is the mass ratio of the fines, equaling $W_f/(W_s+W_f)$.

Assuming all the fines are erodible, the void ratio of coarse grains is

$$e_s=(V_w+V_f)/V_s \quad \text{……. (3.2)}$$

and the void ratio of fines is

$$e_f=V_w/V_f \quad \text{……. (3.3)}$$

From Equations (3.1), (3.2) and (3.3), and assuming that the specific gravities of the coarse and the fine grains are the same, the following equation is obtained:

$$f_f=e_s/(1+e_s+e_f) \quad \text{……. (3.4)}$$

Equation (3.4) indicates that the possible maximum value for f_f is reached under ideal conditions, namely, the coarse grains in the binary mixture specimen are loosely packed, while the fines are densely packed inside the voids between the coarse grains. Since the maximum void ratio of the No. 3 sand is 1.009 (the primary fabric formed by silica No. 3 is loosely packed) and the minimum void ratio of silica No. 8 is 0.703 (the fine particles, silica No. 8, are densely packed), the possible maximum mass ratio of the erodible fines is 37%. A series of four binary mixtures is determined as the test soils based on the above equation. The fine contents of the four mixtures are 25%, 20%, 16.7% and 14.3%, respectively, which are less than the calculated possible maximum value. The grain size distributions, the specific gravity and the maximum and the minimum void ratios of the four tested soils are shown in Fig. 3.6 and Table 3.4.

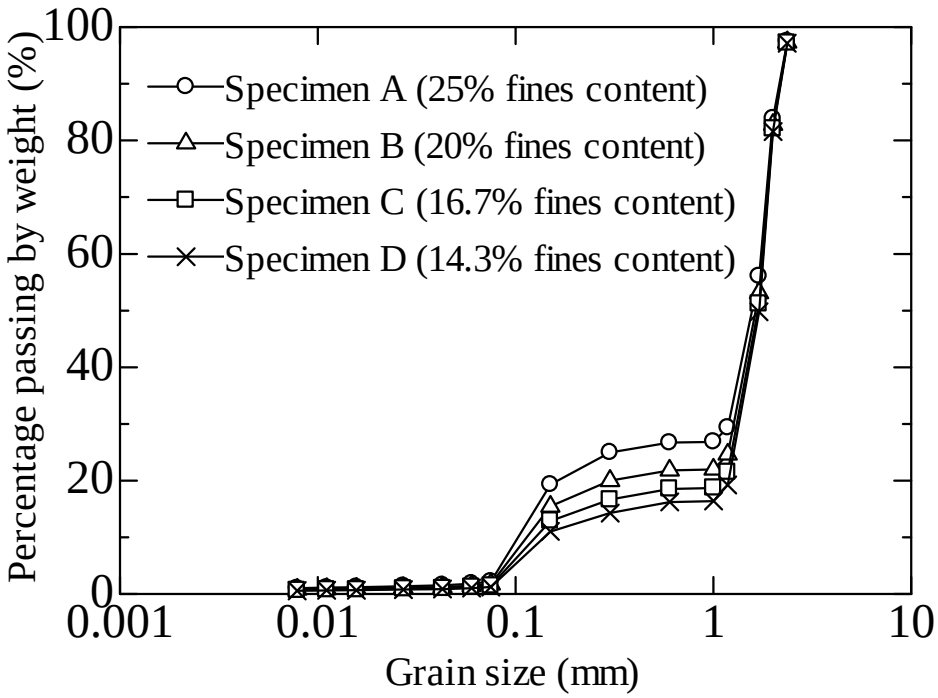

Figure 3.6 Grain size distributions of four soils

Table 3.4 Soil parameters of the four specimens

Specimen No.	A	B	C	D
Specific gravity	2.63	2.63	2.63	2.63
Maximum void ratio	0.756	0.764	0.775	0.795
Minimum void ratio	0.367	0.373	0.385	0.402
Void ratio range(1)	0.389	0.391	0.39	0.393

Note:
(1) Difference in void ratio between loosest and densest sand states

A plot of void ratios against fine contents is shown in Fig. 3.7. The demarcation line, located between the maximum and the minimum void ratio lines, is determined by $e_s=e_{c\_max}$ (Thevanayagam and Mohan 2000), where intergranular void ratio e_s is defined as

$$e_s = \frac{e + FC}{1 - FC} \quad \text{……. (3.5)}$$

The soil behavior around this line may be influenced by both coarse grains and fines. If those fines which actively play a role in transferring loads are eroded, the soil strength may be changed accordingly. In this series of tests, the relative densities of the specimens are expected to cover this demarcation line. Two different relative densities are finally selected for each soil specimen, as shown in Fig. 3.7 and Table 3.5.

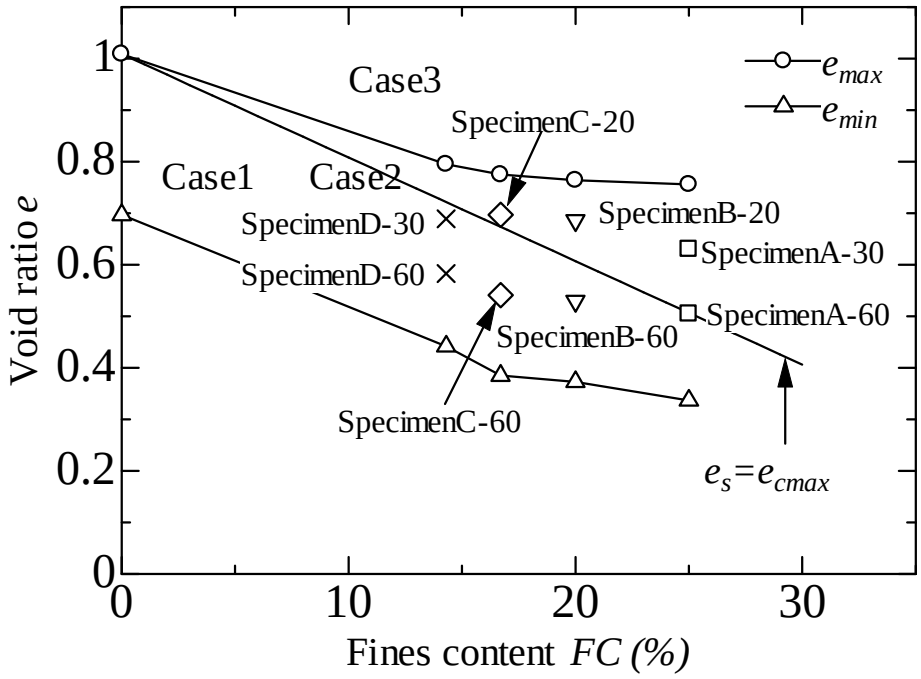

Figure 3.7 Intergranular matrix phase diagram

Table 3.5 Soil specimens for seepage test

Specimen No.	Fines content (%)	Relative density (%)	Initial void ratio
A-30	25	30	0.63
A-60	25	60	0.51
B-20	20	20	0.69
B-60	20	60	0.53
C-20	16.7	20	0.70
C-60	16.7	60	0.54
D-30	14.3	30	0.69
D-60	14.3	60	0.58

3.3.3 Vulnerability of mixtures to internal erosion

To ensure that internal erosion will occur during the seepage tests, the vulnerability of the four mixture soils to internal erosion is assessed by five currently available methods proposed by the U.S. Army Corps of Engineers (1953), Istomina (1957), Kezdi (1979), Kenney and Lau (1985, 1986), Burenkova (1993) and Mao (2005). The results are summarized in the Figs. 3.8 ~ 3.12 and Table 3.6.

The analysis results indicate that gap-graded soil which is deficient in certain size grains appears to be susceptible to erosion. The four soils are potentially unstable and vulnerable to internal erosion if seepage takes place.

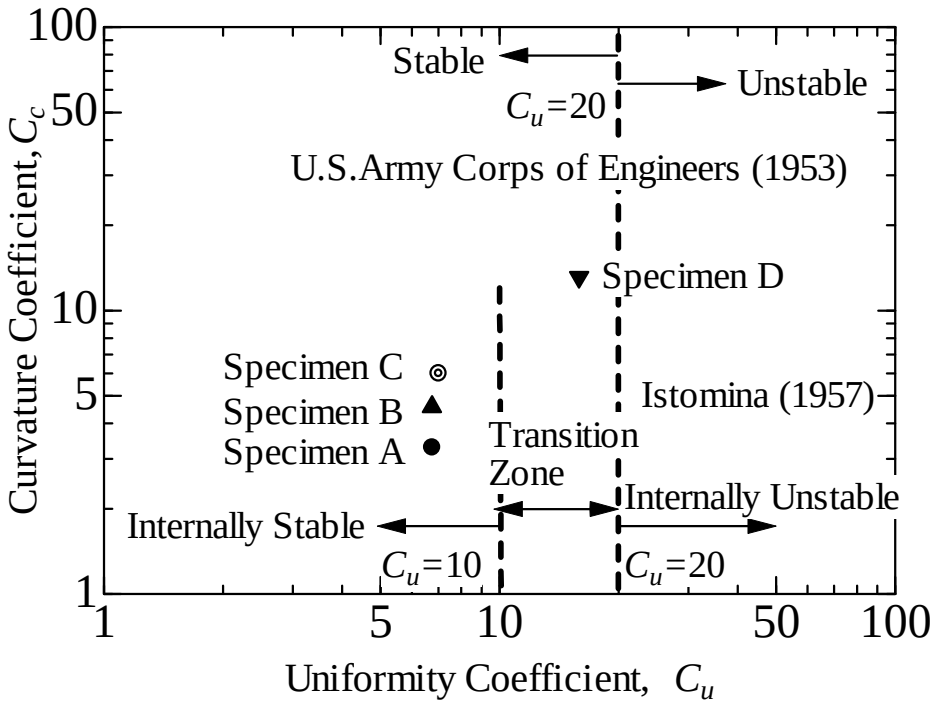

Figure 3.8 Classification of erosion characteristics based on U.S.Army Corps of Engineer (1953) and Istomina (1957)

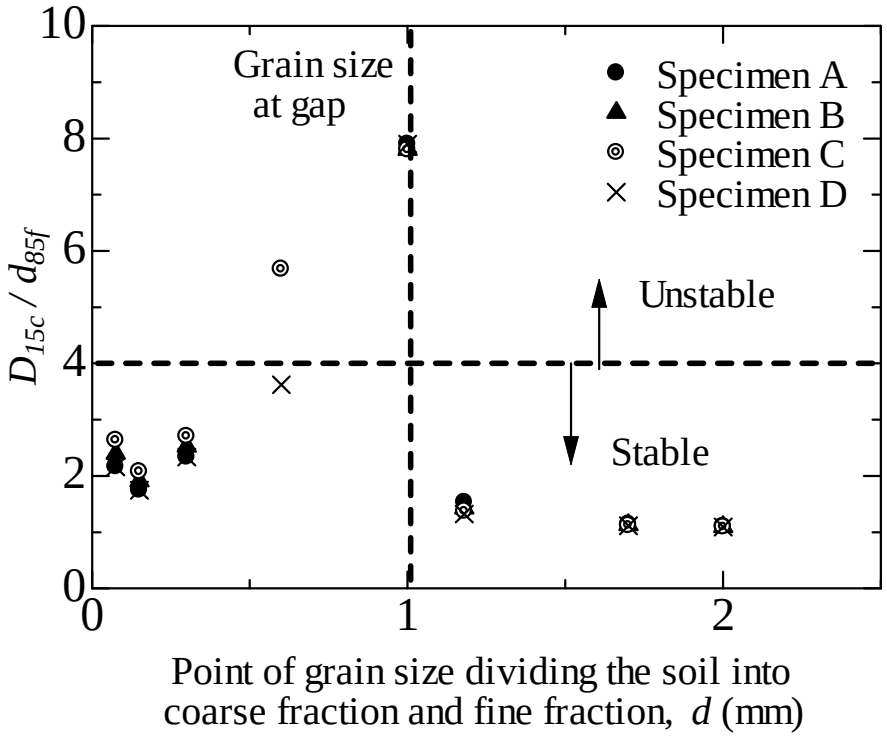

Figure 3.9 Classification of erosion characteristics based on Kezdi (1979)

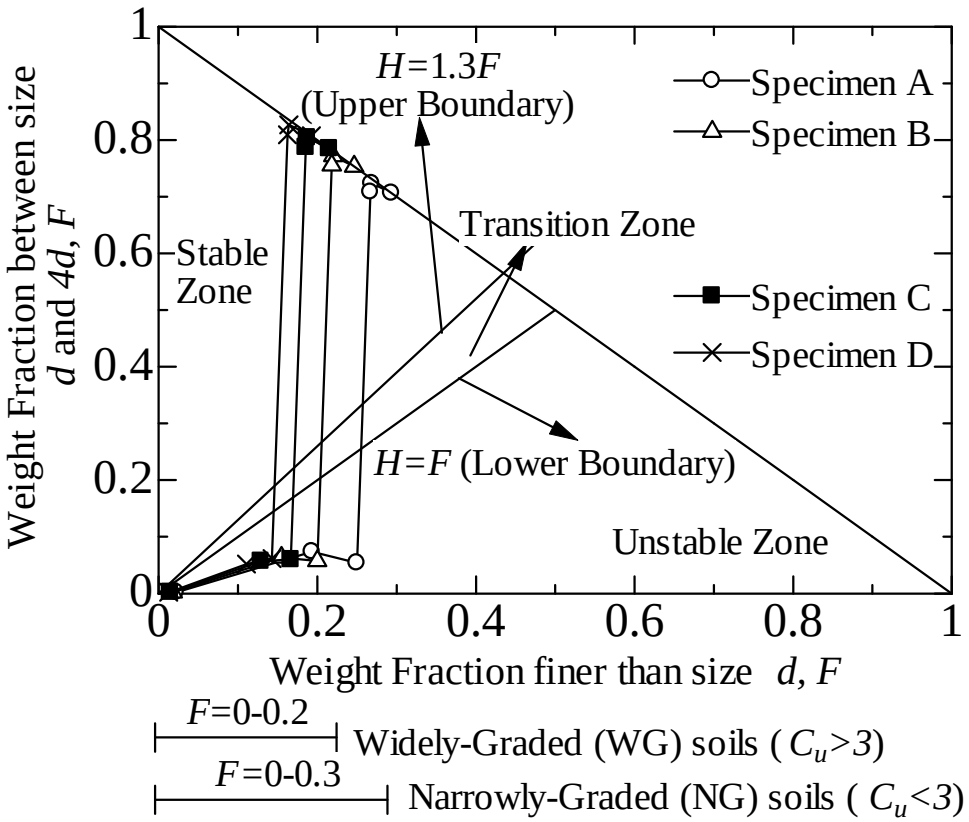

Figure 3.10 Classification of erosion characteristics based on Kenny and Lau (1985, 1986)

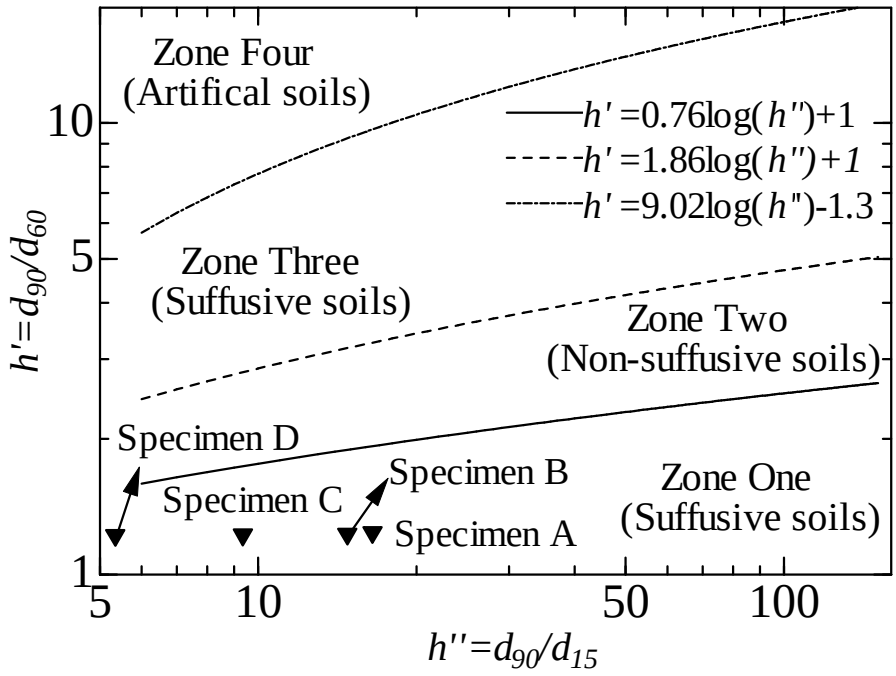

Figure 3.11 Classification of erosion characteristics based on Burenkova (1993)

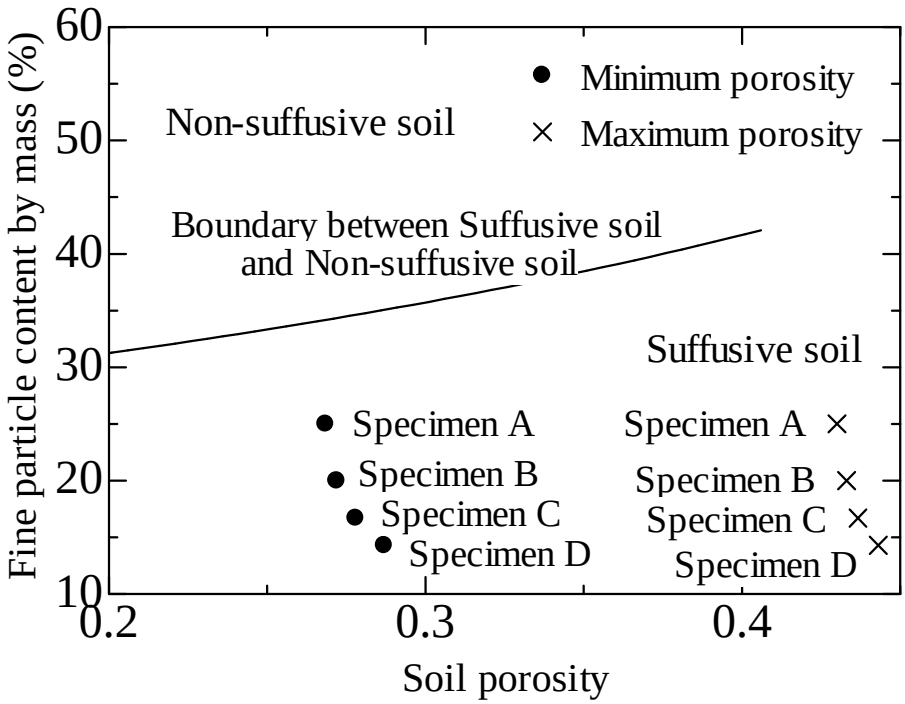

Figure 3.12 Classification of erosion characteristics based on Mao (2005)

Table 3.6 Assessment of specimen vulnerability to internal erosion by current methods

Specimen	Methods used to assess internal stability					
	U.S. Army (1953)	Istomina (1957)	Kezdi (1979)	Kenney & Lau (1986)	Burenkova (1993)	Mao (2005)
A	S	S	U	U	U	U
B	S	S	U	U	U	U
C	S	S	U	U	U	U
D	U	U	U	U	U	U

Note: “U” means Unstable; “S” means Stable

3.3.4 Soil preparation

To prevent the segregation of the two different sized particles, the moist tamping method is employed (Ladd 1978; Frost and Park 2003). This method achieves uniform specimens by the concept of “undercompaction”; each layer is compacted to a lower density than the desired value by a predetermined amount due to the fact that the compaction of succeeding sand layers would also densify the layers below. It has been proven reliable by other scholars (Bradshaw and Baxter 2006; Yang *et al*. 2008). The specimen preparation procedures are as follows (Fig.3.13): determine the oven-dried weights of both silica No. 3 and No. 8 for tests according to the prescribed fine content and relative density. Adjust the water content to an appropriate value. Usually, for the larger fine content specimen, a greater water content is preferred (e.g., the initial water content of specimen A is 8%, while that of specimen D is 5%). Thoroughly mix the

soils with water to ensure that the fine particles are distributed as uniformly as possible. This procedure is usually done at least 16 hours before use. The specimen is prepared layer by layer. Weigh the amount of material required for each layer, and place it into the cell with a scoop. A tamping rod is used to compact the soil to the required height determined by “undercompaction”. Upon completion, weigh the specimen to check the relative density again and record it. This process usually takes two hours. Saturation of the specimen is performed in a vacuum tank. De-aired water is purged into the specimen from the bottom inlet at a slow rate. This process takes approximately 5 ~ 6 hours to ensure saturation quality.

(a) Glass marbles

(b) Completion of layer 1

(c) Completion of layer 4

(d) Completion of layer 10

Figure 3.13 Specimen preparation procedures

3.4 Observed soil behavior in fixed-wall seepage test

Typical soil behavior observed in the seepage tests will be presented first, including the onset of internal erosion, hydraulic conductivity change, migration of fine grains and percentage of fines loss. By controlling three variables, which are fines content, soil relative density and imposed hydraulic gradient, the factors which influence the hydraulic gradient at which internal erosion would initiate, hydraulic conductivity change and fines loss due to internal erosion could be studied. After internal erosion, the eroded soil specimens are produced, against which CPT will be conducted to find the changes of soil strength.

3.4.1 Definitions

A critical hydraulic gradient for soil stability i_c was proposed by Terzaghi (1948) to determine a zero effective stress condition, which is given by

$$i_c = \frac{G_s - 1}{1 + e} \quad \text{……. (3.6)}$$

It is related to the void ratio and the specific gravity of soil particles. It is always accompanied by the phenomenon of the “boiling” or “heaving” of both coarse and fine particles. For cohesionless soils, i_c is approximately equal to 1.

The critical hydraulic gradient for internal erosion, i_s corresponds to the minimum hydraulic gradient at which the first sign of internal erosion appears when the imposed hydraulic gradient gradually increases, indicated by the slight rushing out of fine grains. It corresponds to the inflection point in the hydraulic gradient and the flow velocity relationship curve, shown in Fig.3.14. The critical hydraulic gradient for internal erosion is defined as:

$$i_s = \frac{i_1 + i_2}{2} \quad \text{……. (3.7)}$$

where i_2 is the hydraulic gradient at which curve slope begin to change; i_1 is the hydraulic gradient just before i_2.

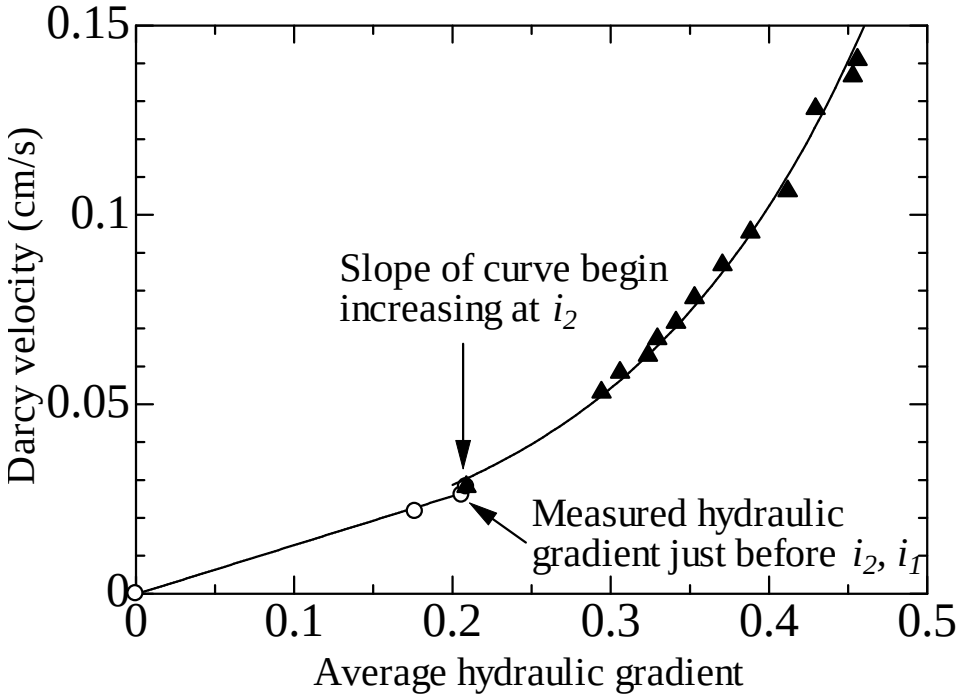

Figure 3.14 Estimation of critical hydraulic gradient for internal erosion

3.4.2 Observed migration of fines

All the test specimens, except specimen D-30, showed internal erosion phenomena. The hydraulic behavior of those specimens, such as the tendency of the flow velocity and the hydraulic gradient relation, is similar. Since the phenomenon observed in specimen A is obvious and typical, the results of specimen A are mainly shown later for discussion. Figure 3.15 presents the observation of the fine grain loss from the top (specimen A-30). Before the onset of the internal erosion, the fine grains stay still. When the critical hydraulic gradient for internal erosion is reached, small “dance-like” movements of fine grains occur. A very light layer of sand silt covers the top surface. Then, a few sand spots or sand volcanoes appear after increasing the hydraulic gradient. Slight movement of the fine grains is found around those spots. At the larger imposed hydraulic gradient, the number of sand spots increases and covers the whole area, and the movement of the fine grains around those spots becomes fiercer. As the hydraulic gradient is further increased, a piping-like phenomenon happens.

Side view of the particle migration can be seen in Fig. 3.16. As is shown, dyed-black fine particles are utilized in three layers to highlight the migration of fines along the vertical direction. The fines content is 25% and initial relative density is 30%. When the hydraulic gradient for internal erosion is arrived, the fines in the upper layer start to dislodge first. With the increasing of imposed hydraulic gradient, the movement of fines in the upper layer seems to be more vigorous and the fines at the middle begin moving. Several visible “pipe channels” are formed and developed, which directly connects to the sand spots or sand volcanoes at the top surface. It is postulated that further increase in the imposed hydraulic gradient would result in more fluidized fines passing through

the “pipe channels” to be washed away. However, it is probable that clogging appears if the size of the fluidized fines (usually evaluated by the representative diameter, e.g., d_{50}) was larger than the diameter of “channels” or local accumulation occurs at certain spots along those channels. It may cause the slight change of internal flow direction and the fines may pass through other available “channels”. If the clogging is critical enough, the hydraulic conductivity may consequently increase.
Or the clogging of fines would be cleared if the imposed hydraulic gradient becomes higher and the “channels” work again. Hagerty (1991a) commented that this temporary clogging changed the flow condition in the soil and made the internal erosion complicated and unpredictable.

Less fines in the bottom layer move at the beginning of internal erosion due to the higher confining pressure. If the imposed hydraulic gradient is high enough, the fines in this layer would start to dislodge. The erosion rate in this layer would be larger due to the higher hydraulic gradient at this layer, which might explain the phenomenon that although the fines in the upper layer dislodge first, the percentage of fines loss in the bottom layer is the highest.

Due to erosion, the distribution of the fines was rather random, leading to the random formation of “pipe channels” inside the soil. With the progress of fines erosion, the coarse grains may correspondingly adjust their relative positions to reach a new equilibrium.

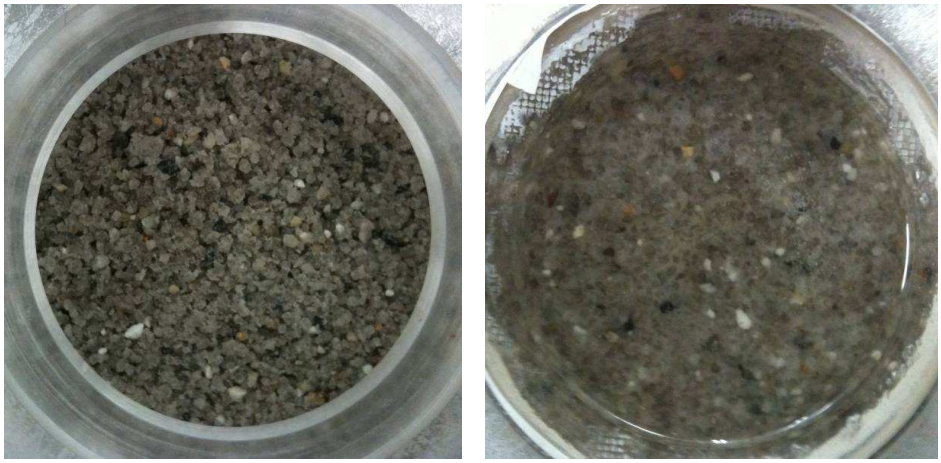

(a) Before internal erosion (b) i=0.15

(c) i=0.17

(d) i=0.19

(e) i=0.20

(f) i=0.23

Figure 3.15 Observed migration of fines from top (specimen A-30)

(a) Before internal erosion

(b) i=0.10

(c) i=0.16

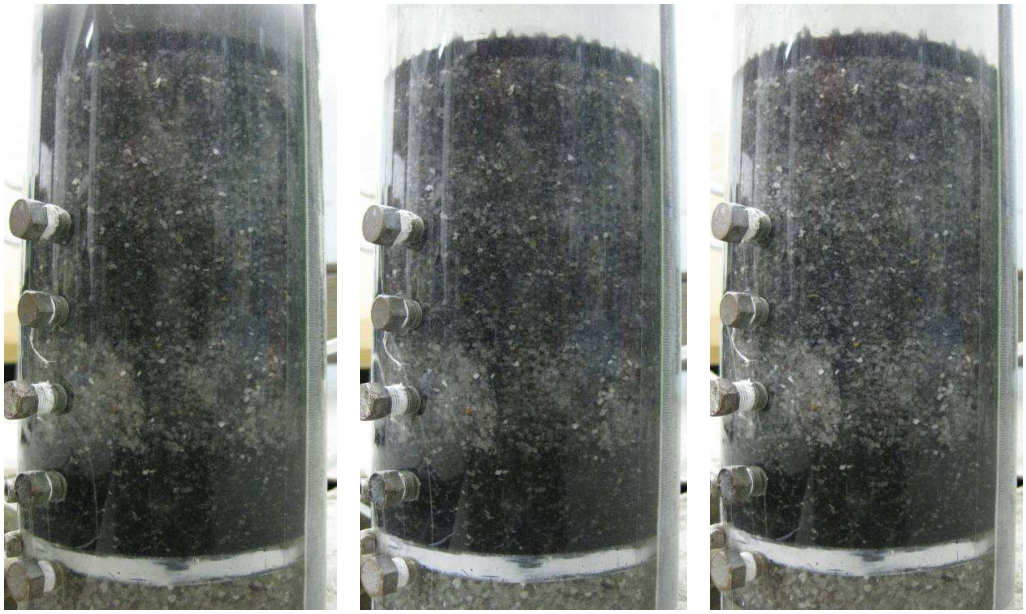

(d) i=0.18 (e) i=0.21 (f) i=0.24

Figure 3.16 Vertical migration of fines

3.4.3 Onset of internal erosion

The typical relationship between the hydraulic gradient and the flow velocity (specimen A-30) is shown in Fig. 3.17. At first, the approximate linear relationship between the hydraulic gradient and the flow velocity, in accordance with Darcy's law, indicates no occurrence of internal erosion. At this stage, the effective porosity, representing the porosity available for contribution to the fluid flowing through the specimens, stays basically the same irrespective of the hydraulic gradient. After reaching the critical hydraulic gradient for internal erosion i_s, the curve slope begins to inflect, corresponding to the first observation of "dance-like" movements of the fine grains. The fines are dislodged by the seepage flow, leading to the increase in effective porosity, and thus, hydraulic conductivity. It can be inferred that when the critical hydraulic gradient for soil stability i_c is reached, the "heaving" phenomenon occurs and the specimen reaches the state of zero effective stress.

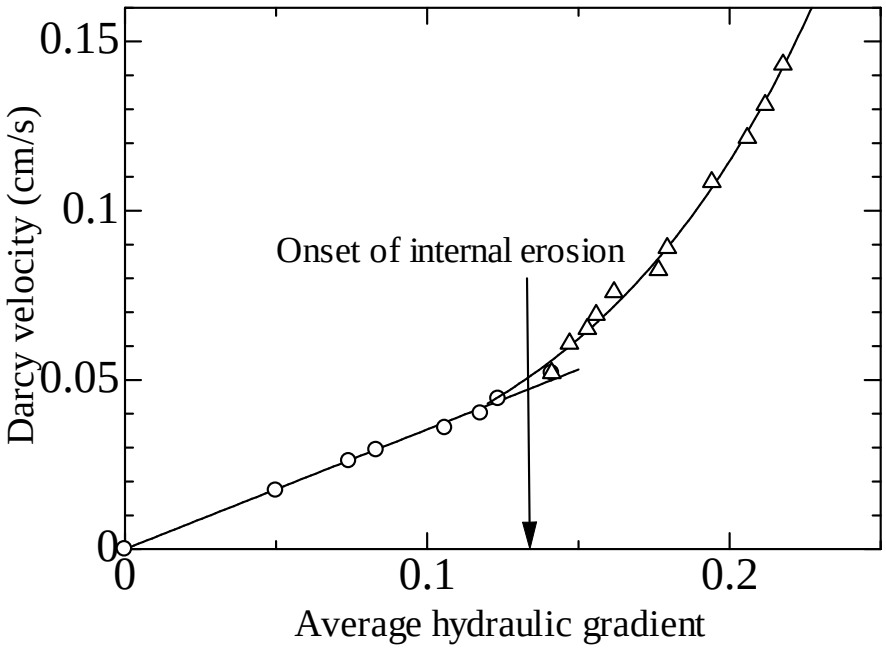

Figure 3.17 Hydraulic gradient and Darcy velocity relation (specimen A-30)

3.4.4 Changes of hydraulic conductivity

Since the amount of fine grain loss varies with the depth, the hydraulic conductivity is not uniform for all depths. In this section, the changes in local hydraulic conductivity are calculated by the local hydraulic gradient assuming that the seepage flow follows Darcy's law. Figure 3.18 shows the relationship between the average hydraulic gradient and the local hydraulic conductivity of each layer for specimen A-30.

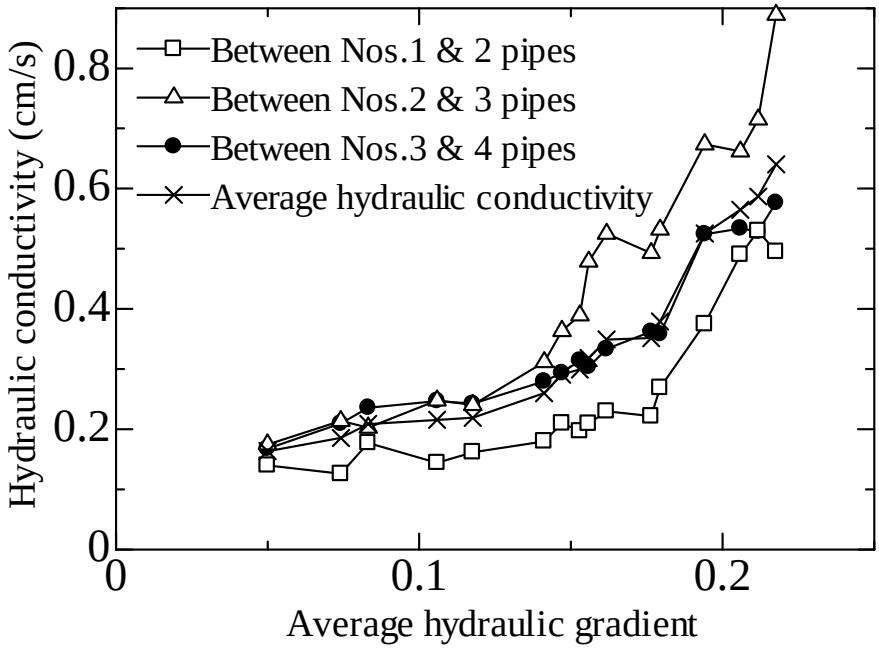

Figure 3.18 Local hydraulic conductivity variance (specimen A-30)

Before internal erosion (i < 0.13), a slight increase in the hydraulic conductivity with the imposed hydraulic gradient can be observed because of the nature of the upward seepage flow test, namely, the upward flow would decrease the effective stress, similar to unloading the soil, and the void ratio would correspondingly increase, leading to the increase in hydraulic conductivity even without internal erosion. However, compared to the drastic increments in hydraulic conductivity, due to the loss of fine grains, the hydraulic conductivity is thought to be basically constant before internal erosion and its increments could be negligible. After the onset of internal erosion, the hydraulic conductivity obviously increases with the imposed hydraulic gradient, resulting in 3 times the initial value when the maximum imposed hydraulic gradient of 0.22 is reached. The loss of fines would lead to the increase in hydraulic conductivity.

3.4.5 Influence of controlled factors

Figure 3.19 shows the variance in the critical hydraulic gradient for soil stability and the critical hydraulic gradient for internal erosion with the different initial fine contents for the dense soil specimen (60% relative density). The calculated critical hydraulic gradient for zero effective stress following, Terzaghi's equation, are 1.08, 1.06, 1.05 and 1.03, and the experimental values of the critical hydraulic gradient for internal erosion are 0.21, 0.23, 0.24 and 0.25, respectively. These values are in accordance with the test results of Skempton and Borgan (1994), namely, migration and the strong piping of fines take place in unstable materials at gradients of about one fifth to one third of the theoretical value. There seems to be a trend for the specimen with a lower fine content to require a larger hydraulic gradient in order to bring about internal erosion. The loose specimens also show the same trend (Fig. 3.20).

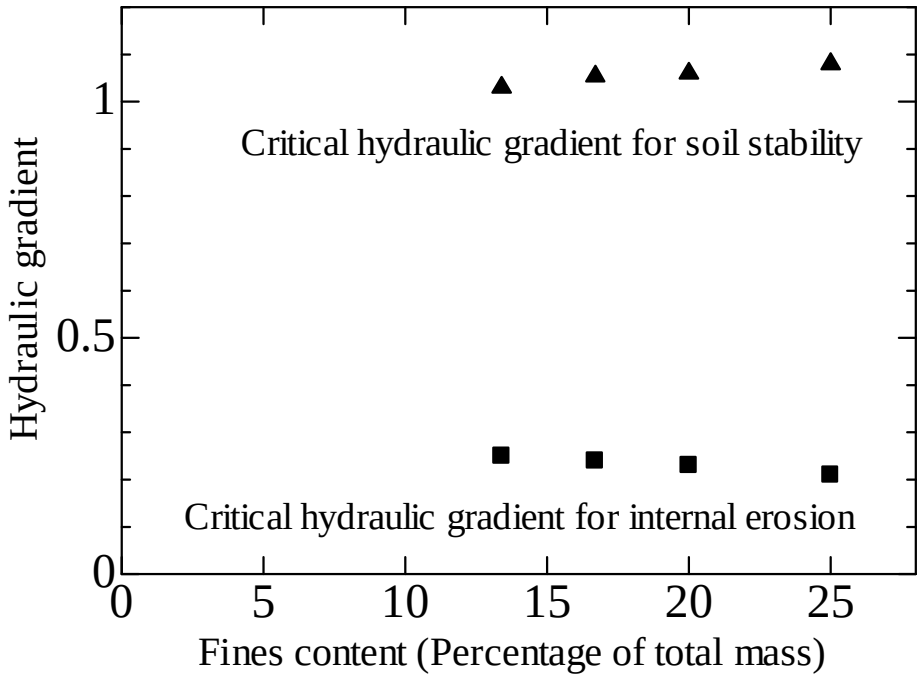

Figure 3.19 Relation between fines content and i_s, i_c for dense specimens

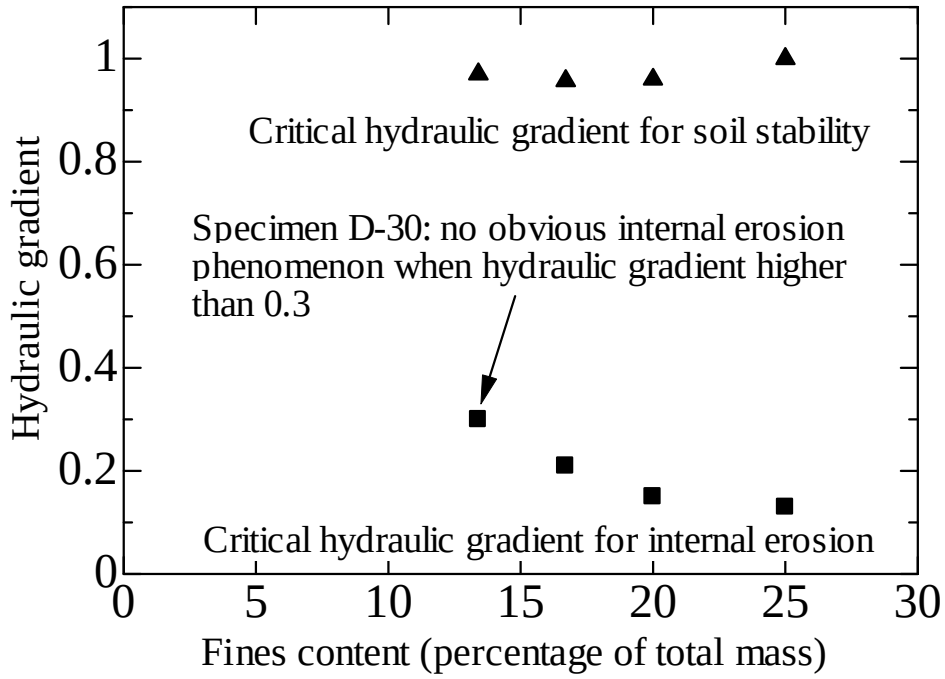

Figure 3.20 Relation between fines content and i_s, i_c for loose specimens

The influence of the relative density on the critical hydraulic gradient for internal erosion is presented in Fig. 3.21. A larger relative density for the specimen with the same fine content leads to a larger value of critical hydraulic gradient for internal erosion.

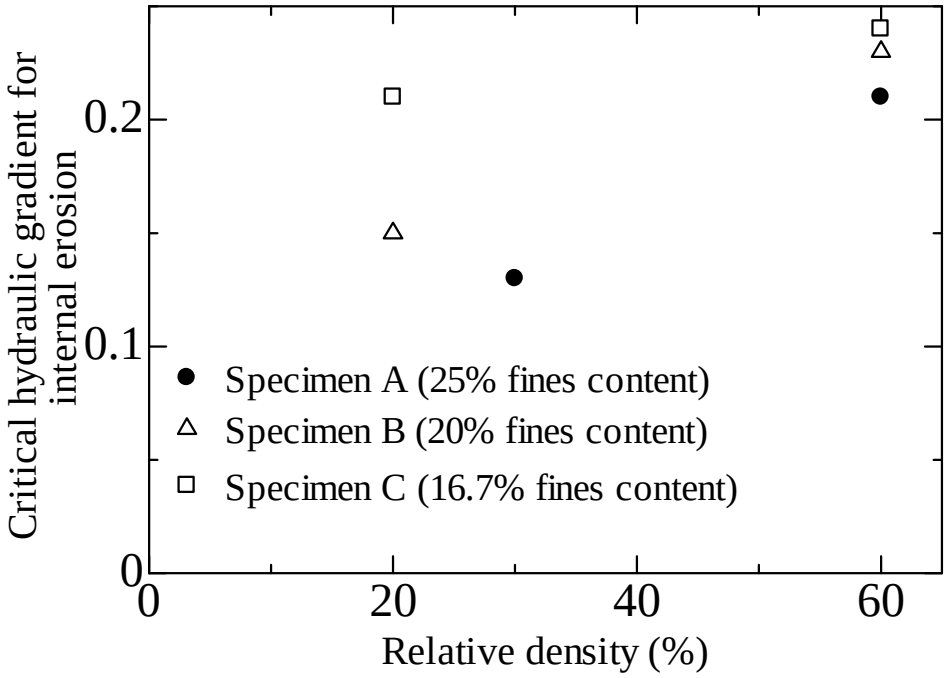

Figure 3.21 Relationship between relative density and i_s

3.4.6 Percentage of fines loss during internal erosion

Typical post-test grain size distribution curves for each zone (Fig. 3.1) of specimen A-60 at i_{max} = 0.45 are shown in Fig. 3.22. The distribution curve for each layer, after the internal erosion shifts downward from the original curve after internal erosion, indicates the tested specimen has experienced fines loss. The extent of the movement proportionally increases with the amount of fines loss. A graphical method proposed by Kenney and Lau (1985) is used to approximately assess the fraction of eroded fine grains, as well as the largest eroded fine grains, based on the changes in the grain size distribution curve. This method has been proven to be effective by many scholars (Wan, 2006; Zhang, 2007). A detailed calculation is shown in Fig. 3.23. The main idea of this method is to extend the initial grain size distribution curve of the test specimen to match the curve after internal erosion. Since the coarse grains stay the same after internal erosion, by extending the vertical scale of the initial grain size distribution curve, the coarse part of the initial curve should match that of the post-test grain size distribution curve. The fraction of eroded fines can be calculated from the amount of movement of the initial grain size distribution curve.

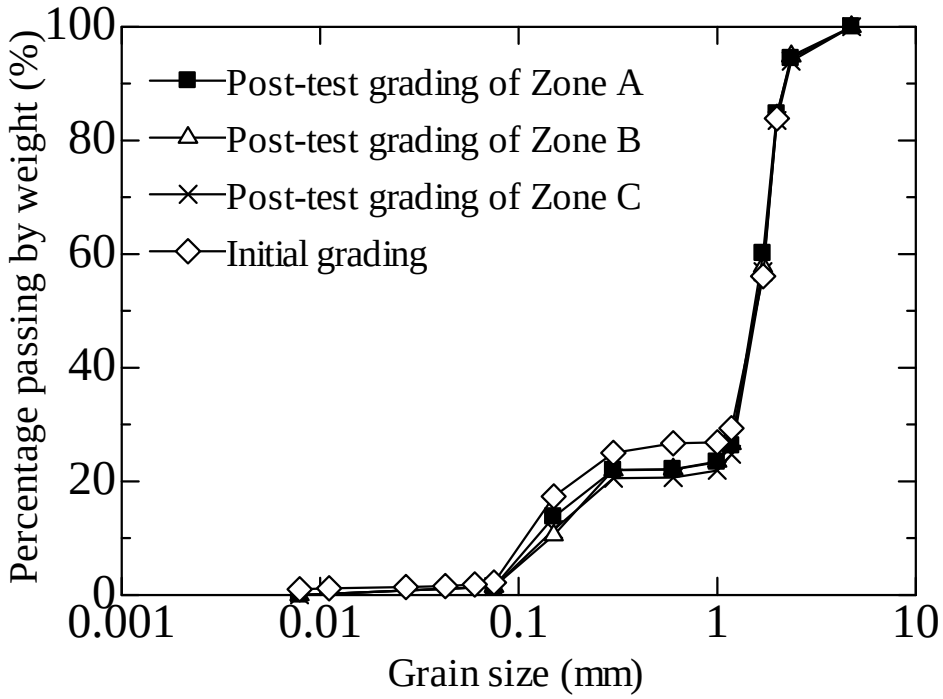

Figure 3.22 Grain size distribution curve with depth

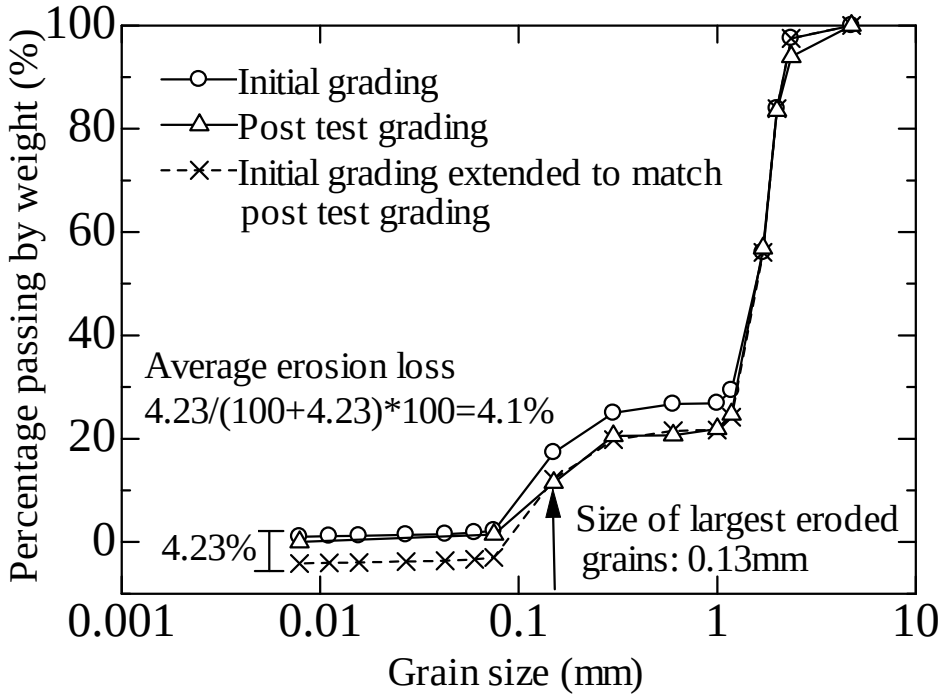

Figure 3.23 Graphical method of fines loss assessment

Table 3.7 presents the fines loss (percentage of total mass) after imposing two different maximum hydraulic gradients for specimen A-60. It is noted that the fine grain loss of the bottom layer is the greatest, since the bottom layer has no "fine grain supply". The fine grains are washed away leading to a large amount of fines loss. For the middle and upper layers, although their fine grains are washed away by the seepage flow, the fine grains from the bottom layer are dragged up by the seepage flow, forming a soil grain supplement to those layers. Due to the open-ended nature of the water channel, more grains will be eroded from the top layer than from the middle layer. This finding is in accordance with Kenney and Lau (1985). They defined the three layers as the top transition zone, the central homogeneous zone and the bottom transition zone. The fines loss in the top and bottom zones is larger than that in the central zone.

For specimens A-60, B-60 and C-60, different maximum hydraulic gradients, larger than the critical hydraulic gradient for internal erosion, are imposed to find its influence on the fines loss. The relationship between the maximum imposed hydraulic gradient and the percentage of fines loss of those specimens with different fine contents are shown in Fig. 3.24. There is a general trend whereby the larger maximum imposed hydraulic gradient means a larger fines loss. Specifically, before the onset of the internal erosion, the soil specimens are stable without any fines loss. Once internal erosion starts, the fines loss increase with the imposed hydraulic gradient. At the same imposed hydraulic gradient, the specimen with the larger fines content shows the potential for more erosion. Due to the relatively large hydraulic conductivity of the tested specimens, a hydraulic gradient of greater than 0.51 cannot be imposed. Since the amount of erodible fine grains in a mixture is definite, the eroded fine grains will not increase unlimitedly with the imposed hydraulic gradient. When a certain hydraulic gradient is

reached, the fines loss will be close to its limit and remain stable irrespective of the hydraulic gradient.

3.4.7 Void ratio and volumetric deformation

An obvious characteristic of internal erosion is the change in soil microstructure, resulting in the increase in void ratio and volumetric deformation. Due to the nature of the upward seepage tests, the precise measurement of the soil deformation during the seepage tests cannot be conducted. By observation, there is a trend after internal erosion, for the tested specimen to subside (Fig. 3.25). The largest deformation is observed at specimen A-60. The volumetric strain caused by internal erosion is about 6%. The specimen deformation is caused by both the loss in soil grains and the possible change in voids due to the soil grain spatial adjustment, as is shown in Fig. 3.26. The largest increase in void ratio occurs if there is no deformation during the internal erosion, corresponding to the Mitchell (1976) assumption that the fine grains occupy the voids between the coarse grains and may not participate in the force transfer. The loss of those fines would not cause any deformation in the soil fabric. The minimum volumetric strain is 0. However, in practice, the internal erosion would always be accompanied by the deformation of the soil structure, which is regarded as a sign of instability. It may be better to consider this possibility as an ideal simplification in theory. The minimum void ratio of the specimen after erosion could be estimated by the greatest compaction that the coarse grains could achieve, resulting from the rearrangement of the soil grains. Under this circumstance, the volumetric deformation of the specimen would reach the maximum value.

Table 3.7 Percentage of fines loss at different depths for specimenA-60

Zone / Max. hydraulic gradient		A	B	C
Percentage of fines loss in mass (%)	0.45	3.00	2.70	4.10
	0.51	3.00	2.94	5.11

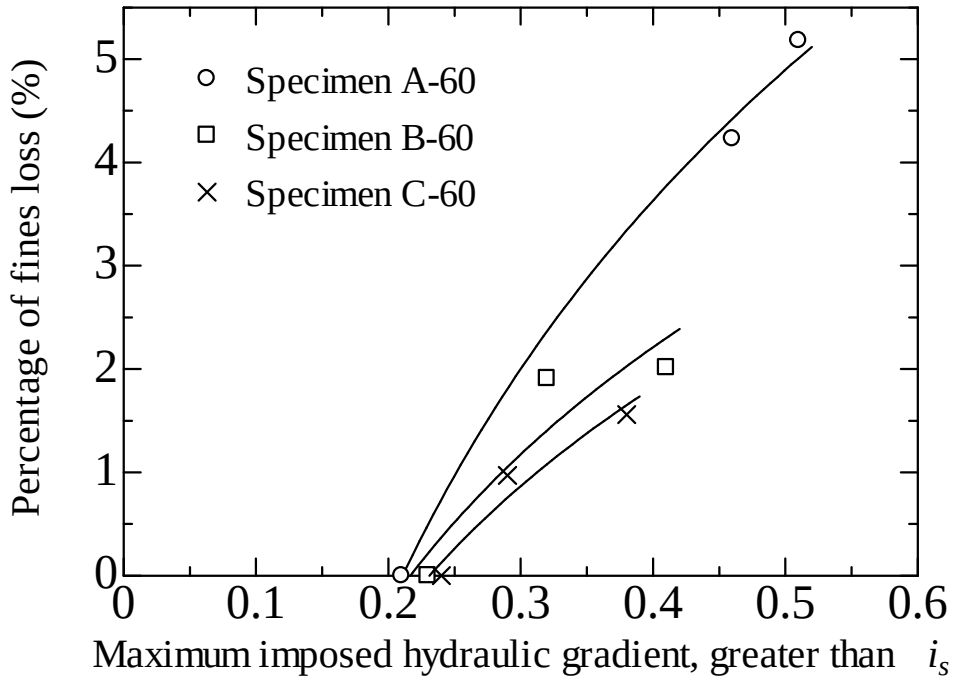

Figure 3.24 Fines loss variance with maximum imposed hydraulic gradient at various fines contents

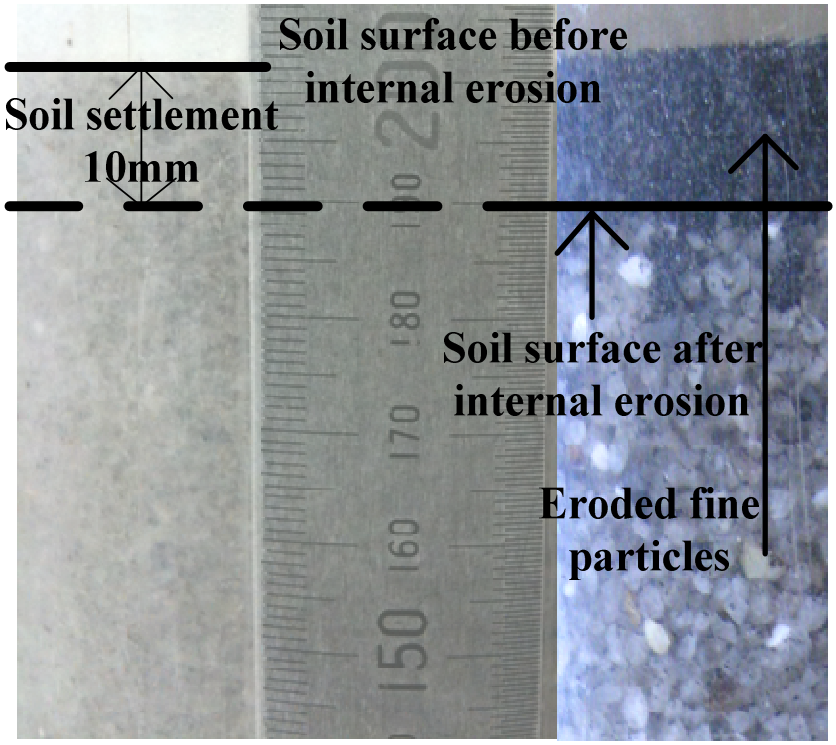

Figure 3.25 Changes in soil volume due to internal erosion (specimen A-60)

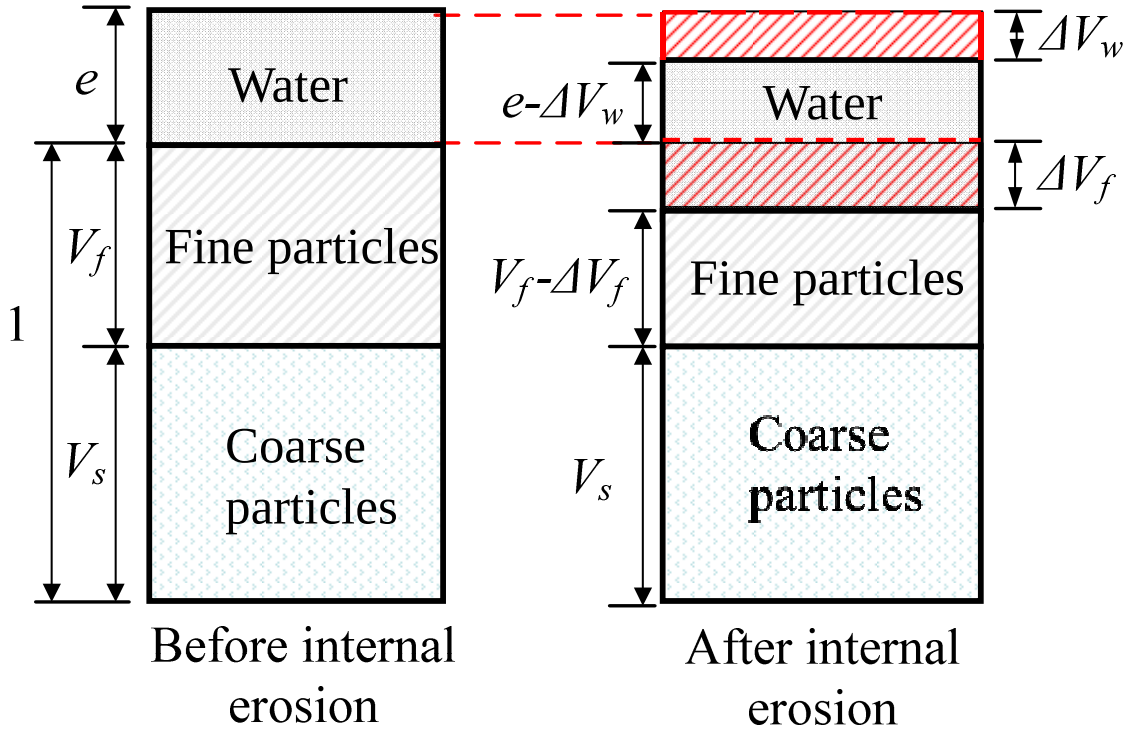

Figure 3.26 Possible volumetric deformation of tested specimen

The soil volumetric deformation is accompanied by the possible loss of those fines actively engaged in the mechanical transfer and the spatial rearrangement of the soil grains, both of which would probably adjust the force transfer path in specimens, and consequently, lead to a reduction in soil strength after internal erosion.

3.5 Cone penetration test (CPT)

3.5.1 Introduction of the miniature cone and test specimens

Due to the difficulties of retrieving undisturbed samples from the seepage cell after the tests, an *in situ* testing technique is needed to characterize the mechanical properties of the specimen. The miniature Cone Penetration Test (CPT) was selected because it offers the continuous measurement of the cone resistance along depth and excellent repeatability. In practice, the friction angle of sand deposits can be estimated from the results of CPTs (Terzaghi, Peck and Mesri 1996). By conducting CPTs before and after the application of the seepage flow to the specimen, the reduction in strength due to the internal erosion can be evaluated. The miniature cone used in the tests is a cylindrical cone tip with a diameter of 10 mm and tip apex angles of 60° (Fig. 3.27). By using an embedded load cell, the resistance at the tip can be measured. A jack is connected to the upper end of the penetrometer to push the cone into the specimens at a constant rate. The data acquisition system allows automatic cone tip resistance recording. The penetration rate is 20 mm/sec, following JGS 1435-2003. The total penetration depth is 160 mm. According to Been, *et al.* (1986), who reviewed the problems associated with calibration chamber tests, the size effect, including grain size and the chamber size effect, and the boundary effect are the most important issues. The diameter ratio of

seepage cell to cone in this research is 10, which might cause the size effect. Some assessments on the size effect in this study can be found in the Appendix A. All the test specimens are listed in Table 3.8.

3.5.2 Cone resistance profile

Profiles of the cone tip resistance for specimens A, B, C and D at 60% relative density are shown in Fig. 3.28. A larger fine content leads to a smaller cone tip resistance. A potential explanation is that for gap-graded soil, coarse grains work as the soil skeleton and the interlocking between them is primary. The fines work as separators between the coarse grains. With more fines content, those "separators" decrease the frictional forces between the coarse grains, resulting in a smaller shearing resistance and, correspondingly, a decrease in the cone tip resistance.

The influence of internal erosion on CPTs is demonstrated by the cone tip resistance profiles obtained before and after the internal erosion. As an example, those of specimen A-60 are shown in Fig. 3.29. After the internal erosion, the cone resistance decreases, indicating that the internal erosion process may have changed the interlocking of the soil grains leading to the decrease in cone resistance. However, the strength reduction may potentially be induced by loss of fines, weakening soil grain interlocking or the size effect. On previous researches, the size effect was closely related to the soil's relative density. As the relative density is not very large (60% maximum), it might be said that the reduction in resistance is mainly caused by the fines loss, not by the size effect.

Figure 3.29 also reveals that the reduction in cone tip resistance has a certain relationship with the maximum imposed hydraulic gradient. Before internal erosion, the soil structure is assumed to remain constant irrespective of the hydraulic gradient. After the onset of the internal erosion, the larger imposed maximum hydraulic gradient results in more fines loss, and therefore, further cone tip resistance reduction.

Figure 3.27 Miniature cone penetrometer

Table 3.8 Number of specimens undertaken by CPT

Specimen No.	Before internal erosion	After internal erosion
A-30	1 test	1 test
A-60	1 test	3 tests(1)
B-20	1 test	1 test
B-60	1 test	2 tests(1)
C-20	1 test	1 test
C-60	1 test	2 tests(1)
D-30	1 test	None
D-60	1 test	1 test

Note:
(1) For the dense specimens, seepage tests ending at different imposed hydraulic gradients are performed.

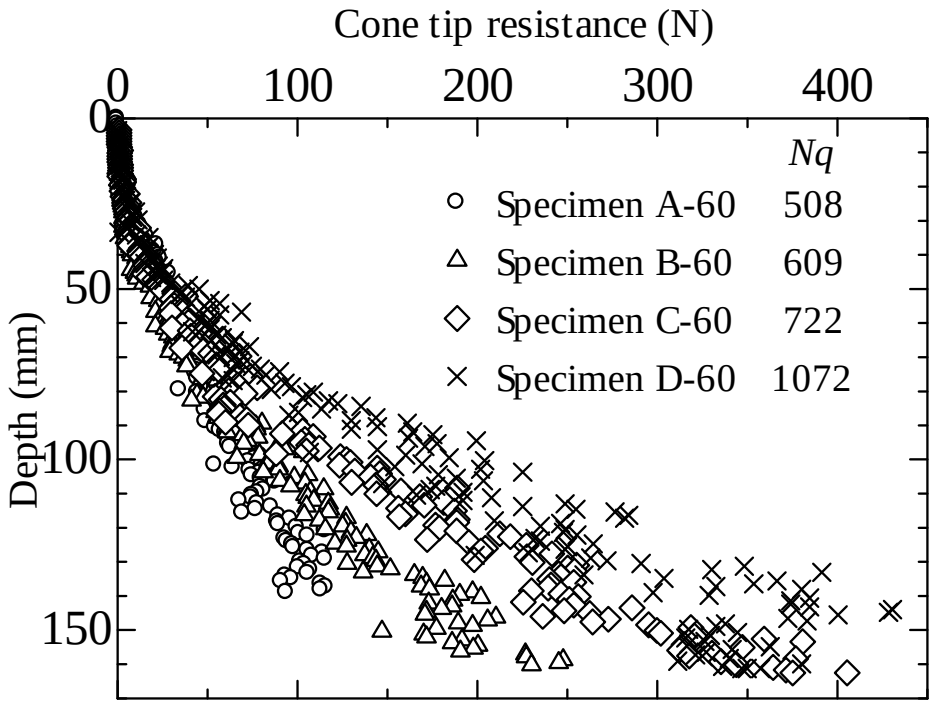

Figure 3.28 Cone resistance of dense specimens

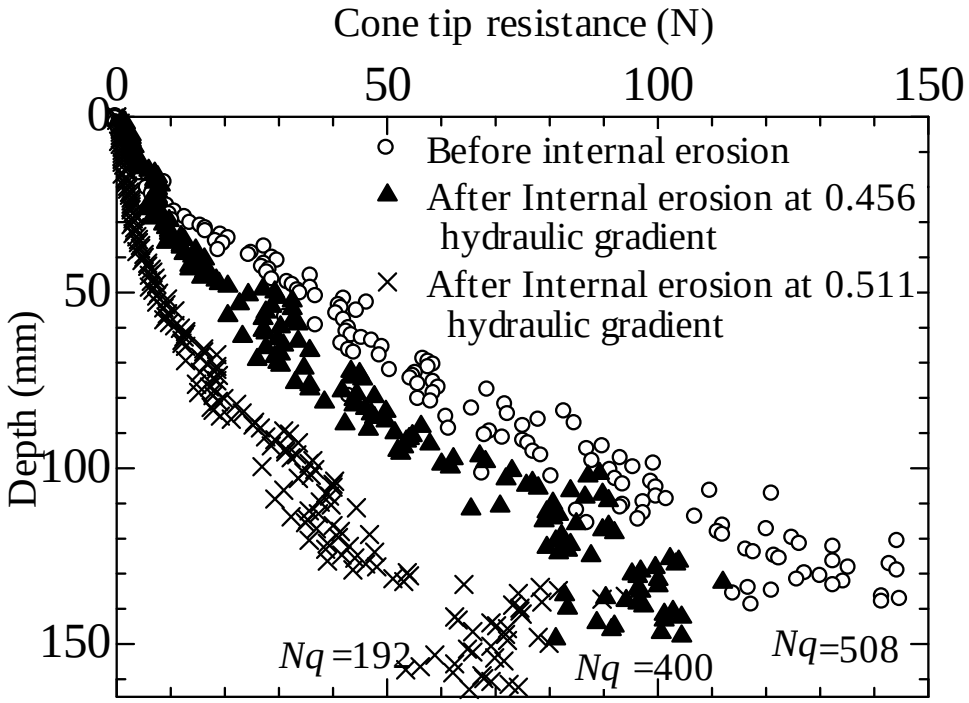

Figure 3.29 Cone resistance before and after internal erosion (specimen A-60)

3.6 Interpretation of resistance profiles

3.6.1 Review of Empirical correlation for CPT

The CPT data are interpreted into a mechanical parameter to make the CPT results easier to understand from an engineering point of view and to compare them with different cases. The approach of the interpretation is to develop empirical correlations between the cone tip resistance and the behavioral properties of soils (e.g., the angle of shearing resistance) based on various theories. Cone tip resistance is the measurement of the CPTs, and the behavioral properties of the soils are obtained from laboratory tests. The most practical model explaining the cone tip resistance is the bearing capacity theory, which is based on the limit equilibrium method proposed by Terzaghi and Peck (1948). This method assumed the failure mechanisms and then determined the failure load by assuming that the soil was a rigid-plastic material. However, it was criticized for not taking the soil compressibility into account, leading to unreliable predictions of the angle of shearing resistance (Vesic 1972). However, Janbu and Senneset (1974) reported a relationship between bearing capacity number N_q, the increment of cone resistance Δq_c and vertical effective stress $\Delta\sigma'_v$, and the angle of shearing resistance with little data scattering which indicated the limited influence of the soil compressibility. Work by Al-Awkati (1975) further proved that, for quartz sands, the shear strength had more influence on the cone resistance than the compressibility, and therefore, the bearing capacity theory could provide reasonable predictions. For silica sand, it is reasonable to empirically correlate the bearing capacity number (N_q) derived from CPTs and the drained angle of shearing resistance (ϕ'), which may commonly be represented as follows:

$$\tan\phi' = A_1 + A_2 \ln(\Delta q_c / \Delta\sigma_v') \quad \text{……. (3.8)}$$

where $\Delta\sigma'_v$ is the vertical effective stress increment at the depths where cone tip resistance increment Δq_c is measured ($N_q = \Delta q_c / \Delta\sigma_v'$). A_1 and A_2 are regression coefficients. Durgunoglu and Mitchell (1975) initially proposed a design chart to determine the angle of shearing resistance based on the bearing capacity theory. The curve fitting yields A_1= 0.215 and A_2=0.131. This method is found to be applicable to sands with low compressibility. Based on the calibration chamber test results on normally consolidated, moderately compressible, predominantly quartz sands, Robertson and Campanella (1983) showed a correlation in the form of a design chart, the regression coefficients of which are A_1= 0.194 and A_2=0.147.

3.6.2 Procedures for interpretation of resistance profiles

Following the common calibration procedure, the interpretation is performed to compare the measured cone penetration resistance, in terms of N_q, and the measured angle of shearing resistance from direct shear box tests. Since the tested specimens (A, B, C, D) mainly consist of silica No. 3, the frictional forces of which are primary in shear strength, several fully saturated specimens consisting only of silica No. 3 sand, are tested as well for calibration purposes. Those cases correspond to the extreme consequences of erosion which indicates all the fines are eroded. Details are given in Table 3.9. The calibration chamber is the same as that used in the seepage tests.

To avoid the possible bottom boundary effects, the cone resistance data for depths of 30 mm~100 mm are selected to evaluate bearing capacity number N_q. The bearing capacity number obtained from the cone resistance profile (Fig. 3.28) of specimens A, B, C and D at a relative density of 60% are shown in Table 3.10. In the same way as with the cone tip resistance, the bearing capacity number also decreases with the fine content. The bearing capacity number can be thought of as a mechanical parameter that can characterize the cone tip resistance. A reduction in the bearing capacity number due to internal erosion can be seen from Fig. 3.29. After internal erosion, the bearing capacity number decreases and the extent of the decrease in the bearing capacity number seems to be dependent on the imposed hydraulic gradient. This trend can be clearly noted from Fig. 3.30, which shows the relationship between the maximum imposed hydraulic gradient and the normalized bearing capacity number (the ratio of the bearing capacity number before and after internal erosion). For specimen A-60, after internal erosion at a hydraulic gradient of 0.45, bearing capacity number N_q decreases by approximately 30%, while at a hydraulic gradient of 0.54, N_q deceases by about 70%.

The angles of shearing resistance of the tested specimens are obtained by conducting constant pressure Direct Shear Box Tests. The apparatus consists of shear boxes, a guide for the shear boxes and a loading system for both vertical force and shear force. The soil specimens are prepared by the moist tamping method, ensuring similar soil conditions as in the seepage tests. Each tested specimen is subjected to shearing at a velocity of 0.2 mm/min, following JGS 0561-2000, to allow volume changes of the specimen, while the effective normal stress on the shear plane is maintained at a constant value. For the same specimen, four different normal stresses, 25kPa, 50kPa,

100kPa and 200kPa, are conducted. Typical shearing results for specimen A-60 are shown in Fig. 3.31.

Table 3.9 Details of tested specimens for interpretation

Specimens	D_r (%)	e	Mineralogy	Shape	N_q
Silica No.3	20	0.95	Mainly quartz	Subangular	26
Silica No.3	60	0.82	Mainly quartz	Subangular	84
Silica No.3	100	0.70	Mainly quartz	Subangular	938
Specimen A	60	0.51	Mainly quartz	Subangular	508
Specimen B	60	0.53	Mainly quartz	Subangular	609
Specimen C	60	0.54	Mainly quartz	Subangular	722
Specimen D	60	0.58	Mainly quartz	Subangular	1072

Table 3.10 Summary of changes in soil strength due to internal erosion

Specimen No.	Normalized bearing capacity number	Angle of shearing resistance (°)		Strength reduction, ΔR (%)	Max. imposed hydraulic gradient
		Before internal erosion	After internal erosion		
A-30	0.86	36.1	35.8	1.0	0.22
B-20	0.96	32.7	32.6	0.3	0.25
C-20	0.95	35.1	35.0	0.3	0.24
A-60	0.33	41.1	39.5	6.1	0.54
B-60	0.78	41.6	41.2	1.4	0.41
C-60	0.71	42.1	41.6	1.8	0.38
D-60	0.67	42.4	41.8	2.1	0.28

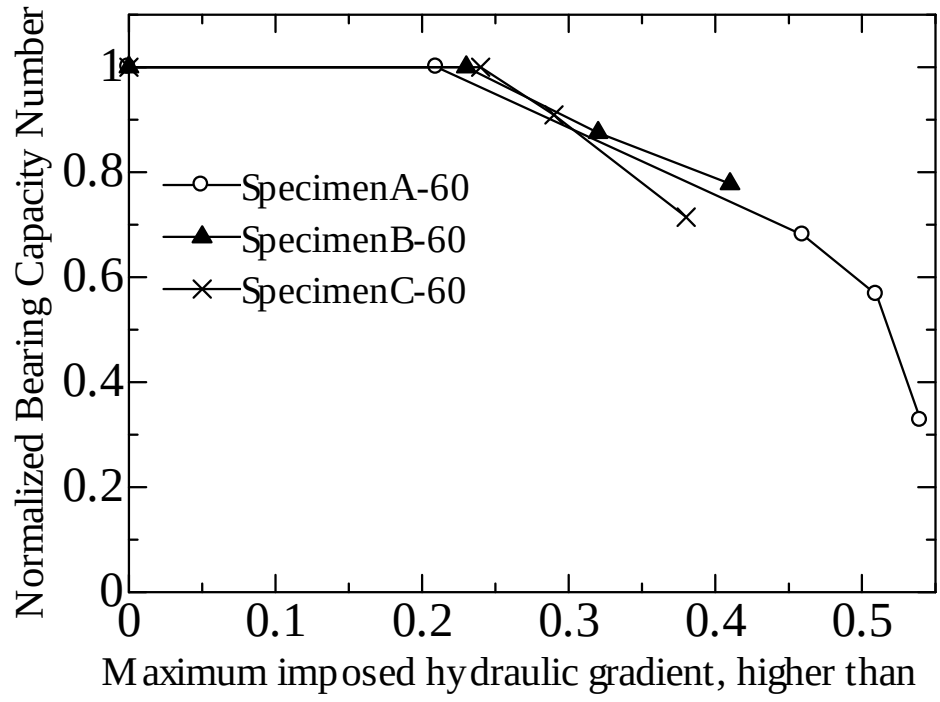

Figure 3.30 Relation between maximum imposed hydraulic gradient and normalized bearing capacity number

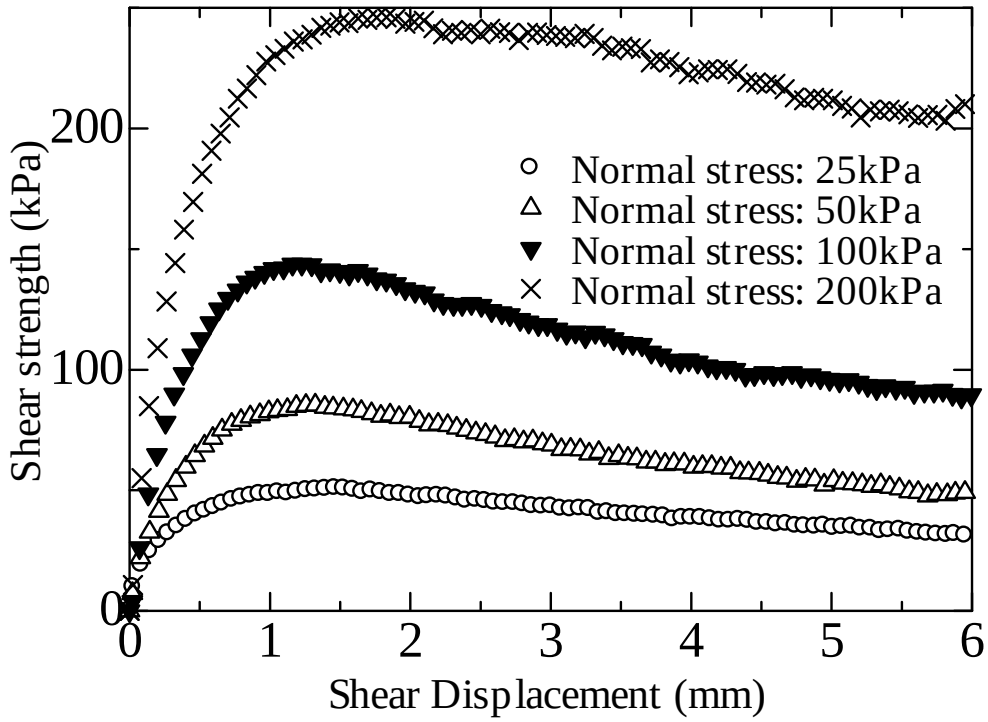

Figure 3.31 Relation between shearing displacement and strength (specimen A-60)

The comparison between the bearing capacity number from the CPT data and the angle of shearing resistance obtained from the direct shear box tests is shown in Fig. 3.32.

Due to the influence of compressibility, there is some scattering in the results. The best fitting curve by the logarithmic function is shown in Equation (3.9).

$$\tan\phi' \approx 0.573 + 0.1\ln(\Delta q_c / \Delta\sigma_v') \quad \text{..... (3.9)}$$

Since this empirical correlation compares two different shear modes, i.e., simple shear in the direct shear box and compression at the cone tip, it underestimates the angle of shearing resistance value due to the influence of compressibility (Robertson and Campanella 1983); and therefore, the strength reduction index in terms of $\tan\phi'$ may not reflect the actual strength reduction quantitatively. However, at least it may shed some light on how the internal erosion affects the strength parameter in general.

3.6.3 Interpreted strength of eroded soil

To make the comparison clear, the strength reduction is defined as the following based on this correlation:

$$\Delta R = 1 - \frac{\tan\phi'_{\text{post-erosion}}}{\tan\phi'_{\text{before-erosion}}} \quad \text{..... (3.10)}$$

Changes in the soil strength due to internal erosion for both the loose and the dense specimens are summarized in Table 3.10. After internal erosion, the cone tip resistance decreases, resulting in a decrease in the estimated angle of shearing resistance. The fines loss varies depending on the imposed hydraulic gradients. The relationship between the maximum imposed hydraulic gradient and the normalized soil strength (1-ΔR) is shown in Fig. 3.33. The larger imposed hydraulic gradient causes a further reduction in soil strength. Up to the imposed hydraulic gradient of 0.5, the changes in strength are gentle, while drastic changes can be seen with imposed hydraulic gradients over 0.5. However, the loss of fines does not increase with the imposed hydraulic gradient unlimitedly. Due to the limitation of the system, a large hydraulic gradient could not be imposed on the specimens. It could be inferred, however, that at a certain stage, the fines loss may be constant irrespective of the imposed larger hydraulic gradient. Correspondingly, an upper limit for the reduction in soil strength, due to the internal erosion, may exist, as shown in Fig. 3.34. It is worth mentioning that the hydraulic gradient addressed here is within the range of i_s and i_c. Out of this range, the soil may be stable or may fail.

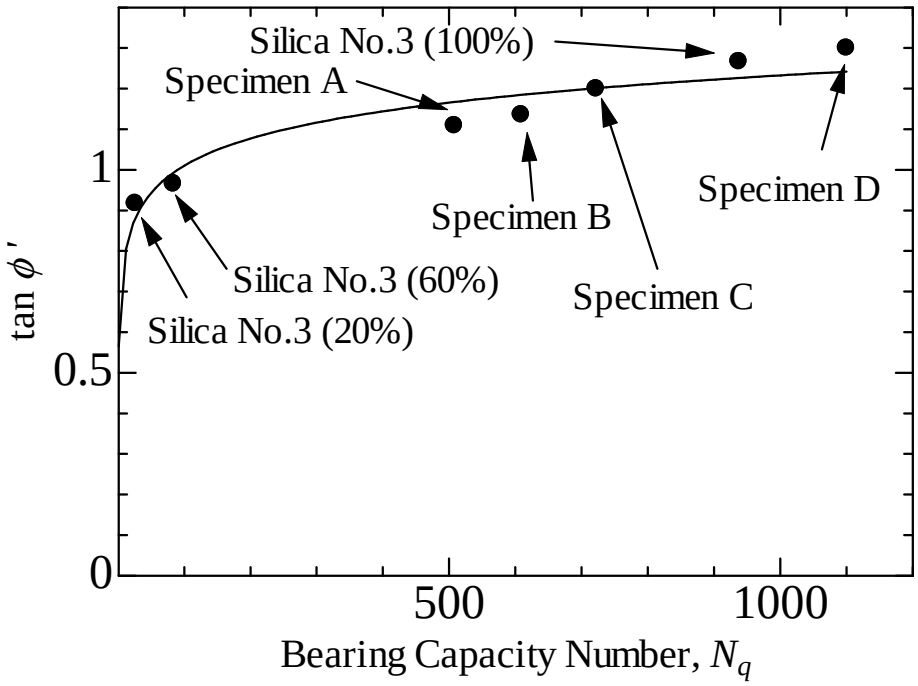

Figure 3.32 Relation between bearing capacity number and tanϕ'

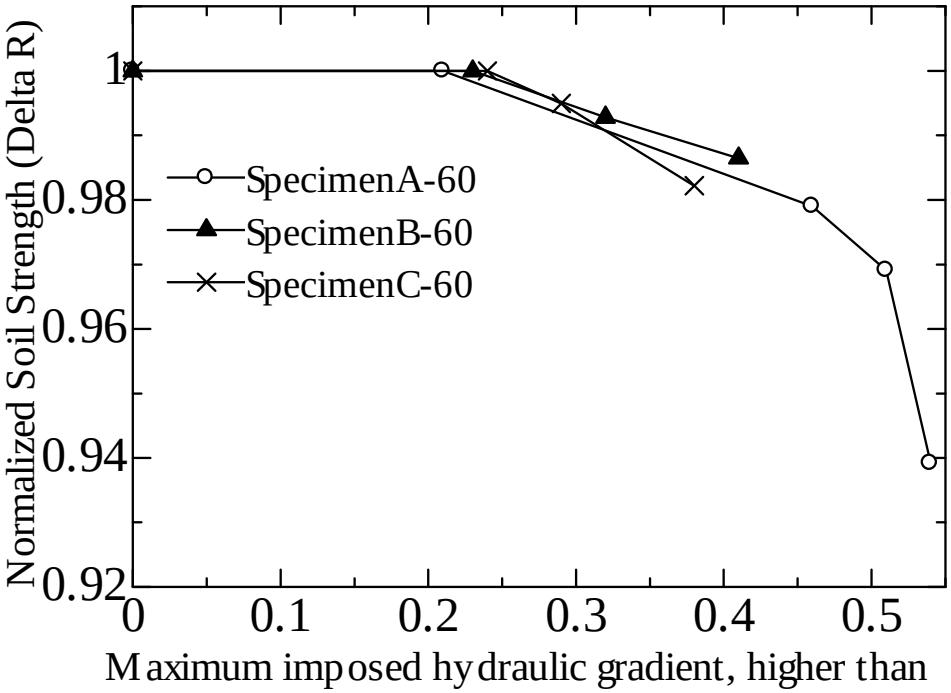

Figure 3.33 Relation between maximum imposed hydraulic gradient and normalized soil strength

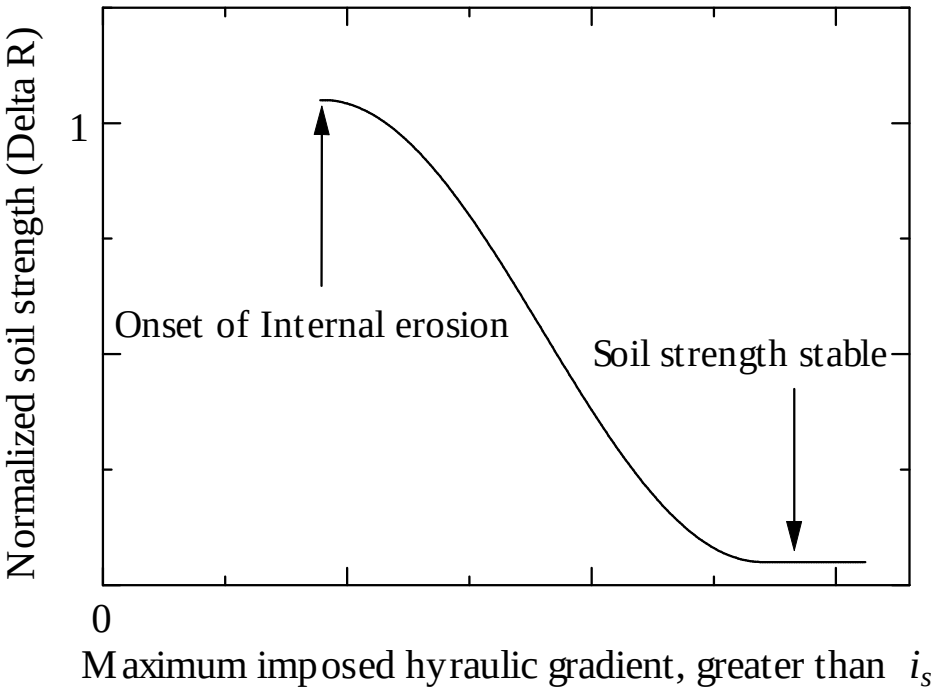

Figure 3.34 Hypothetical strength reduction curve against maximum imposed hydraulic gradient

3.7 Conclusions

The influence of internal erosion on soil strength has been experimentally studied through a series of one-dimensional upward seepage tests at a constant water head and cone penetration tests. By giving an upward seepage flow to the gap-graded soil specimens, internally eroded soils are created. The mechanical consequences of internal erosion are examined by cone penetration tests on internally eroded specimens.

Before the internal erosion, the relationship between the average hydraulic gradient and Darcy velocity is basically linear. After the onset of erosion, the slope of the relationship is no longer linear, indicating that the hydraulic conductivity of soils drastically increases with the progress of the internal erosion. The hydraulic gradient for internal erosion is found to be about one fifth to one third of the critical hydraulic gradient for soil stability. The lower the fines content, the larger the hydraulic gradient required to cause internal erosion. Those specimens containing the same mass ratio of fines as the larger relative density require a larger critical hydraulic gradient to initiate the internal erosion. The loss of fines proportionally increases with the imposed hydraulic gradient.

The internal erosion causes a reduction in cone tip resistance, the extent of which may be related to the imposed hydraulic gradient. A larger imposed hydraulic gradient, indicating a greater loss of fines, would lead to further cone resistance reduction. Drastic changes in the strength can be seen with hydraulic gradients over 0.5. The internal erosion causes the angle of shearing resistance of a soil specimen to decrease within a certain hydraulic gradient range.

CHAPTER 4

NEWLY DEVELOPED FLEXIBLE-WALL SEEPAGE PERMEAMETER

4.1 Introduction

It is universally recognized that seepage-induced erosion would lead to catastrophic consequences: approximately half of the dam failures are because of soil erosion (Richards and Reddy, 2007). Although it is such a huge potential risk for the earth structure safety, hitherto, few laboratory tests have been fully developed to comprehensively assess the mechanical consequences of internal erosion on sands by taking account of both monotonic and cyclic loadings. One of the main difficulties lies in guaranteeing a high saturation degree in soil specimens during erosion test, which may be hardly fulfilled in a conventional apparatus. Without a comparatively high saturation degree, laboratory tests on those internally eroded soils might not be well performed. Moreover, since internal erosion is chronic phenomenon, it would be better if the laboratory erosion tests could last for relatively long period. Upon those difficulties, this chapter presents a newly developed triaxial seepage apparatus, capable of maintaining back pressure in a soil specimen during erosion test and directly obtaining the mechanical response of internally eroded soils.

4.2 Description of apparatus

The newly developed triaxial internal erosion apparatus could directly investigate not only the hydraulic characteristics of soils at the onset and the progress of internal erosion but also the change of soil mechanical behaviors induced by internal erosion. It is applicable for testing non-cohesive soils. The design is improved after preliminary one-dimensional seepage tests in a fixed-wall permeameter of Chapter 3. The apparatus mainly consists of a constant-flow-rate control unit, an automated triaxial system and eroded soil collection unit. The recorded variables include the pressure differences generated by the seepage flow, soil axial and radial strain, cumulative eroded soil mass and pore pressures. The whole system allows independently synchronous control of the hydraulic condition and the stress state of tested specimens. Photograph of the overall system and the triaixial permeameter are shown in Fig. 4.1 and 4.2, respectively. The schematic illustration of the new apparatus is noted in Fig. 4.3.

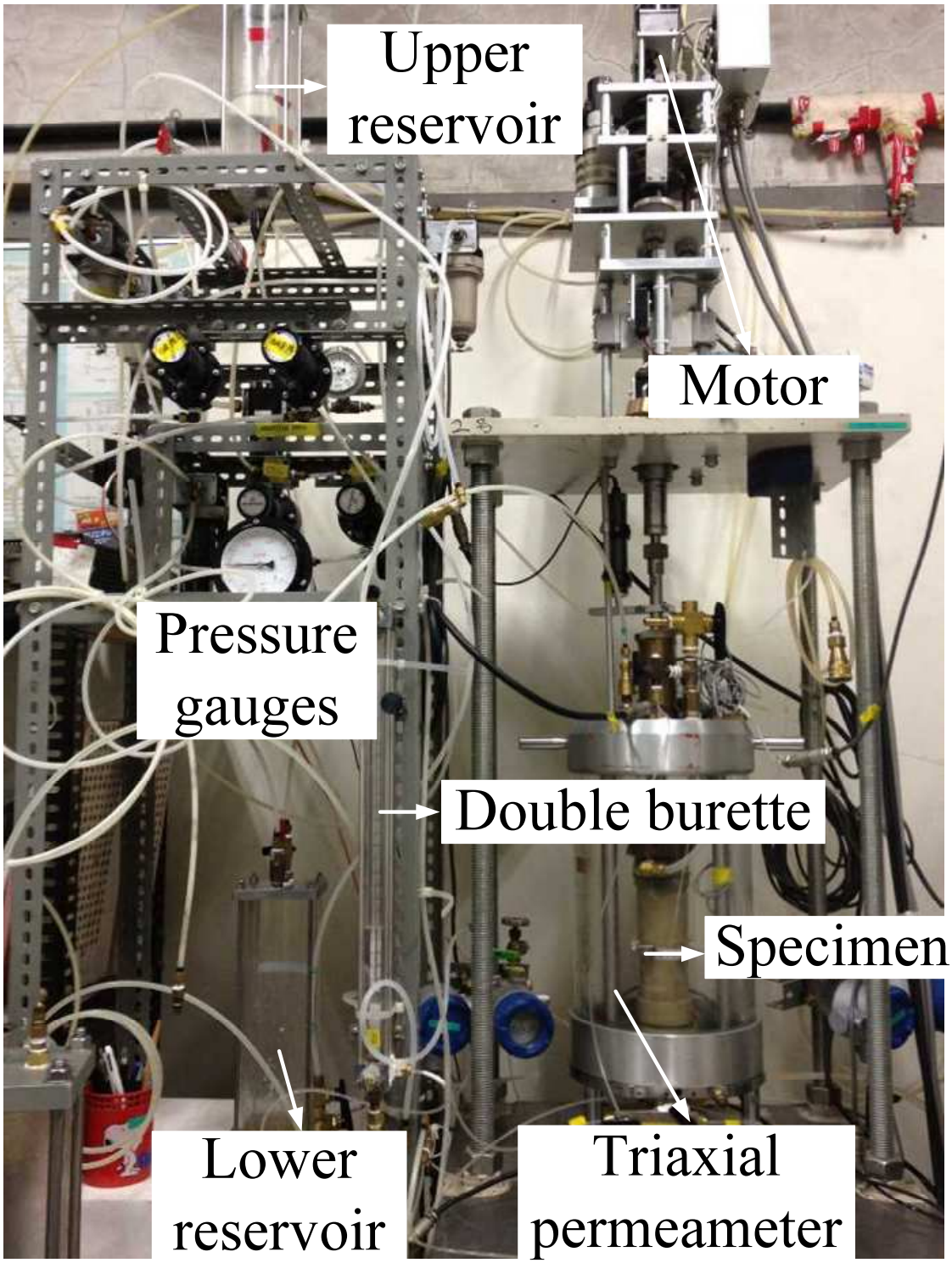

Figure 4.1 Photograph of whole system

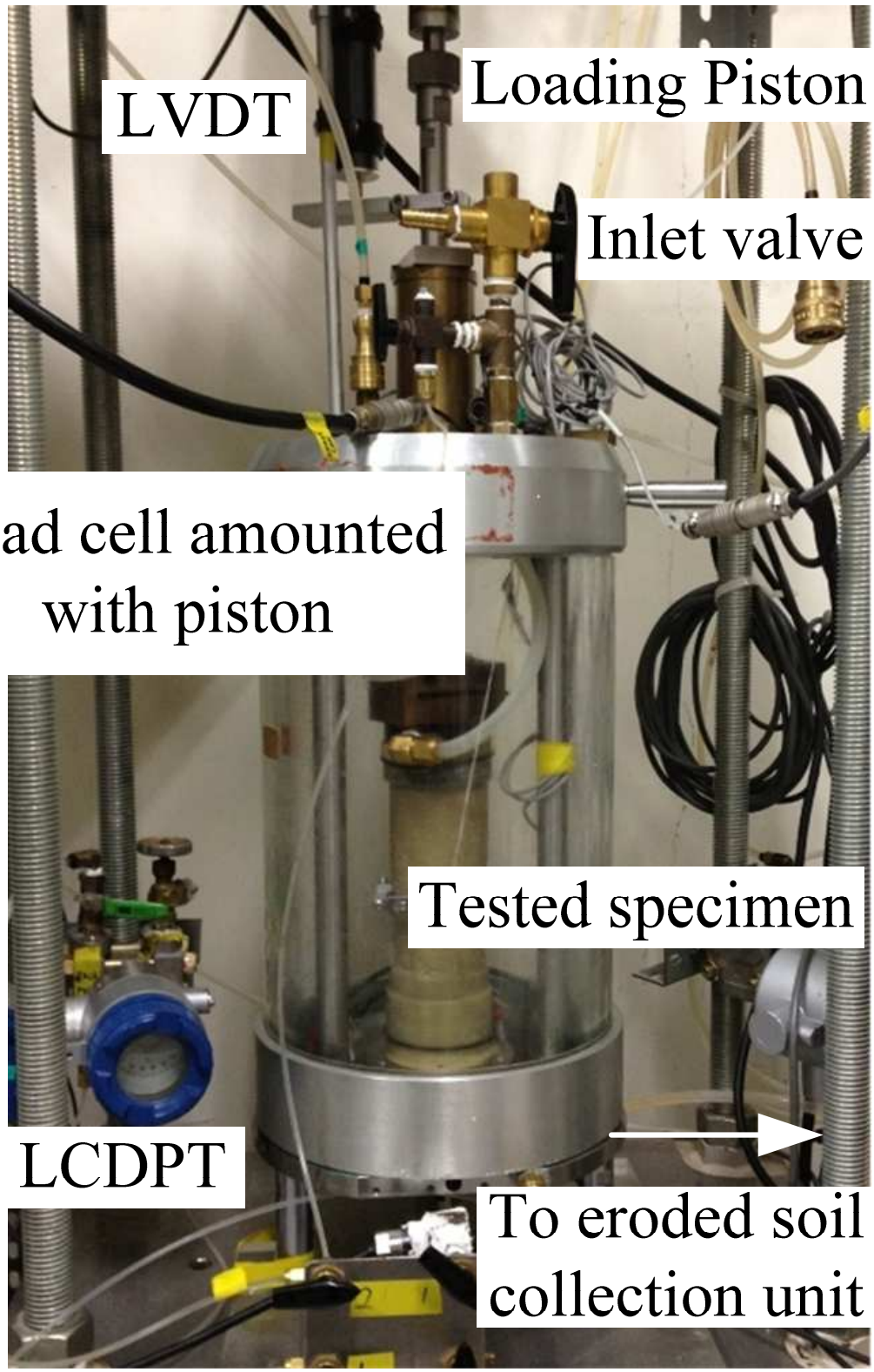

Figure 4.2 Photograph of triaixial permeameter

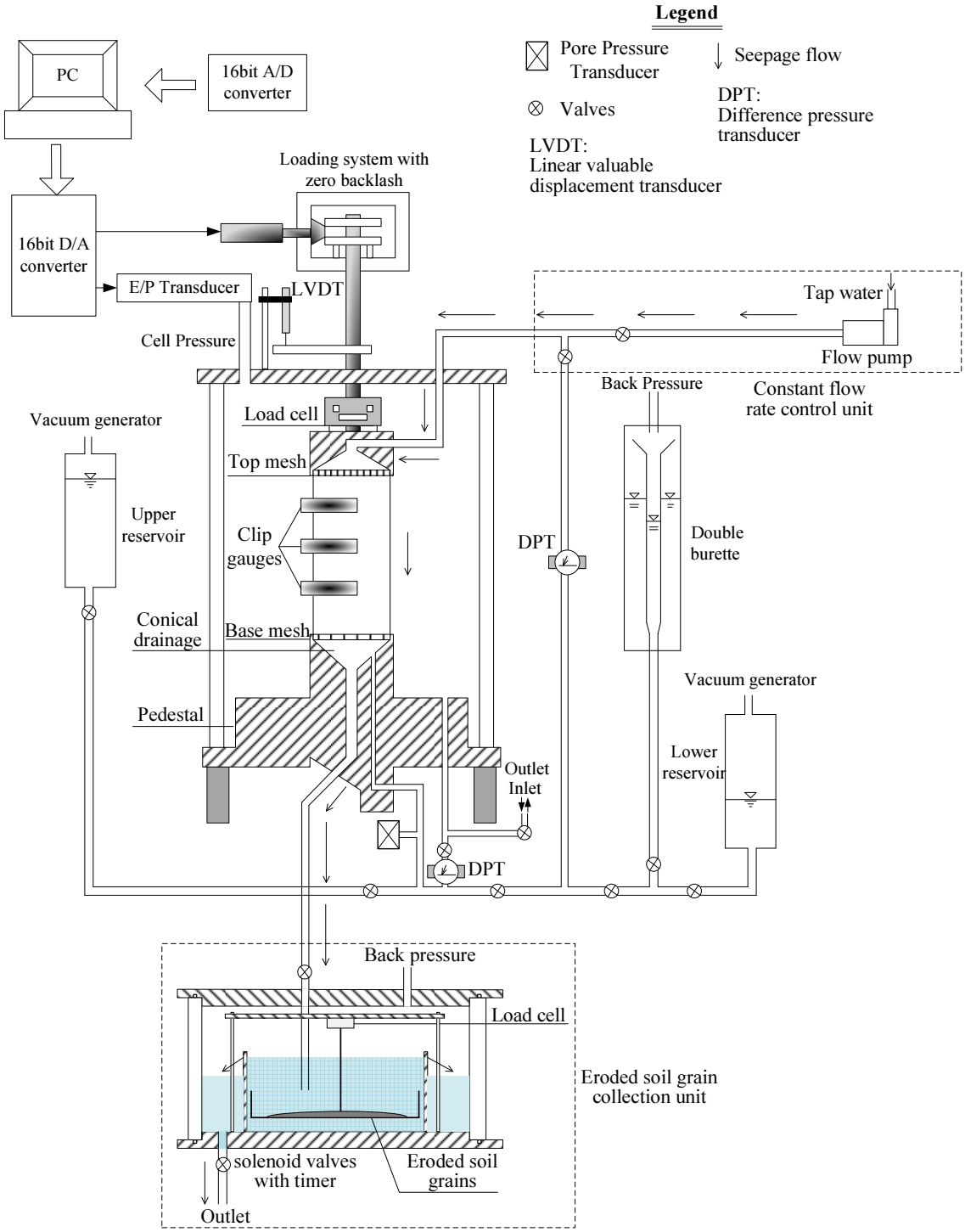

Figure 4.3 Schematic diagram of triaxial seepage test assembly

4.2.1 Constant flow rate control unit

Hydraulic gradient and Darcy velocity are the vital parameters for hydraulics. For those sands with large hydraulic conductivity (>0.001m/s), seepage test by the hydraulic-gradient-control method may not be appropriate because of the comparatively small hydraulic gradient to trigger and maintain the internal erosion. An accurate control of

the hydraulic pressure and estimation of the head loss in tubes, valves and fittings is necessary, which however is difficult in practice. The flow-rate-control mode, on the other hand, could avoid the above-mentioned difficulties. Richard and Reddy (2010) concluded that flow velocity might be the fundamental characteristic responsible for erosion in non-cohesive materials, which could yield more consistent results. In this apparatus, the seepage test is performed by the constant-flow-rate method. The control unit is composed of a rotary pump with the maximum flow rate of 1360mL/min for pumping water flow through the specimen and a low capacity differential pressure transducer (LCDPT) for measuring the pressure drop from the top to the bottom of tested specimens. The output of LCDPT is highly linear within the range of 0~20kPa. To maintain the flow rate constant, all the flow channels are designed to be the same size: 7.5mm-in-diameter plastic tubes with a relatively large amount of stiffness are used. To minimize the effect of tube stiffness on the measurement of deviator stress, the tube is arranged in spiral (Fig. 4.4). For common triaxial equipment, an annular porous stone is typically used at the interface between soil and water in the top cap. However, in this apparatus, instead of porous stone, a perforated plate is mounted in the top cap, which directly attaches to the specimen, to minimize the possible water head loss (The same as is at the pedestal, the details of which will be given later). The seepage water is pumped from a water tank, which is filled with water and kept at room temperature, at least 24 hours before use. Because the back pressure is maintained during seepage tests, the volume of the indissolved air bubbles in seepage flow may be shrunk and their influence on the soil saturation degree may be minimized. During the experiment, the range of the assigned inflow rate must ensure the resulting pressure drop is well below the confining pressure to prevent the separation of membrane from the soil specimen.

4.2.2 Automated control unit

The automated triaxial system used, which is capable of investigating either the static or cyclic soil behavior, could conduct measurements and controls by PC through 16-bit A/D and D/A converters. The triaxial cell allows test specimens of 70mm in diameter and 150mm in height. The main tie bars of the cell are internal which permits connections of top cap and load cell, and attachment of strain transducers before sealing down the pressure cell. The vertical load could be automatically applied by a motor-gear system at any rate. The maximum load is 50kN. The system has zero backlash on reversal of the load, which would realize the continuous cyclic loading without any stress relaxation. The cell pressure is applied by the air pressure which is maintained constantly at 700kPa through an automatic air compressor. All the pressure lines are connected to a drying system to remove any condensed water. The control of the cell pressure is by E/P (Electronic to Pneumatic) transducers, which are linked to a PC through a 16-bit D/A board. The axial load is measured by the load cell internally mounted above the top cap, which eliminates the effects of any friction on the loading shaft. The soil effective pressure is known from another Difference Pressure Transducer, which joins the specimen base and cell. Pore pressure is obtained at the base of a specimen by a pressure transducer mounted at the pedestal. All the measuring devices are connected to amplifiers and then to a PC through a 16-bit A/D converter. All of the controls of the triaxial testing and data recording are through a program with the interactive visual interface, written in Visual C++.

Figure 4.4 Details of spiral tube

The base pedestal is specially designed to accommodate the internal erosion test (Fig. 4.5). The main component is the drainage system to prevent the possible accumulation

of eroded soil at the bottom, which would cause clogging. It includes a conical trough and a plastic tube fitted at the outlet of the trough, directly connected to the soil collection system. This space gives freedom in determining the filter, either the granular type or the wire mesh with openings. A paradox comes up in the filter determination. For soil element test, it is significant to ease the influence of boundary frictions on the measured material properties. In practice, to minimize the non-uniformity in stresses and strains induced by end restraint, a lubrication layer, such as a silicone grease layer or latex rubber is utilized (Kuwano *et al.*, 2000). However, that layer would cause great water head loss and serious clogging during erosion test because of the high viscosity. A compromise in free ends may be necessary. In this apparatus, the filter is the 5mm-thick steel mesh with a smooth surface (Fig. 4.6). The opening size of the mesh follows the recommendation of Japan Dam Conference which specified that the mesh should fully hold the coarse grains and permit the erosion of fines (Uno, 2009). The adopted opening size is 1mm in this apparatus.

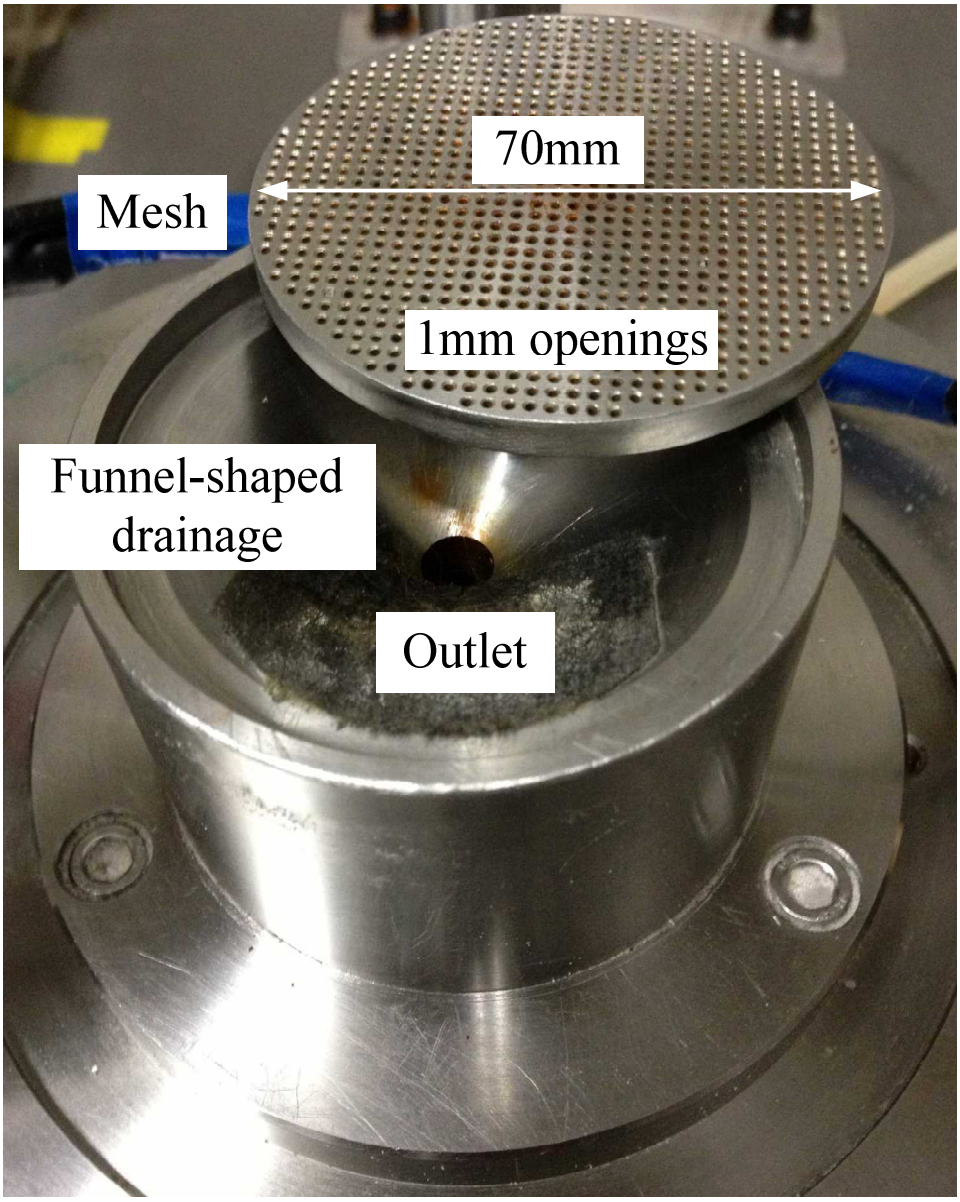

Figure 4.5 Base pedestal

Figure 4.6 Two 5mm-thick meshes (1mm opening)

4.2.3 Eroded soil collection unit

The main component of the eroded soil collection unit is the pressurized sedimentation tank (Fig. 4.7). The acrylic tube is mounted between a steel top and base plate, and is sealed by means of O-rings and five external tie rods. Inside of the tank, a 160mm-in-diameter acrylic cylinder full of water is built in. During the seepage tests, the discharge effluent with dislodged fines directly flows into the cylinder through a pipe that connects the inlet valve and the cylinder. The end of the pipe is fully submerged in the cylinder to prevent the admission of air bubbles into the tested soil specimen. The cumulative eroded soil mass is gained by continuously weighing the light tray, which is fully submerged in the cylinder to collect the eroded soil grains. The waterproofed load cell that has high sensitivity could record the cumulative eroded soil weight within a continuous period. The theoretical resolution of the load cell is 0.00015N (approximately 0.015g). Because of the magnitude of noise and zero shift induced by the data collection system, some deviations may exist. To drain off the seepage water, a solenoid valve with timer is fixed at the outlet drainage line. The valve is capable of opening and closing at a determined interval of time. During erosion tests, the back pressure in the tested soil specimen is maintained through the sedimentation tank.

4.2.4 Transducers for measurement

A submersible load cell is employed to measure the soil response in vertical direction. The soil effective stress is measured by a Difference Pressure Transducer (DPT), which joins the specimen base and cell (Fig.4.8). Pore pressure is obtained at the base of a specimen by a pressure transducer mounted at the pedestal. During seepage test, a Low Capacity Differential Pressure Transducer (LCDPT) is utilized for measuring the

pressure drop from the top to the bottom of tested specimens. To reconfirm the hydraulic drop, another pressure transducer is installed to monitor the water pressure at the top of tested specimens. The cumulative eroded soil mass is gained by the submersible load cell with high sensitivity (Fig.4.9). An outer Linear Variable Differential Transformer (LVDT) (Fig.4.10) is used to monitor the vertical displacement while three pairs of clip gauges with the capacity of ±2mm are attached to tested specimens to gain the radial deformation (Fig.4.11). The voltage output of each transducer is adjusted to fit within the optimized range of the 16 bit A/D converter. The calibration procedures are conducted against a reference standard (Head, 1998). The calibration and regression characteristics of the transducers are summarized in Table 4.1.

Figure 4.7 Eroded soil collection unit (sedimentation tank)

Figure 4.8 Difference Pressure Transducer

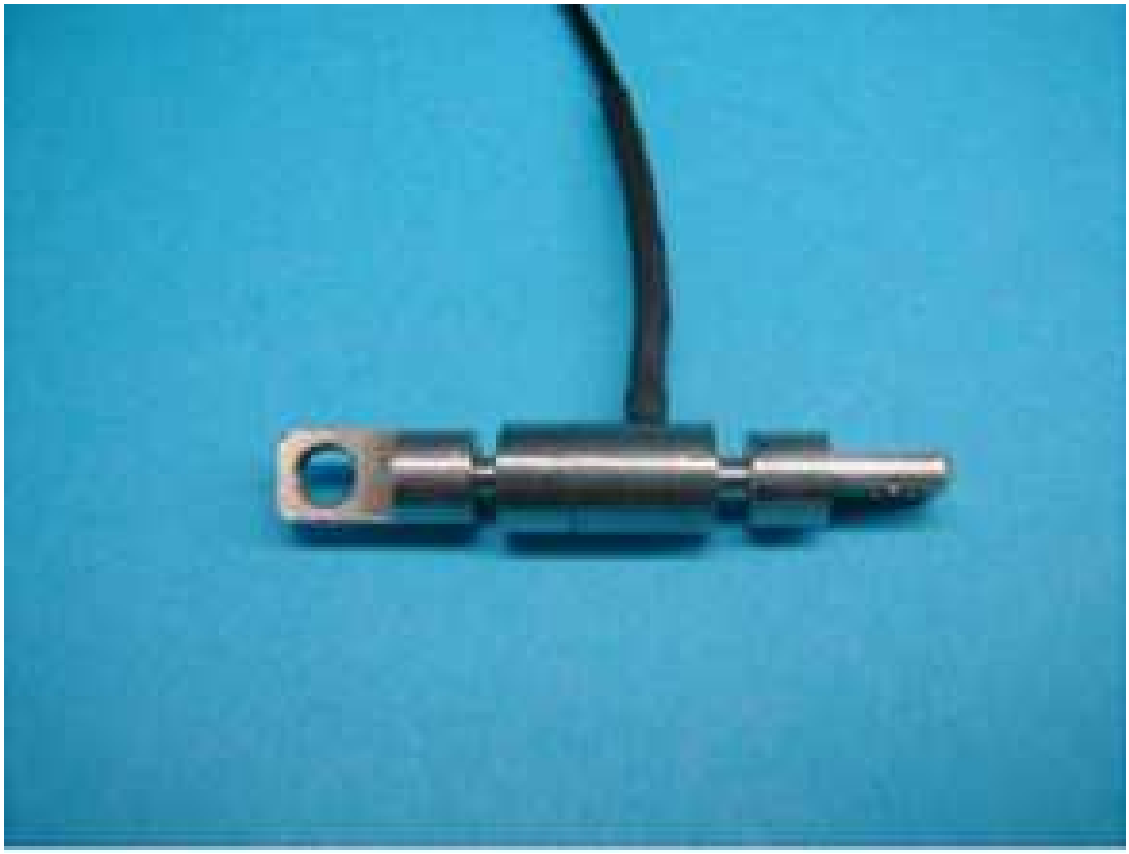

Figure 4.9 Miniature load cell

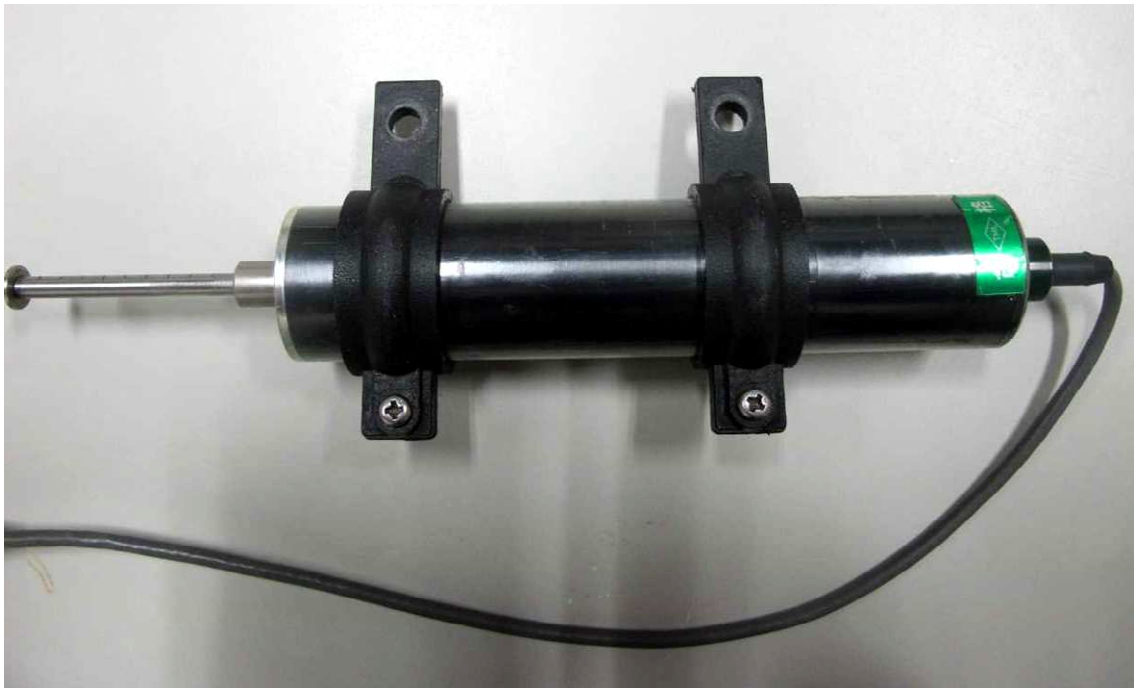

Figure 4.10 Linear Variable Differential Transformer (LVDT)

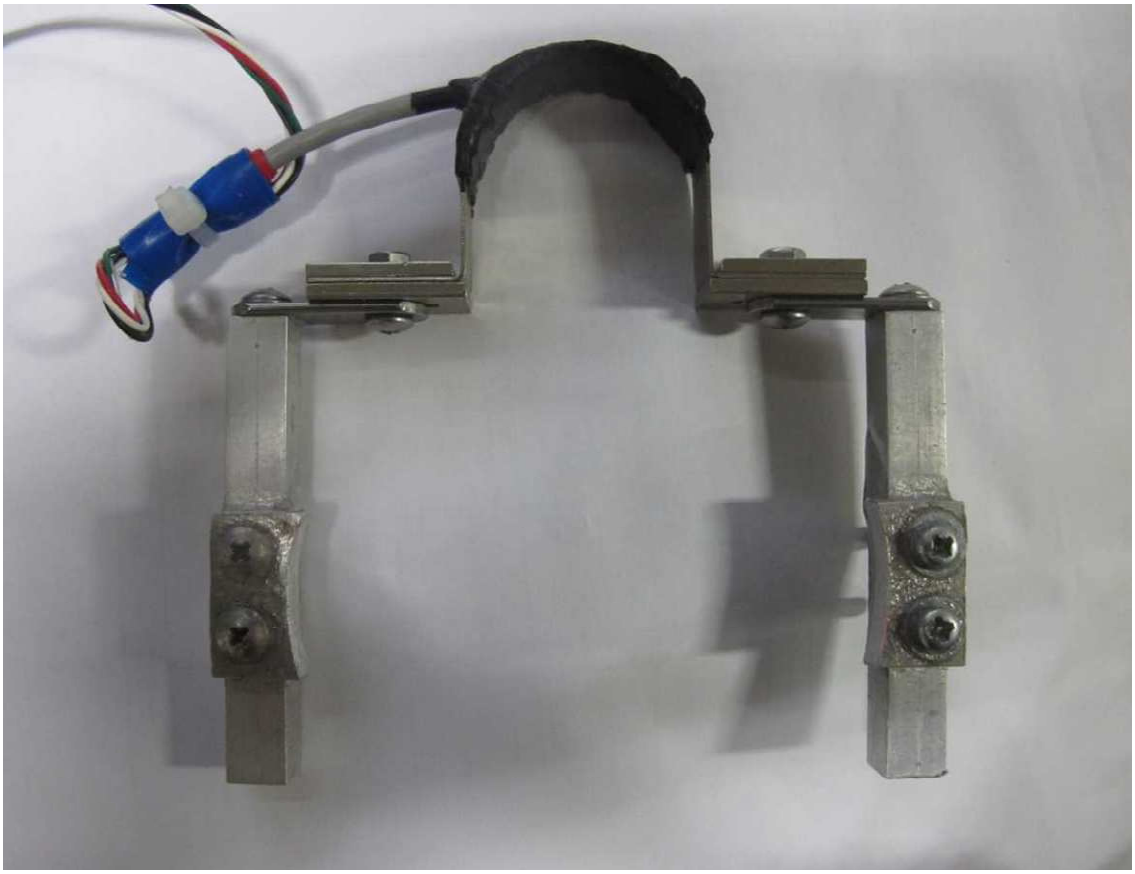

Figure 4.11 Radial Displacement Transducer (RDT)

Table 4.1 Calibration and regression characteristics of transducers

Trans.	Calibrated against	Range	Type of regression	Coefficient of correlation	Accuracy[9] (%)
Load cell[1]	Dead Weight	0~1500 (N)	Linear	0.99999	0.48
LVDT[2]	Micrometer	0~20 (mm)	Linear	1.00000	0.08
DPT[3]	Pressure gauge	0~400 (kPa)	Linear	0.99999	0.09
LDPT[4]	Pressure gauge	0~20 (kPa)	Linear	0.99997	0.92
PPT (Top) [5]	Pressure gauge	0~400 (kPa)	Linear	1.00000	0.35
PPT (Base) [5]	Pressure gauge	0~400 (kPa)	Linear	1.00000	0.40
Load cell[6]	Dead Weight	0~0.5 (kg)	Linear	1.00000	0.10
RDT1[7]	Micrometer	-2~+2 (mm) [8]	Linear	1.00000	0.28
RDT2[7]	Micrometer	-2~+2 (mm) [8]	Linear	1.00000	0.17
RDT3[7]	Micrometer	-5~+5 (mm) [8]	Linear	1.00000	0.25

Note:
(1) Load cell for measuring axial load (N);
(2) Linear Variable Differential Transformer for measuring axial deformation (mm);
(3) Difference Pressure Transducer for measuring effective stress (kPa);
(4) Low Difference Pressure Transducer for measuring pressure drop during seepage test (kPa);
(5) Pore Pressure Transducer for measuring water pressure at top and bottom of tested specimen, respectively (kPa);
(6) Miniature load cell for measuring cumulative eroded soil mass (g);
(7) Radial Displacement Transducer (mm);
(8) "-" and "+" means extension and compression, respectively;
(9) Percentage of the maximum error in a calibrated range.

4.3 Test procedures

The purpose of the study is to investigate the erosion characteristics of the cohesionless soil and its mechanical consequences. Therefore, the main testing procedures include erosion tests on the reconstituted soil specimens, monotonic compression or cyclic shearing tests on the eroded specimens, and post-erosion grain size distribution analysis. A detailed description of each procedure is presented as following:

4.3.1 Before test

Deaerated water should be prepared before tests by filling the reservoirs with tap water and constantly applying the possibly maximum vacuum for at least 24 hours. Zero balance and span adjustment of all the transducers and E/P transducers should be conducted. To fully remove the air in connection lines, the prepared deaerated water should be run through all the pipes for minutes. Then dismantle the cell and check the pressure lines. It is significant that all the pressure lines are free from air bubbles.

4.3.2 Specimen preparation

The tested specimen is 70mm in diameter and 150mm in height. The technics of moist tamping (Ladd, 1978) is employed to prevent the segregation of the two different sized grains. The method is developed based on the fact that when typical sand is compacted in layers, the compaction of each succeeding layer may further densify the layers below. The concept of "undercompaction, U_n" is recommended to assess the effects of densification. It indicates how great a percentage a layer should be to be less densified than the target value. In this study, a non-linear average undercompaction criterion, which is proved to be reliable in generating uniform soil conditions (Jiang *et al.*, 2003), is adopted. The average undercompaction of each layer in a moist tamped specimen is shown in Fig. 4.12.

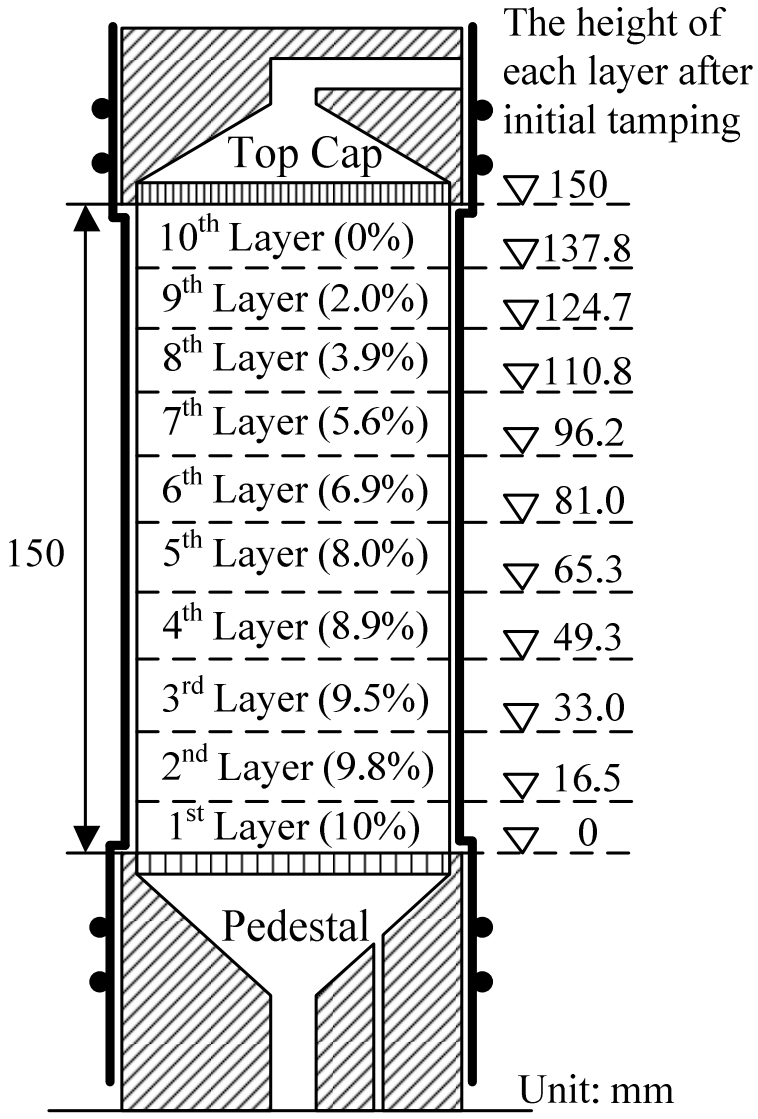

Figure 4.12 Average undercompaction of each layer

The specimen preparation procedures are as follows: determine the oven-dried weights of clean sand for a test according to the fines content and relative density. The initial water content is determined as 10% from previous trial and error, at which a uniform specimen would be achieved. Thoroughly mix the soils with deaerated water to make sure the distribution of fines in a specimen is uniform. Equally separate the wet mixture into 10 pieces and keep them in a zipped bag to equalize moisture at least 16 hours before use. The specimen is prepared layer by layer. Weigh the amount of material required for each layer, and place it into the mold by scoop. Each layer is compacted to the required height determined by “undercompaction”. The initial soil weight could not be directly checked after preparation. Therefore, the after-test oven-dry weight of the soil specimen together with the eroded soil weight should be checked.

4.3.3 Saturation and consolidation

The vacuum saturation procedure (ASTM D4767-11; JGS 0525-2000), including two stages, is adopted in this study. The top and bottom of the tested specimen is connected to two separate reservoirs. After specimen preparation, vacuum is introduced into the specimen through both water reservoirs gradually until it reaches -80kPa. The pressure difference between the specimen pressure and the cell pressure is kept constant as 20kPa during the incremental introduction of vacuum. Deaerated water is allowed to be slowly injected into the specimen upwardly. The inflow rate should be sufficiently slow to avoid the filtration of soil grains in the specimen. After three-quarters of the deaerated water has flowed through the specimen, slowly return the specimen pressure to 0kPa and increase the cell pressure to 20kPa, keeping the pressure increment constant as 20kPa throughout the process. The remaining deaerated water of the upper reservoir is then injected into the specimen again. A total water volume of 10.4 (normalized value in terms of pore volume) has been flowed through the soil specimen. The inlet valve of sedimentation tank should be closed completely to avoid any possible soil grain loss.

The application of back pressure begins after the completion of the vacuum saturation procedure. In this apparatus, back pressure could be applied from either the double burette or the sedimentation tank (Fig. 4.3). Both of them are pressurized simultaneously and connected to the tested specimen. Initially the valve connected to the sedimentation tank is closed. The cell pressure and back pressure are increased incrementally with the drainage valves to the double burette, which is connected to the top and bottom of the specimen, opened. The size of each increment is 50kPa. For the majority of tests, a B-value of higher than 0.95 could be achieved after applying a back pressure of 100kPa. At this circumstance, the pressure inside the sedimentation tank reaches 100kPa as well. Then close the double burette valve and slowly open the sedimentation tank valve. Minor adjustments might be necessary to ensure the back pressure reaches 100kPa and then wait until the readings from pressure gauges become stable. The recordings of the load cell inside the sedimentation tank indicate that there is hardly fines loss because of the application of back pressure.

The consolidation is performed by an automatic control system. Cell pressure gradually increases up to the target value at a fairly low increment (i.e., 1kPa/min) to avoid soil grains migration. Axial stress, controlled by a motor, increases correspondingly to keep

the determined effective stress ratio (effective axial stress/effective radial stress) constant. In this study, soil specimens are isotropically consolidated until the preferred stress state is reached. After consolidation, the specimens are ready for erosion tests.

4.3.4 Erosion test

From the erosion test, the detection of critical Darcy velocity is expected, at which internal erosion initiates. To sufficiently demonstrate the mechanical effects of internal erosion on soils, the imposed inflow rate for each specimen should be held constant as a reference. After several trial tests, an inflow rate of 310mL/min for the tested soil is selected because the loss of fines at this rate is significantly large, which would highlight the differences between the eroded specimen (ES) and the non-eroded specimen (NS) in terms of stress-strain relationship. The procedure for the inflow rate increments in this study is shown in Fig. 4.13. Based on the test results of Chapter 3, the initiation of internal erosion would occur at a fairly low Darcy velocity, which is approximately 0.02~0.12cm/s (i.e., equivalent to the inflow rate of 48mL/min~277mL/min through a 70mm-in-diameter circular section) depending on the density and fines content of the tested specimen. Therefore, the initial increment of inflow rate is set approximately at 10(mL/min)/min: increase the inflow rate to 10mL/min in 1min and allow the seepage flow to become steady for the next 1min. The trial tests indicate that a short duration (e.g. 1min) is sufficient to stabilize the seepage flow. As long as erosion initiates, the amounts of eroded fines would increase with the increase of inflow rate. The increments of inflow rate at this stage could be relatively larger to shorten the test. Then in this study, the inflow rate is increased to the target value of 310mL/min at increments of 50(mL/min)/min once the it reaches 100mL/min. This inflow rate of 310mL/min will be maintained constant until (1) the recorded hydraulic gradient is steady; (2) the effluent become clear and clean by visual observation; (3) there are no further eroded fines loss (i.e., <0.2g per 10min); and (4) there are no further increases in the axial and radial strain of the tested specimen. Commonly, the erosion test would be terminated after 3 hours. The inflow rate is decreased gradually till there is no pressure difference between the top and bottom of the specimen. Then close the inflow valve and let the specimen stay still until the readings of the pressure gauges become stable. The B-value is checked again.

The stress state of the specimen during the erosion test is maintained the same level as after isotropic consolidation. The cumulative eroded fines mass is recorded automatically by the load cell inside of the sedimentation tank. The balance of the light tray is realized by the following procedure: before the erosion test, the cylinder is filled with deaerated water so that the light tray is fully submerged. After applying the target pressure of 100kPa to the sedimentation tank, the tray would reach equilibrium within 10min. Then set the readings of “eroded soil mass” as zero and start recording. During the erosion tests, it is found that the readings of the cumulative eroded soil mass were influenced by the impact force, generated from the flow jet. It became obvious if larger inflow rate was assigned. To minimize the effect of the impact force on the light tray, a funnel with a 15mm-in-diameter opening at the end has been fastened on the steel frame to surround the inlet pipe. The position of the funnel outlet is aligned with the tray center. The details are shown in Fig. 4.14. It works as a buffer that could decrease the

velocity of flow jet as well as a drainage that could facilitate the eroded fines uniformly settled down onto the light tray. The axial displacement, radial deformation and the pore water pressure difference generated by the seepage flow is recorded at every 1s automatically.

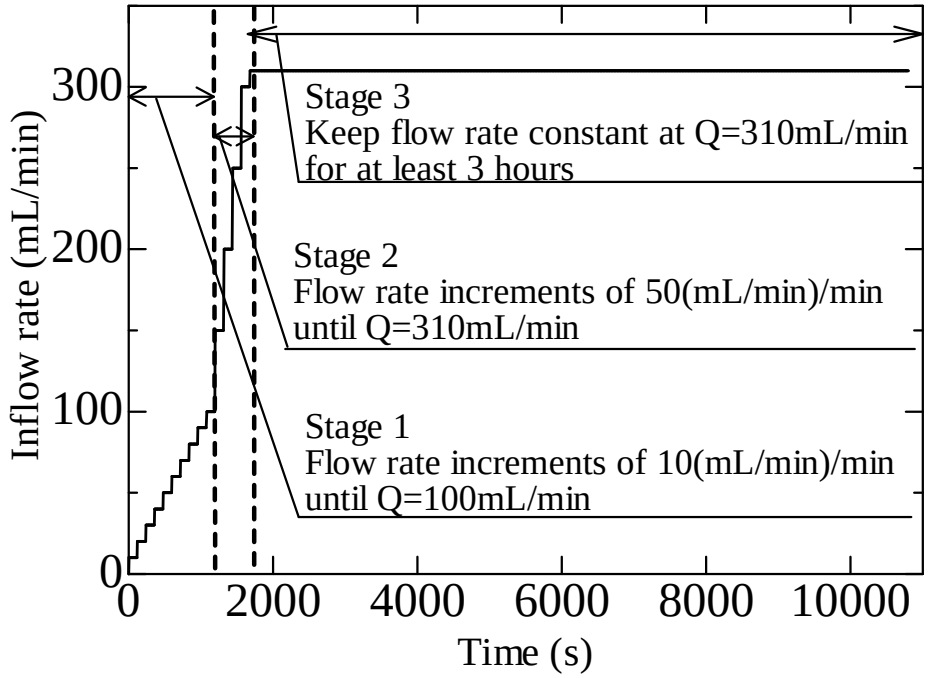

Figure 4.13 Inflow rate increments for seepage test

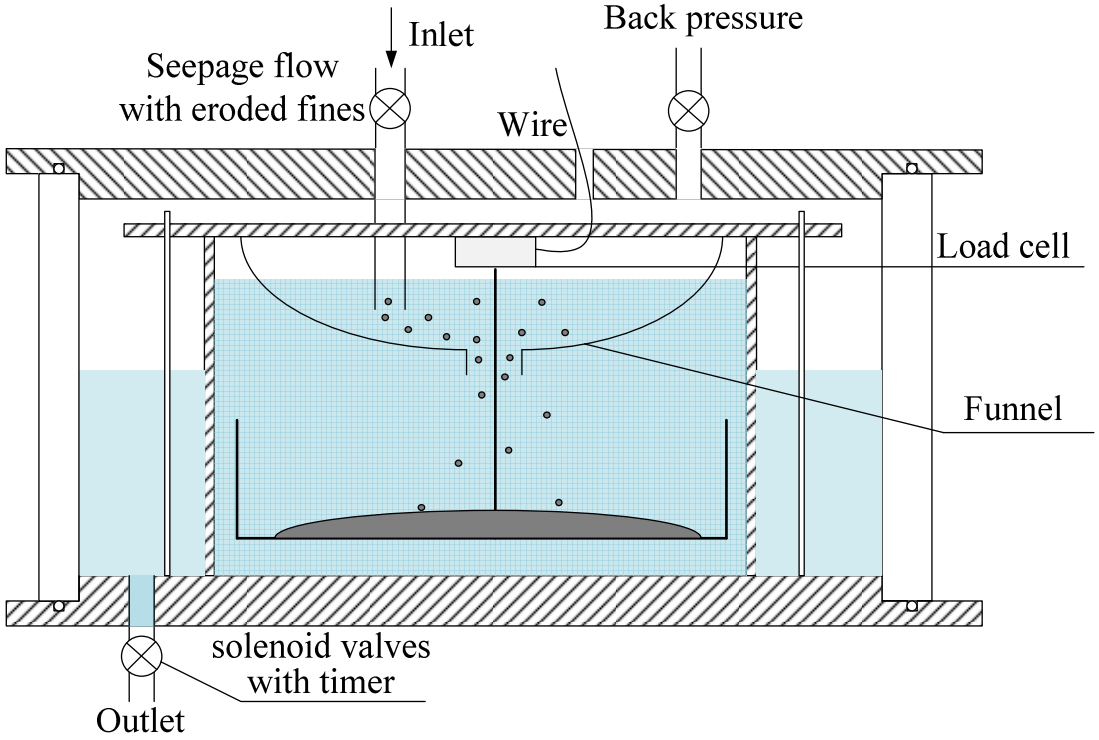

Figure 4.14 Schematic diagram of improved eroded soil collection unit

4.3.5 Undrained and drained monotonic tests

Undrained and drained compression test is performed at the same stress state as that of erosion test to investigate the mechanical consequences of internal erosion. The compression test is displacement controlled with the axial strain rate of 0.1%/min, following the standard criteria (ASTM D4767-11; ASTM D7181-11; JGS 0524-2000; JGS 0525-2000), to allow the pore pressure to reach equilibrium. The confining pressure is maintained constant, whereas axial displacement increases at the designated strain rate. Axial stress could be obtained from the load cell amounted to the piston. The recorded data from the eroded soil collection unit indicate that there is hardly fines loss as a result of compression.

4.3.6 Undrained cyclic tests

To quantify the effect of internal erosion on the cyclic resistance, undrained cyclic tests are performed on the eroded specimens. After erosion test, the soil specimens are subjected to a cyclic shear stress in axial direction under the same effective confining pressure as that of erosion test with a determined cyclic stress ratio. The axial strain rate is 0.5%/min, which is sufficiently slow to allow the equilibrium of pore pressure in the tested specimens.

4.4 Summary

A newly developed triaxial internal erosion apparatus, capable of directly investigating not only the hydraulic characteristics of soils at the onset and the progress of internal erosion under preferred stress state but also the mechanical behaviors of those internally eroded soils, is presented. By introducing a sedimentation tank, back pressure could be maintained in the tested specimens during erosion test to ensure a relatively high saturation degree. A measurement system of the cumulative eroded soil mass is installed in the tank to continuously record the eroded soil mass. Erosion tests are performed by constant-flow-rate control manner with the measurement of the induced pressure difference between the top and bottom of the tested specimens. Volumetric strain of the soil specimen could be assessed by measuring the axial and radial deformation. The mechanical consequences of internal erosion could be evaluated by directly performing undrained and drained compression tests or undrained cyclic tests on the eroded soil.

The soil specimens are prepared by moist tamping method, which could prevent the segregation of fines from coarse grains. Full saturation is achieved by standard vacuum procedure followed by the application of back pressure on specimens. The reconstituted specimens are isotropically consolidated into target mean effective stress and then seepage tests are conducted at the same stress state. For the soil strength test stage, the axial strain rate is maintained sufficiently slow to ensure the full equilibrium of pore pressure in specimens.

CHAPTER 5

SOIL HYDROMECHANICAL BEHAVIOR IN TRIAXIAL SEEPAGE TEST

5.1 Introduction

A comprehensive understanding of the erosion mechanisms and the post-erosion soil behavior is beneficial to the estimation of erosion progress and is helpful for the retrofit of internally eroded soil structures, such as levees. In this chapter, by using the newly developed triaxial seepage apparatus capable of maintaining back pressure in the soil specimen during seepage test and directly measuring the cumulative eroded soil mass within the test period, the erosion mechanism for saturated gap-graded cohesionless soil under the isotropic confining pressure is elaborated. The representative erosion-induced variation of soil hydraulic conductivity, volumetric strain and void ratio is presented first. Then the influence of the effective confining pressure and initial fines content is discussed by the comparison of the testing data with the representative data.

5.2 Tested specimens

Gap-graded soils, like sandy gravels, are more prone to internal erosion due to its deficiency in certain grain size (Skempton and Brogan, 1994). They may be detected at the earth dams that have been suffered from years of erosion or the construction site with substandard procedure of soil mixing leading to the omission of amounts of soil grains. In this study, the tested sand includes two types of silica sand (silica No.3 and No.8) with the same specific gravity of 2.645 but different dominant grain sizes, the same is described in Chapter 3. They are commercially available sands, frequently used as industrial polishing materials. The silica sand is mainly composed of quartz, and categorized as sub-round to sub-angular material. Before testing, they are fully washed and dried to remove possible impurities. Micro observation of the dry mixtures of silica No.3 and No.8 by a digital microscope at a total magnification of 100X is shown in Fig.5.1. According to the Standard Practice for Classification of Soils for Engineering Purposes (ASTM D2487-11), silica No.3 and No.8 corresponds to medium sand and fine sand, respectively. With larger grain size, silica sand No.3 works as the coarse fractions which are regarded as soil skeleton in the mixture, whereas, silica No.8 is the erodible fines. Hereafter, without specification, the term “fines” is referred to silica No.8 for simplicity even though it is not strictly classified as fines. In Chapter 3, the estimated maximum mass fraction of fines is approximately 37% for the tested mixtures derived from the geometrical restriction: the volume of fines should be less than that of the voids between coarse grains. A series of fines content (mass ratio) of 35%, 25% and 15% is adopted. The grain size distribution and the physical properties of the mixture are shown in Fig. 5.2 and Table 5.1.

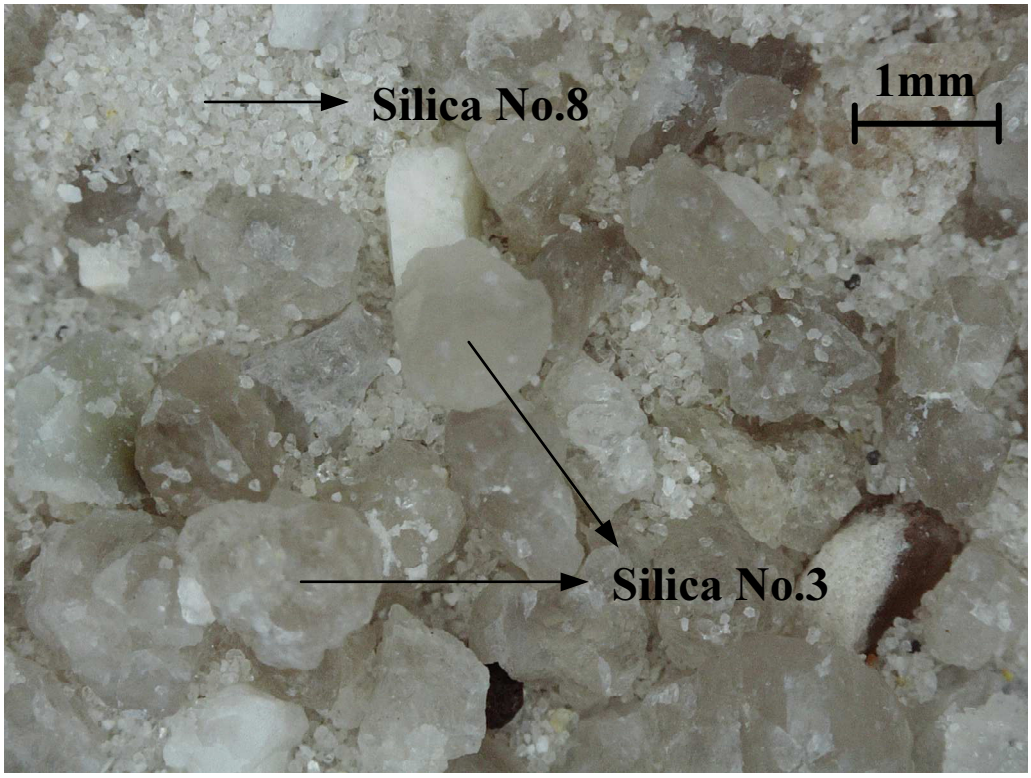

Figure 5.1 Microscopic observation of dry mixtures of silica No.3 and No.8 by a digital microscope

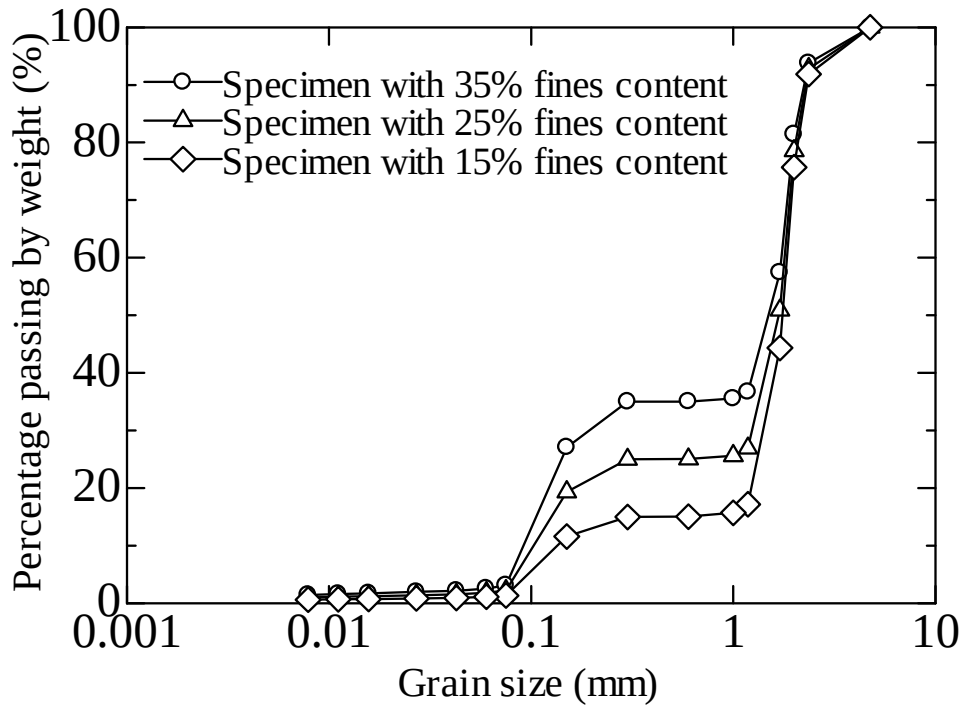

Figure 5.2 Grain size distribution curves of the mixtures

Table 5.1 Physical properties of tested soil

Physical property	Specimen 35	Specimen 25	Specimen 15
Specific gravity, G_s	2.65	2.65	2.65
Fines content (%)	35	25	15
Maximum void ratio, e_{max}	0.74	0.77	0.79
Minimum void ratio, e_{min}	0.36	0.37	0.53
Median particle size d_{50}	1.54	1.68	1.78
Effective particle size d_{10}	0.038	0.038	0.10
Uniformity coefficient C_u	45.9	47.7	18.7
Curvature coefficient C_c	0.59	33.6	22.6
$(H/F)_{min}$ (1)	0.05	0.08	0.15
$(D_{15c}/d_{85f})_{gap}$	7.9	7.9	7.9
Conditional factor of uniformity, h' (2)	1.3	1.2	1.2
Conditional factor of uniformity, h'' (3)	8.5	9.3	6.2
Grain description	Subround - subangular		

Note:
(1) F is the weight fraction of the soil finer than size d; H is the weight fraction of the soil in the size ranging from d to $4d$.
(2) $h'=d_{90}/d_{60}$
(3) $h''=d_{90}/d_{15}$

Similarly, the vulnerability of the mixture to internal erosion is assessed by currently available methods U.S. Army Corps of Engineers (1953), Istomina (1957), Kezdi (1979), Kenney and Lau (1985, 1986), Burenkova (1993) and Mao (2005). The details of the evaluation are shown in Table 5.2, which indicates that the mixtures are potentially unstable for soil erosion.

Several internally unstable specimens are tested to understand the erosion mechanism. A summary of the test cases is shown in Table 5.3. Each specimen with moisture content reaches the target void ratio following the procedures of moist tamping method. The applied mean effective stress is 50kPa, 100kPa and 200kPa, which approximately corresponds to the earth pressure of 5m, 10m and 20m in depth, respectively. Three specimens, named 35E-50-R, 35E-100-R and 35E-200-R, are tested under the same effective stress state as that of Specimens 35E-50, 35E-100 and 35E-200 to confirm the repeatability of the test results and test apparatus.

Table 5.2 Assessment of the mixture's vulnerability to internal erosion

Criteria	The mixture is internally stable if	Specimen 35	Specimen 25	Specimen 15
U.S. Army (1953)	$C_u < 20$	U[(1)]	U	S[(1)]
Istomina (1957) [Ref. Kovacs (1981)]	$C_u \leq 20$	U	U	S
Kezdi (1979)	$(D_{15c}/d_{85f})_{max} \leq 4$	U	U	U
Kenney and Lau (1985, 1986)	$(H/F)_{min} \geq 1$ $(0 < F < 0.2)$	U	U	U
Burenkova (1993)	$0.76log(h'')+1<h'<1.86log(h'')+1$	U	U	U
Mao (2005)	$4P_f(1-n) \geq 1$[(2)]	U	U	U

Note:
(1) "U" means Unstable; "S" means Stable;
(2) P_f is the fines content by weight in soil; n is the porosity, derived from Table 5.3.

Table 5.3 Details of test conditions

Specimen	Fines content before erosion (%)	Initial void ratio	Post consolidation void ratio	Post erosion void ratio	p' (kPa)
35E-50	35	0.64	0.59	1.09	50
35E-100	35	0.60	0.55	0.92	100
35E-200	35	0.59	0.55	0.80	200
25E-50	25	0.61	0.57	0.81	50
15E-50	15	0.68	0.68	0.78	50
35E-50-R	35	0.62	0.60	1.00	50
35E-100-R	35	0.60	0.56	0.95	100
35E-200-R	35	0.64	0.57	0.77	200

5.3 Representative soil behavior during erosion

Parametric study is performed in this series of tests. Two variables in this study are effective confining pressure (50kPa, 100kPa and 200kPa) and initial fines content (35%, 25% and 15%), which are considered of great significance for soil internal erosion phenomena. Firstly, the characteristics of erosion are described by interpreting the hydraulic gradient, cumulative eroded soil mass and volumetric deformation of the tested specimens with 35% initial fines content under the effective confining pressure of 50kPa (specimen 35E-50). One of the consequences of erosion is the variation in grain size distribution curve, which would be helpful to illustrate the spatial progression of erosion. Then, the influence of the two variables is discussed by the comparison of the

testing data of others specimens with those of specimen 35E-50.

5.3.1 Maintained back pressure

The saturation degree of the tested specimen would usually decrease during the period of the seepage test because of the air bubbles generated in the specimen induced by the pore pressure reduction. Commonly, the inflow is at the higher pressure with air dissolved. Due to the head loss during seepage test, the pore water pressure in the tested specimens is lower. Thus, dissolved air may probably separate out and form air bubbles in the tested specimen. As a result, the saturation degree would decrease. Evans and Fang (1988) proved that the decrease in saturation degree would cause the reduction in the measured hydraulic conductivity by approximately three orders of magnitude, which may result in a misleading understanding of the hydraulic behavior of tested soils. Furthermore, falling in the saturation degree may reduce the quality of compression test on the internally eroded specimens. As a countermeasure, a back pressure of 100kPa is maintained to the tested specimens from the sedimentation tank, shown in Fig. 5.3. Although slight deviations from 100kPa exist due to the regular opening/closing of drainage valve of sedimentation tank, basically the back pressure is maintained constant in the tested soil specimen. Usually, the B-value drops after seepage test. For most of the soil specimens, that value is still higher than 0.93, which is considered as fully saturated in this research.

5.3.2 Evolution of hydraulic gradient and hydraulic conductivity

The hydraulic gradient is derived from the recorded pressure drop induced by seepage flow and the specimen length corrected by deducting the vertical deformation. With the progress of erosion, hydraulic gradient would vary correspondingly. That variation of specimen 35E-50 at the initial 900s and 0s~11000s in the erosion test is plotted in Fig. 5.4. At 480s, a moderate drop of hydraulic gradient is noticed (Q=50mL/min, v=0.021cm/s), which is considered as the sign of the onset of internal erosion (Fig. 5.4a). The effluent becomes slightly turbid with very small amounts of suspending fines. At this moment, the reading from the eroded soil collection unit is basically zero, indicating that no eroded fines are detected. It is postulated that at this stage the process of filtration of fine grains diffuses within the specimens. A sharp increase of the hydraulic gradient is detected at 880s (Q=100mL/min, v=0.042cm/s) at which the increment of the inflow rate begins increasing from 10(mL/min)/min to 50(mL/min)/min (Fig. 5.4b). This sharp increase may relate to the influence of “hammer effects” which refers to the phenomenon that a sudden increase or decrease in Darcy velocity would affect the hydraulic properties of soil specimens (Tomlinson and Vaid, 2000). It may induce the unexpected movement of soil grains that would affect the detection of critical Darcy velocity. Another possibility might be explained by the temporary clogging of fines among the constrictions of coarse grains when large amounts of fines begin eroding off. The hydraulic gradient dramatically drops after the “peak” with the erosion of a large amount of fines. It is postulated that the soil grains gradually change their position for self-balance at this stage and correspondingly, the specimen would deform. After a period, the soil packing will reach a new equilibrium without further erosion and consequently, the hydraulic gradient becomes constant.

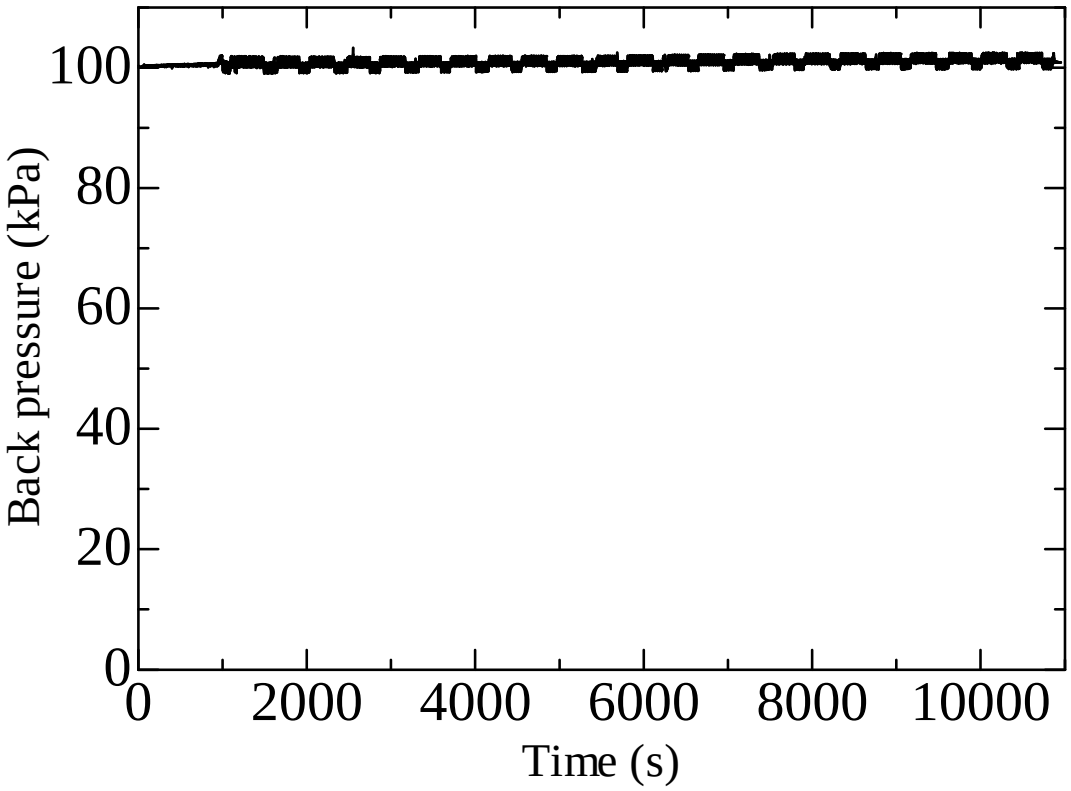

Figure 5.3 Maintained back pressure within seepage test period (specimen 35E-50)

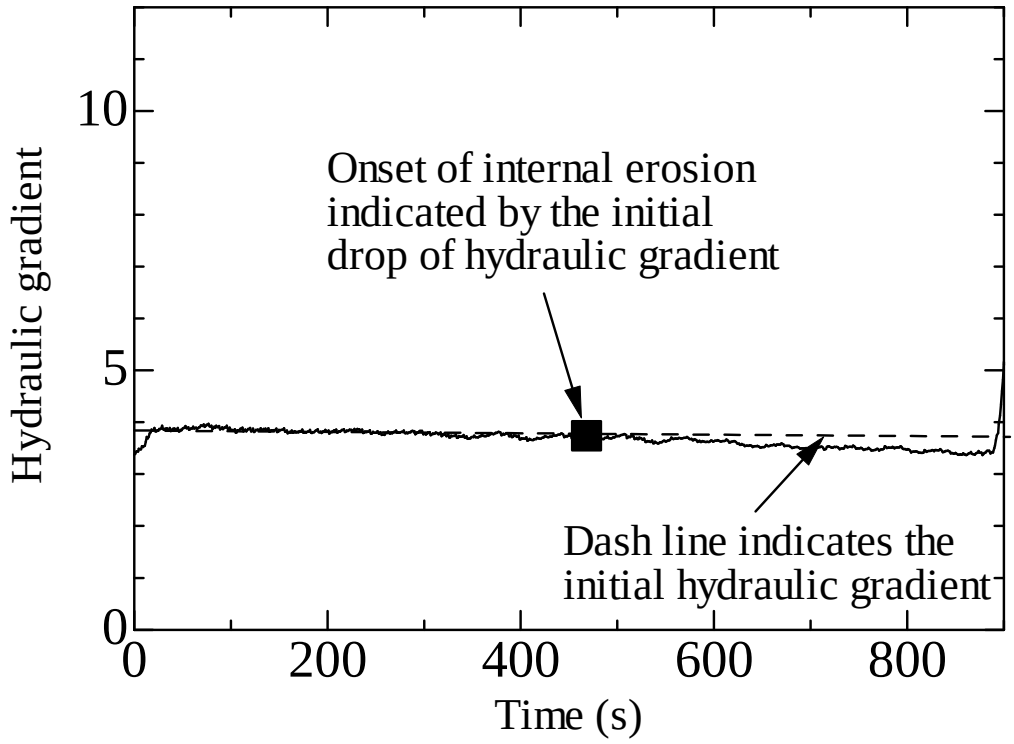

(a) 0s~900s of seepage test

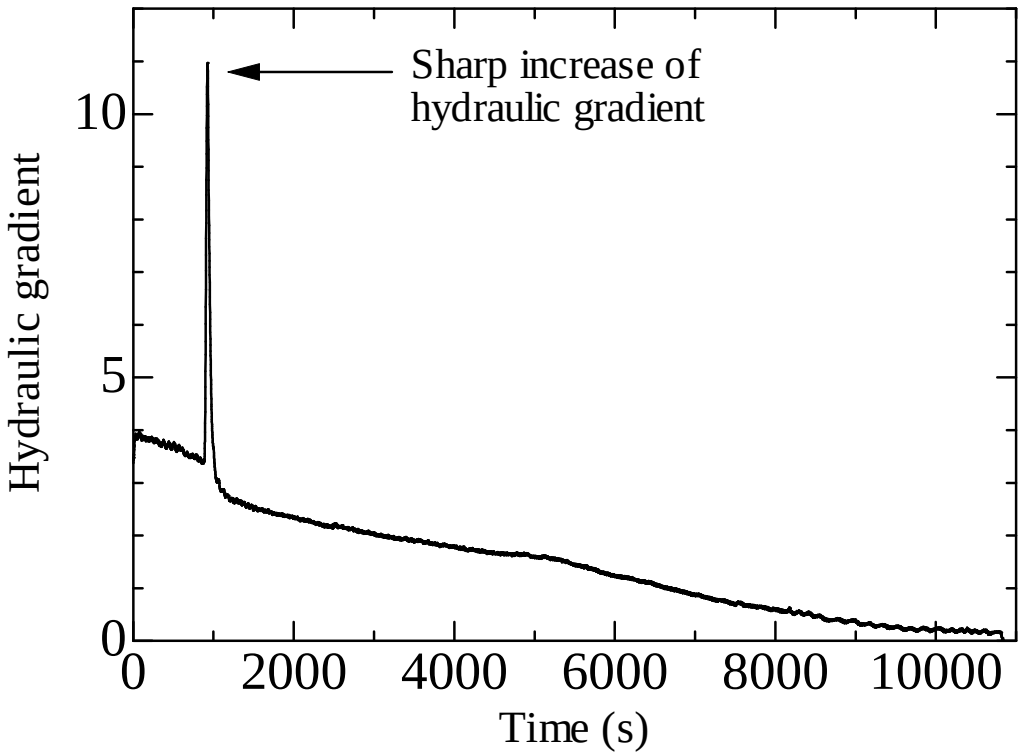

(b) Whole time period of seepage test

Figure 5.4 Hydraulic gradient within seepage test period (specimen 35E-50)

On condition that Darcy velocity and hydraulic gradient is known, hydraulic conductivity could be calculated following Darcy's law that describes the flow of a fluid through a porous medium. A condition of laminar flow during seepage test is validated by ensuring the Reynolds number less than 10. The validation procedure and calculation details are similar to that illustrated in Chapter 3. In this study, the inflow is constantly provided by a pump with a constant rate. Discharge rate is unknown due to the difficulties in conducting measurement in a pressurized tank. The Darcy velocity in this assessment is derived from the inflow rate and the cross-sectional area corrected by the radial deformation. Figure 5.5 shows the variation of hydraulic conductivity with the period of erosion test. Before the onset of internal erosion, hydraulic conductivity keeps constant at 0.006cm/s. At the initial drop of hydraulic gradient, hydraulic conductivity begins increasing at 480s (Q=50mL/min, v=0.021cm/s, Fig. 5.5a). An obvious increase of hydraulic conductivity is observed after the sharp increase of hydraulic gradient (Fig. 5.5b). It could be understood that with the progress of internal erosion, the fines are gradually dislodged causing the increasing of pore size. Thus, hydraulic conductivity increases. It may be argued that the temporary clogging, which leads to the sharp increase of hydraulic gradient, should decrease the hydraulic conductivity. In this study, the formation and dissipation of the temporary clogging is found to be rapid in a short period probably because of the relatively large hydraulic conductivity of the tested soil. Therefore, a mere increasing of hydraulic conductivity is obviously noted in Fig.5.5b. Seepage flow would carry a significant amount of fines through the channels formed by voids among coarse grains. It is possible that the movement of fines is impeded at a channel, the size of which is not sufficiently large for the passing of fines and

consequently, it may result in the clogging among coarse grains. With the increasing accumulation of fines at channels, the size of effective pore throats would further decrease and thus, hydraulic conductivity would drop. This phenomenon is usually detected after a significantly longer period. In this study, the decrease of hydraulic conductivity from 8500s probably indicates the possible occurrence of clogging. The maximum hydraulic conductivity detected is approximately 150 times larger than the initial value.

5.3.3 Cumulative eroded soil mass with time

The evolution of the percentage of cumulative fines loss with time is plotted in Fig. 5.6 where the recorded cumulative eroded soil mass is normalized by the total weight of specimen. Corresponding to the instantaneous increase of hydraulic gradient, large amounts of fines are eroded away, which might cause the increment of porosity and the re-adjustment of the inter-grains position. The erosion rate decreases with the progress of internal erosion. By the end of the test (t=11000s, Q=310mL/min, v=0.14cm/s), approximately 25% fines are lost and 13% fines remain in the tested specimen.

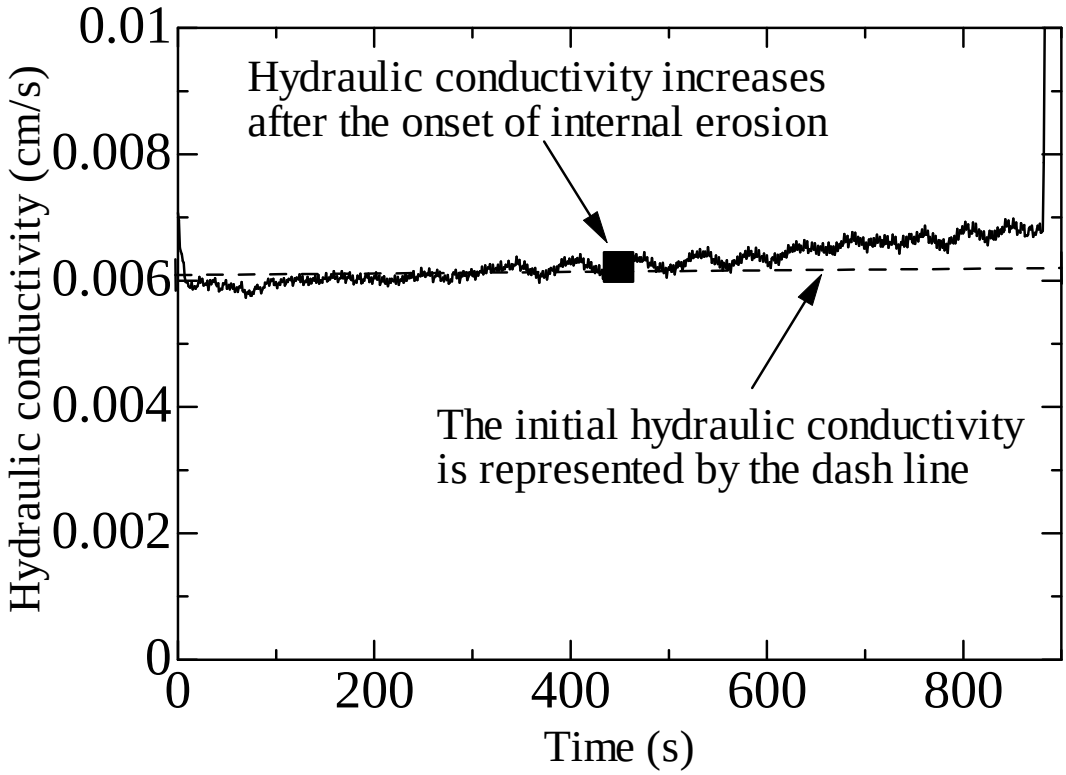

(a) 0s~900s of seepage test

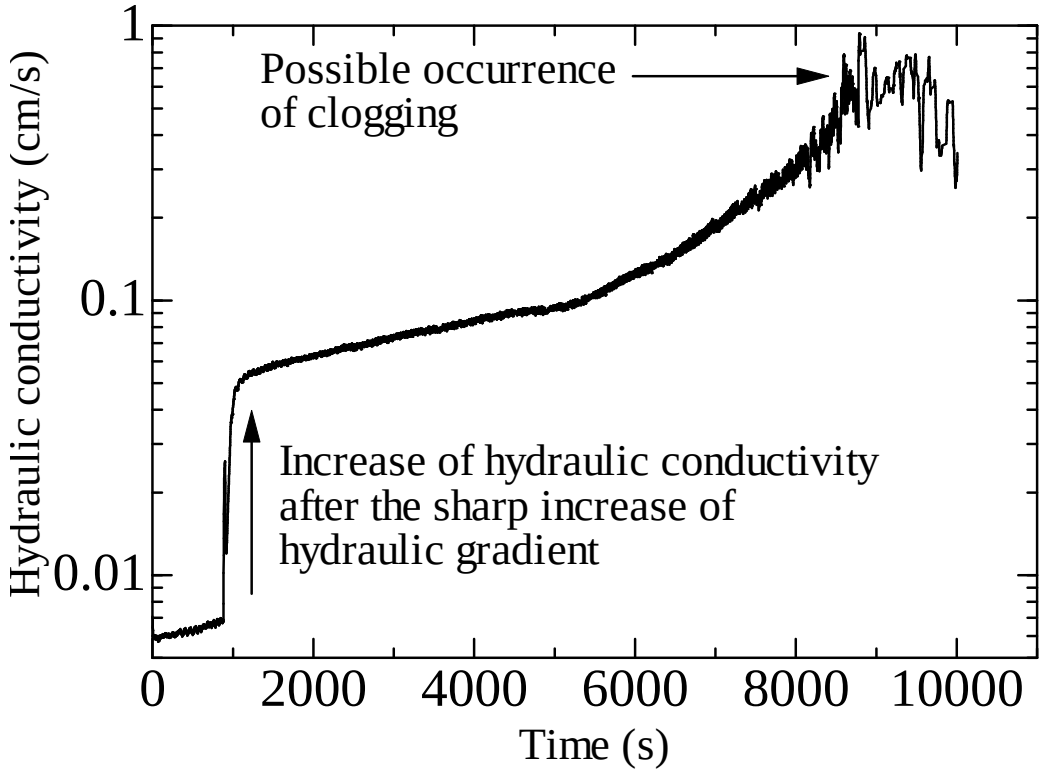

(b) Whole time period of seepage test (semi-log scale)

Figure 5.5 Hydraulic conductivity within seepage test period (specimen 35E-50)

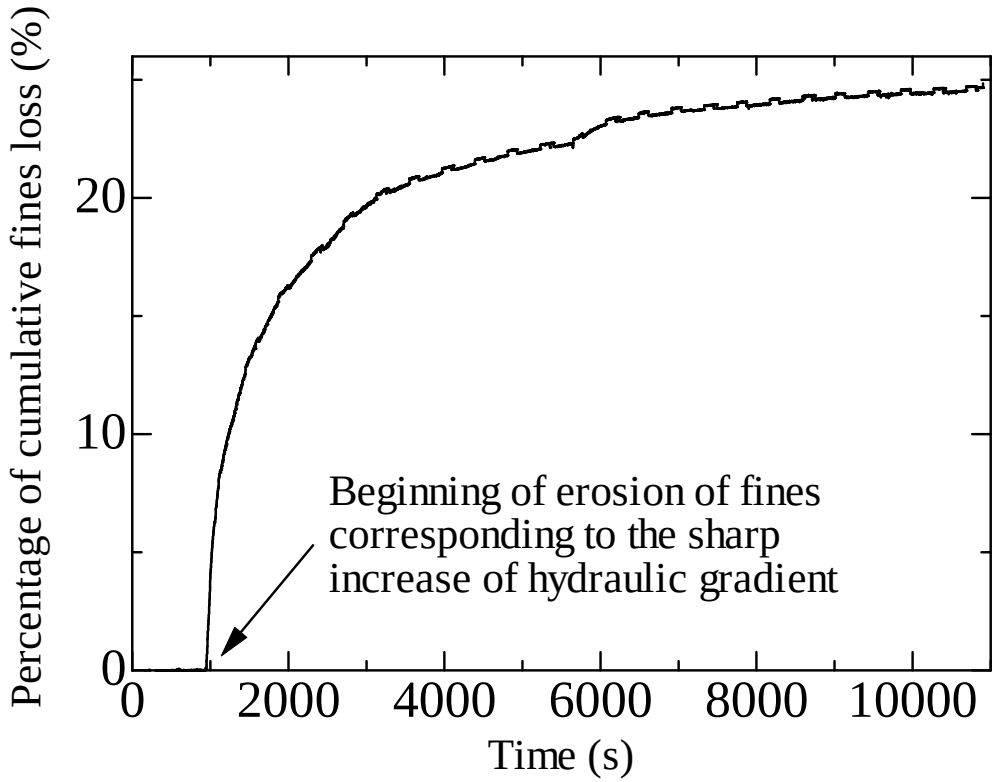

Figure 5.6 Percentage of cumulative fines loss within seepage test period (specimen 35E-50)

5.3.4 Soil volumetric deformation

Incessant erosion of fines from the tested specimen may result in the re-arrangement of soil grains, consequently leading to the volumetric deformation. Figure 5.7 presents the soil specimen deformation in terms of volumetric strain during the erosion test. At the stage 1 of the seepage test when the inflow rate increases from 0 until 100mL/min by 10(mL/min)/min, the volumetric strain approximately increases by 2.3% because of the test apparatus. The rotary pump used in the test would produce jet flow on the soil specimen when increasing the inflow rate, i.e., at the beginning of each stage. This jet flow leads to the soil deformation, which is considered as a limitation of the current water circulation system of the apparatus. Generally, the tested specimen is prone to be contractive with the progress of erosion. In stage 3 when the inflow rate is kept constant, two obvious jumps in deformation are detected around 2400s and 5600s. It is postulated that along with the constant loss of fines, the coarse grains would correspondingly re-arrange their positions to reach a new equilibrium in a short period, which might be an explanation of the sudden and rapid collapse of earthen structure induced by erosion. Moffat *et al.* (2011) described the relatively rapid volumetric deformation of soil as the characteristic of suffusion (internal erosion).

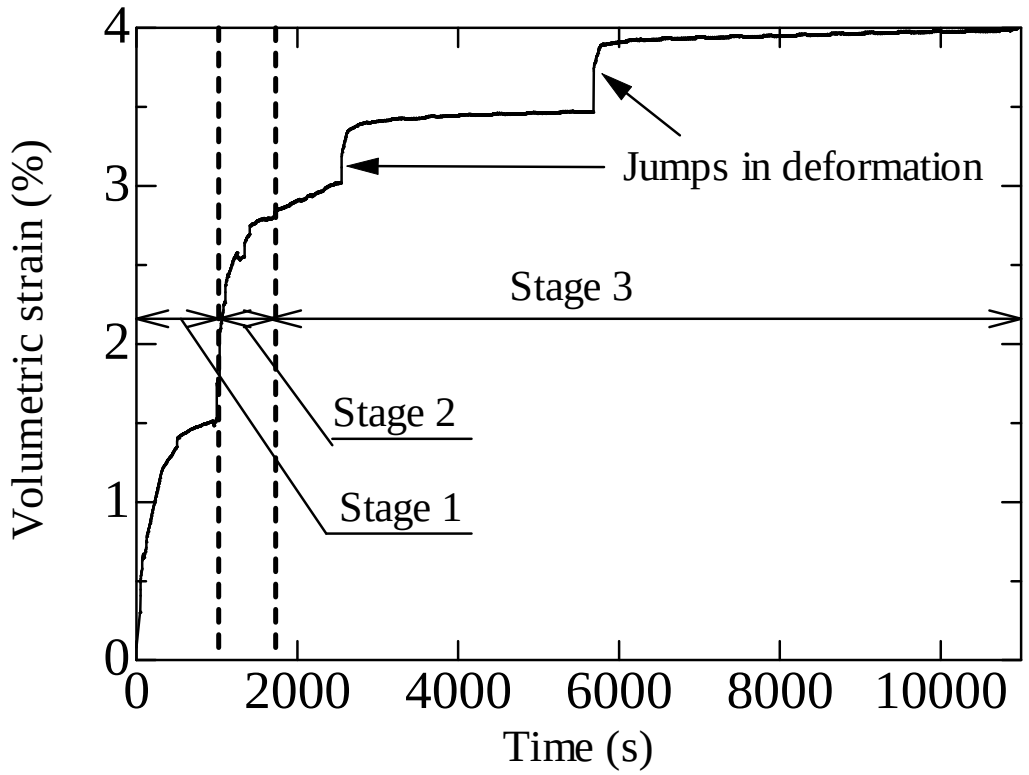

Figure 5.7 Volumetric strain within seepage test period (specimen 35E-50)

5.3.5 Post-erosion grain size distribution

The variation in grain size distribution could reflect the changes in the geometry of soil specimens due to internal erosion. Kenney and Lau (1985) concluded that fine grain losses resulting from erosion could cause the post-erosion distribution curve shifts downward from original curve. The extent of the movement proportionally increases with the amount of fine grain loss. Chang and Zhang (2011b) experimentally demonstrated that comparing to the fines loss in the bottom layer and the middle layer, that loss in the upper layer is larger. In this test, the post-erosion specimen is equally divided into two layers: top layer and bottom layer. The grain size distribution curve is determined by sieving test on those soils that have been oven-dried at 110°C for 24h. Figure 5.8 presents the typical grain size distributions of a post-erosion soil specimen. The post-erosion curves of both upper layer and bottom layer move downward from the original curve, the extent of which is corresponding to the loss of fines. Moreover, the fines loss in the upper layer is more than that in the bottom layer.

5.3.6 Influence of effective confining pressure

The effect of effective confining pressure on erosion mechanism is complicated. At the larger confining pressure, the fines are expected to be densely packed among coarse grains and the interstitial spaces may be narrower. For the soil specimens with the higher confining pressure, the seepage flow might dislodge fewer fines. However, the force transfer mechanism of granular material is much more complex. Due to the boundary frictions, force-arching may develop at the intersections of the bottom boundary, which may hold the fines from erosion. At the higher confining pressure, it is possible that the force-arching is failed, which, instead, might cause further erosion of fines (Tomlinson and Vaid, 2000). In this study, constant-flow-rate seepage tests on the specimens with 35% initial fines content under three different effective confining pressures (50kPa, 100kPa and 200kPa) are conducted. Through the period of seepage test, the mean effective stress is kept the same as that of consolidation (e.g., p'=50kPa, q=0kPa). The influence of effective confining pressure is demonstrated by comparing the test data in terms of Darcy velocity, hydraulic conductivity, percentage of cumulative fines loss and volumetric strain.

The Darcy velocity for stage 3 under different effective confining pressures is presented in Table 5.4. It indicates that the velocity is basically the same in each case, which provides a reference for the following comparison. Figure 5.9 shows the normalized hydraulic conductivity, which is the ratio of hydraulic conductivity after and before the internal erosion. For specimen 35E-50 whose effective confining pressure is 50kPa, the post-erosion hydraulic conductivity increases nearly 150 times while that increment for specimen 35E-100 and 35E-200 is 100 and 80, respectively. With the progress of internal erosion, the specimen would gradually become heterogeneous and consequently, the local velocity filed exhibits significant spatial fluctuations. It is possible that the local flow velocity is much larger than the overall macroscopic velocity. Under larger effective confining pressure, the progress of internal erosion may slow down and therefore, the maximum value of the local velocity field is lower. On the other hand, the fines might be tightly packed and the interlocking between soil grains is firmer under

larger effective confining pressure. Thus, fewer fines would overcome the interlocking forces and would be dislodged from the specimen, as is shown in Fig. 5.10. As is discussed, the extent of the increasing in the hydraulic conductivity is closely associated with the amounts of fines loss. For the specimen with less extent of increasing in hydraulic conductivity (i.e., specimen 35E-200), the fines loss is expected to be less (Fig.5.10). Similarly, the volumetric strain induced by erosion of fines is the least in specimen 35E-200 and the largest in specimen 35E-50, shown in Fig.5.11.

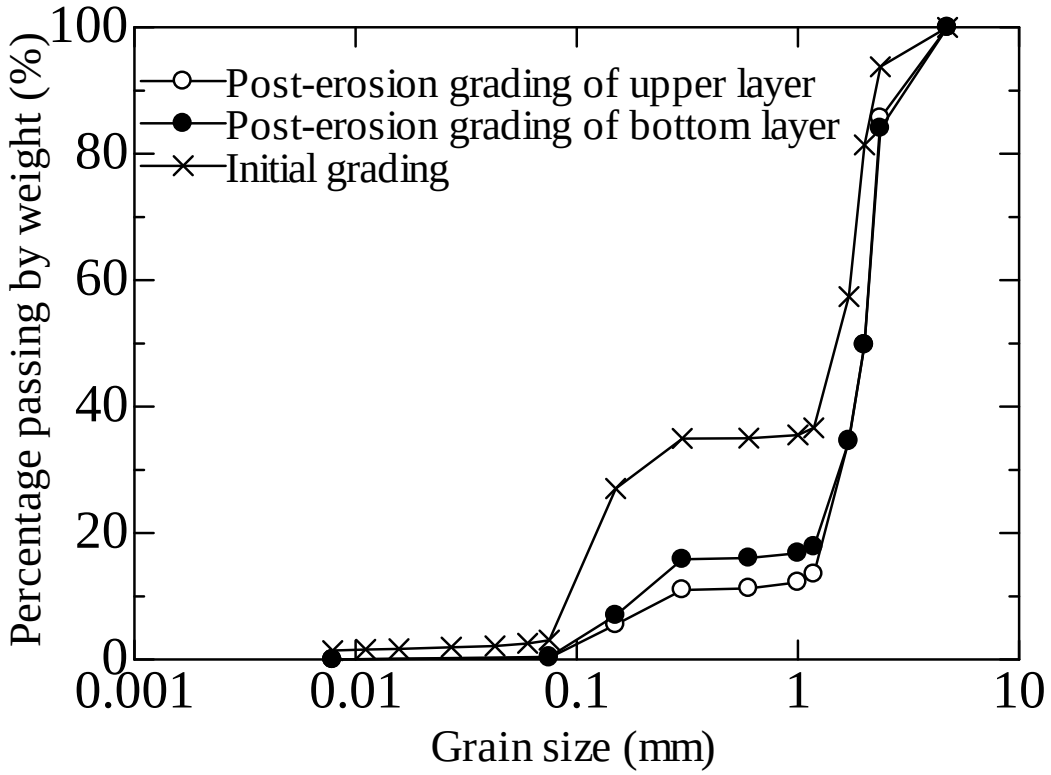

Figure 5.8 Grain size distribution curves of the post-erosion specimen (specimen 35E-50)

Table 5.4 Assigned Darcy velocity in seepage tests

Specimen	Darcy velocity (cm/s)
35E-50	0.144
35E-100	0.150
35E-200	0.146
25E-50	0.145
15E-50	0.138

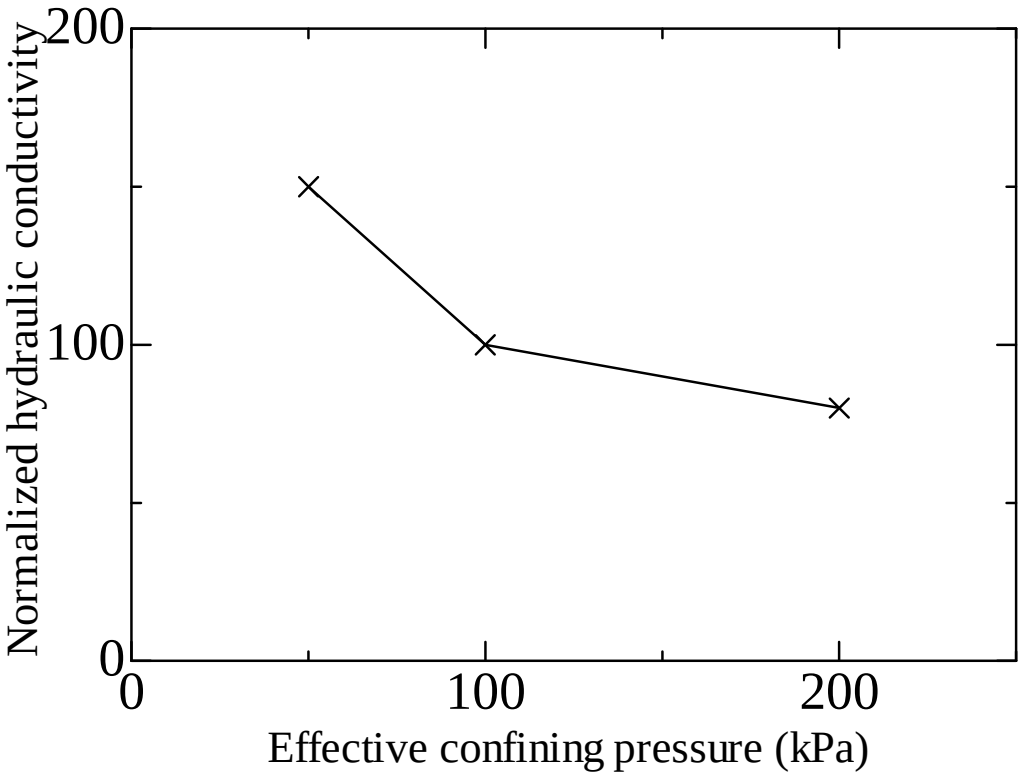

Figure 5.9 Effective confining pressure versus normalized hydraulic conductivity for specimens with 35% initial fines content

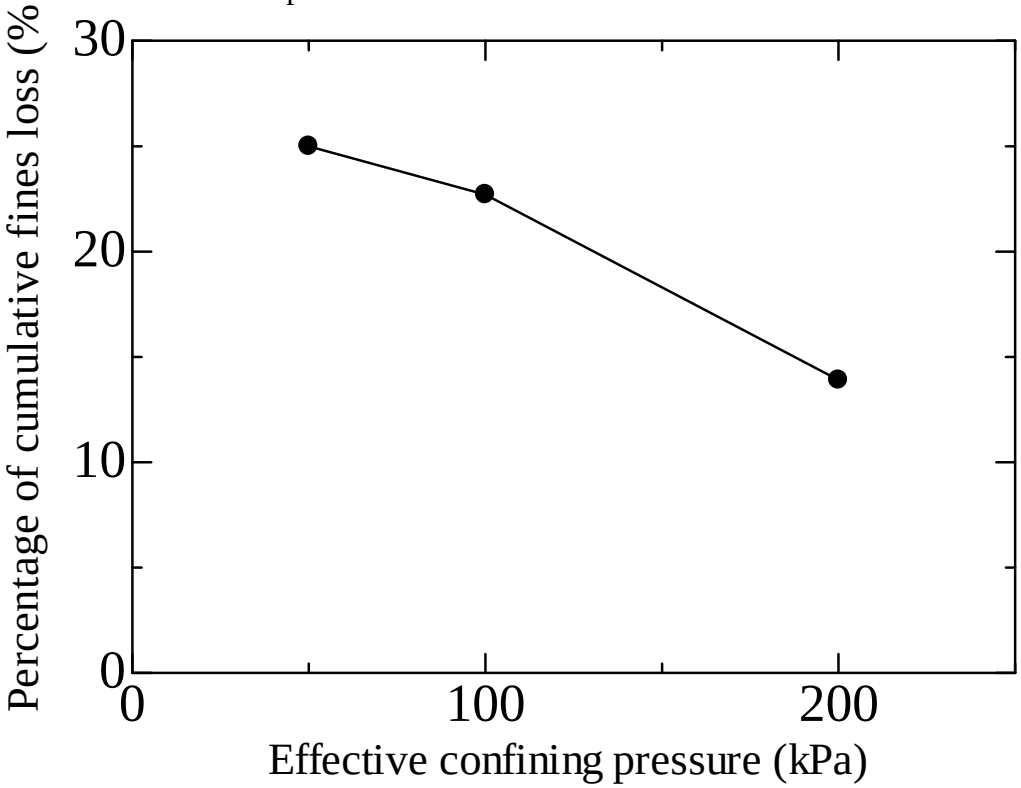

Figure 5.10 Percentage of cumulative fines loss versus effective confining pressure for specimens with 35% initial fines content

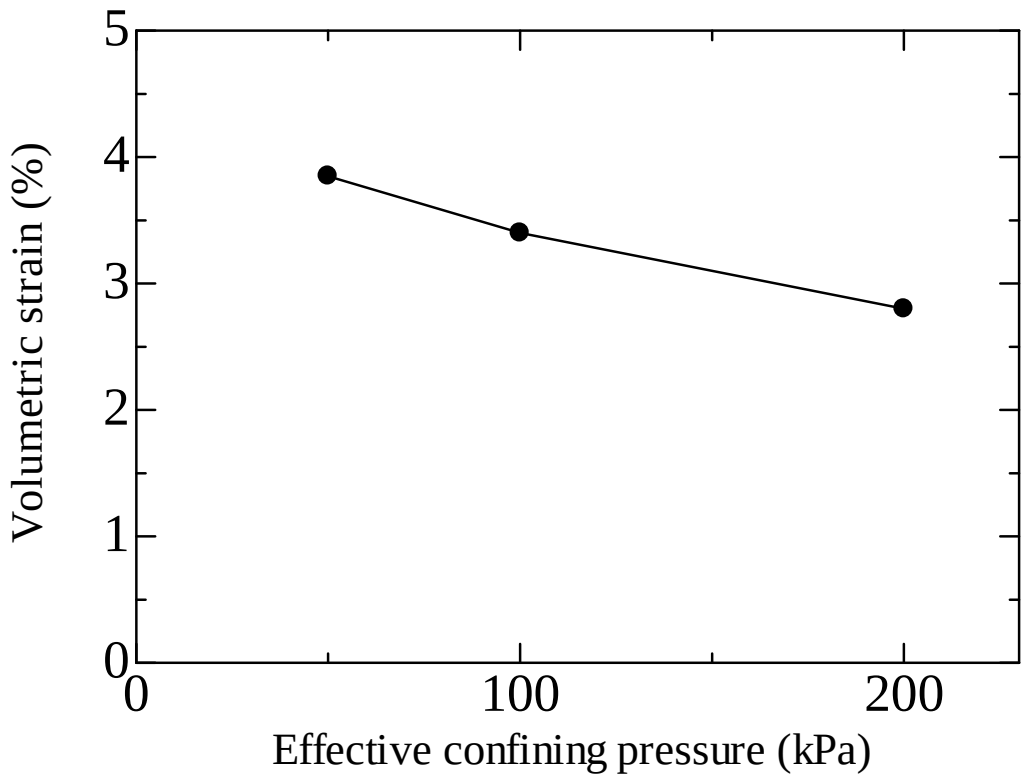

Figure 5.11 Internal erosion induced volumetric strain versus effective confining pressure for specimens with 35% initial fines content

5.3.7 Effects of soil initial fines content

The initial fines content actually characterizes the effect of soil packing, which may offer a physical explanation for the soil hydromechanical behavior. The schematic microstructure of the soil specimen with respective 35%, 25% and 15% fines content is shown in Fig. 5.12. Majority of fines is considered to be locked within the voids of coarse grains for the specimen 15E-50 with 15% initial fines content, in contrast with specimen 35E-50 with 35% initial fines content, where the fines may not only fill the voids but also probably separate the coarse grains. If internal erosion initiates, the fines simply occupied the voids may be easily eroded away while those fines separating the coarse grains may hardly move because of the higher contact force on them. Suppose that the fines are merely considered as voids, at the same relative density, the voids size among the coarse grains of specimen 35E-50 would be larger than that of specimen 15E-50. A larger void size would commonly allow for greater fines loss. Therefore, the specimen with larger initial fines content is assumed to show much greater extent of erosion.

The Darcy velocity assigned on the specimens with different initial fines contents under an effective confining pressure of 50kPa is noted in Table 5.4. The similar value of flow velocity for each specimen is regarded as a reference for comparison. The initial relative density of each specimen is set the same as 30%. The normalized hydraulic conductivity versus initial fines content is presented in Fig. 5.13 indicating that the largest increase of hydraulic conductivity occurs in specimen 35E-50. Figure 5.14 and 5.15 show the

percentage of cumulative fines loss and erosion-induced volumetric strain versus initial fines content, respectively. It can be seen that cumulative fines loss is larger for specimen 35E-50 and correspondingly, the erosion-induced volumetric strain is larger.

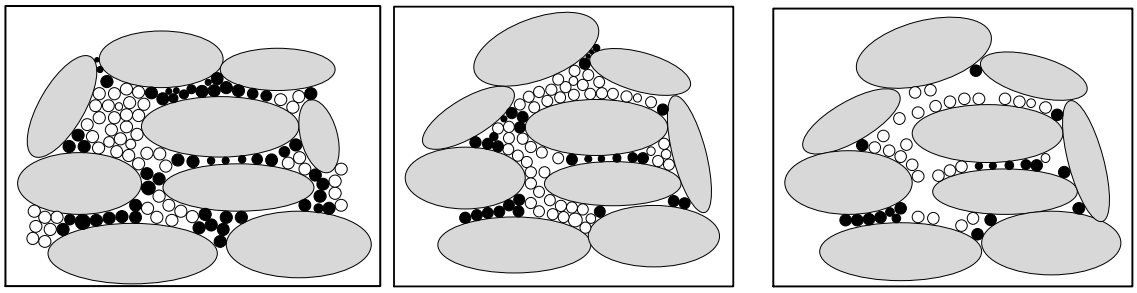

(a) 35% initial fines content (b) 25% initial fines content (c) 15% initial fines content

Figure 5.12 Schematic diagram of possible soil microstructure (the empty grains are erodible)

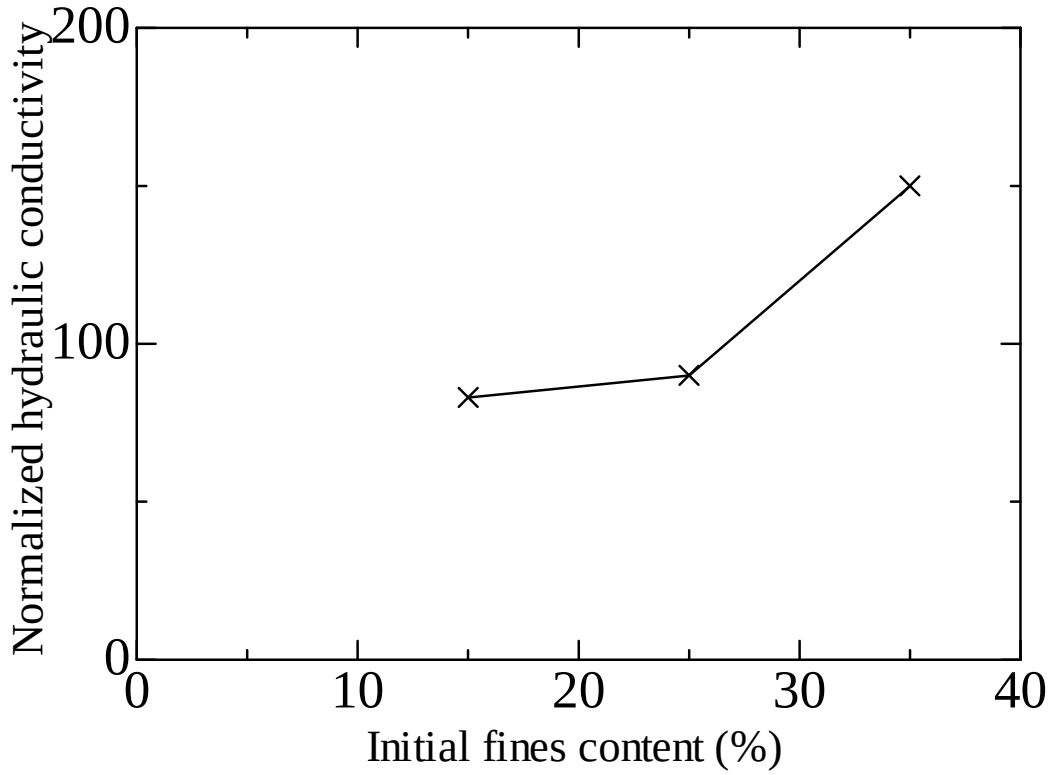

Figure 5.13 Normalized hydraulic conductivity versus initial fines content under an effective confining pressure of 50kPa

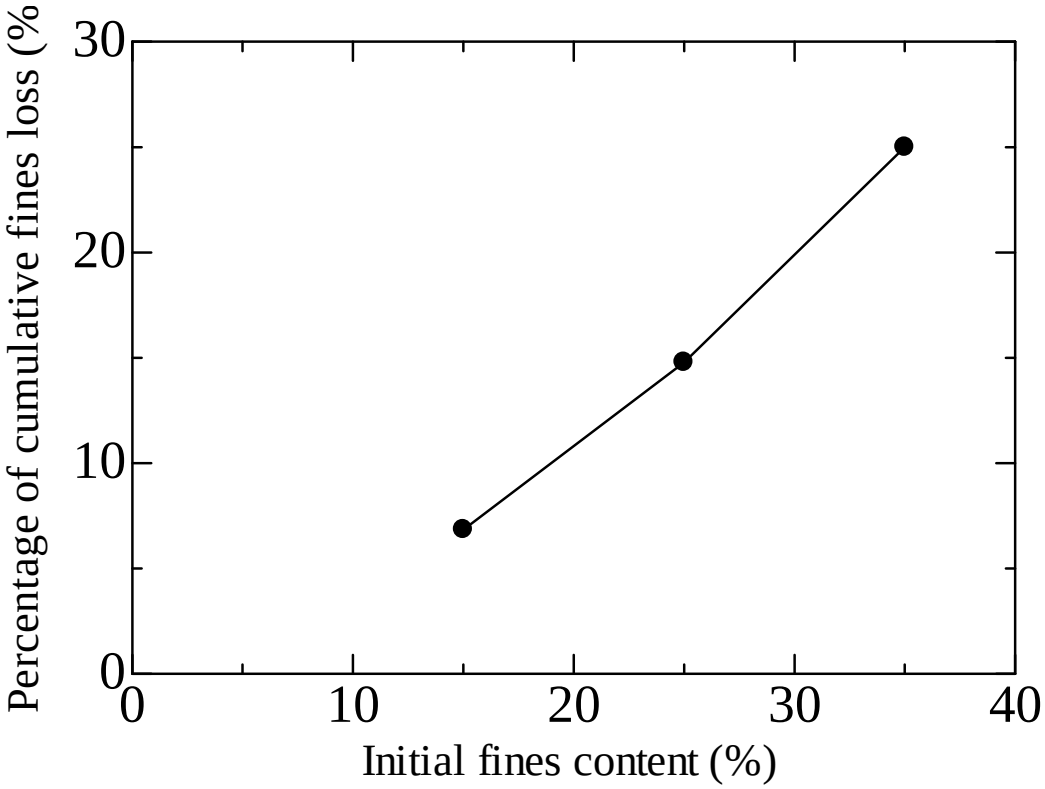

Figure 5.14 Percentage of cumulative fines loss versus initial fines content under an effective confining pressure of 50kPa

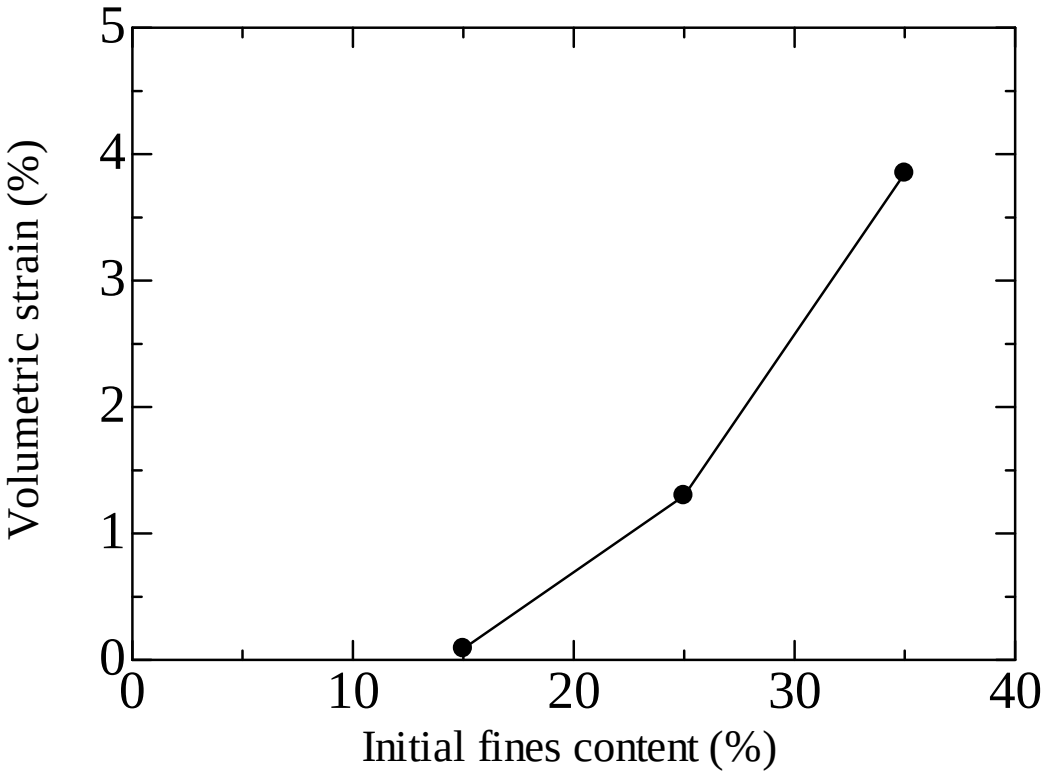

Figure 5.15 Internal erosion induced volumetric strain versus initial fines content under an effective confining pressure of 50kPa

5.3.8 Test repeatability

The repeatability is confirmed by comparing the key parameters among tested specimens with 35% initial fines content, shown in Table 5.5. Irregular deviation exists among the hydraulic gradient and hydraulic conductivity, which might be influenced by the inhomogeneity of the specimens. However, the percentage of cumulative fines loss and volumetric strain are basically the same, which might indicate the consistency of erosion law for each test case.

5.4 Evolution law of void ratio

Change of void ratio is caused by the fines loss (ΔV_f) and possible intergranular re-arrangement (ΔV_w), as is shown in Fig. 5.16. To address the problem, it is postulated that the void ratio change follows two steps: (1) as soon as internal erosion initiates, no deformation occurs due to the dislodgement of fines, the total volume of the tested specimen remains the same and the volume of eroded fines would be occupied by water at the same volume if the saturated soil is taken into consideration. e_0 indicates the void ratio induced by erosion of fines with soil deformation, which can be given by:

$$e_0 = \frac{e_c + \Delta FC}{1 - \Delta FC} \quad \text{..... (5.1)}$$

Table 5.5 Repeatability of seepage tests

Specimen	Maximum hydraulic gradient	Post-erosion hydraulic conductivity (cm/s)	Percentage of cumulative fines loss (%)	Volumetric strain (%)
35E-50	11.7	2.8	25.0	3.9
35E-50-R	10.1	1.9	22.4	3.8
35E-100	5.68	0.8	22.7	3.2
35E-100-R	7.17	1.0	22.7	3.6
35E-200	10.5	0.8	13.9	2.8
35E-200-R	7.76	1.5	16.7	2.8

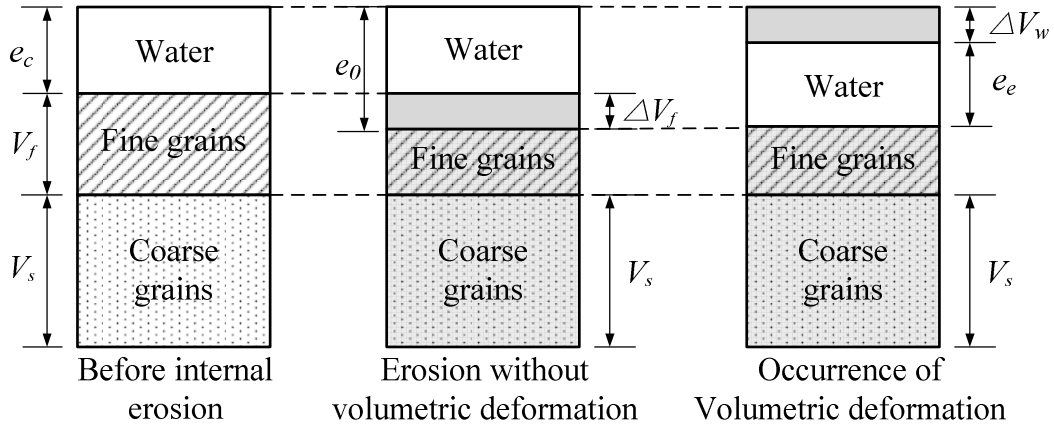

Figure 5.16 Soil erosion induced variation in soil phase relation

Where ΔFC indicates the percentage of cumulative fines loss by mass, which equals to the percentage by volume if the specific gravities of the coarse and the fine grains are the same; (2) with the erosion of large amounts of fines, the metastable structure might be formed which would easily trigger the re-arrangement of soil grains into a stable packing. Correspondingly, a volumetric deformation (ε_v) and therefore a change in void ratio would take place, which equals to $\varepsilon_v(1+e_0)$. The post-erosion void ratio could be obtained as:

$$e_e = e_0 - \varepsilon_v(1+e_0) = (1-\varepsilon_v)(\frac{e_c + \Delta FC}{1-\Delta FC}) - \varepsilon_v \quad \ldots\ldots\ldots (5.2)$$

As is indicated by Eq. (2), change of void ratio is closely dependent on the volumetric strain during internal erosion. If no deformation occurs, a large post-erosion void ratio would be obtained. Further, if the specimen shows dilative behavior during erosion, the largest void ratio would be gained, which may again accelerate the erosion progress. By contrast, a contraction behavior during this process may delay the increase of void ratio even decrease the void ratio after internal erosion. At this circumstance, the lower limit of void ratio could be determined by the greatest density that the coarse grains could achieve. The corresponding volumetric deformation of the specimen would reach the maximum value. Scholtès *et al.* (2010) conducted the simulations of grain extraction by the similar approach. The deformation of granular assembly was obtained by the analysis of inter-particle sliding resistance. McDougall *et al.* (2004, 2013) proposed a parameter, indicated by Λ, to quantitatively illustrate the dissolution-induced volume change of soil. It is defined as the ratio of the increments of void volume to that of solid volume. A value of -1 indicates no change in volumetric strain and the increase in void ratio is the maximum.

A plot of the amount of axial, radial and volumetric strain versus cumulative eroded fines loss is depicted in Fig. 5.17 to interpret the deformation characteristics during soil erosion. The positive axial, radial and volumetric strains indicate the contractive behavior of the tested specimen. Initially, the inflow rate is small and few fines are eroded away while the jet flow induced by the flow pump causes certain amounts of strain. From the beginning of stage 2, large amounts of fines are dislodged and soil deformation develops correspondingly. The phenomenon of the jumping of radial strain frequently occurs while the axial strain develops smoothly. Chang and Zhang (2012) proposed that the soil deformation is mostly determined by the potential of buckling of the strong force chains through the coarse grains and fine grains mainly provide lateral supports for those chains. Since the mass of coarse fractions keeps constant during internal erosion, failure of a force chain may let the remaining force chains to keep on supporting the soil specimen and therefore, the axial strain smoothly develops. On the other hand, the fines loss is continuous with the progress of soil erosion, which would continuously weaken the lateral supports. At certain circumstances, when the remaining fine grains are not strong enough to provide the lateral support, sudden radial deformation may occur, which is represented as “jumps” in radial strain. Another potential possibility relates to the strain-measuring techniques employed in the triaxial testing. The axial strain is recorded by an external LVDT, directly connected to the loading piston and top cap. Since the top cap equally spaced around the top surface of

the tested specimen, the measured axial strain actually represents the average displacement and therefore, the recorded curve develops smoothly. For the radial strain determination, on the other hand, it is obtained from three clip gauges attached at the different spots along the specimen. The inherent assumption is that the average of the discrete radial deformations is representative of the overall radial strain. Comparing to the whole body measurements of axial strain, the discrete local radial deformation might be discontinuous with possible abrupt irregularities.

The estimated void ratios derived from Equations (5.1) and (5.2) for the specimens with 35% initial fines content under an effective confining pressure of 50kPa, 100kPa and 200kPa are presented in Fig. 5.18, which clearly indicates the contribution of volumetric strain to the void ratio change. For specimen 35E-50, the calculated void ratio considering merely the fines loss is 1.13 and because of the volumetric deformation that value approximately decreases by 3.5% to 1.09. The calculated value of Λ is -0.91 for the specimen, indicating a limited influence of volumetric strain on the increments of void ratio. At the higher confining pressure, with less loss in fines, the volumetric deformation of the tested specimen and void ratio change is comparatively less. Compared to the soil state before erosion, the post-erosion void ratios commonly increase, which might alter the mechanical response of the tested soil in terms of stress-strain relationship.

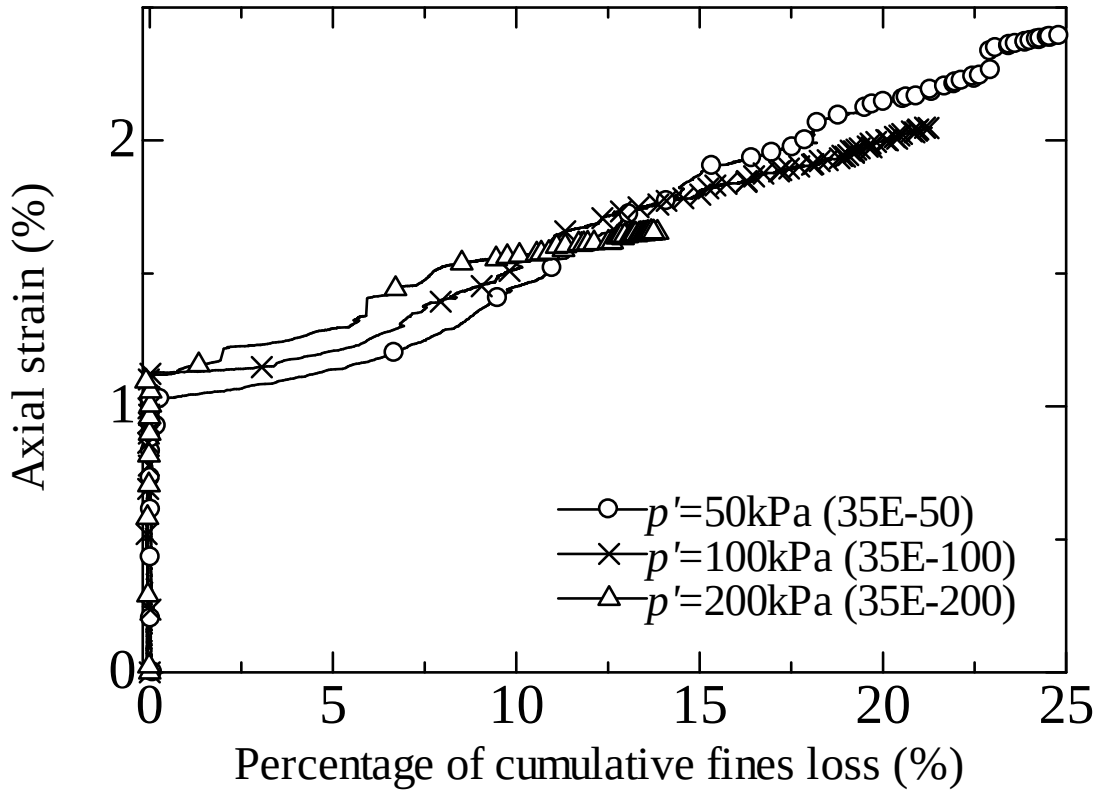

(a) Axial strain changes

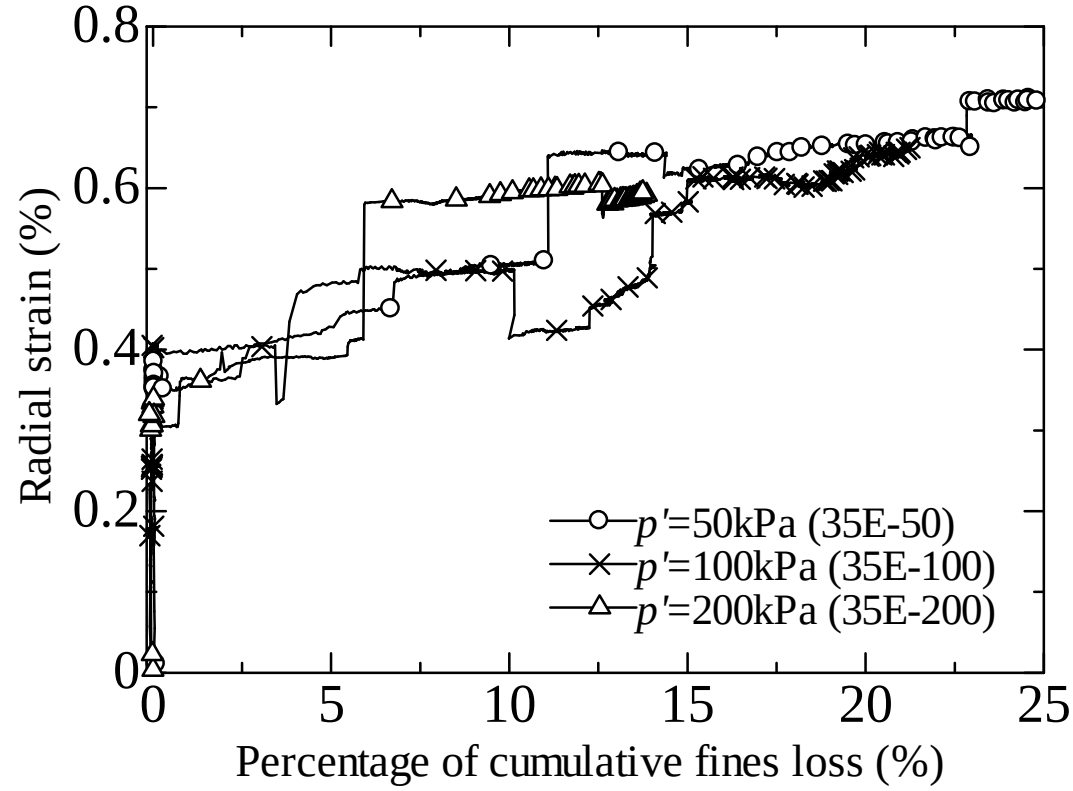

(b) Radial strain changes

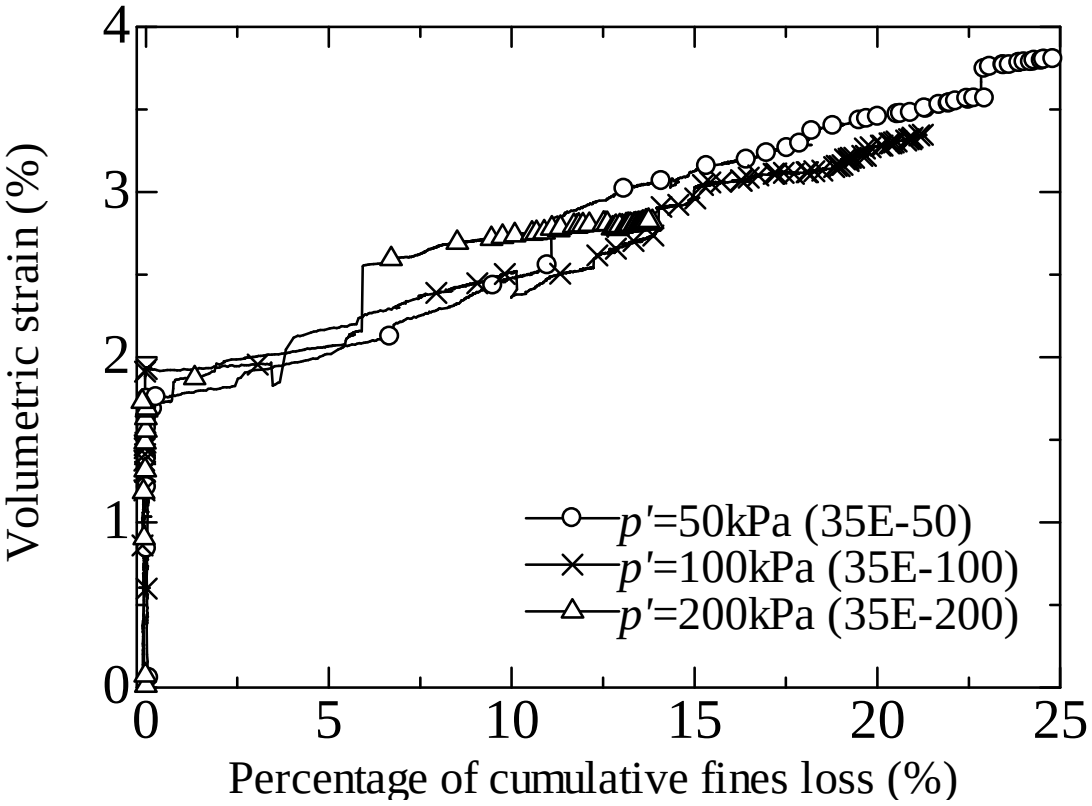

(c) Volumetric strain changes

Figure 5.17 Axial, radial and volumetric strain versus percentage of cumulative fines loss under different effective confining pressures for specimens with 35% fines content

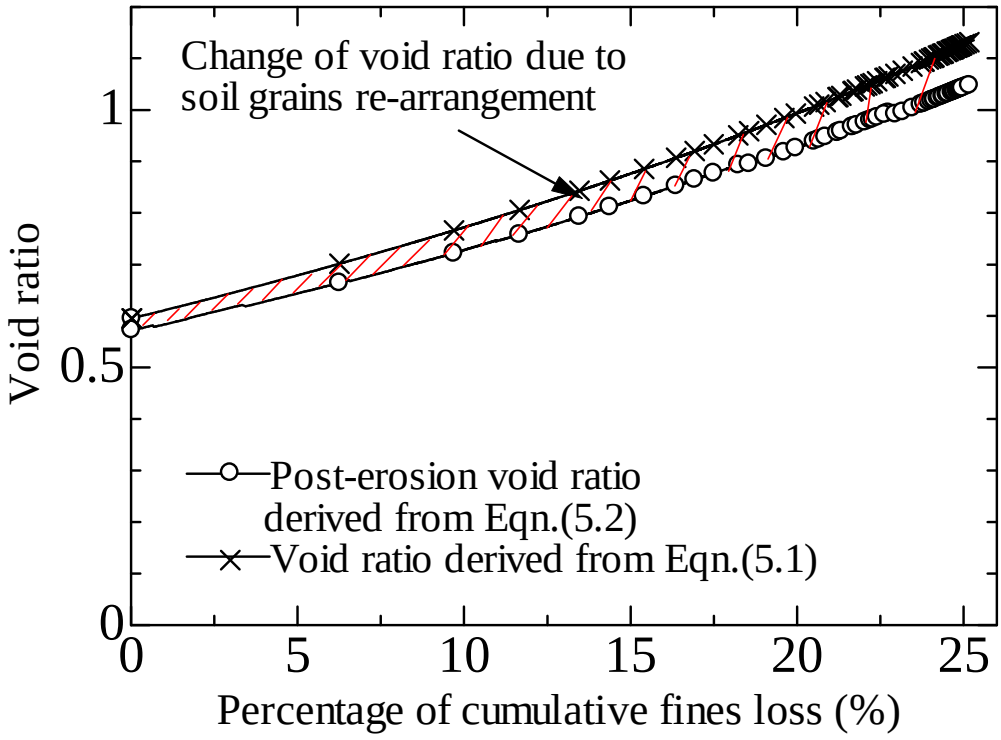

(a) An effective confining pressure of 50kPa (specimen 35E-50)

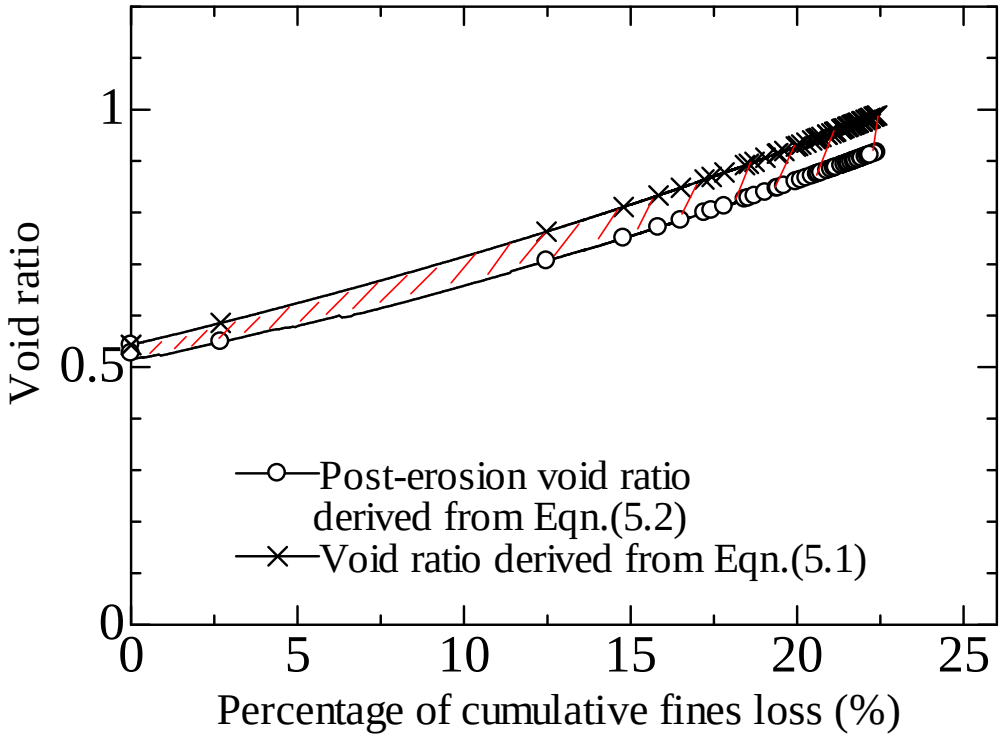

(b) An effective confining pressure of 100kPa (specimen 35E-100)

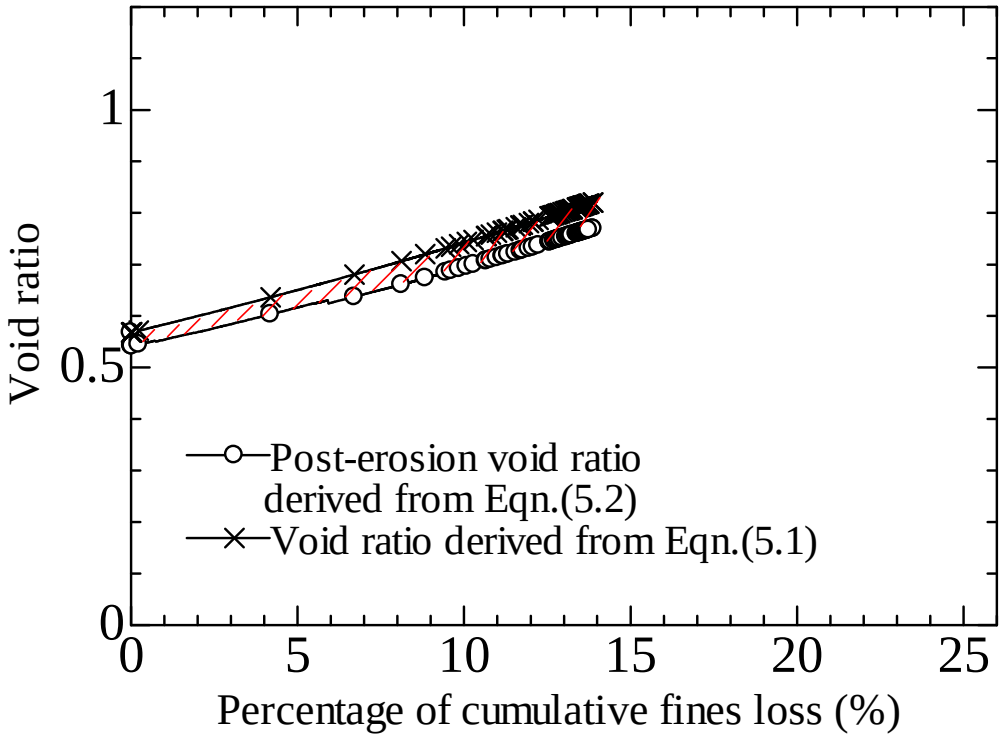

(c) An effective confining pressure of 200kPa (specimen 35E-200)
Figure 5.18 Void ratio versus percentage of cumulative fines loss under different effective confining pressures

5.5 Erosion law

The constitutive law for erosion is mostly empirical, derived from laboratory tests. For cohesive soil, Reddi *et al.* (2000) proposed an expression of shear stress to evaluate the initial surface erosion. Afterwards, a number of internal erosion analysis adopted this concept with the assumption that as long as the seepage flow exerted shear stress is larger than the critical shear stress, erosion occurs. However, if the size of the flow path within the specimen and that of the eroded fines are considered, there is high possibility of occurrence of soil redeposition and clogging. In this study, the erosion by definition refers to the effective dislodgement and transport of the fines, which would be detected at the exit of the tested specimens. The test results are summarized in Figs. 5.19 and 5.20 in terms of evolution of (a) percentage of cumulative fines loss with time and (b) erosion rate with time under different effective confining pressures and initial fines content. It is noted that both the cumulative eroded soil mass and maximum erosion rate decrease with the effective confining pressure and increase with the initial fines content within the test range. The erosion rate reaches the peak at the beginning of stage 2 and then drops with time to a constant value. This tendency is in accordance with the finding of Reddi *et al.* (2000), who conducted the internal erosion test by a flow pump.

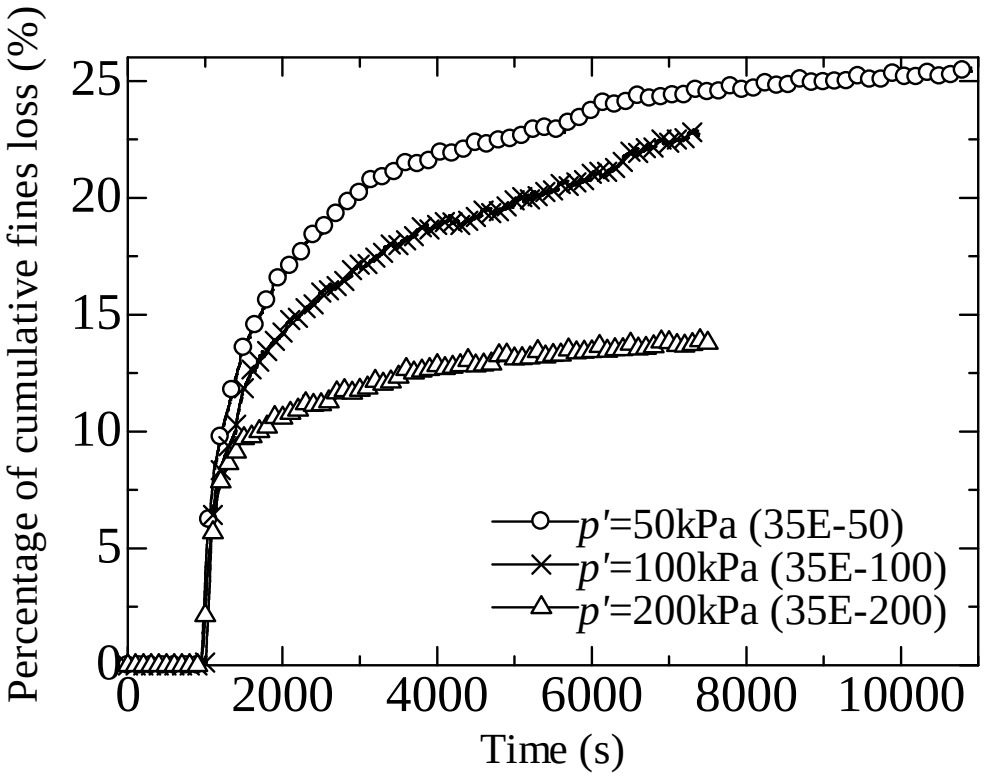

(a) Percentage of cumulative fines loss with time under different effective confining pressures for specimens with 35% initial fines content

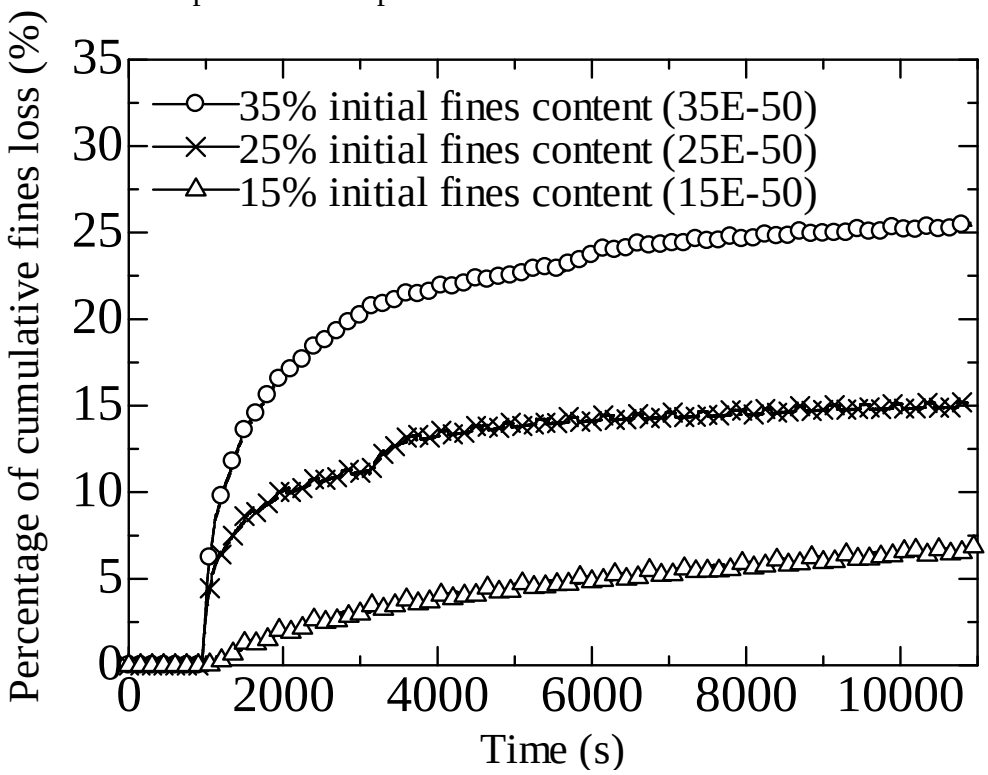

(b) Percentage of cumulative fines loss with time for specimens with different initial fines contents under an effective confining pressure of 50kPa

Figure 5.19 Percentage of cumulative fines loss within seepage test period

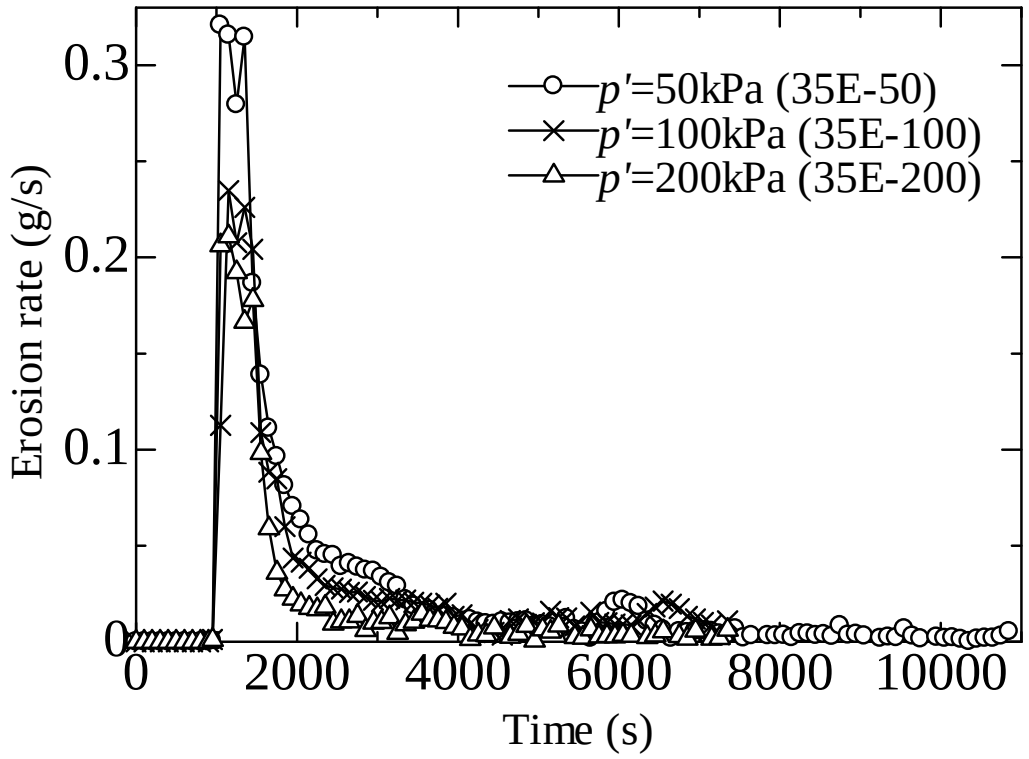

(a) Erosion rate with time under different effective confining pressures for specimens with 35% initial fines content

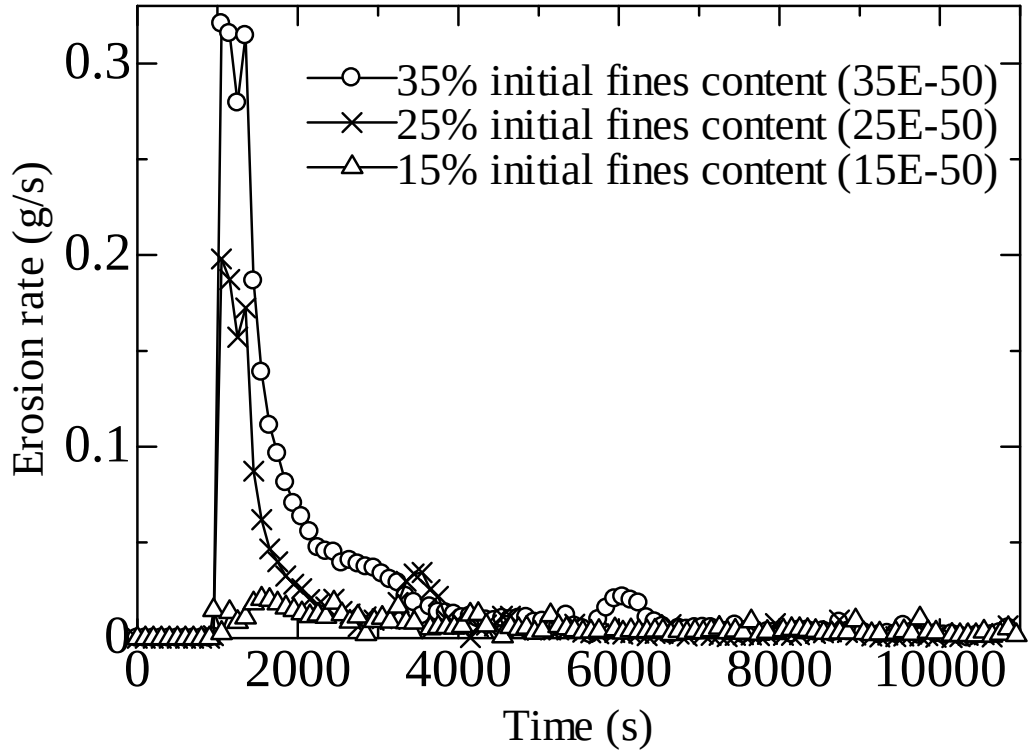

(b) Erosion rate with time for specimens with different initial fines contents under an effective confining pressure of 50kPa

Figure 5.20 Evolution of erosion rate within seepage test period

5.6 Conclusions

The mechanisms of internal erosion for saturated sand with different initial fines contents at isotropic stress states are presented in this paper. The binary mixtures consist of two types of silica sands (silica No.3 and No.8) with different dominant grain sizes. With larger grain size, the silica No.3 works as the soil skeleton in the mixtures while the fine silica No.8 is the erodible fines. Erosion tests are performed by the constant-flow-rate control in triaxial apparatus. The back pressure is applied to ensure the full saturation of tested soil. Cumulative eroded soil mass is continuously recorded by a consecutive monitoring system. The mechanical consequences of internal erosion are assessed by conducting drained compression tests on eroded soil specimens.

Hydraulic gradient dramatically drops with the progress of internal erosion, indicated by the erosion of large amounts of fines. Correspondingly, hydraulic conductivity, derived from Darcy's law, keeps increasing at this stage. Afterwards, the soil grains would gradually reach a new equilibrium when the hydraulic gradient and cumulative eroded soil mass become constant. A moderate decrease of hydraulic conductivity is detected after a significantly long period of test time, which might be caused by the clogging of fines inside tested specimens. Erosion of fines would result in the increase of contractive volumetric strain. The post-erosion grain size distribution analysis indicates that the fines loss is larger in the upper layer. The saturation degree drops after internal erosion test with the B-value larger than 0.93.

Assigned the seepage flow with the same velocity, the specimens under the larger effective confining pressure show less increments in hydraulic conductivity within the test range. The percentage of cumulative fines loss and volumetric strain induced by internal erosion is the least in the specimens under the effective confining pressure of 200kPa and the largest in the specimens under the effective confining pressure of 50kPa.

Comparing the erosion test results of the specimens with 35%, 25% and 15% initial fines content, respectively, the largest change of hydraulic conductivity occurs in the specimen with 35% initial fines content. Fines loss is larger for the specimens with larger initial fines content and correspondingly, the internal erosion induced volumetric strain is larger. The change of void ratio is closely dependent on the volumetric strain during internal erosion. In this series of erosion tests, the tested specimens show contractive behavior and the post-erosion void ratio increases.

CHAPTER 6

MECHANICAL RESPONSES OF INTERNALLY ERODED SOIL

6.1 Overview

The coarse grains may rearrange their inter-position into a new equilibrium and consequently, eroded soil will become loose. The stress ~ strain relationship of the internally eroded soil might be greatly altered compared with the original soil. There is a high possibility that the strength of the post-erosion soil decreases due to the destructive function of internal erosion. Sugita *et al.* (2008) reported flow slide of several embankments constructed on catchment topography (i.e., swamps and valleys) during Noto Peninsula Earthquake of Japan. Because of the ground configuration, those embankments may have been suffering from years of internal erosion and chronically become too weak to resist seismic shakings. Although soil erosion might be a huge threat for the stability of existing earthen structures, unfortunately, few studies could deliver comprehensive investigations about the consequences of soil erosion from the perspective of soil mechanics. This chapter mainly discusses the mechanical consequences of internal erosion on a series of non-cohesive soils. By utilizing the modified triaxial apparatus, undrained and drained monotonic tests are performed on the eroded specimens, which would be helpful to fully understand the mechanical characteristics of eroded non-cohesive soil. Of special interests are the comparison of soil behavior between the eroded soil and the original soil without erosion. Associated with the results of monotonic compression tests, internally eroded specimens have been tested under a series of cyclic loading to illustrate the cyclic failure and determine its cyclic strength.

Since the direct consequences of internal erosion include the reduction in fines content and increase in void ratio, knowledge of the mechanical influence of nonplastic fines and void ratio might be helpful to understand the responses of the internally eroded non-cohesive soil. It is universally recognized that the presence of nonplastic fines in a soil could create a “metastable” soil structure (Terzaghi, 1956) that greatly influences the mechanical characteristics of soil. Generally the median grain size of the skeleton sands (D_{50}) ranges within 1mm to 0.1mm corresponding to medium ~ fine sand, whereas that of the nonplastic fines (d_{50}) is predominantly smaller than 0.075mm corresponding to the silt passing a No.200 U.S. standard sieve (ASTM D2487-11). Regarding the mechanical function of nonplatic fines debates still exist in literature. Kuerbis *et al.* (1988, 1989) conducted undrained triaxial tests on Brenda mine tailings sand with fines contents of up to 22.3% and noted that for those specimens with a constant void ratio of the skeleton sand, an increase in fines content would cause slightly more dilative behavior. Adopting the similar comparison basis which is a similar void ratio of the skeleton sand, Pitman *et al.* (1994) tested Ottawa sand with the contents of crushed quartz fines and kaolinite up to 40%. The results of the undrained triaxial compression tests indicated a slightly more dilative soil response generating a sand with larger liquefaction resistance. Salgado *et al.* (2000) mixed Ottawa sand with up to 20% silcosil

and created several soil specimens with similar relative density. The results of drained triaxial tests presented an increase in the dilatancy with the increase of fines content. Undrained compression tests on the old alluvium sand of Singapore with 0% and 9% content of silt-size quartz conducted by Ni *et al.* (2004) showed that at the same void ratio of skeleton sand, nonplastic fines increased the undraind strength and, at worst, act like voids. But contrary behavior was observed by others. Zlatovic and Ishihara (1995) noted that for Toyoura sand mixed with up to 30% of silt contents, the increasing of nonplastic fines contents would trigger increased contractive soil behavior in undrained triaxial testing. Similarly, Lade and Yamamuro (1997) observed that an increase in the contents of Nevada fines would reduce the volumetric dilative tendency in both undrained and drained triaxial compression tests, even though the relative density was increased. Undrained triaxial tests conducted by Monkul and Yamamuro (2011) on the Nevada sand-B with contents of Loch Raven silt up to 20% indicated that the presence of nonplastic fines would increase the soil contractibility resulting in a soil vulnerable to liquefaction.

Because of the extreme diversity in mineralogical and geometric characteristics of soil grains the published contradictory results may not present a persuasive picture of the mechanical effects of fines content. Lade and Yamamuro (1997) pointed out that the understanding of consequent experimental conclusions should be on the basis of a legitimate and logical comparison, such as soil preparation method, relative density or grading curve. The most direct comparison base is fines content which would be regarded as a variable for the classification of silty sand behavior. If clean sand is mixed with increasing amounts of fines, usually the e_{max} & e_{min} and void ratio range (difference between e_{max} and e_{min}) would change correspondingly. In this approach, a chevron-shaped relation of e_{max} & e_{min} and fines content is commonly utilized (Lade *et al.*, 1998; Cubrinovski and Ishihara, 2002), as is shown in Fig.6.1 with the superimposed of corresponding soil microstructure evolution. In this plot, the soil grain is assumed to be spherical. Within the span of the percentage of fines content in a soil, it has been divided into three zones: coarse fractions dominance zone (CZ), transitional zone (TZ) and fine fractions dominance zone (FZ). Within CZ, small amounts of fines fill within the voids among coarse fractions. Thus an increasing in the fines content results in a proportional reduction of e_{max} and e_{min}. That is to say, the overall volume of sand will stay constant irrespective of the increasing in the fractions of fines. At this circumstance, the strength of the binary mixtures is mainly provided by the coarse fractions as a result of the phenomenon that strong force chains preferentially pass through larger grains (Voivret *et al.*, 2009) and fines may hardly participate in force transformation, acting like a void. It enters the TZ when the dominant network of coarse fractions begins to be destroyed and fine fractions start to participate the network. A value of threshold fines content (FC_{th}) may exist to indicate the state that the fines fully occupy the voids of coarse fractions where the e_{max} and e_{min} of the binary soil reach the smallest value. Soil fabric will transform from “fines floating on sands” to “sands floating on fines” (Vallejo, 2001; Yamamuro and Covert, 2001; Huang *et al.*, 2004; Yang *et al.*, 2006; among others). FC_{th} is unique for each particular soil and no universally acceptable value exists. Papadopoulou and Tika (2008) determined a value of 35% as a threshold value for Assyros quartz sand from the movement of critical state line in *e~logp’* space. Carrera *et al.* (2011) regarded a fines content of 50% as transitional fines content for Stava

tailings. Chang and Meidani (2012) suggested a range of 25% ~ 35% to denote the transition zone. The anticipated soil behavior would depend on how great the fines involve in the force chains. It is of significance to figure out whether nor not the fines effectively work as separators between coarse gains. Since soil fabric is complicated and unpredictable, the prediction of transitional soil behavior, so far, is still ambiguous, which Chang and Meidani (2012) comment as "a gray area". Nocilla *et al.* (2006) concluded that for transitional soil, unique normal consolidation line and critical state line may not exist. Beyond this zone, an increasing in fine fractions content would completely isolate the coarse fractions, resulting in FZ. Instead of acting like a void, the fines would constitute the dominant network, which determines the soil mechanical behavior. The discussion of this paper will be confined in the coarse dominance zone (CZ) and transitional zone (TZ), as is denoted in Fig.6.1.

Instinctively, void ratio, usually referred as a state variable for the prediction of soil responses, might be another available comparison base. But a sequence of experimental investigations has proven that the void ratio might be an inappropriate indicator. For instance, Lade and Yamamuro (1997) observed that silty sands liquefied statically even at almost dense state (up to a relative density of 60%) and demonstrated that the void ratio of silty sands would not effectively represent the number of solid contacts compared with that of clean sand. Realizing the difficulties of describing the fines content-dependent soil behavior merely by "void ratio" due to the complicated role of fines participating in force transform, Mitchell (1976) introduced a concept of "void ratio of the granular phase, e_s" assuming that the volume of fines is a part of the voids of coarse fractions. It is also referred as intergranular void ratio (Thevanayagam *et al.*, 1998, 2000), granular void ratio (Lupini *et al.*, 1981) or skeleton void ratio (Pitman *et al.*, 1994; Lade *et al.*, 1998). Thevanayagam and Mohan (2000) developed this concept and further subdivided the mechanical behavior of the sands within coarse dominance zone (CZ) and transitional zone (TZ), shown in Fig.6.2. The space between the maximum void ratio and minimum void ratio, indicating the achievable void ratio range, has been divided by a demarcation line corresponding to $e_s \approx e_{c\_max}$. Accordingly, the mechanical behavior of silty sand is classified into three categories. Specimens within Case 1 have smaller void ratio and the intergranular void ratio of coarse fractions is less than the maximum void ratio, indicating a comparatively stable packing of soil grains. The soil behavior largely depends on the coarse fractions. By comparison, specimens of Case 3 have a larger void ratio and the intergranular void ratio is larger than the maximum void ratio of the coarse fractions. In this case, the coarse grains are probably separated by the fines, resulting in an unstable packing of soil grains. The shear strength of the soil could be significantly influenced by the shear resistance along the fines. In between, Case 2 has an intermediate void ratio. The intergranular void ratio is approximately equal to the maximum void ratio of the coarse fractions. The anticipated soil behavior would depend on the percentage of fines wedged among the coarse fractions. Furthermore, to quantitatively reveal the function of fines, a parameter "*b*", presenting the percentage of the active fines participating in the force transformation in the network, has been included to derive the intergranular void ratio (Thevanayagam *et al.*, 2002, 2007). It is usually called "equivalent intergranular void ratio, e_s^*". Several studies proved that a unique critical state line may exist in the $e_s^* \sim logp'$ space, irrespective of fines content. However, the determination of "*b*" is subjective and

empirical, which again relates with the mineralogical and geometric characteristics of soil grains (Rahman *et al.*, 2011). The approximate regions of the tested specimens in this study are denoted in Fig.6.2, which indicates that their behaviors largely depend on extent of fines participating in the force chains and furthermore, the soil microstructure.

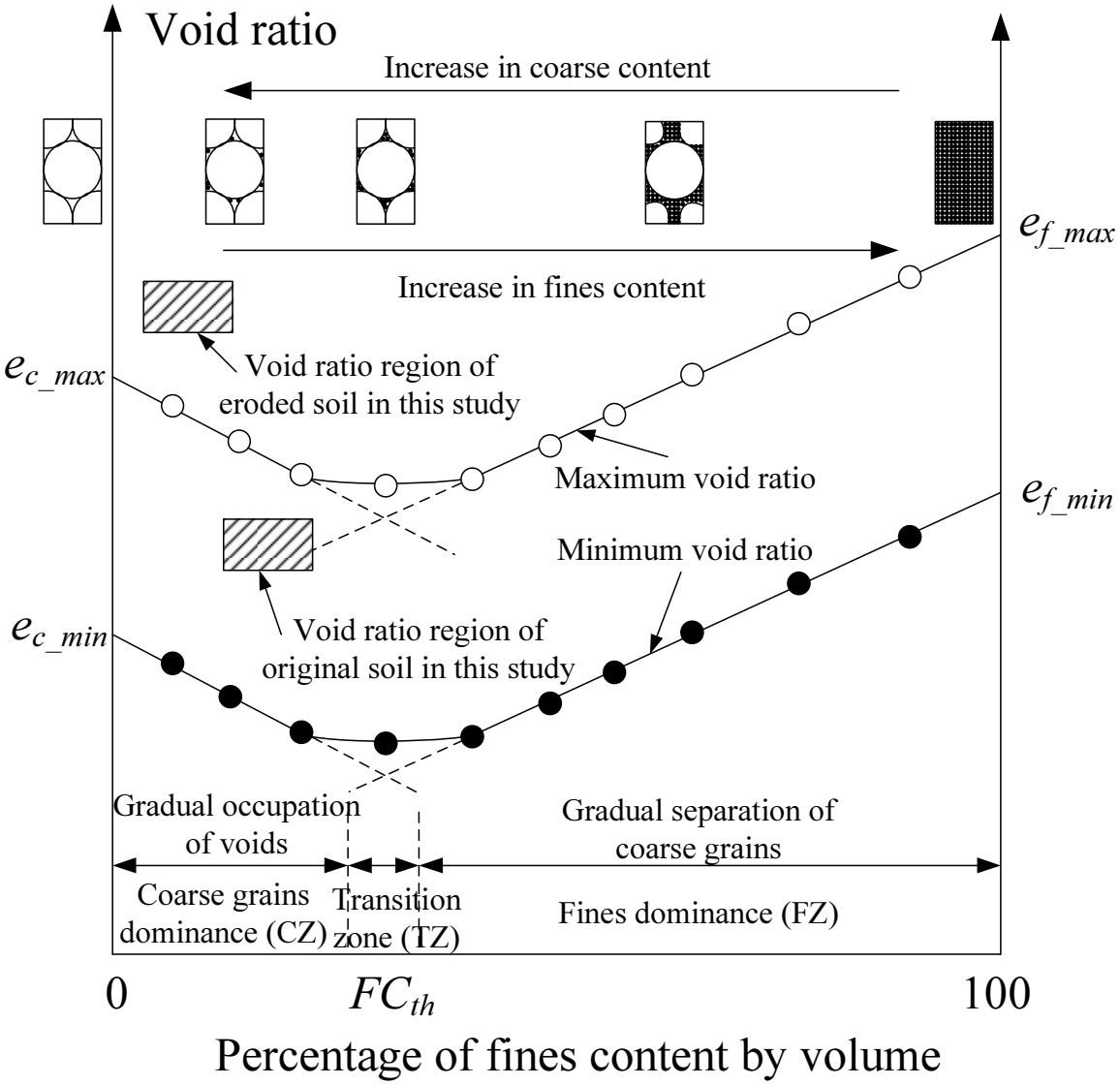

Figure 6.1 Relation of percentage of fines content and maximum & minimum void ratio with superimposed soil microstructure evolution

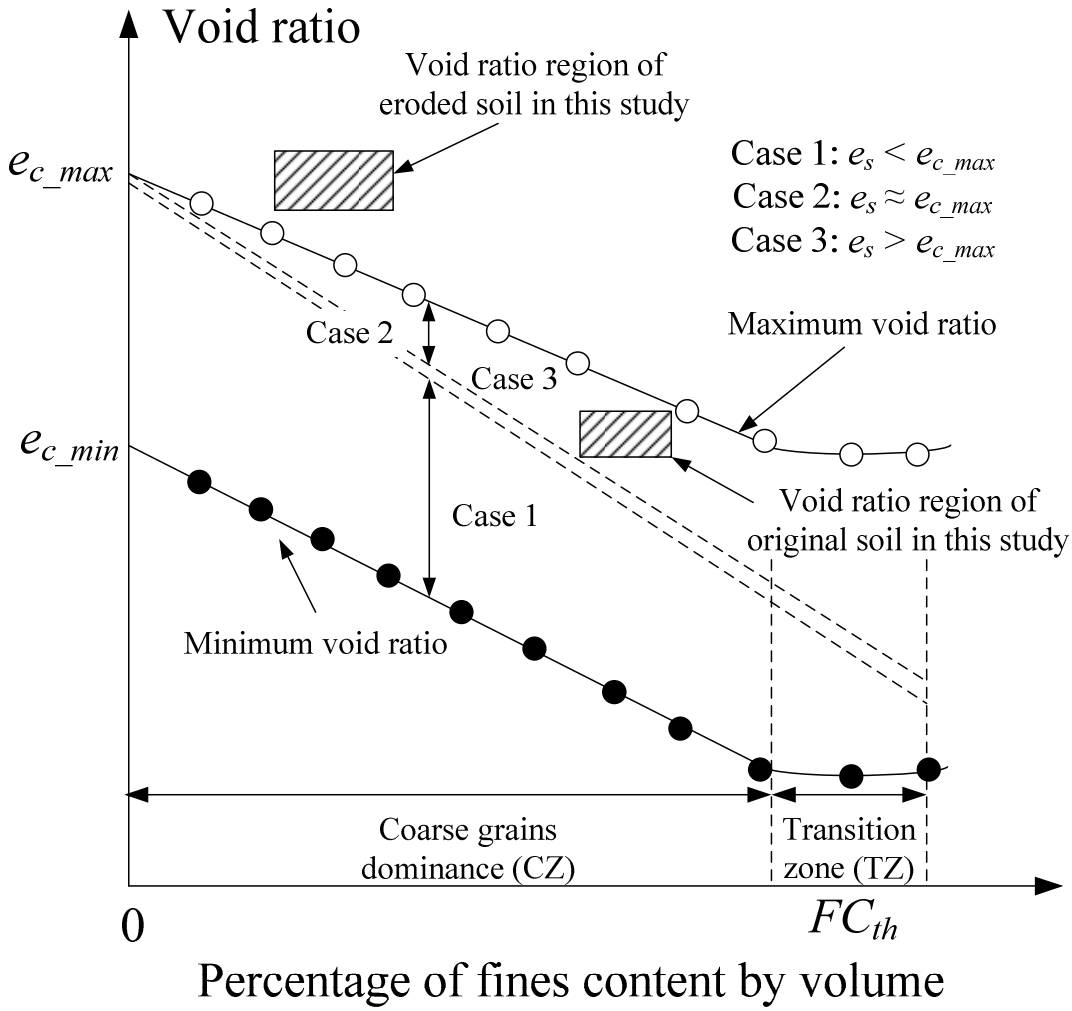

Figure 6.2 Intergranular matrix phase diagram

Other influential factors on the silty sands behavior have been discussed in detail in literature. For instance, Murthy *et al.* (2007) explained the increase of friction angle with addition of silt in sands by the relative angularity between the fine and the coarse grains. The more silt will contribute to increase the friction angle if the more angular the silt grains are and the more rounded the coarse grains are. Høeg *et al.* (2000) concluded that the reconstituted silty specimens prepared by moist tamping method showed a larger peak deviator stress compared with the specimens by slurry method and water pluviation method. Monkul and Yamamuro (2011) analyzed the effect of median grain size ratio (D_{50c}/d_{50f}) and concluded that a "metastable" soil structure tended to be developed at a sufficiently large size ratio. The influence of soil grading was discussed by Carrera *et al.* (2011) who summarized that the locations of critical state line and normal compression line vary with the soil grading curves.

6.2 Tested specimens

As is introduced in section 5.2, the tested specimens are the binary mixtures of the two sands by three different fines contents (mass ratios), which are 35%, 25% and 15%. The

grain size distribution of the mixtures (Fig.5.2) indicates that all of the three specimens are gap-graded. Fig.6.3 shows a plot of e_{max} & e_{min} and void ratio range (difference between e_{max} and e_{min}) against fines content, which notes that the tested specimens with the maximum fines content of 35% belong to coarse dominance zone (CZ). The mechanical responses are largely dependent on how great the fines are participating in the force chains, as is described in Fig.6.2. The increasing void ratio range with the increase of fines content may result in a larger degree of possible variation in the packing of the sand and the specimens with significantly large amounts of fines may be more compressible. A summary of the test cases in this chapter is shown in Table 6.1. The initial void ratio refers to the void ratio of tested specimens under an effective confining pressure of 20kPa prior to consolidation. Each specimen with moisture is tamped to the target void ratio by the standard moist tamping method to avoid the segregation of the two kinds of grains with different dominant size. The tamping on each specimen is in a systematic manner to guarantee an identical input energy. The effective confining pressures during tests are 50kPa, 100kPa and 200kPa, which approximately correspond to the earth pressure of 5m, 10m and 20m in depth, respectively. Controlled specimens (35N, 35N-50(-D), 35N-100(-D) and 35N-200(-D)) at the same stress state without internal erosion are tested for the comparison purpose. The test program follows section 4.3. A schematic diagram of the test procedure in Cambridge stress field is presented in Fig.6.4.

The internally eroded specimens (35E, 35E-50(-D), 35E-100(-D) and 35E-200(-D)) are created by conducting the seepage test at a constant inflow rate of 310mL/min in the modified triaxial cell. As is discussed in section 5.5, the cumulative eroded soil mass decreases with the increasing of effective confining pressure and increases with the increasing of initial fines content within the test range. The changes in fines content and void ratios have been summarized in Table 6.2, where the equivalent intergranular void ratio is derived by adopting a b value of 0.7, recommended by Ni *et al.* (2004) for quartz sand with a fines content of 9%. It is indicated that with the significant loss of fines, the post-erosion void ratios of tested specimens greatly increase. Comparison of the specimens with 35% initial fines content under different effective confining pressures indicates the least increment in void ratio is found at the specimens with the largest effective confining pressure and however their intergranular void ratios are somewhat similar, approximately at 1.30. It may be regarded as a comparison base for interpreting the eroded soil behavior. A plot of the positions of the tested specimens within the void ratio ~ fines content space is shown in Fig.6.5. The post-erosion specimens own significantly large values of void ratio, even larger than the maximum void ratio, and thus an extremely loose soil state is expected. A larger fines content and a smaller void ratio is detected for the specimens on which seepage tests are performed under larger effective confining pressure, compared with the specimens under lower effective confining pressure. The positions of tested specimens are all above the demarcation line, indicating that the packing of coarse grains is unstable and effectively separated by fines, and the soil behavior is affected by those active fines participating in the force chains. Due to the characteristics of internal erosion, local clogging or accumulation of fines might occur and consequently, a particular packing of soil grains might be formed. Therefore, different from the normal mechanical behavior of sand, an exceptional soil behavior is discovered, which will be discussed later.

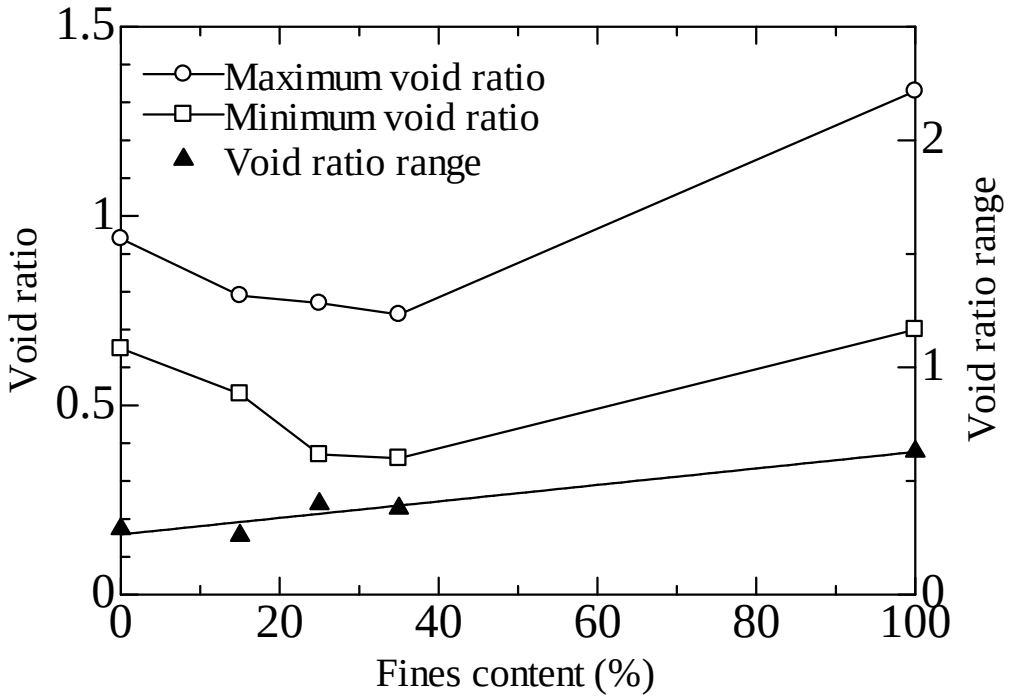

Figure 6.3 Relation of e_{max} & e_{min} and void ratio range against fines content

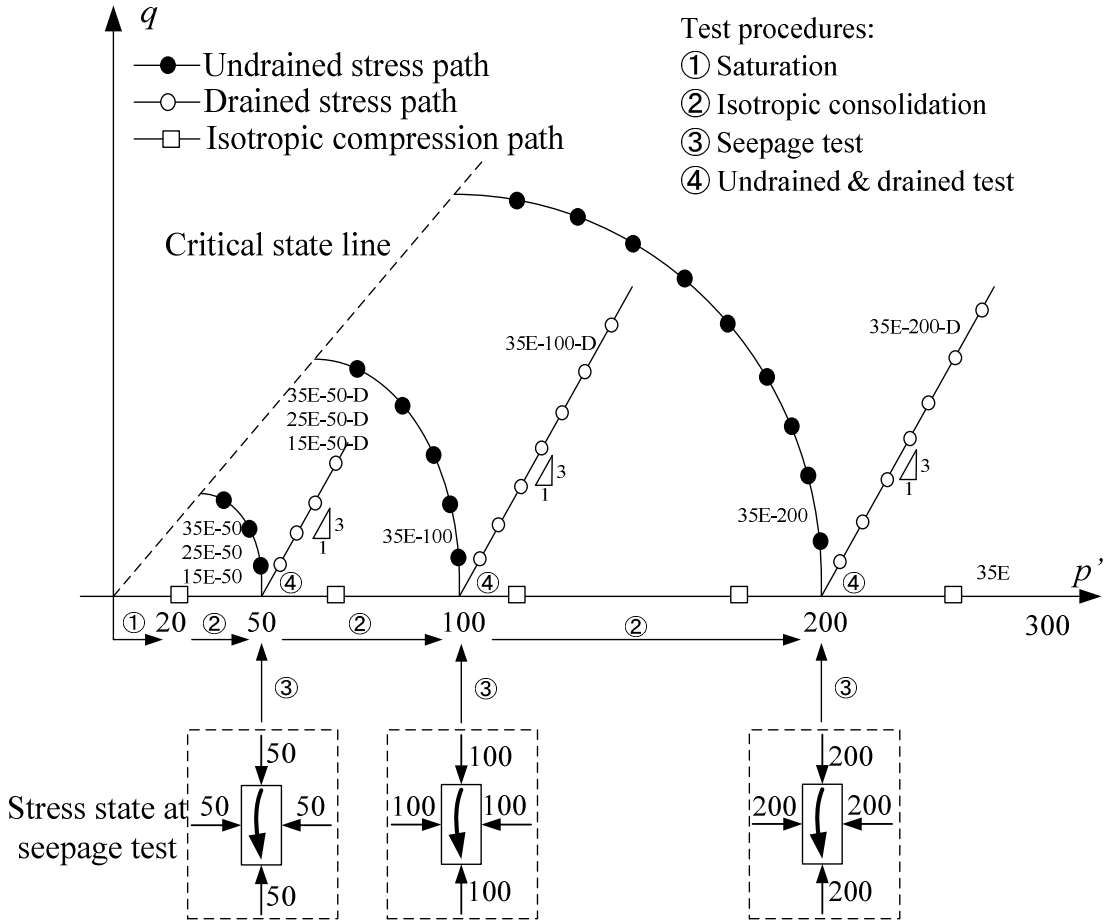

Figure 6.4 Schematic diagram of test procedures in Cambridge stress field superimposed with test cases

Table 6.1 Details of tested specimens

Specimens	Initial fines content before erosion (%)	Initial void ratio (e_i)	Initial confining pressure (kPa)	Post consolidation void ratio (e_c)	Type of compression
35E[(1)]	35	0.61	50	0.58	Isotropic compression
35E-50	35	0.59	50	0.56	Undrained
35E-100	35	0.60	100	0.55	Undrained
35E-200	35	0.59	200	0.55	Undrained
35E-50-D	35	0.59	50	0.55	Drained
35E-100-D	35	0.60	100	0.56	Drained
35E-200-D	35	0.64	200	0.57	Drained
25E-50	25	0.61	50	0.58	Undrained
15E-50	15	0.68	50	0.68	Undrained
25E-50-D	25	0.61	50	0.58	Drained
15E-50-D	15	0.68	50	0.68	Drained
35N[(1)]	35	0.61	------	------	Isotropic compression
35N-50	35	0.60	50	0.56	Undrained
35N-100	35	0.60	100	0.54	Undrained
35N-200	35	0.59	200	0.54	Undrained
35N-50-D	35	0.59	50	0.55	Drained
35N-100-D	35	0.61	100	0.56	Drained
35N-200-D	35	0.59	200	0.54	Drained

Note:
(1) Specimens named with “E” means erosion test is performed at a constant inflow rate of 310mL/min;
(2) Specimens named with “N” means the original soil without erosion.

Table 6.2 Summary of post-erosion soil conditions

Specimen	Post-erosion fines content (%)	Decrement of fines content by (%)	Post-erosion void ratio	Increment of void ratio by (%)	Intergranular void ratio(1)	Equivalent intergranular void ratio(2)
35E	13.33	61.91	1.03	77.59	1.34	1.11
35E-50	13.10	62.57	0.99	76.79	1.30	1.07
35E-100	15.90	54.57	0.92	67.27	1.29	1.02
35E-200	22.00	37.14	0.80	45.45	1.30	0.92
35E-50-D	13.52	61.37	1.01	83.64	1.32	1.09
35E-100-D	15.92	54.51	0.92	69.64	1.29	1.02
35E-200-D	24.53	29.91	0.77	35.09	1.34	0.91
25E-50	12.08	51.68	0.82	41.40	1.08	0.89
15E-50	8.75	41.67	0.79	16.18	0.97	0.84
25E-50-D	11.99	52.04	0.81	39.66	1.06	0.88
15E-50-D	9.98	33.47	0.78	14.71	0.97	0.83

Note:
(1) Intergranular void ratio $e_s=(e+FC/100)/(1-FC/100)$
(2) Equivalent intergranular void ratio $e_s^*=[e+(1-b)FC/100]/[1-(1-b)FC/100]$

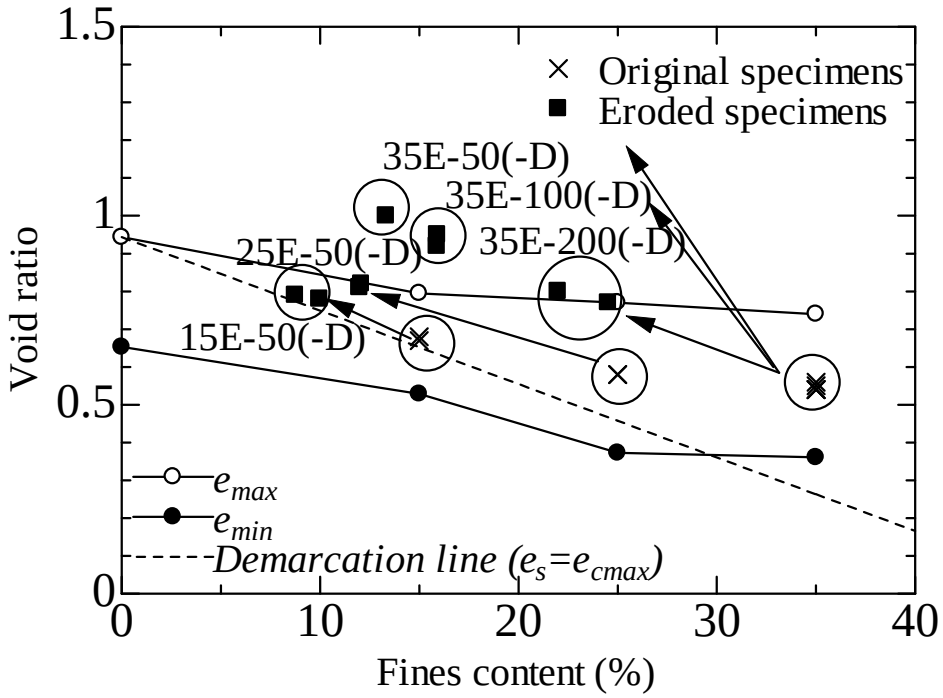

Figure 6.5 Plot of tested specimens in fines content ~ void ratio space

6.3 Summary of test results

6.3.1 Isotropic compression and swelling

The variations of specific volumes during isotropic compression tests are plotted in $v \sim \log p'$ space, shown in Fig.6.6. The original specimens refer to the specimens with 35% and 25% fines content, respectively. The eroded specimen denotes the post-erosion specimen, originally with an initial fines content of 35% before internal erosion and a fines content of 13% and specific volume of 2.03 after internal erosion at an effective mean stress of 50kPa. For the original specimens, the location of NCLs moves downwards as the fines content is increased and the two lines seem to be in parallel. The NCLs are flatter within the range of low mean effective stress, whereas gradually steepen with the increasing of mean effective stress and therefore, a unique gradient of NCL (ν) may not exist. Carrera *et al.* (2011) found a similar trend and noted that as the p' tends towards zero the NCLs of tested specimens have similar low gradient with a horizontal asymptote. In contrast, the swelling lines are in parallel for each specimen and a unique value of swelling line gradient (κ) would be determined as 0.033 and 0.021 for the specimen with fines content of 35% and 25%, respectively. Because of the significant increase of specific volume after erosion, the NCL of eroded specimen significantly ascends and curves compared with the original specimens. Similar trend that the NCL becomes steepen as p' increases and the swelling lines seem to be parallel is detected. Comparison of the coefficient of compressibility of the eroded specimen and original specimen at mean effective stress of 50kPa, 100kPa, 200kPa and 300kPa along with the gradient of swelling lines is summarized in Table 6.3. Commonly, the compressibility degrades with the increasing of mean effective stress, whereas at large stress level (i.e., 300kPa) it becomes slightly larger which might result from the adjustment of inter-positions among soil grains. Since the mineralogy and grain shape of the skeleton sand and fines are similar, the movement of NCLs may largely depend on the packing of soil grains and their relative movements rather than the difference in the soil nature. In terms of the eroded specimen 35E, the compressibility is lower at low mean effective stress and becomes larger at large mean effective stress compared with the original specimen before internal erosion (35N), which might reflect the influence of erosion on the soil fabric. A temporary strengthened soil packing might be formed, which results in an initial low compressibility. With the subsequent isotropic compression, this strengthened packing might be deteriorated at a mean effective stress between 100kPa and 200kPa, and consequently, eroded specimen shows larger compressibility at larger pressure due to the looser soil state. Further evidence of the temporary strengthened soil packing will be noted at the discussion of monotonic drained test results.

Table 6.3 Summary of isotropic compression indices

Soil	FC (%)	Specific volume at p'=50kPa	Coefficient of compressibility m_v (10^{-4}/kPa)(1)				Gradient of swelling line (κ)
			p'=50kPa	p'=100kPa	p'=200kPa	p'=300kPa	
35N	35	1.58	2.48	1.57	1.04	1.23	0.033
35E	13	2.03	1.66	1.39	1.29	2.64	0.051

Note: (1) changes in volume per unit volume for a unit change of effective stress

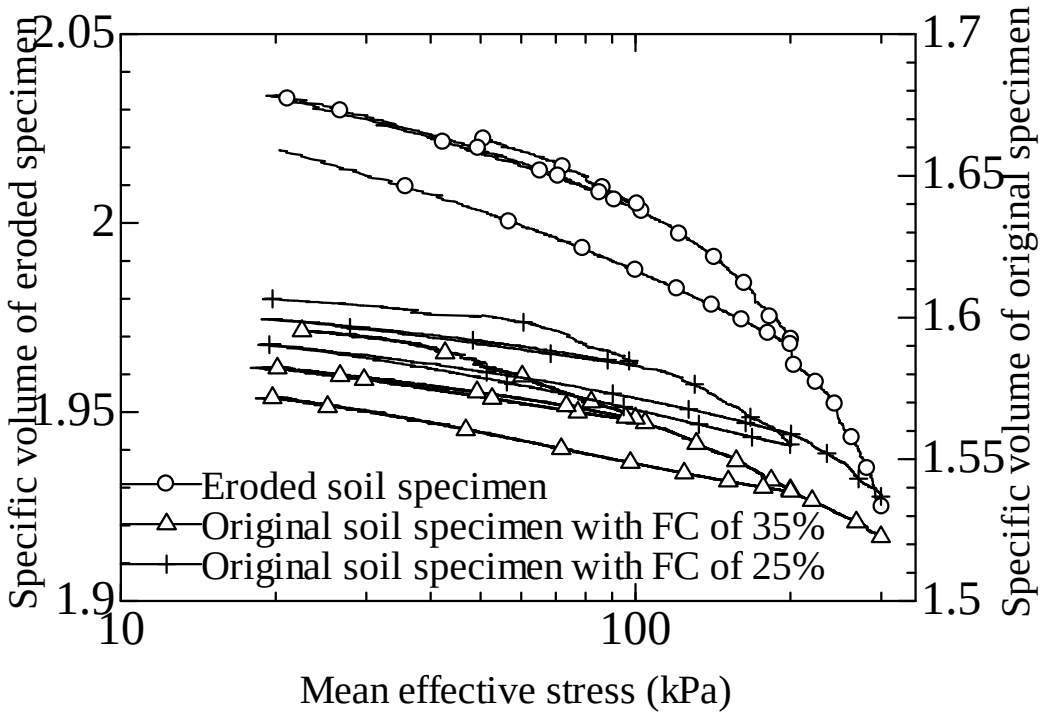

Figure 6.6 Normal compression lines of eroded specimen and original specimen

6.3.2 Monotonic drained tests

A series of three drained monotonic tests have been conducted on the eroded specimens under the initial effective confining pressure of 50kPa, 100kPa and 200kPa, respectively. Although the post-erosion void ratios of the specimens are different, the intergranular void ratios are basically equal (i.e., approximately 1.30). If the intergranular void ratio is accepted as the effective reference for the comparison of the mechanical behavior of eroded soils, the differences in the drained response may be mainly caused by the effective confining pressure and the particular post-erosion packing of soil grains. The relation curves of deviator stress and axial strain accompanied with the evolution of volumetric strain are plotted in Fig.6.7(a and b), respectively, which indicates a typical contractant volumetric behavior of loose sand. The deviator stress gradually develops and maintains constant at a peak value, whereas the contractive volumetric strain will rise to maximum and keep stable. Unfortunately, the tests in this study were terminated at the axial strain of about 13% ~ 17%, which may not be sufficiently large to present the full drained responses of eroded specimens. A better hyperbolic curve fitting is adopted by the following equations to approximate the contractant soil behavior at drained condition (Duncan and Chang, 1970; Ferreira and Bica, 2006):

$$q = \sigma_1^{'} - \sigma_3^{'} = \frac{\varepsilon_a}{a + b\varepsilon_a} \quad \text{……. (6.1)}$$

$$\varepsilon_v = \frac{\varepsilon_a}{c + d\varepsilon_a} \quad \text{……. (6.2)}$$

Where *a*, *b*, *c* and *d* are the constants which could be determined by hyperbolic fitting of original data. The extrapolated curves up to 20% are shown in Fig.6.7(a and b) by dash

lines, where an exceptional response of the volumetric strain at failure departure from clean sand is detected, as is displayed in Fig.6.8. Herein, failure is defined as the soil state wherein the deviator stress obtained at an axial strain of 15% (ASTM D4767-11; ASTM D7181-11). The plot, presenting the relation of volumetric strains at failure against initial effective confining pressure, indicates a reduction in volumetric strain with the increasing of effective confining pressure. Because of the dilatancy tendency under low confining pressure, at this circumstance, the clean sand commonly fails at lower volumetric strain and corresponding with further increase in effective confining pressure, increasing contractive volumetric strain in clean sand is expected. The inconsistent pattern of behavior detected for eroded specimens may imply a distinguished packing of soil grains from clean sand. Although the intergranular void ratios of the eroded specimens 35E-50-D, 35E-100-D and 35E-200-D are somehow similar, the fines contents vary approximately from 13% to 24%. The different responses in volumetric strain may indicate the differences in the extent of the participation of fines in the tested specimens. For specimen 35E-50-D, the fines may fully participate in the force chains and because of the relative larger compressibility of fines, a larger volumetric strain is noted. By contrast, the fines in specimen 35E-200-D may less participate in the force transformation and therefore, the volumetric strain is mainly induced by the coarse grains resulting in a less volumetric strain. Due to the progress of internal erosion, the distribution of fines in the specimens might be different depending on the effective confining pressure, the “b” value indicating the extent of the participation of fines might be different for each specimen. To fully understand the mechanism, a micro observation of the migration of fines during erosion test and compression test might be necessary.

A temporary declining in soil stiffness at the initial stage of shearing with respect to the axial strain ranging from 0% ~ 1% is observed. Figure 6.9 displays the variation of secant stiffness at the initial 1% of axial strain. The soil stiffness has been normalized by mean effective stress in order to compare the cases with different effective confining pressures and accentuate the uniqueness of internal erosion induced packing of soil grains. For the comparison purpose, the secant stiffness of clean silica No.3 sand with an initial void ratio of 0.88 during drained compression under an effective confining pressure of 50kPa is superimposed. Generally, the tested specimens show identical pattern of stiffness variation with the largest initial stiffness and exponentially reducing with axial strain. Compared with the loose clean silica No.3 at the relative density of approximately 20%, the eroded specimens still show much lower secant stiffness and therefore, an extremely loose fabric is expected for the internally eroded specimens. Furthermore, temporary drops in soil stiffness are observed for eroded specimens 35E-50-D, 35E-100-D and 35E-200-D, at the axial strain of 0.5%, 0.4% and 0.2%, respectively. It is considered as the evidence of the deterioration of the temporary reinforced soil packing that is developed by the progressive accumulation of fines among coarse grains during erosion. Under larger effective confining pressure, the reinforcement may be easily destroyed at subsequent compression and therefore, the stiffness drop in specimen 35E-200-D is found at lower axial strain. To validate the assumption, a direct observation of the post-erosion packing of soil grains by advanced testing technique might be necessary.

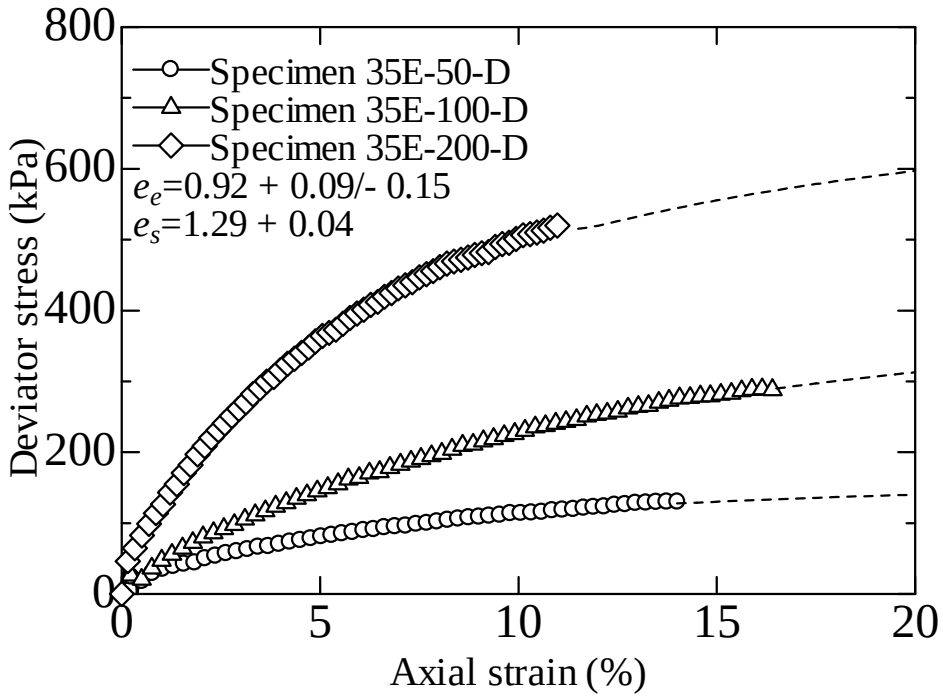

(a) Relation of axial strain and deviator stress

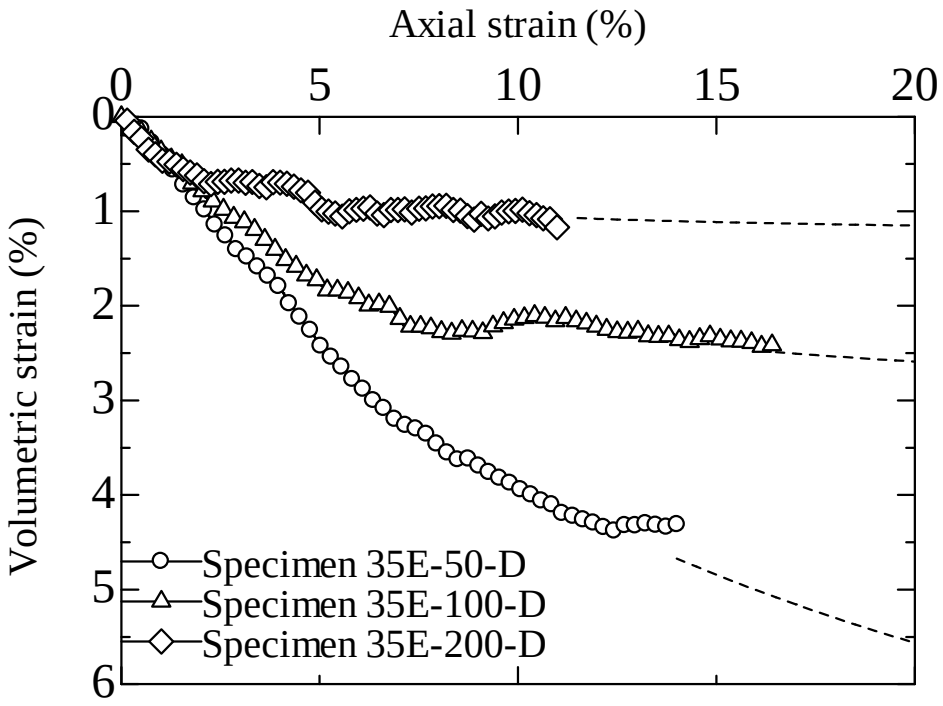

(b) Relation of axial strain and volumetric strain

Figure 6.7 Drained monotonic tests on eroded specimens under different effective confining pressures

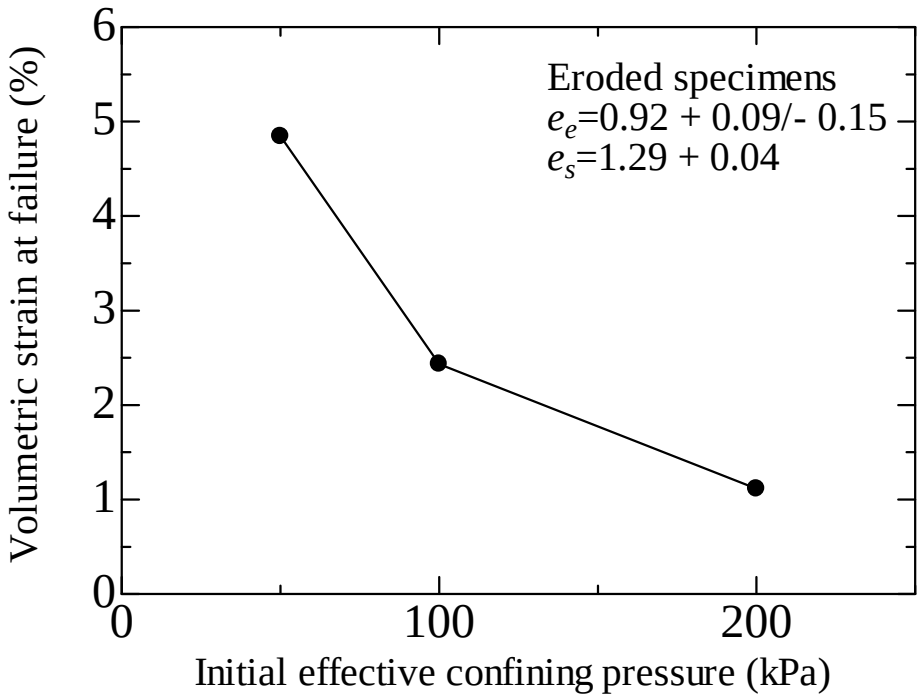

Figure 6.8 Volumetric strain at failure of eroded specimens against initial effective confining pressure

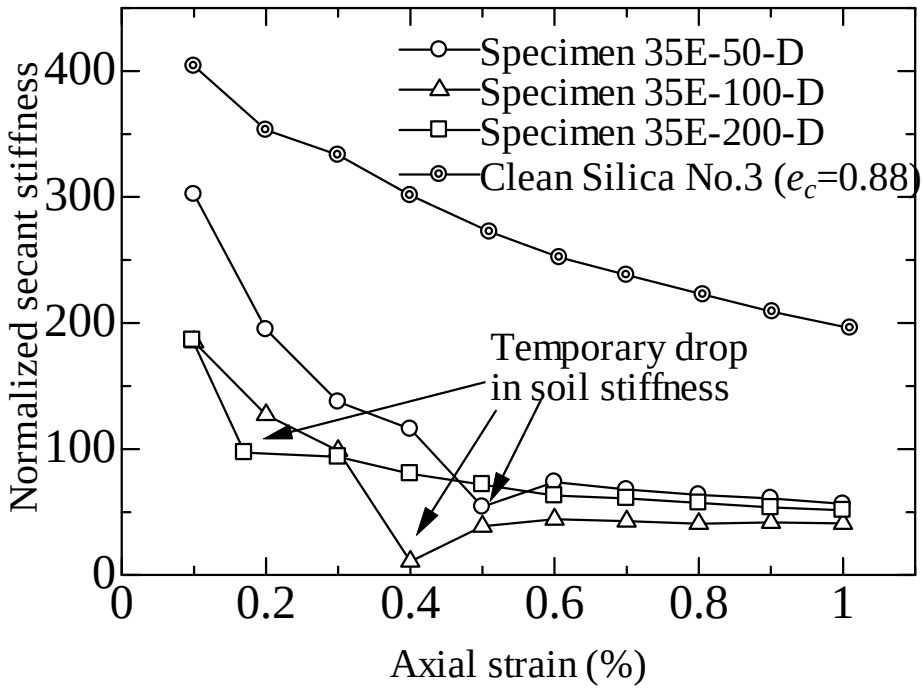

Figure 6.9 Normalized secant stiffness within 1% of axial strain superimposed with the stiffness of loose silica No.3

A majority of experimental investigations has revealed that an axial strain of 30% ~ 40% is necessary for achieving critical state of sand in drained test. However, in this

study, the critical state might not be reached and extrapolation of the data is somehow necessary. The identification of critical state line is fulfilled by plotting the stress ~ dilatancy relation of the drained tests on eroded specimens and extending the curve to the point of intersection with the zero dilatancy axis, shown in Fig. 6.10. Scattering though, an unique critical stress ratio $(q/p')_{cs}$ could be evaluated as 1.43 and accordingly, the derived critical friction angle is 35.27°. The derived critical state line (CSL) will be plotted in the Cambridge stress field for interpreting the undrained test results.

6.3.3 Monotonic undrained tests

Similarly, undrained monotonic tests have been conducted on the eroded specimens that have suffered internal erosion under an effective confining pressure of 50kPa, 100kPa and 200kPa, respectively. The post-erosion intergranular void ratios are similar, which is considered as the comparison base for interpreting the data. The differences in the undrained responses of eroded specimens are mainly caused by the effective confining pressure and the packing of soil grains formed after internal erosion. Figure 6.11(a and b) presents the undrained responses of the eroded specimens in terms of stress ~ strain curves and excessive pore pressure evolutions, respectively. The post-erosion void ratio and intergranular void ratio of the tested specimens are indicated in Fig.6.11a. Generally, the deviator stress of the eroded specimens reaches a marked peak at low axial strain, approximately 1%, followed by the temporary strain softening and then becoming dilative as the phase transformation point is arrived, which shows the typical characteristics of temporary liquefaction. It is recognized that temporary liquefaction appears at the condition where the undrained deviator stress achieves an initial peak and then drops to a minimum value, resulting from the rapid development of excessive pore water pressure and consequently, declining in effective stress. The state at which the undrained deviator stress reaches a local and temporary minimum is named as “quasi-steady state”. As the increasing of effective confining pressures, an increasing stability is observed since the quasi-steady deviator stress increases. The subsequent straining triggers the dilation in the eroded specimens causing the declining of excessive pore pressures and then rising of effective stress. This progress could be seen in Fig.6.11b, where excessive pore pressures build up to a peak within the initial 1% of axial strain and then maintained at the peak temporarily, followed by slight reduction with further compression. To quantitatively evaluate the temporary liquefaction potential of the eroded specimens under different effective confining pressures, a plot of the ratio of quasi-steady deviator stress to initial peak stress (q_{ss}/q_{peak}) against initial effective confining pressure is shown in Fig.6.12. A q_{ss}/q_{peak} of zero indicates complete drop of deviator stress to zero, whereas that of unit stands for a stable soil behavior (Yamamuro and Lade, 1997). It is seen that the increasing effective confining pressure results in the rising of stress ratio, indicating an increasing stability. Further evidence of the increasing stability with increasing of stress level is shown by plotting the mobilized friction angle at peak with effective confining pressure in Fig.6.12. A smaller mobilized friction angle is detected under lower effective confining pressure, indicating a greater potential of contractiveness. This pattern of behavior may be understood by the change of volumetric strain in the drained test, shown in Fig.6.7b. A larger contractive volumetric deformation is detected under lower effective confining pressure. Thus, it seems that the high compressibility may inhibit the dilation and consequently decrease

the mobilized friction angle. However, this tendency is contrary to the behavior of clean sand. Because of the trend of increasing dilatancy under lower effective confining pressure, the stress ratio of clean sand should decrease with increasing of effective confining pressure, implying an unstable soil behavior at larger stress level. Similarly, since the intergranular void ratio is basically the same for each case, the reverse soil responses should be associated with the packing of soil grains after internal erosion. This reverse pattern of behavior may pose a potential threat for the stability of eroded earth structure. Internal erosion commonly appears within the core of a dam and embankment where low confining pressure is expected. The reverse behavior of eroded soil that it becomes unstable under low confining pressure with the occurrence of temporary liquefaction may probably trigger the failure of the earthen structures.

Since the eroded specimens display reverse behavior from clean sand, it is necessary to assess their instability potential. Instability, also named as “prefailure instability”, refers to the soil state wherein large plastic strains occurs because of the soil being incapable of consistently sustain a given stress, which is commonly observed in saturated loose sand at undrained conditions (Lade and Pradel, 1990). The concept of “instability region” is utilized to evaluate the instability potential of a soil, locating somewhere between the critical state line (CSL) and instability line (IL). The instability line is determined by a series of locus points connecting the stress origin and the peak points of the effective stress paths, derived from undrained compression tests under different initial effective confining pressures, in the Cambridge stress field. A plot of undrained tests data in the stress space, superimposed with CSL derived from drained tests and IL, is shown in Fig.6.13. Temporary liquefaction occurs in the three eroded specimens indicated by an initial peak deviator stress followed by decline. Beyond the quasi-steady state, the specimen exhibits dilative tendency, resulting in a deviator stress larger than the initial peak at large axial strain (i.e., larger than 10%). The peak deviator stress increases with the increasing of effective confining pressure. In terms of the instability line, a nonlinear relation is detected within the range of 50kPa ~200kPa effective confining pressure, which might be attributed to the variation of effective friction angle with the increasing effective confining pressure. The nonlinear relation under the low mean effective stress region is considered as the typical undrained behavior of silty sand by Yamamuro and Poul (1997). They inferred that under large effective confining pressure (i.e., 6000kPa) where grain crushing dominances mechanism of shearing on sand the effective friction angle will maintain constant and the instability line will become linear.

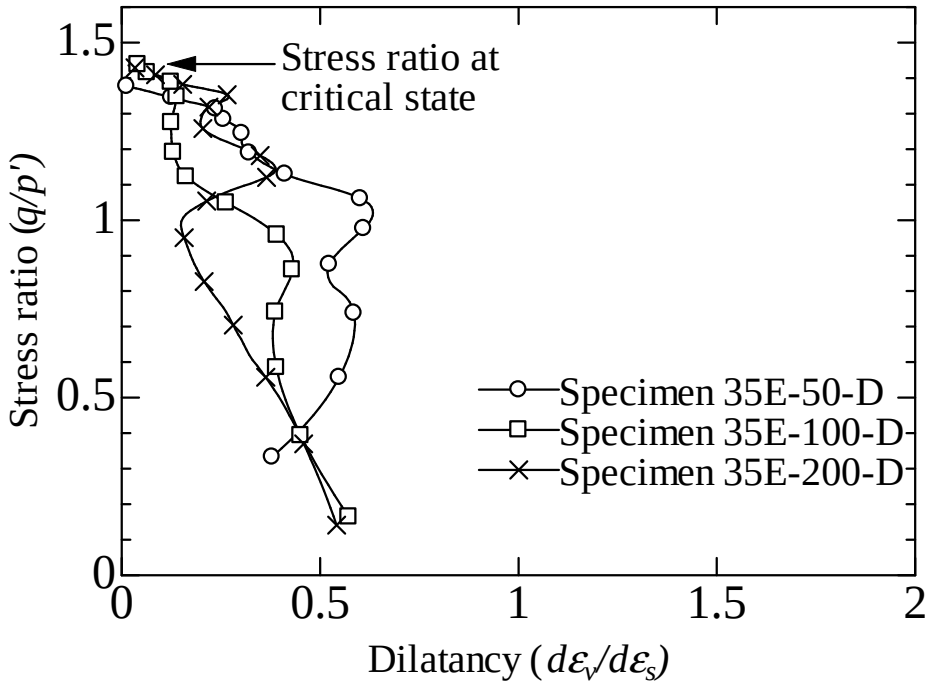

Figure 6.10 Relation of stress and dilatancy for drained tests on eroded specimens

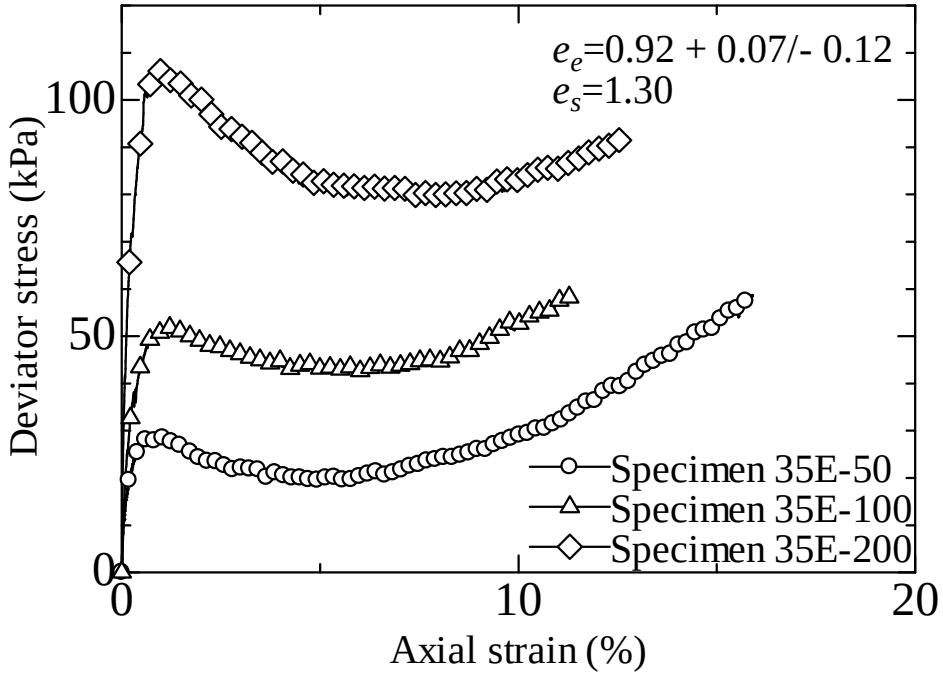

(a) Relation of axial strain and deviator stress

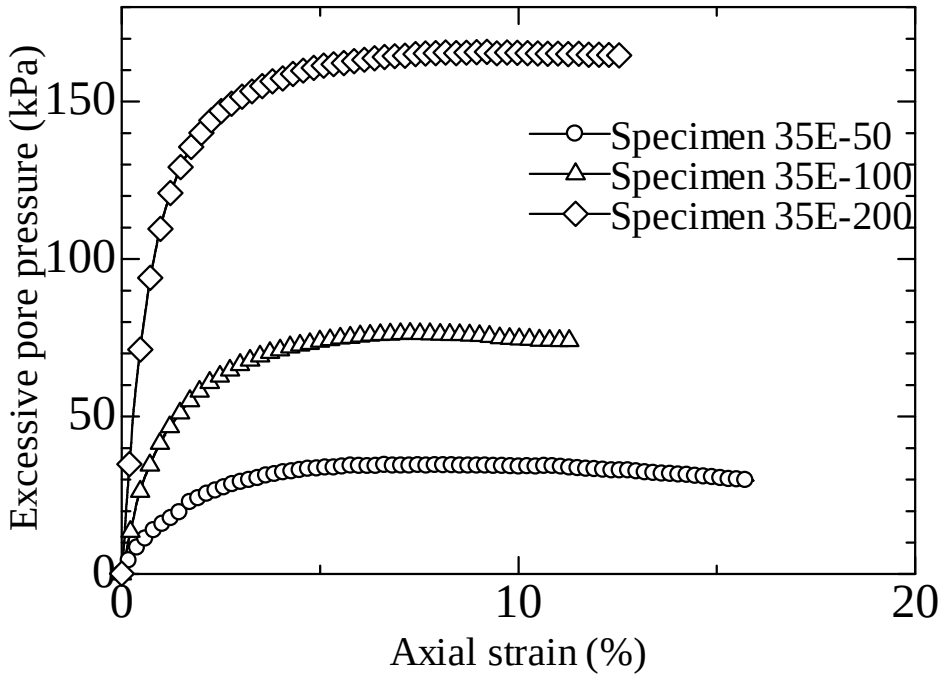

(b) Excessive pore pressure generation with axial strain

Figure 6.11 Undrained monotonic tests on eroded specimens under different effective confining pressures

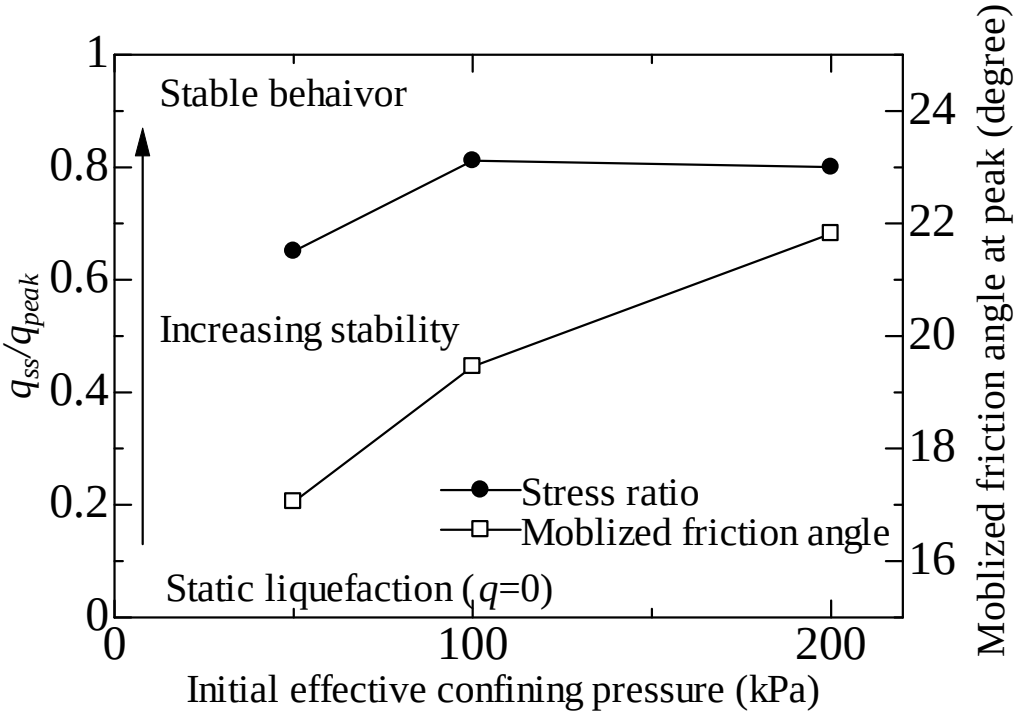

Figure 6.12 Relation of stress ratio and mobilized friction angle against initial effective confining pressure

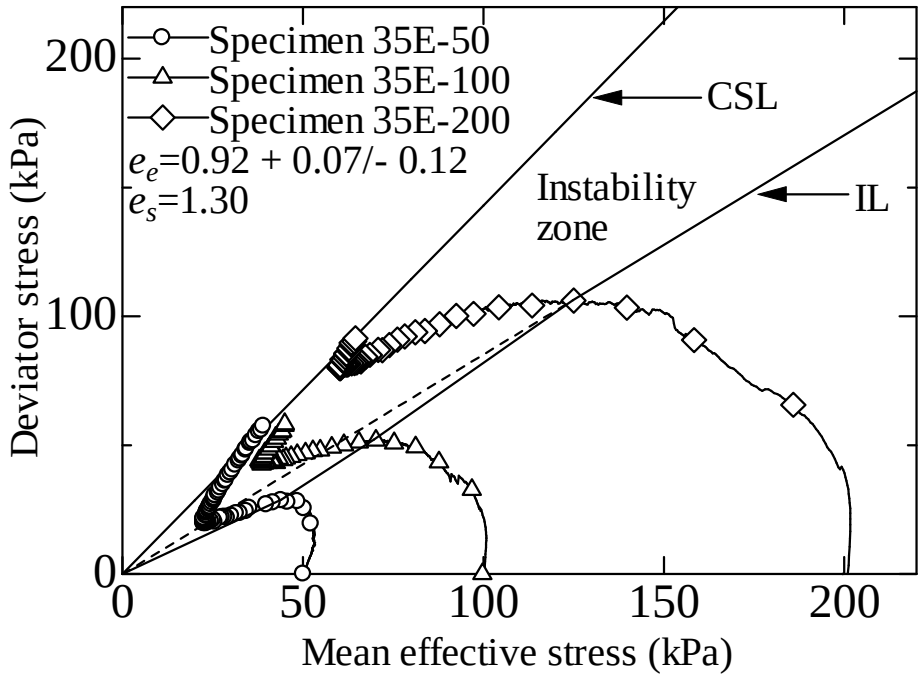

Figure 6.13 Effective stress path of undrained tests in Cambridge stress field superimposed with critical state line, instability line and instability zone

6.4 Exceptional behavior of internally eroded soil

Monotonic compression tests on internally eroded specimens have revealed the exceptional soil responses from clean sand. The eroded soil displays typical contractive pattern of behavior in the drained tests, whereas in terms of undrained responses the eroded soil initially becomes contractive and succeeding dilative. With the increasing of effective confining pressure the eroded soil exhibits a less volumetric strain in the drained tests and a greater mobilized friction angle in the undrained tests. Meanwhile, a decline in soil secant stiffness at drained tests is detected within the initial 1% axial strain. Since the intergranular void ratio of the tested specimens are approximately the same and the effective confining pressure may not be sufficiently large to trigger grain crushing (i.e., a maximum effective confining pressure of 200kPa in the compression tests), the soil responses should be dominated by the post-erosion grain configuration in the specimens and the rearrangement of their interpositions during shearing.

6.4.1 Mechanical influence of fine silica No.8

Firstly, the presence of fines in soil specimens, creating a soil packing fundamentally different from clean sand, may alter the soil responses at shearing. The mechanical influence of silica No.8 on the mixtures is indicated in Fig.6.14(a and b) by plotting the axial strain and undrained deviator stress relation, and corresponding effective stress path in *p'-q* diagram of the specimens with fines contents of 35%, 25%, 15% and 0%, respectively, under an initial effective confining pressure of 50kPa. The skeleton sand consists of the coarse silica No.3 sand. The reconstituted specimens with fines are prepared by moist tamping method with an initial relative density of approximate 30%.

The moist tamped specimen of clean silica No.3 is targeted at the largest achievable void ratio to accentuate its dilative tendency even at loose condition. It is obviously noted that the presence of silica No.8 would decrease the soil strength and inhibit the dilatancy tendency. The initial slopes of the effective stress paths increase with the decreasing in fines content, indicating a lower rate of pore pressures generation for the specimen with less fines content. This rate is controlled by the contractive volumetric deformation potentials in the specimens. By comparison, the specimen without fines shows complete dilative behavior, whereas that with 35% fines content displays contractant deformation throughout the compression. It is inferred that the fine silica No.8 may lubricate the skeleton No.3 grains and therefore, smoothes the contacts among the coarse grains. The loss of effective contacts and the large compressibility of fines cause the soil stiffness to decrease and the compressibility to increase. In terms of undrained condition, the consistent shearing may force the fines to slide into the voids and correspondingly the coarse grains move into a better contact, causing dilatancy at larger axial strain. The loose specimens with larger amount of silica No.8 may prolong the initial contractive tendency due to the function of “lubrication”. Similarly, a larger effective confining pressure may accelerate the progress of the sliding of fines into voids, which overcomes the initial contractive effects of fines, and consequently, the tested specimens show larger mobilized friction angle under larger effective confining pressure. Similar evidences of the existence of the lubricated soil grain configuration could be referred to Thevanayagam *et al.* (2000, 2007). The particular function of fines and resulting packing of soil grains may explain the observed initial contractive and succeeding dilative behavior in the undrained test and the increasing mobilized friction angle with the increasing of effective confining pressure, as is shown in Fig.6.13.

6.4.2 Distinctive packing of soil grains after internal erosion

The mechanical function of fines could not offer reasons for the temporary decline in secant soil stiffness observed in the drained tests. If the presence of fines assumes to be sufficient to explain the exceptional behavior of eroded soil, a similar mechanical response should be expected between the eroded specimens and the reconstituted specimens with similar fines content and initial void ratio. Further tests have been performed to validate this assumption. The reconstituted specimen with 15% initial fines content is prepared by moist tamping method, targeting at the largest achievable void ratio. Because of the occurrence of large volumetric deformation during consolidation, the void ratio before compression is 0.81, still less than the post-erosion void ratio of 0.99. Figure 6.15(a and b) indicates the drained responses of the two specimens in terms of stress ~ strain relationship and corresponding development of volumetric strain. Due to the larger void ratio, the eroded specimen mostly gains less strength. However, the volume change curves seem to somewhat departure from the associated understanding. The looser eroded specimen behaves less contractively comparing to the denser reconstituted specimen at the initial compression. Careful examination of the soil response within the initial 1% axial strain leads to another inconsistent pattern of behavior, shown in Fig.6.15c. The initial secant stiffness of eroded specimen is larger than that of the reconstituted specimen and a sudden drop in deviator stress is detected around 0.5% axial strain, after which soil strength and secant stiffness keep lower than that of the reconstituted specimen throughout the test range.

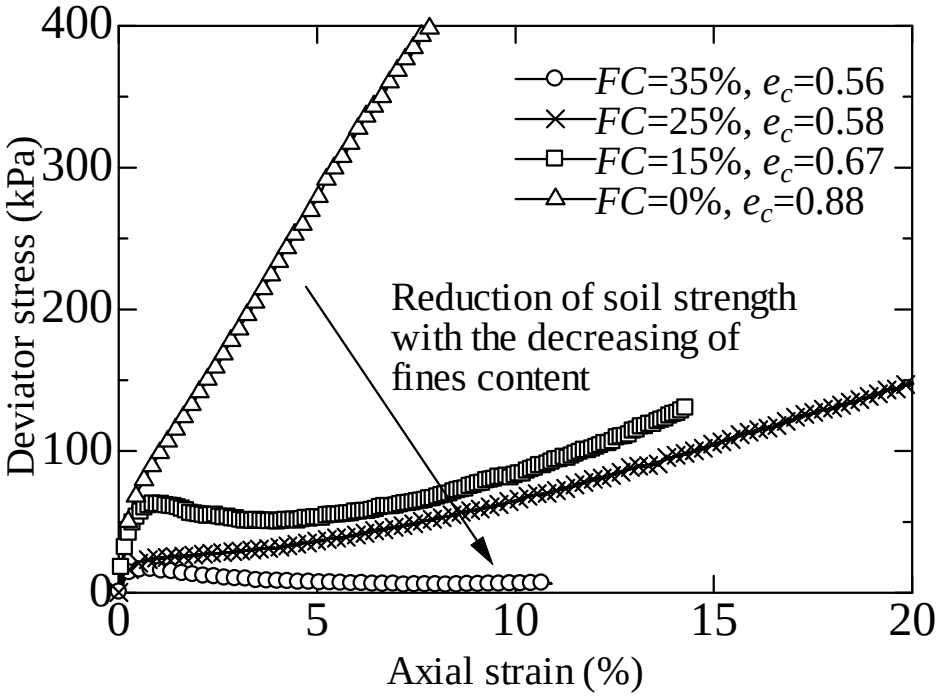

(a) Relation of axial strain and deviator stress

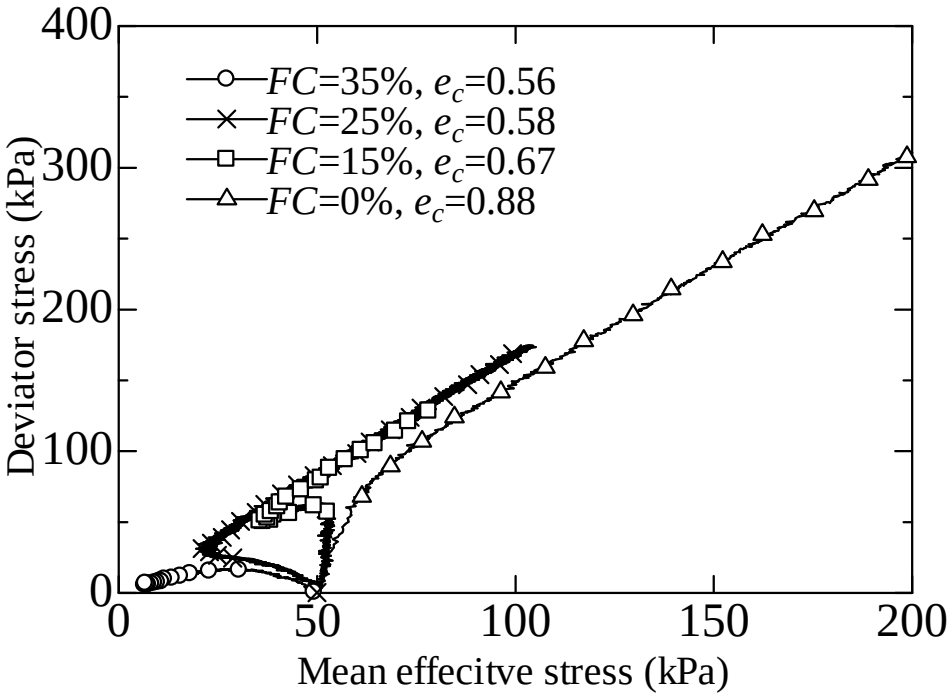

(b) Relation of mean effective stress and deviator stress

Figure 6.14 Undrained monotonic tests on eroded specimens with different contents of silica No.8 under an effective confining pressure of 50kPa

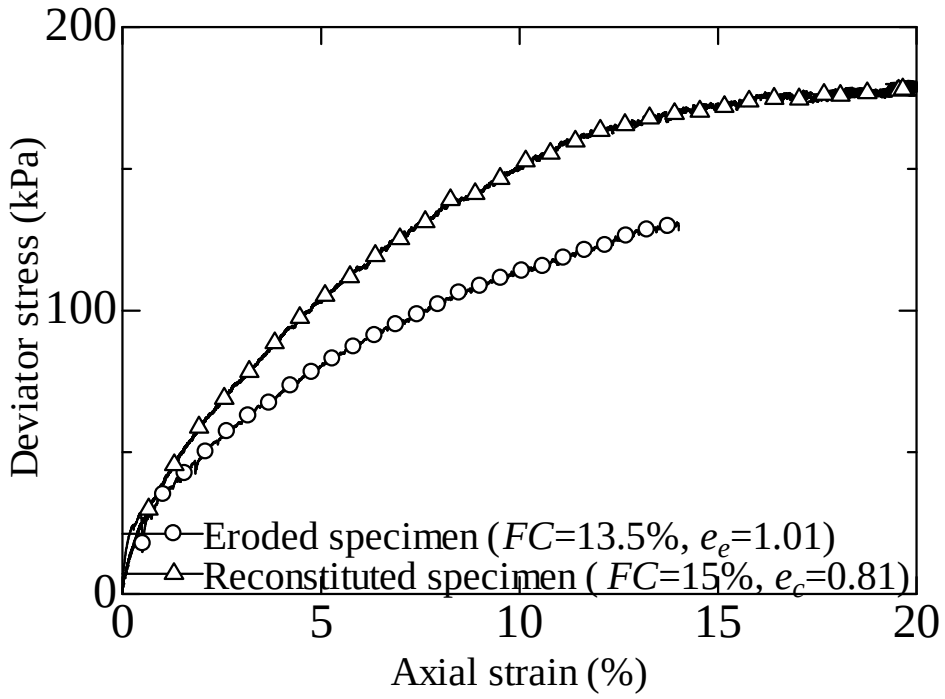

(a) Relation of axial strain and deviator stress

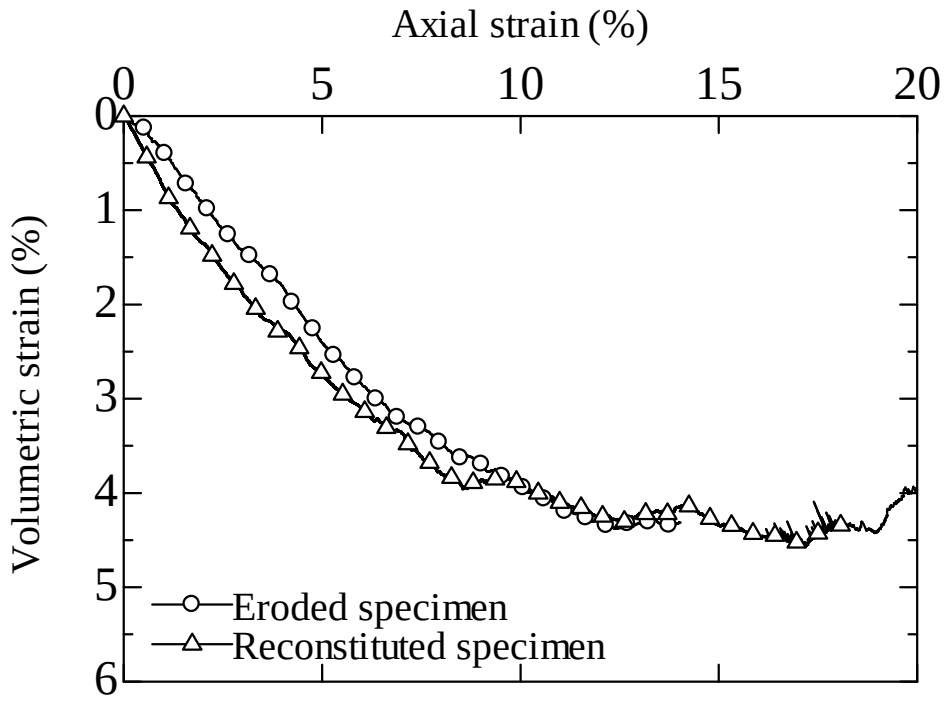

(b) Relation of axial strain and volumetric strain

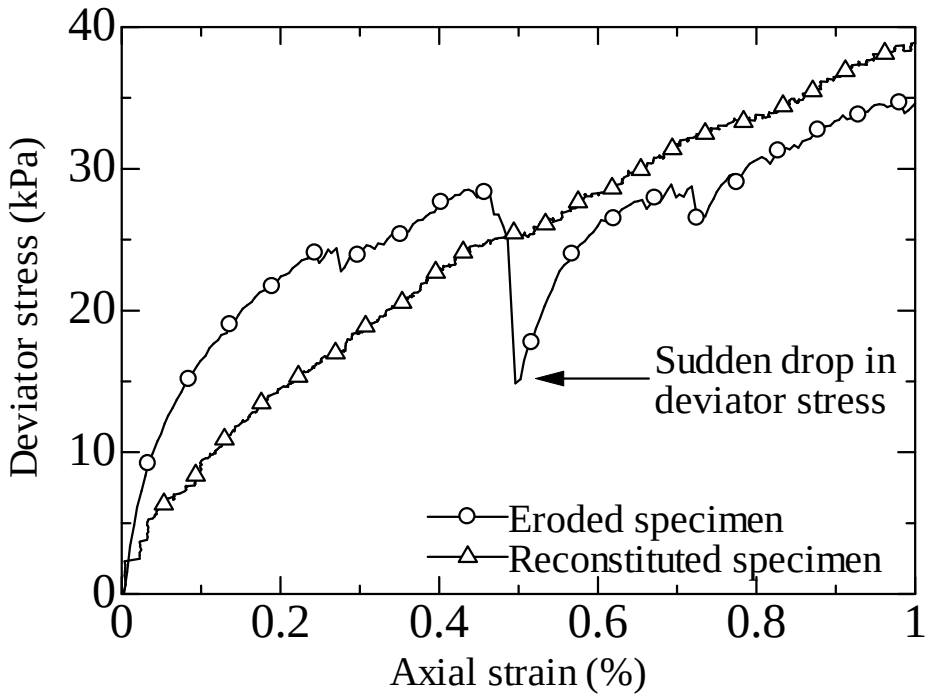

(c) Evolution of deviator stress within the initial 1% axial strain

Figure 6.15 Drained responses of the eroded specimen and the reconstituted specimen with similar void ratio and initial fines content under an effective confining pressure of 50kPa

To avoid the influence of possible errors rising from testing procedures on the observed phenomenon, undrained monotonic test has been performed on the eroded specimen and the reconstituted specimen with similar initial fines content and void ratio, as is shown in Fig.6.16(a and b). Looser though the eroded specimen displays a similar peak deviator stress as that of the reconstituted specimen at an axial strain of about 1%. After peak, the reconstituted specimen becomes fully dilative within the test range, whereas, the eroded specimen experiences temporary strain softening, followed by dilatancy. In terms of stress field, the two effective stress paths somehow converge at larger axial strain because of the similar fines content. Obvious different behavior is observed at the initial stage of shearing, the initial slope of stress path of eroded specimen is larger than that of reconstituted specimen, indicating a lower rate of pore pressure generation. The eroded specimen is initially less contractive than the reconstituted specimen even if the void ratio is larger.

The above two tests together with the results of isotropic compression of eroded specimens have indicated that internal erosion may create a distinctive packing of soil grains different from either clean sand or manually reconstituted fines-containing sand. Specifically, compared with the reconstituted specimens with similar void ratio and initial fines content, the eroded specimen becomes much stiffer. It is inferred that along with the seepage flow amounts of fines keep being dislodged and coarse grains rearrange their positions into a new equilibrium. Because of possible clogging, fines might accumulate at the spots where the constriction size is smaller than that of fines. Due to the rearrangement of grains, those accumulated fines may actively participate in

force chains. Different from the function of “lubrication”, those “surviving” fines after internal erosion would probably perform like reinforcement or jamming. Thereafter, the reinforced post-erosion soil packing renders the eroded specimen much stiffer and less compressible. With the subsequent compression the reinforcement will be deteriorated and the eroded specimen may behave like typical fines-containing sand. To further validate this assumption, a microscopic observation of the post-erosion packing of soil grains might be necessary.

6.4.3 Influence of initial fines content on eroded soil response

The differences in initial fines content directly result in a different soil packing before internal erosion, which will exert an influence on the progress of internal erosion and the post-erosion soil packing. An understanding of the effects of initial fines content may shed light on the evolution of soil packing during erosion and consequently, the mechanical responses of eroded soil. In a specimen, a fraction of fines fill the voids, whereas another fines separate the coarse grains. Since the effective stress of the fines occupied the voids among the coarse grains is less than that of wedged between the coarse grains (Skempton and Brogan, 1994), the fines in the voids may be vulnerable to internal erosion and probably dislodged by seepage flow. Erosion of the fines effectively separating the coarse grains may occur at larger Darcy’s flow corresponding with the rearrangement of coarse grains into new equilibrium. Majority of the “surviving” fines after consistent 3h internal erosion probably are those wedged between coarse grains and actively participating in the force chains. Because of the larger voids size among coarse grains of the specimen with 35% initial fines content (specimen 35E-50(-D)) compared with other specimens (specimen 25E-50(-D) and 15E-50(-D)), if the relative density is similar and fines are merely considered as voids, greater erosion of fines may appear. Under the same effective confining pressure of 50kPa, the specimens show approximately similar post-erosion fines content (i.e., 10%~16%) but different post-erosion void ratios, as is shown in Table 6.2. The postulated evolution of soil packing induced by erosion is indicated in Fig.6.17, which is developed from Fig.5.12.

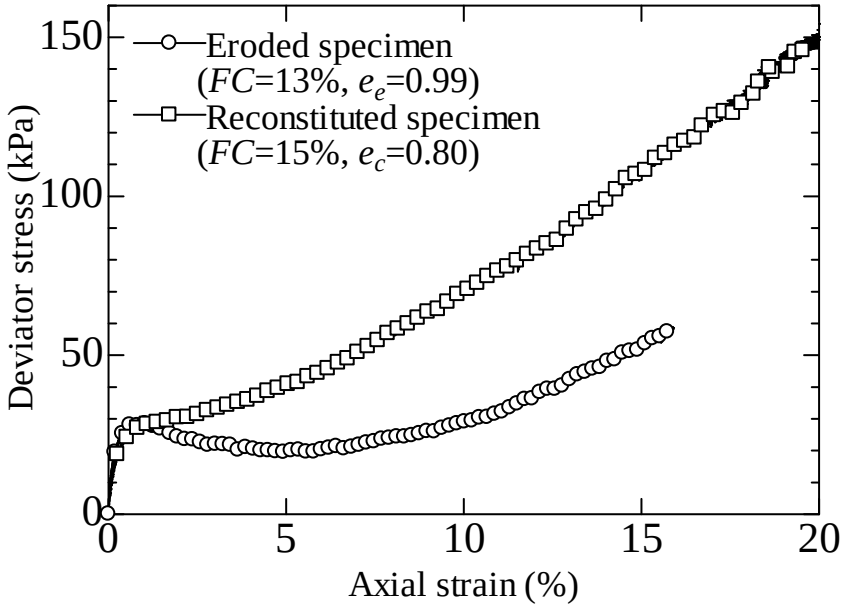

(a) Relation of axial strain and deviator stress

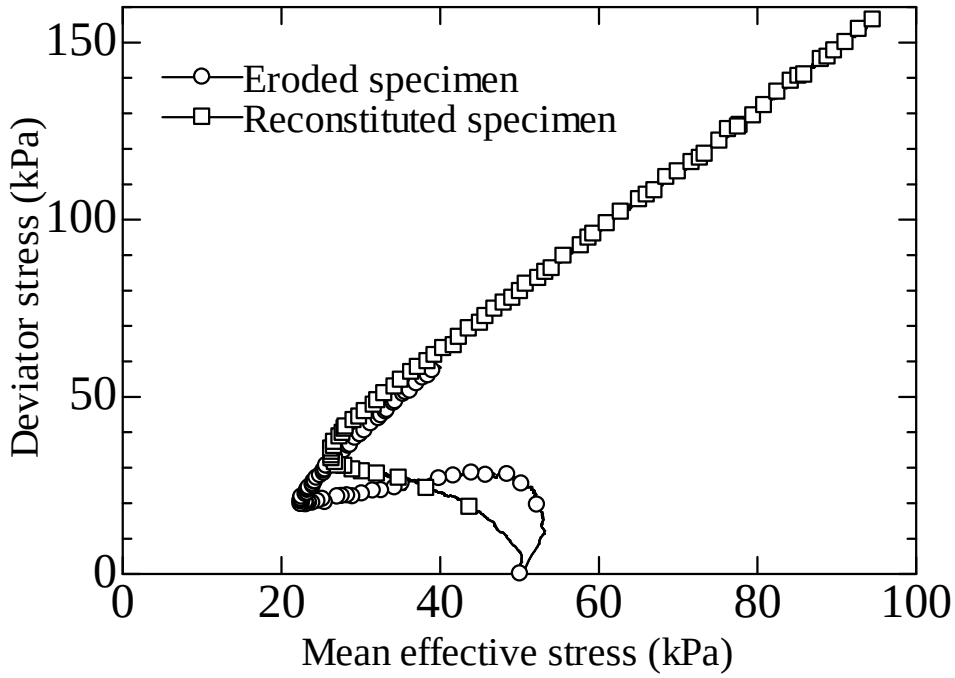

(b) Relation of mean effective stress and deviator stress

Figure 6.16 Undrained responses of the eroded specimen and the reconstituted specimen with similar void ratio and initial fines content under an effective confining pressure of 50kPa

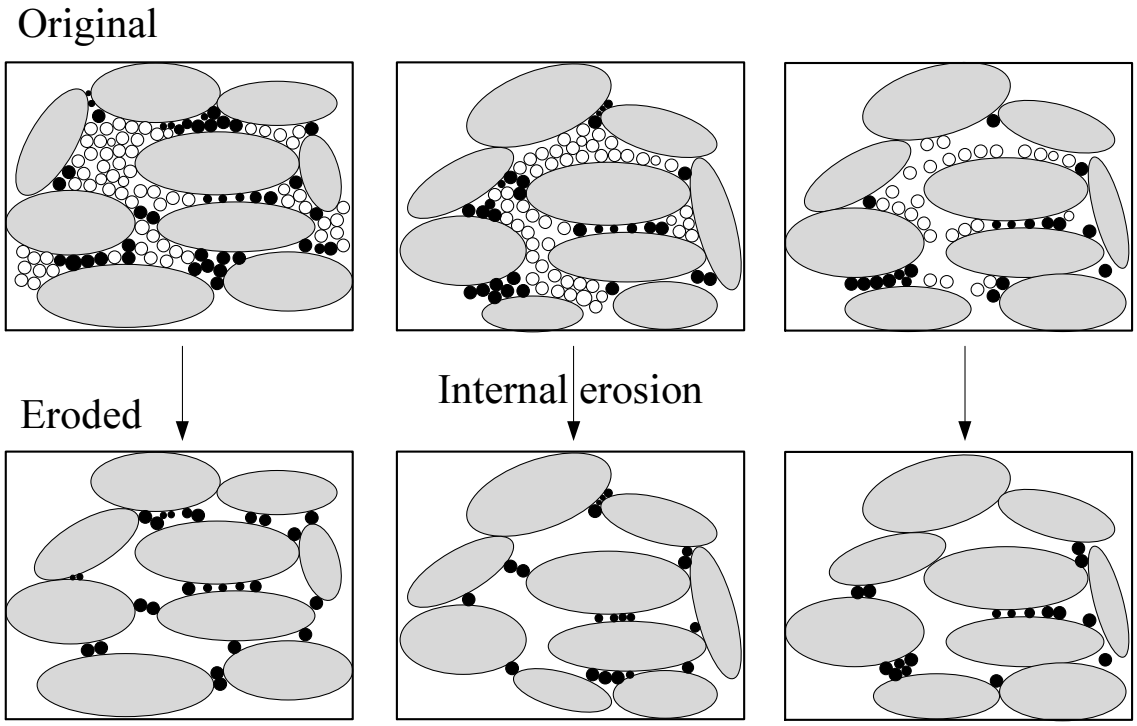

(a) 35% initial fines content (b) 25% initial fines content (c) 15% initial fines content

Figure 6.17 Postulated evolution of packing of soil grains during internal erosion (development of Figure 5.12)

Because of the obvious differences in post-erosion void ratio, the drained and undrained responses of those eroded specimens should be different. Figure 6.18(a and b) shows the results of monotonic drained test on specimen 35E-50-D, 25E-50-D and 15E-50-D under an effective confining pressure of 50kPa. Specimen 35E-50-D, which is the loosest, exhibits the lowest soil strength and secant stiffness. In terms of volumetric strain, three specimens show similar amounts of contractive strain within the initial 6% axial strain, where the compression of fines might dominate the mechanical response. Subsequent drained compression causes the specimen 15E-50-D, which is the densest, become dilative at an axial strain of 14%, and similarly the looser specimen 25E-50-D exhibiting dilatancy at an axial strain of 19%. The loosest specimen 35E-50-D does not show dilative behavior within the test range. Figure 6.19(a and b) presents the undrained responses of the eroded specimens in terms of stress ~ strain curves and effective stress paths, respectively. The post-erosion void ratio and intergranular void ratio of the tested specimens are indicated in Fig.6.19a. The deviator stress reaches a marked peak at low axial strain, approximately 1%, followed by the temporary strain softening and then becoming dilative as the phase transformation point is arrived. The slope of the effective stress paths appear to be somehow similar at the initial stage of shearing and gradually that of specimen 35E-50, which is the loosest, shows the smallest slope value, indicating a tendency of generating larger pore pressure. Subsequent compression may result in a unique CSL because of the similarity in the initial fines content. The test results further prove that a distinctive soil packing may be developed after internal erosion which displays similar initial soil stiffness. Ouyang (2013) analyzed the effects of initial fines content on the mechanical responses of eroded specimens in detail and noted that a larger initial soil stiffness is observed at the eroded specimens compared with the original specimens. Internal erosion would broaden the instability region, indicating the occurrence of deviator stress declining in the earlier stage of shearing.

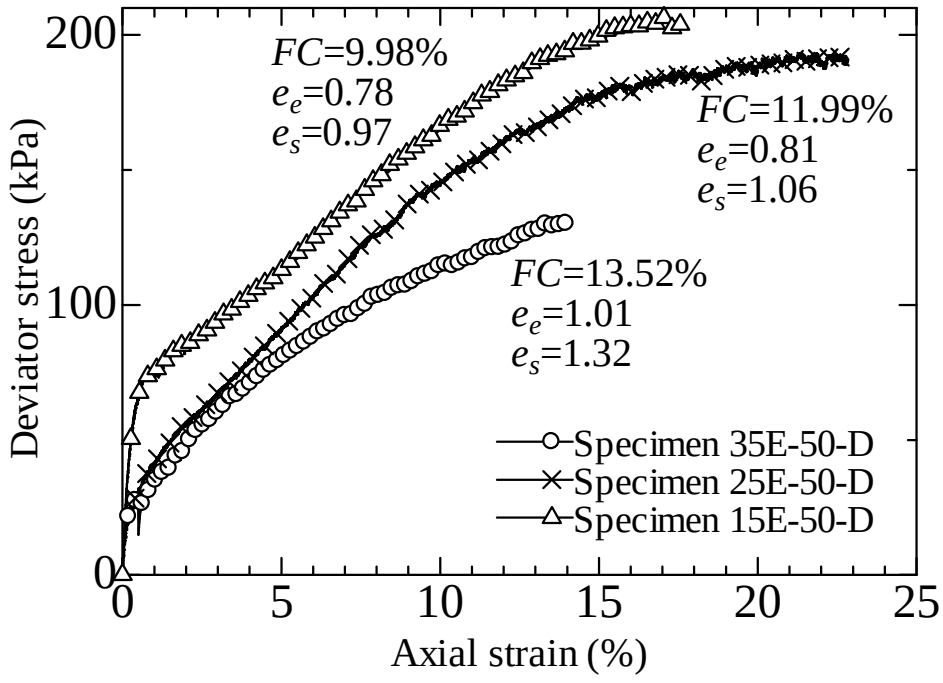

(a) Relation of axial strain and deviator stress

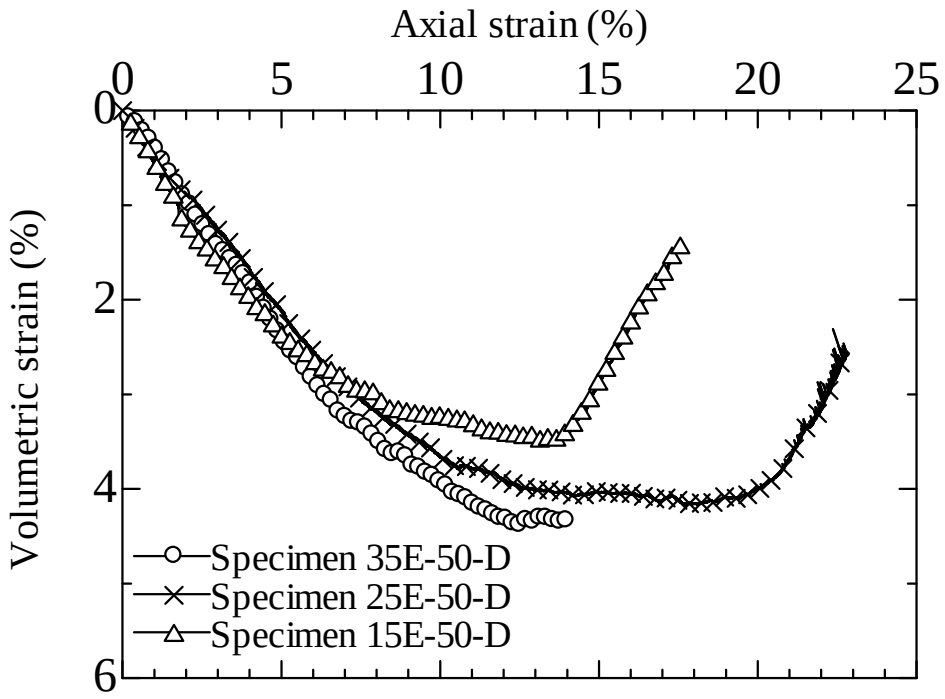

(b) Relation of axial strain and volumetric strain

Figure 6.18 Drained responses of eroded specimens with different initial fines contents under an effective confining pressure of 50kPa

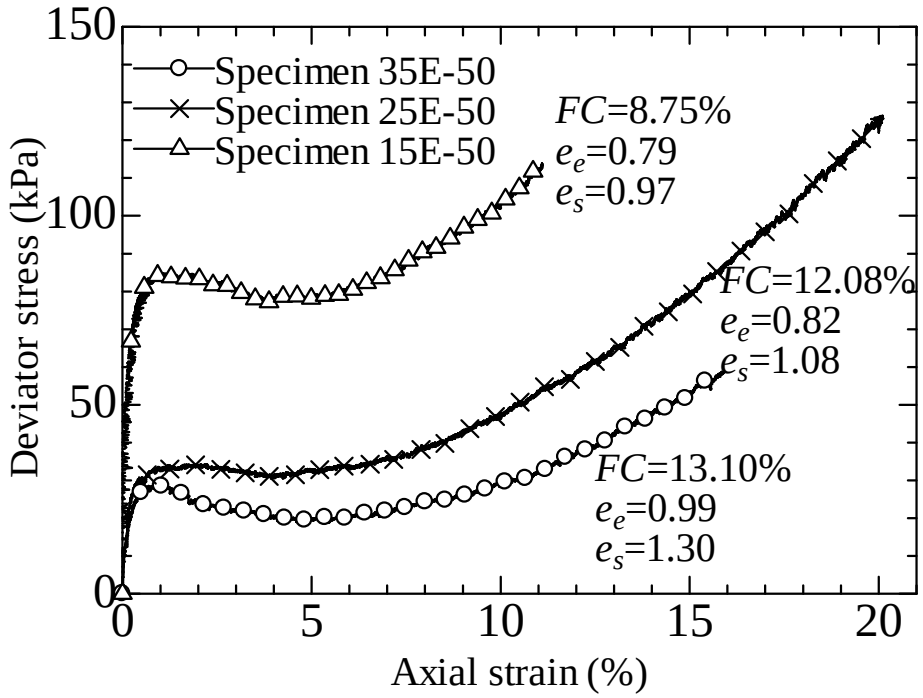

(a) Relation of axial strain and deviator stress

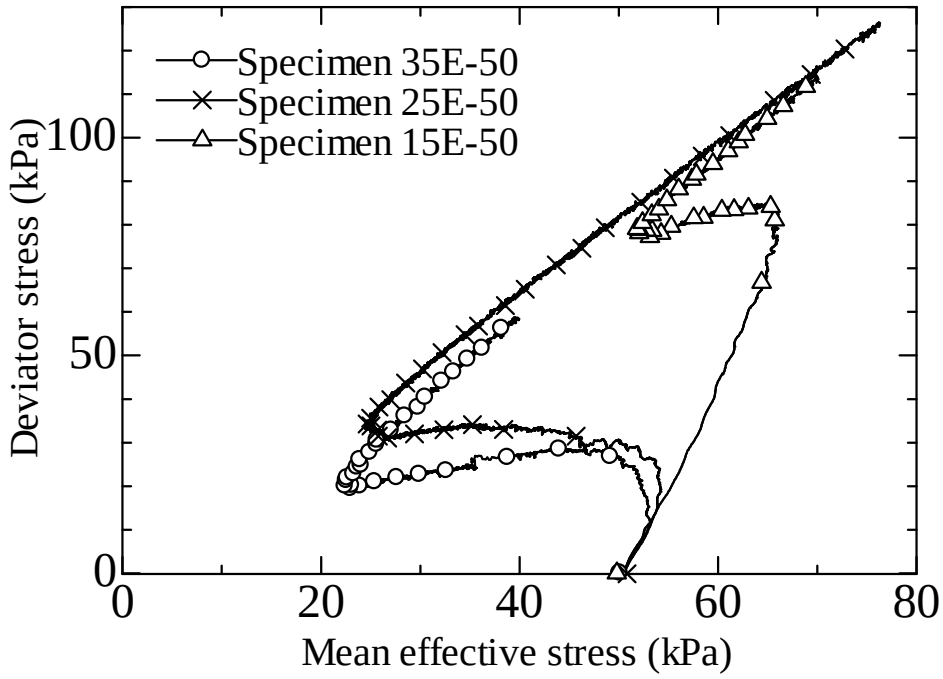

(b) Relation of mean effective stress and deviator stress
Figure 6.19 Undrained responses of eroded specimens with different initial fines contents under an effective confining pressure of 50kPa

6.5 Comparison of mechanical behaviors of eroded/original soil

6.5.1 Mechanical behavior of original soil before internal erosion

Though the mechanical behavior of eroded soil is preliminarily revealed in the above discussion, a direct comparison of the mechanical behaviors of original soil before internal erosion and eroded soil might be necessary to explicitly assess the instability potential of the earthen structure suffered from internal erosion and helpful for the retrofitting of internally eroded structures, such as levees. The original specimens before erosion consist of specimen 35N-50(-D), 35N-100(-D) and 35N-200(-D), shown in Table 6.1. Drained and undrained monotonic compression tests have been performed on those specimens under the effective confining pressure of 50kPa, 100kPa and 200kPa, respectively. The drained test results are summarized in Fig.6.20 in terms of evolution of (a) deviator stress and (b) volumetric strain with axial strain at different effective stress levels. The extrapolation of the tested data by a hyperbolic curve fitting is superimposed in the figures, indicating by dash lines. Similar to eroded specimens, those original specimens before internal erosion with the fines content of 35% exhibit a typical contractant volumetric behavior of loose sand. Within the test range, a larger deviator stress is detected under larger effective confining pressure. Reverse volume-change behavior of loose silty sand is observed. Under low effective confining pressure the existence of highly compressible fines among the coarse grains results in large volumetric strain. With the increasing effective confining pressure, the fines are shoved into the voids among coarse grains resulting in a stiffer grain configuration and consequently, less volumetric strain. Yamamuro and Covert (2001), who observed a similar temporary reduction in volumetric strain at the range of low effective confining

pressure (i.e., 25kPa ~ 100kPa), noted that this reverse volume-change behavior might be the characteristics for the majority of loose silty sands. The derived critical stress ratio $(q/p')_{cs}$, by plotting the stress ~ dilatancy relation of the drained tests, is evaluated as 1.5 and accordingly, the derived critical friction angle is 36.87°. Figure 6.21 shows the undrained response of original soil consisting of (a) relation of axial strain and deviator stress, and (b) effective stress path in the *p'*-*q* diagram. The original specimens reach a peak at low axial strain, approximately 1% ~ 1.5%, followed by strain softening. The after-peak deviator stress maintains constantly at a lower value without the sign of further dilatancy. Correspondingly, excessive pore pressures progressively develop and keep constant at the peak within the test range. An examination of the mobilized friction angle at peak (see Fig.6.22) shows that a lower mobilized friction angle is detected under lower effective confining pressure, indicating a greater potential of compression, which is in accordance with the pattern of behavior of volumetric strain observed in the drained test, shown in Fig.6.20b. Thus, a nonlinear relation of instability line is detected within the range of 50kPa ~ 200kPa effective confining pressure. The initial slope of the effective stress paths appear to increase with the increasing of effective confining pressure, which again implies the tendencies of relatively larger contractive volumetric deformation of the original specimens under lower effective confining pressure. Intuitively, the instability zone of original specimens, the zone sandwiched between the CSL and IL, becomes smaller than that of eroded specimens. Detailed comparison of the original specimens and the eroded specimens will be presented in the following with respect to the changes in soil strength and secant stiffness.

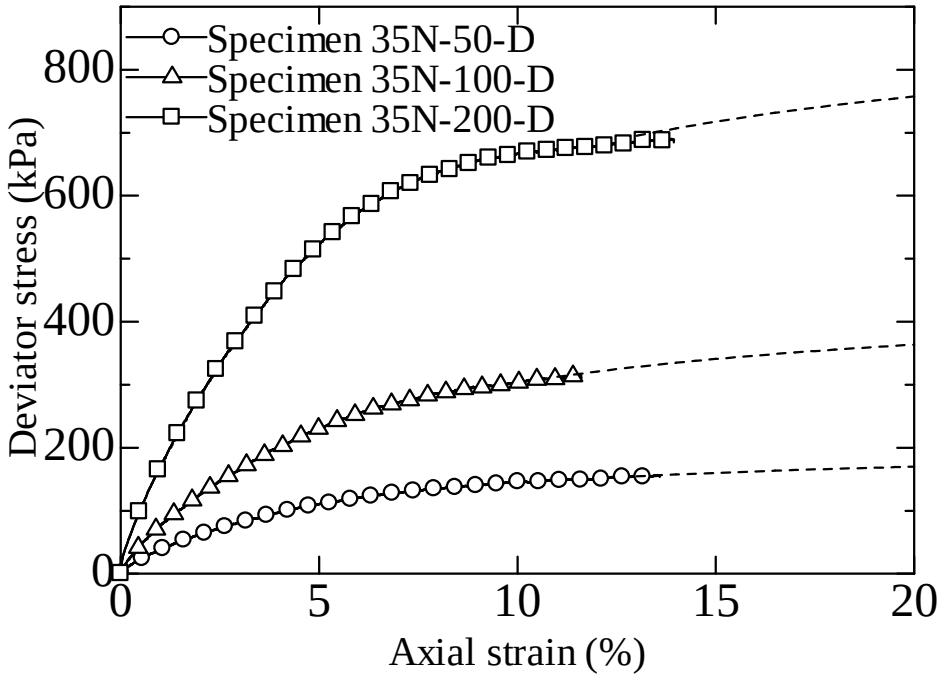

(a) Relation of axial strain and deviator stress

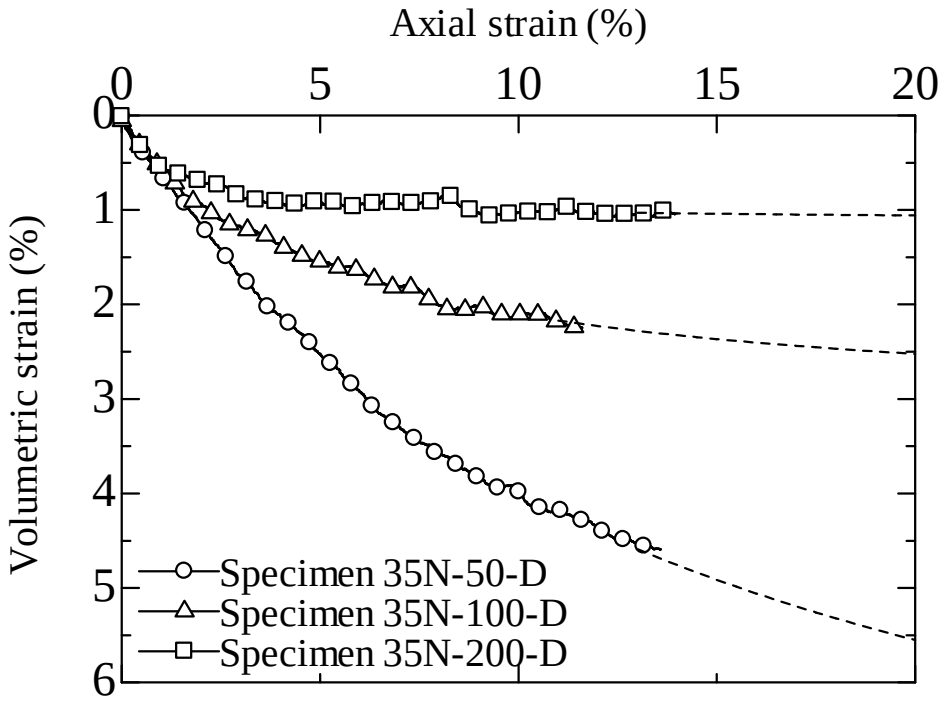

(b) Relation of axial strain and volumetric strain

Figure 6.20 Drained monotonic tests on original specimens under different effective confining pressures

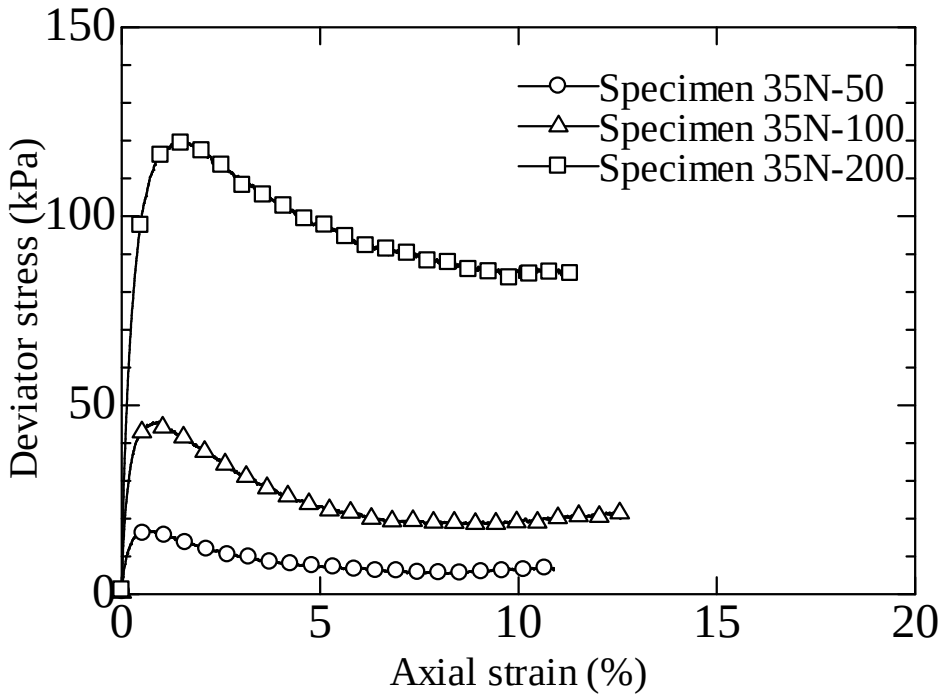

(a) Relation of axial strain and deviator stress

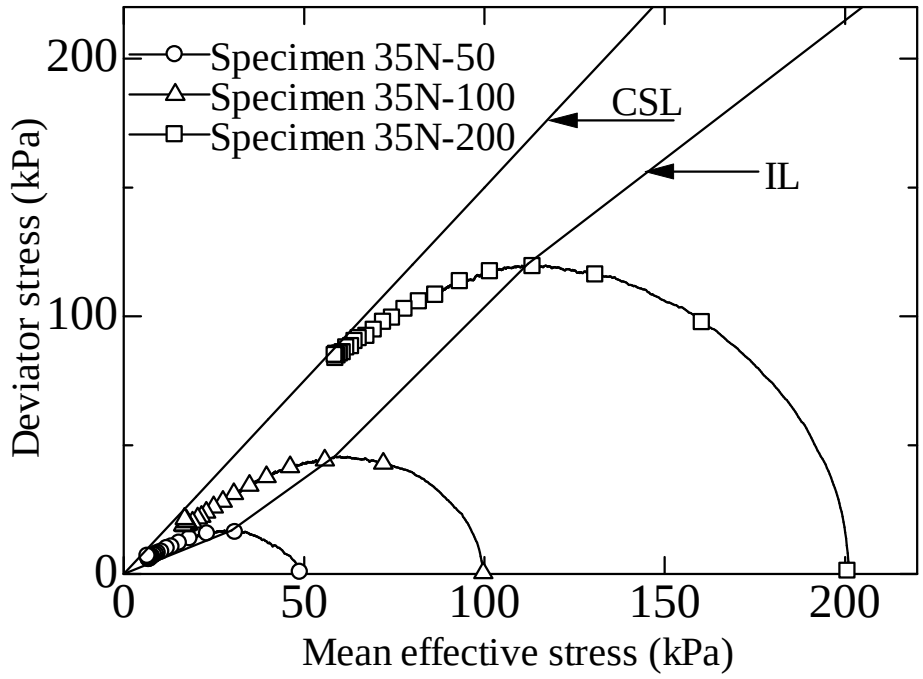

(b) Effective stress paths in stress field superimposed with critical state line and instability line

Figure 6.21 Undrained monotonic tests on original specimens under different effective confining pressures

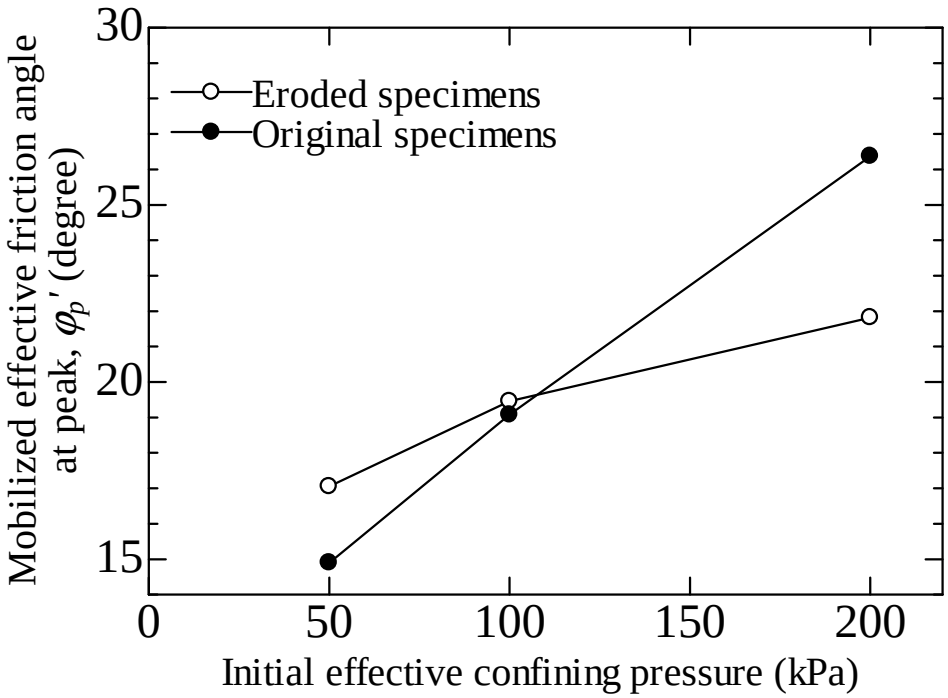

Figure 6.22 Evolution of mobilized effective friction angle at peak with initial effective confining pressure

6.5.2 Soil strength

The term “soil strength” is commonly referred to a representative stress of a soil element (i.e., shear stress) at the state of failure. In this study, the soil strength is assessed by the following four criteria: ASTM failure criterion, Ishihara’s residual strength criterion, Mohr-Coulomb criterion and Lade’s instability criterion. ASTM states that failure corresponds to “the maximum principal stress difference (maximum deviator stress) attained or the principal stress difference (deviator stress) at 15% axial strain, whichever is obtained first during the performance of a test” (i.e., ASTM D4767-11). In this series of tests, the undrained stress ~ strain curves exhibit a peak at the initial stage of shearing, whereas the drained responses are typically contractant within the test range. Thus, the undrained strength refers to the peak deviator stress obtained and the drained strength corresponds to the deviator stress at an axial strain of 15%. A summary of the soil strength before and after internal erosion against initial effective confining pressure is indicated in Fig.6.23, where the soil strength is plotted in a logarithmic scale. It is seen that the drained strength of eroded specimens is less than that of original specimens by 20% in average, irrespective of initial effective confining pressure. The variation of undrained strength, however, seems to relate with the initial effective confining pressure. The undrained strength increases by 69% and 14% after internal erosion for the specimens under an initial effective confining pressure of 50kPa and 100kPa, respectively. For the specimen under an effective confining pressure of 200kPa, the post-erosion undrained strength decreases by 12%. The derived coefficient of compressibility from isotropic compression tests may shed light on the contradictory observations of soil strength. As is shown in Table 6.3, the compressibility of the eroded specimen 35E is lower than that of the original specimen 35N under the effective confining pressure of 50kPa and 100kPa, whereas it turns to be larger under the confining pressure of 200kPa. Correspondingly, the eroded specimens will be stiffer under lower effective confining pressure (i.e., 50kPa and 100kPa) and therefore, a larger peak deviator stress is achieved. However, in terms of the larger effective confining pressure (i.e., 200kPa), the eroded specimens show contrary pattern of behavior and become more compressible, causing a lower undrained peak. This founding accords with the results of Chang and Meidani (2012) who concludes that the eroded specimens on which erosion occurs under lower confining pressure will become dilative, whereas the post-erosion specimens under larger confining pressure show much contractive response with a lower undrained strength.

Ishihara (1996) noted that fines-containing sands may develop amounts of deformation while keeping the magnitude of deviator stress at the lowest level at quasi-steady state (QSS) under undrained conditions, which should be considered in engineering practice. The deviator stress at QSS is defined as the residual strength (S_{us}) derived by

$$S_{us} = \frac{q_{ss}}{2} cos\phi_{ss} \text{ ……. (6.3)}$$

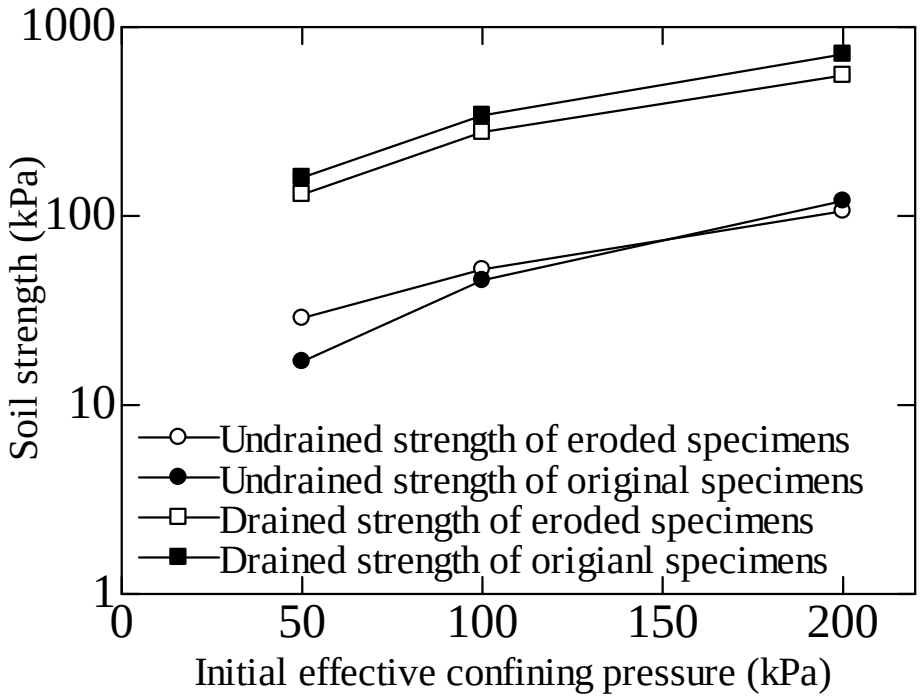

Figure 6.23 Soil strength of eroded specimens and original specimens

The original specimens do not exhibit the further dilation after the quasi-steady state but keep at a constant deviator stress. At this circumstance, this constant value is utilized to determine the residual strength. A plot of the normalized residual strength (normalized with p_0') against initial effective confining pressure is indicated in Fig.6.24. Within the test range, the residual strength of eroded specimens is larger than that of the original specimens. An interesting point is the intercept in the vertical axis observed for the eroded specimens. Ishihara (1996) noted that a linear relation between the normalized residual strength and initial effective confining pressure beginning from the stress origin is expected for the reconstituted sands, as the original specimens shown in the plot. However, the eroded specimens appear to gain the strength even under zero confining pressure, similar to "cohesion", which may again prove the existence of the temporary reinforced soil packing after internal erosion. The reinforcement seems to be stiffer for the specimens under low effective confining pressure during seepage test. Under an effective confining pressure of 200kPa, the normalized residual strength is similar for both specimens, indicating the probable deterioration of the strengthened soil packing.

To further demonstrate the mechanical influence of internal erosion, the tested specimens are replotted in the v ~ log p' space where the NCLs and QSSLs are superimposed, shown in Fig.6.25. The behavior of eroded specimens might be understood by two steps. After the initial isotropic consolidation, the specimens experience internal erosion under a constant effective confining pressure where the void ratio increases. Under each effective confining pressure, the tested specimens would reach one void ratio and consequently, a linear relationship seems to be able to be determined between void ratio and effective confining pressure, which is named as "erosion line" in this paper. It quantitatively reveals the changes in void ratio during internal erosion. Similar to the NCLs, the locus points in the "erosion line" corresponds

to a soil fabric generated by internal erosion given by the initial void ratio and soil stress state. The change of void ratio during erosion is caused by the fines loss and possible rearrangement of the soil grains. As is discussed in section 5.4, the increasing of void ratio mostly depends on the loss of fines which is commonly considered to be unique for a given condition (Sterpi, 2003; Cividini *et al.*, 2009). Figure 6.25 indicates the associated QSSL after internal erosion and its distance from erosion line would be utilized to evaluate the soil residual strength. The QSSL moves upward associated with a change in the curve slope after internal erosion.

As for Mohr-Coulomb criterion, the soil strength, usually referred as shear strength, is derived from cohesion and frictional resistance. Since the normal consolidated specimens in this study consist of silica sand, the source of shear strength is mainly the friction resistance between soil grains, quantitatively assessed by “friction angle”, and the cohesion is expected to be none. The critical friction angle of eroded specimen and original specimen, derived from drained monotonic tests, is 35.27° and 36.87°, respectively. At the same normal stress, the shear strength decreases by 5.7%. It is worthy to stress again that the eroded specimens are created at the same assigned flow rate of 310mL/min. Analysis of Chapter 3 notes that the erosion induced decreasing of shear strength seems to somehow relate with the imposed hydraulic gradient. A soil would lose greater shear strength at larger imposed hydraulic gradient. Similarly, it is expected that at larger assigned flow rate (i.e., larger than 310mL/min), a greater loss of shear strength may occur.

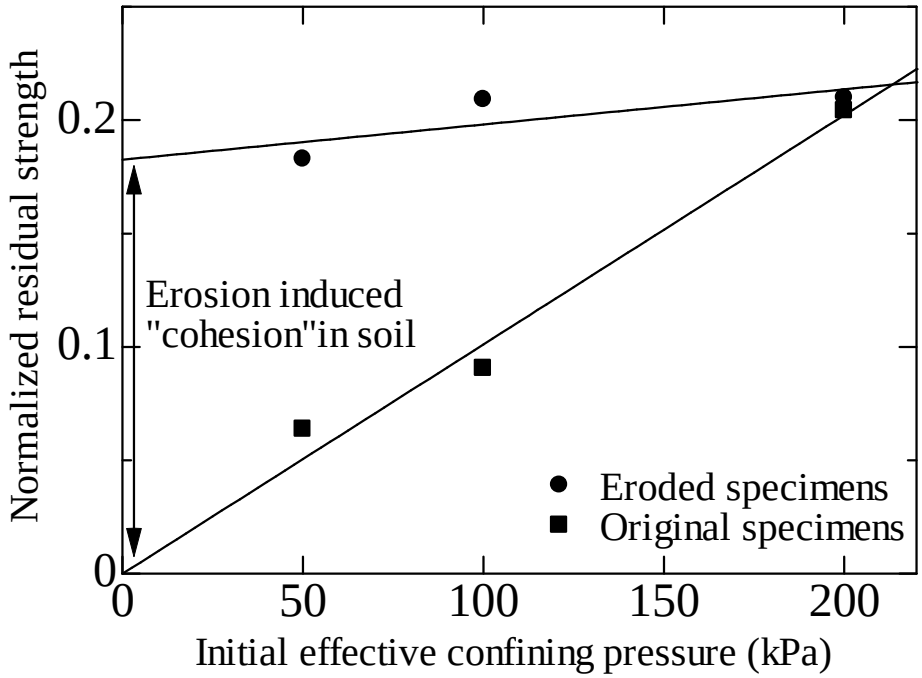

Figure 6.24 Residual strength against initial effective confining pressure

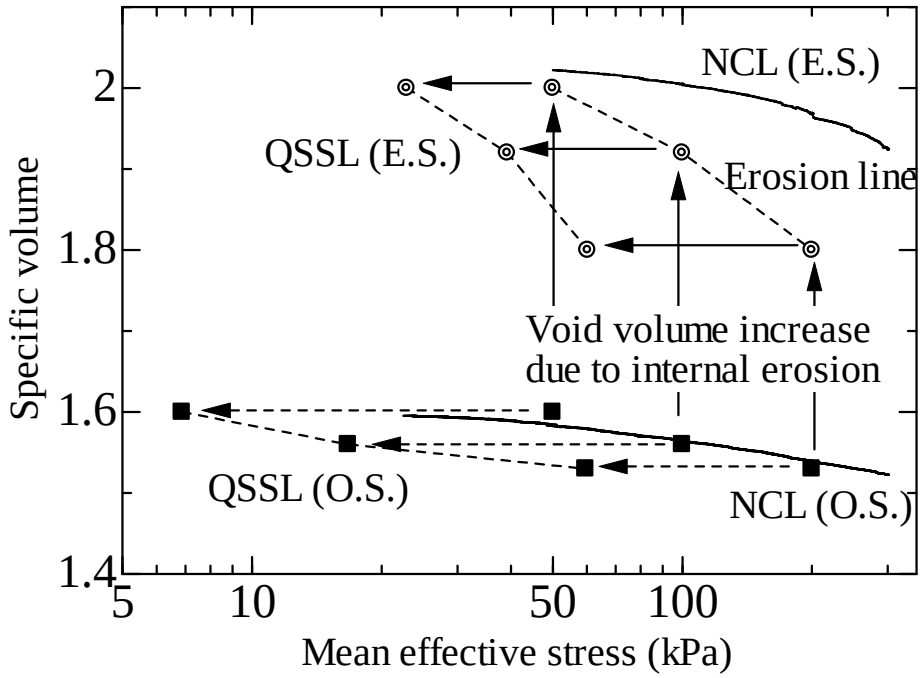

Figure 6.25 Plot of tested specimens in $v \sim \log p'$ space (O.S. means original specimens; E.S. means eroded specimens)

Lade *et al.* (1990, 1997 and 1998) assessed the potential of the soil state wherein the onset of the declining of undrained deviator stress occurs and flow liquefaction may be triggered by the concept of instability line. In this approach, the instability potential of a soil is evaluated by "instability region", which locates between CSL and IL. A summary of the critical state lines, derived from drained tests, and instability lines of the eroded specimens and original specimens is shown in Fig.6.26. Due to the increasing effective friction angle with effective confining pressure, IL is nonlinear under lower effective confining pressure. A larger instability region is observed for the eroded specimens, indicating that under the same mean effective confining pressure the eroded specimens may lose its strength or initially liquefy at the earlier stage of shearing wherein lower deviator stress is generated.

6.5.3 Secant stiffness

The normalized secant stiffness of the eroded specimens and the original specimens with respect to the initial effective confining pressure within the initial axial strain of 1% is shown in Fig.6.27. Since the original specimens are alike in terms of the initial fines content and void ratio, the variation of normalized secant stiffness with axial strain at initial 1% displays identical patterns of behavior. The stiffness reaches the initially largest value and decreases with subsequent compression. However, as for the eroded specimens, besides the similar pattern of declining of secant stiffness with axial strain, they also exhibit distinctions in three aspects. Firstly, the initial secant stiffness becomes larger than that of the original specimens, which may be explained by the unique soil packing created by internal erosion. The majority of "surviving" fines may actively participate in the force transportation and function as jamming which reinforces the soil

packing. Afterwards with further straining, the temporary reinforcement is deteriorated wherein drops in secant stiffness are observed in eroded specimens. Under larger effective confining pressure (i.e., specimen 35E-200-D), the deterioration may occur at earlier stage of shearing. Finally, due to the extremely loose state of the eroded specimens, the secant stiffness keeps lower than the original specimens.

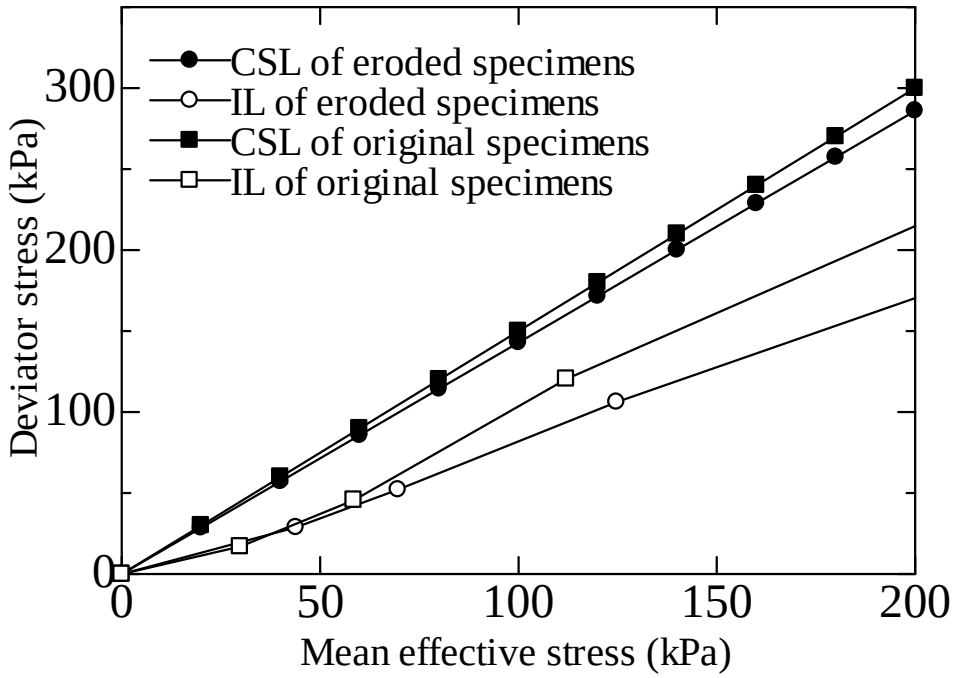

Figure 6.26 Critical state lines and instability lines in Cambridge stress field

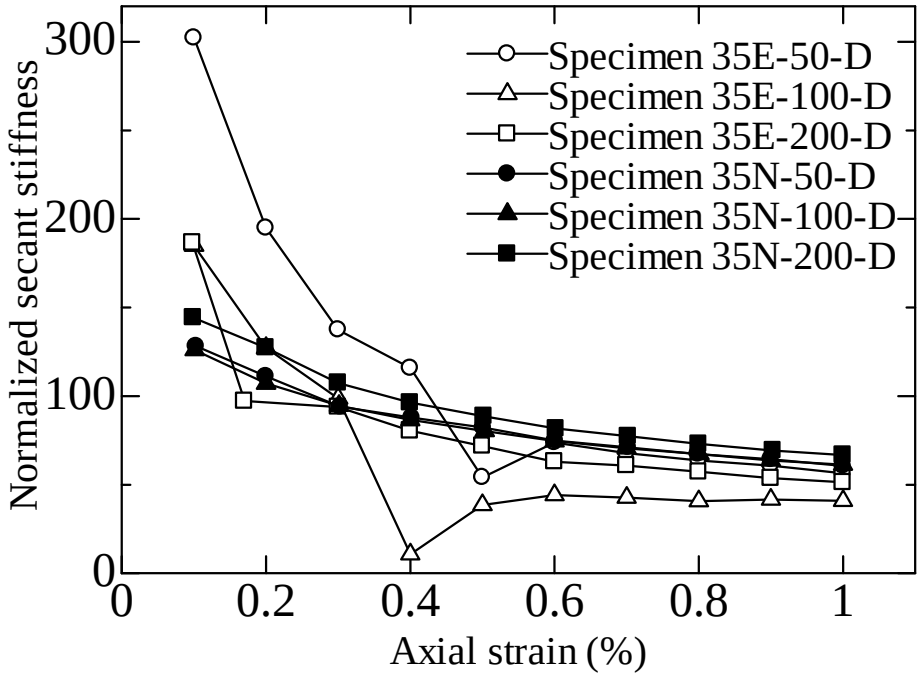

Figure 6.27 Secant stiffness of eroded specimens and original specimens

6.5.4 Dilatancy tendency of undrained responses after internal erosion

A direct comparison of the undrained responses of eroded specimens (Fig.6.11) and original specimen (Fig.6.21) indicates a much dilative after-peak behavior of the eroded specimens, which is contrary to common sense. Because of the erosion of fines and the resulting post-erosion loose soil state, the eroded soils are expected to be contractive. It may be understood by the mechanical function of fines. As is discussed above, for the reconstituted specimens, silica No.8 lubricates the coarse grains and inhibits the dilatency tendency in respect that the contacts between coarse grains may be far less. Due to internal erosion, amounts of fines are dislodged and the remaining fines in the specimen may actively support the packing of soil grains. Loose though, the eroded specimens show larger stiffness and peak deviator stress. The subsequent compression displaces the fines into the voids and creates much better contacts between coarse grains. At this circumstance, the strong dilatency tendency of silica No.3 surpasses the contractive tendency induced by the increase in the void ratio after internal erosion and therefore, the eroded specimens exhibit dilative behavior at larger axial strain. Similar pattern has been observed by Yamamuro and Covert (2001) who noted that the existence of large amounts of silt in loose sand specimens may prolong the contractive quality to larger values of axial strain.

6.6 Cyclic responses of eroded soil

Since the mechanical behaviors of the eroded specimens somehow depart from the common senses, further undrained cyclic tests have been conducted to validate the feasibility of the stress conditions, gained from monotonic undrained compression, at which temporary liquefaction initiates. By interpreting the test results, a quantitative assessment of the influence of internal erosion on cyclic strength would be provided.

6.6.1 Summary of tested specimens

A summary of the tested specimens are indicated in Table 6.4 denoting the fines content and void ratio before cyclic loadings. Original specimens (35N-0.07, 35N-0.10 and 35N-0.12) at the same stress state without internal erosion are tested for the comparison purpose. It is noted that the intergranular void ratios of tested specimens approximately equal to 1.35+/-0.04, which may be regarded as a base for the comparison between original specimens and eroded specimens. As is discussed above, a distinctive soil packing might be developed during internal erosion and therefore, relatively larger initial soil stiffness is expected for the eroded soil. During the cyclic tests, the tested specimens are subjected to two-way loading of compression and extension in axial direction under the same effective confining pressure as that of erosion test. The series of cyclic tests are conducted under an initial effective confining pressure of 50kPa with determined cyclic stress ratio (CSR) as derived by

$$CSR = \frac{\sigma_{cycd}}{2\sigma_r'} \quad \text{……. (6.4)}$$

Three CSRs are determined for original specimens and eroded specimens, respectively,

to assess the cyclic strength. The tested specimens are compressed and extended regularly at an axial strain rate of 0.5%/min, which is sufficiently slow to allow the equilibrium of pore pressure in the tested specimens with an average B-value of 0.93. The axial resistance of soil specimens is collected by the feedback signal of load cell to constantly check whether the determined CSR is reached. If reached, the system could reverse the loading without backlash to avoid any stress relaxation. Necessary corrections, such as the diameter of the tested specimen, have been inserted into the control program. Excessive pore pressures, axial and radial displacement are simultaneously recorded.

6.6.2 Undrained cyclic responses

Figures 6.28 ~ 6.30 show the cyclic behavior of the eroded specimens under the cyclic stress ratio of 0.12, 0.15 and 0.20, respectively, with the monotonic compression data superimposed. The critical state line and phrase transformation line are denoted in the figures as a basis of comparison to test the stress conditions required to trigger cyclic liquefaction. The specimens show non-reversal loading condition: the plastic axial strain develops with cyclic loops. Initially, their behavior follows the “flow deformation” pattern, which refers to the continuous development of axial strain with the decreasing of mean effective stress. However, this trend is inhibited as soon as the specimen is loaded sufficiently to initiate dilation with further straining. Vaid and Chern (1985) termed this phenomenon as “limited flow deformation”. It is noted that true liquefaction, indicated by zero mean effective stress and deviator stress, is not reached in the test. The effective stress paths show dilative response as soon as the phrase transformation line is touched and then asymptotically moves towards CSL associated with dilatancy. Ishihara and Towhata (1982) pointed out that the stress path of dilative soil consists of three parts: under loading (increase of deviator stress), unloading (decrease of deviator stress) , and that near true liquefaction. The stress ~ strain curves and effective stress paths mostly follow the pattern of behavior established by the monotonic test, except for the extension. The deviator stress at extension somehow is beyond the critical state line which might be attributed to the large stiffness of the membrane utilized.

The cyclic behavior of the original specimens under the cyclic stress ratio of 0.07, 0.10 and 0.12, respectively, is indicated in Figs. 6.31~6.33 with the monotonic compression data superimposed. The original specimens display typical behavior of “flow deformation”. Fundamentally, the stress ~ strain curves and effective stress paths follow the pattern of behavior derived from the monotonic compression. By comparison, the original specimens would fail after less cyclic loops than that of eroded specimens. A plot of cyclic resistance ratio versus number of cycles required to cause 5% double amplitude strain for original and eroded soil is shown in Fig.6.34. It indicates that the CSR causing 5% double amplitude strain in 20 cycles, defined as cyclic strength, increases from 0.08 to 0.16 after internal erosion. This increment of cyclic strength may be attributed to the distinctive soil packing after internal erosion. The fines which used to serve as lubrication become jamming and actively participate in force chains. Consequently, the cyclic strength may increase.

Table 6.4 Details of tested specimens of cyclic testing

Specimens	Fines content (%)	Void ratio before cyclic loading	Intergranular void ratio	Effective confining pressure (kPa)	Cyclic stress ratio (CSR)
35E-0.12	13.52	1.01	1.32	50	0.12
35E-0.15	13.88	0.99	1.31	50	0.15
35E-0.20	13.51	1.01	1.32	50	0.20
35N-0.07	35	0.55	1.39	50	0.07
35N-0.10	35	0.55	1.39	50	0.10
35N-0.12	35	0.56	1.40	50	0.12

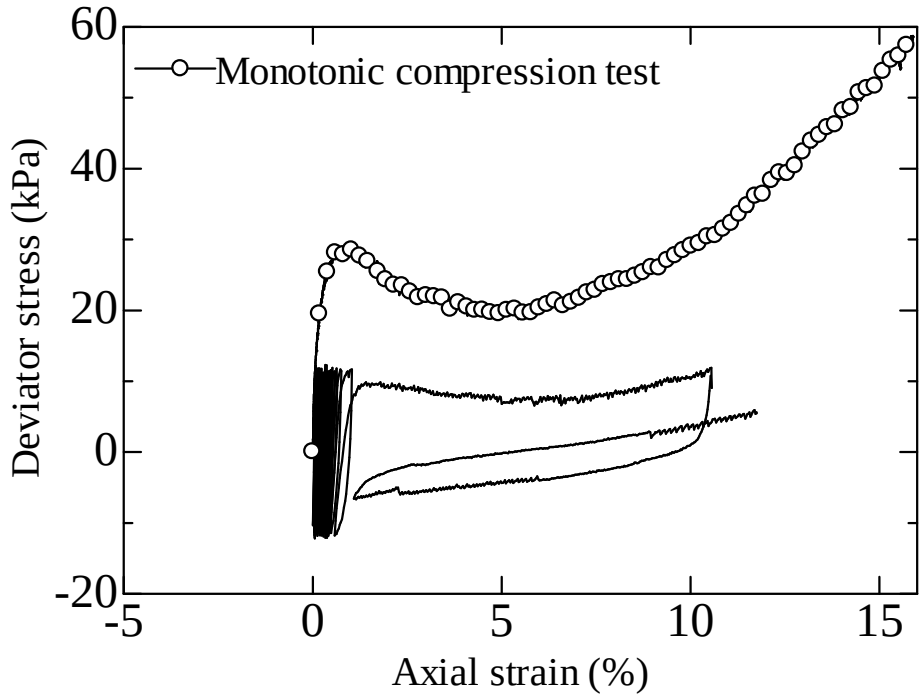

(a) Relation of cyclic deviator stress and axial strain with superimposed monotonic compression test data under undrained condition

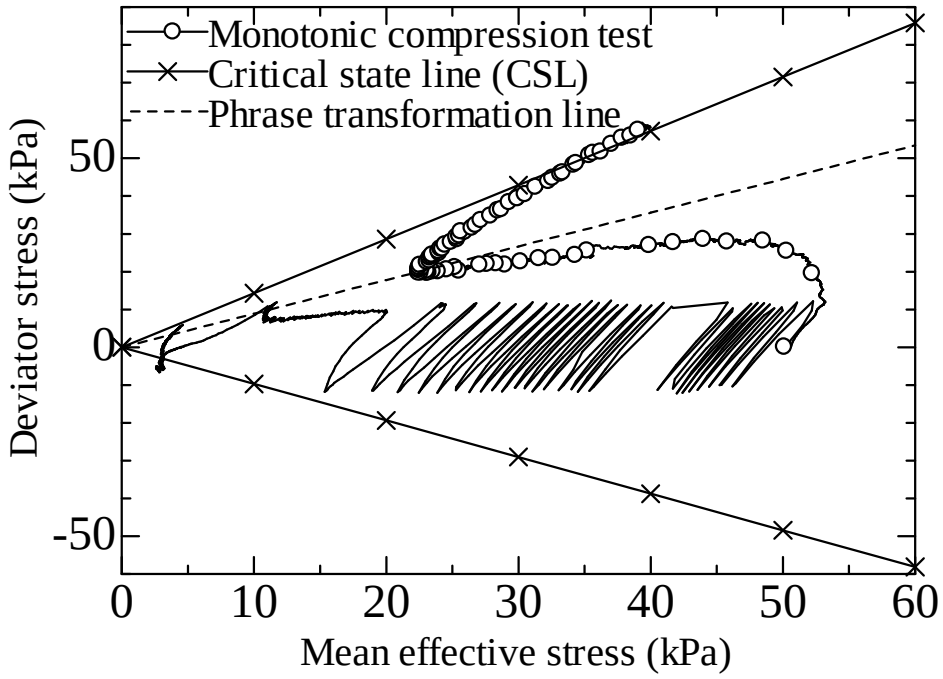

(b) Relation of cyclic deviator stress and mean effective stress with superimposed monotonic compression test data under undrained condition

Figure 6.28 Cyclic behavior of eroded specimens (CSR=0.12)

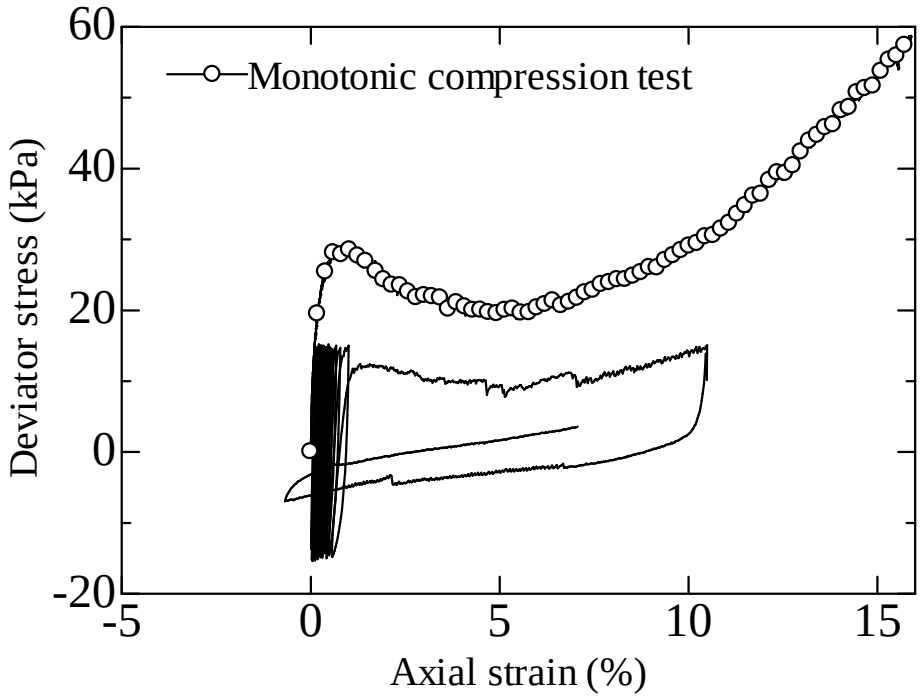

(a) Relation of cyclic deviator stress and axial strain with superimposed monotonic compression test data under undrained condition

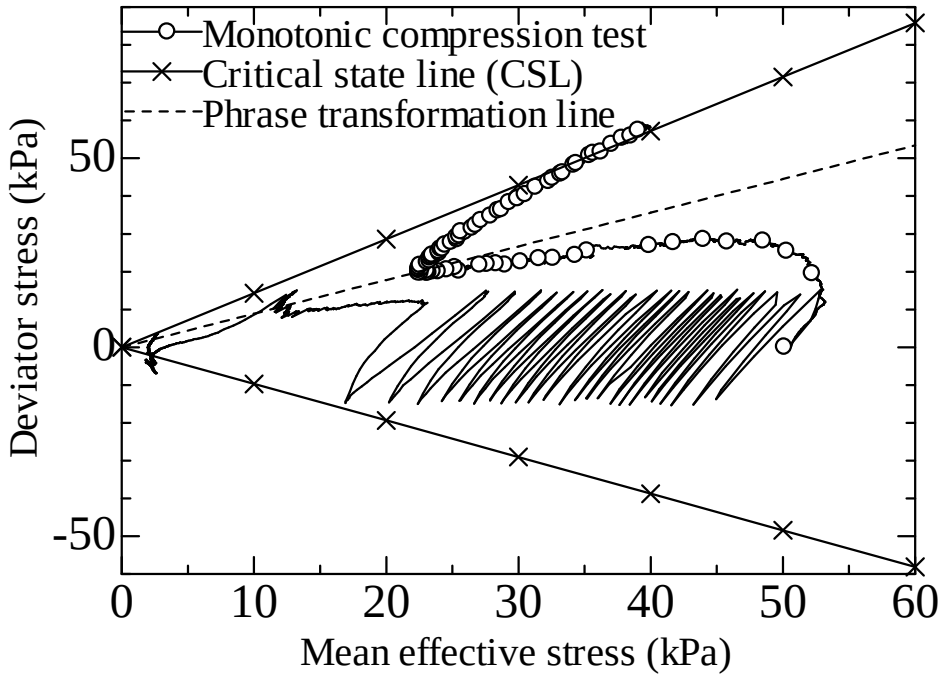

(b) Relation of cyclic deviator stress and mean effective stress with superimposed monotonic compression test data under undrained condition

Figure 6.29 Cyclic behavior of eroded specimens (CSR=0.15)

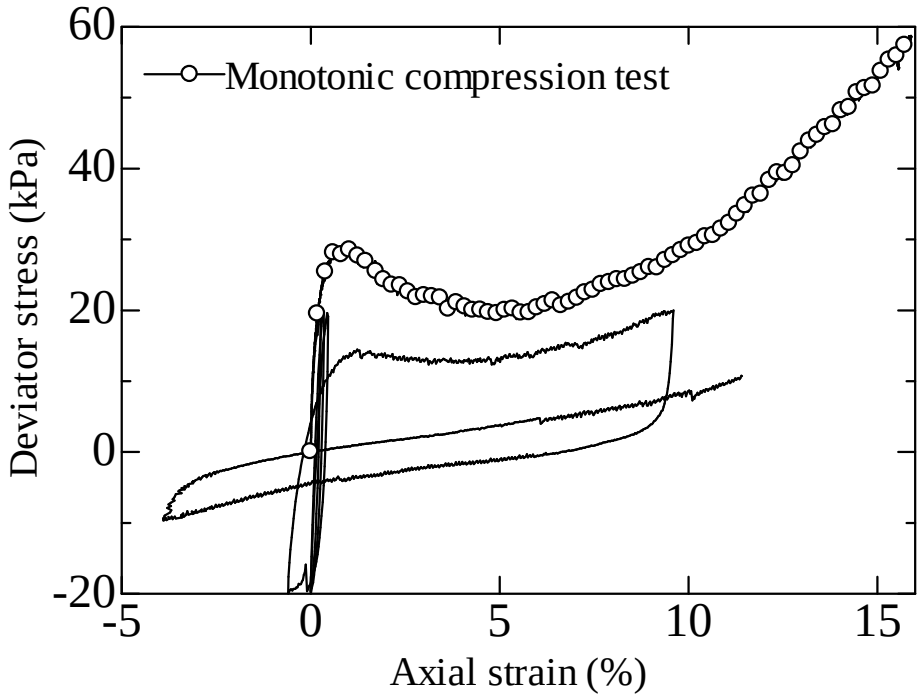

(a) Relation of cyclic deviator stress and axial strain with superimposed monotonic compression test data under undrained condition

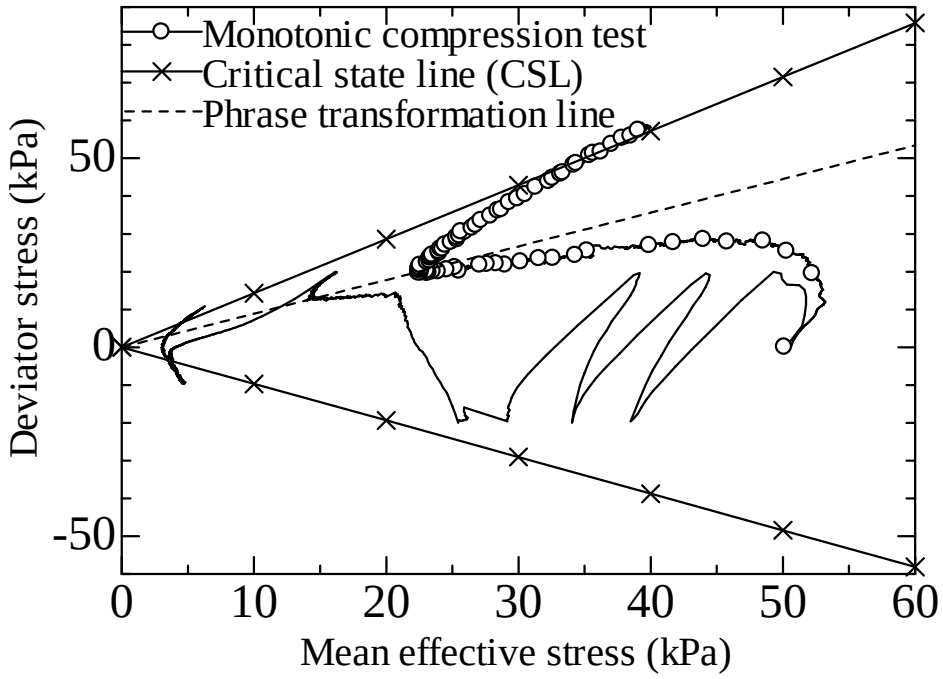

(b) Relation of cyclic deviator stress and mean effective stress with superimposed monotonic compression test data under undrained condition

Figure 6.30 Cyclic behavior of eroded specimens (CSR=0.20)

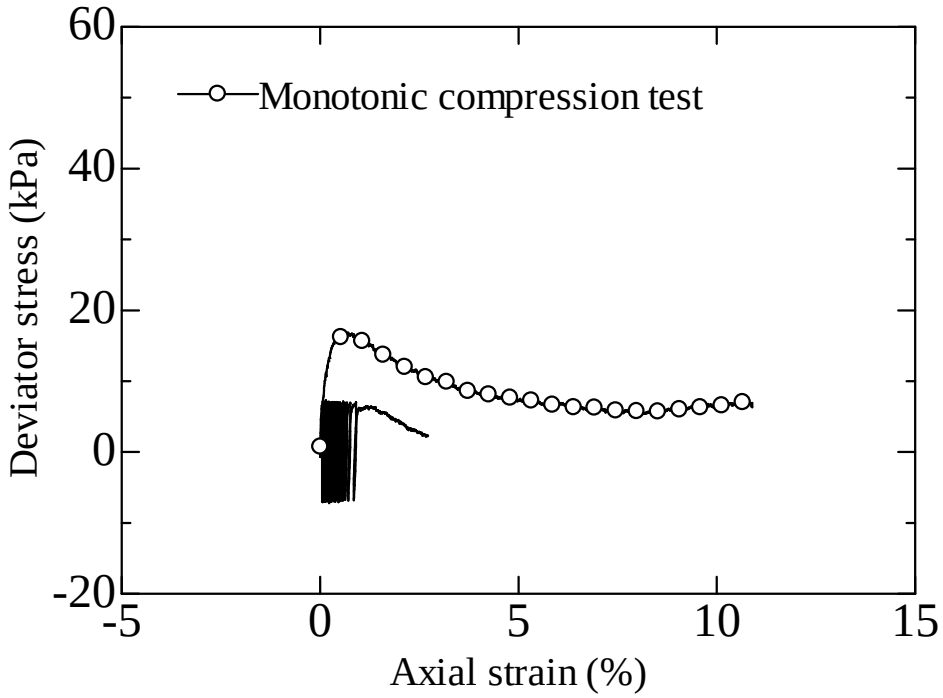

(a) Relation of cyclic deviator stress and axial strain with superimposed monotonic compression test data under undrained condition

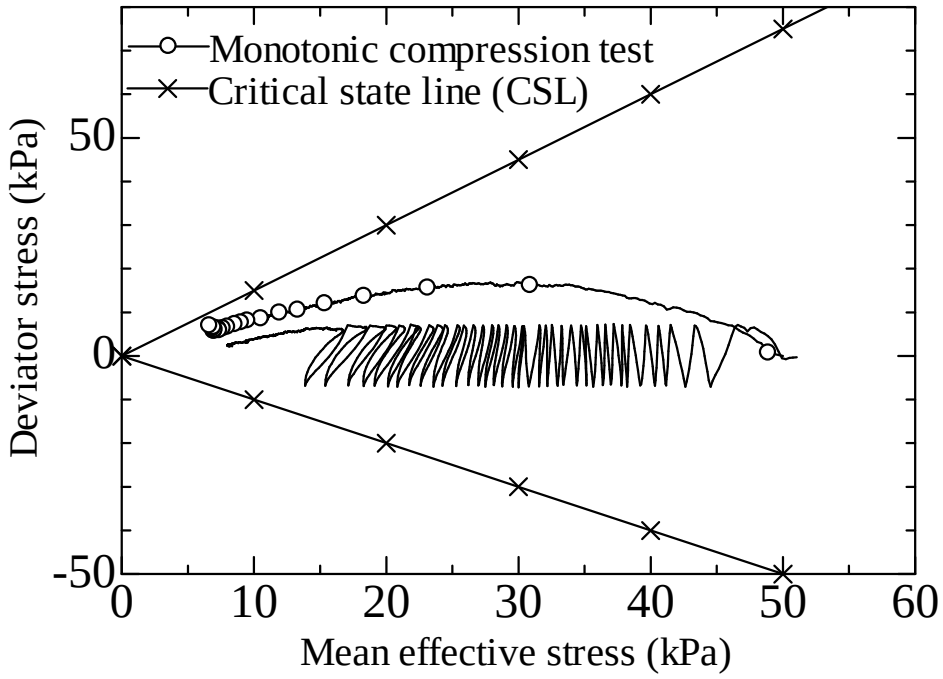

(b) Relation of cyclic deviator stress and mean effective stress with superimposed monotonic compression test data under undrained condition

Figure 6.31 Cyclic behavior of original specimens (CSR=0.07)

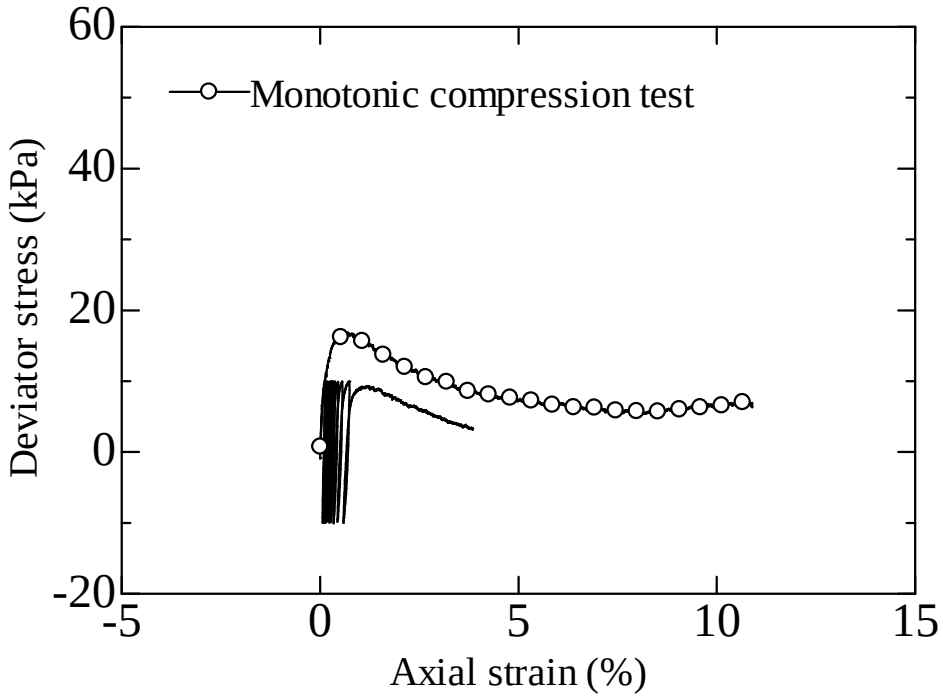

(a) Relation of cyclic deviator stress and axial strain with superimposed monotonic compression test data under undrained condition

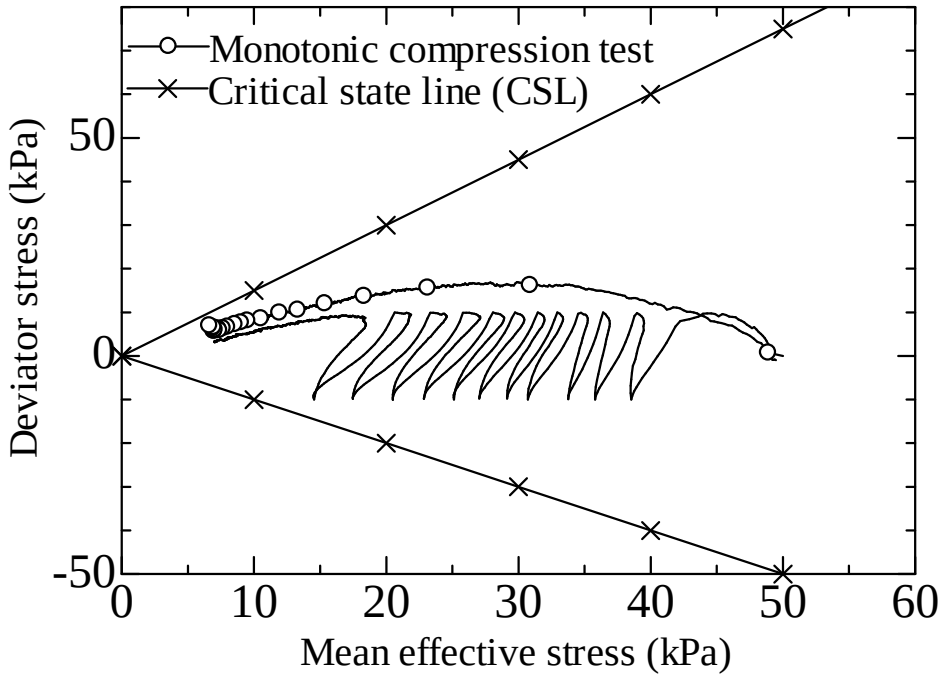

(b) Relation of cyclic deviator stress and mean effective stress with superimposed monotonic compression test data under undrained condition

Figure 6.32 Cyclic behavior of original specimens (CSR=0.10)

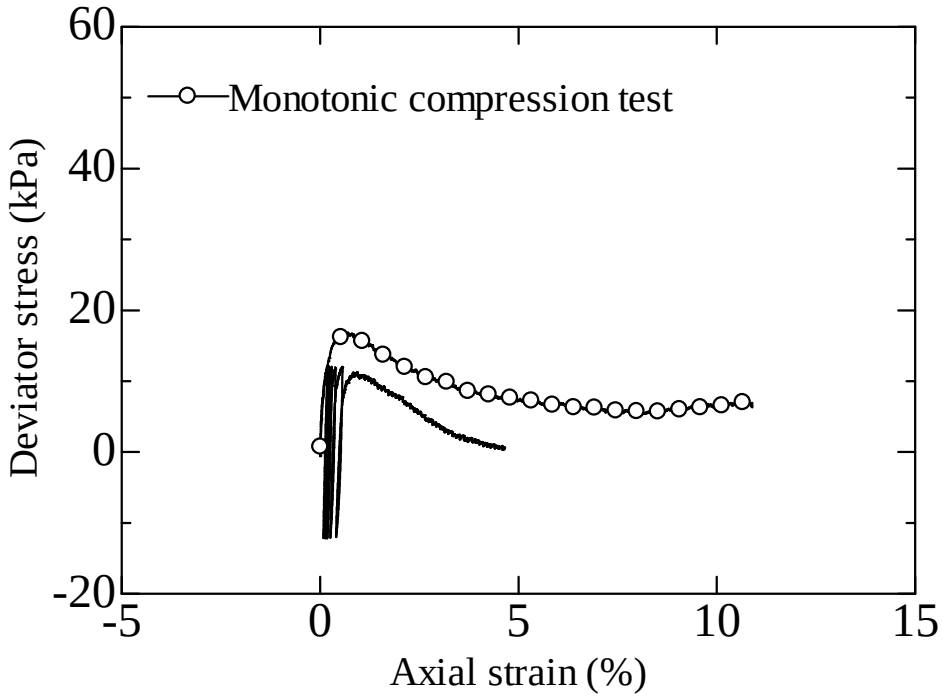

(a) Relation of cyclic deviator stress and axial strain with superimposed monotonic compression test data under undrained condition

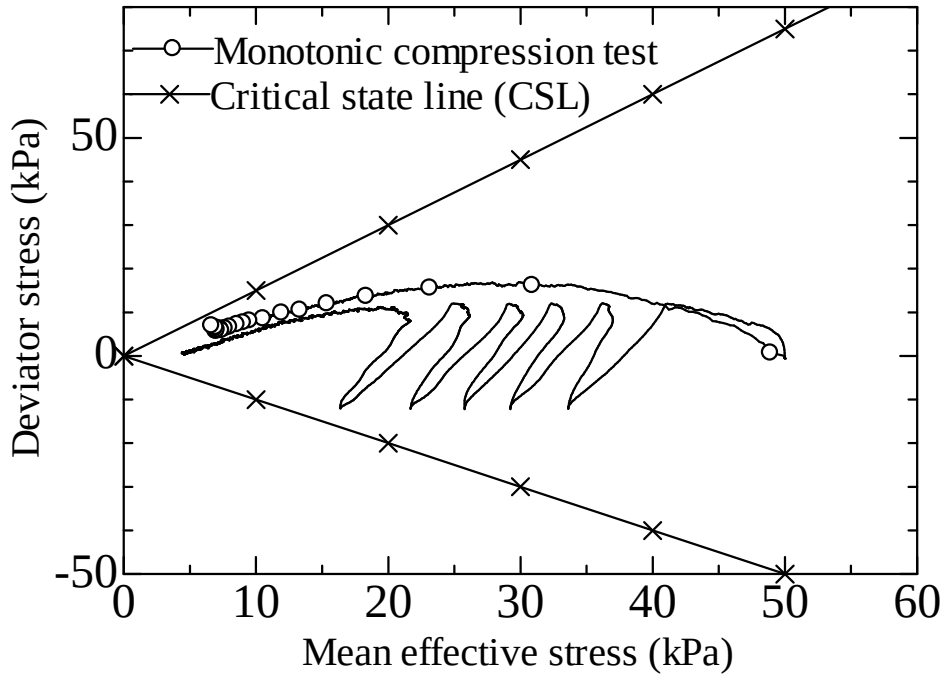

(b) Relation of cyclic deviator stress and mean effective stress with superimposed monotonic compression test data under undrained condition

Figure 6.33 Cyclic behavior of original specimens (CSR=0.12)

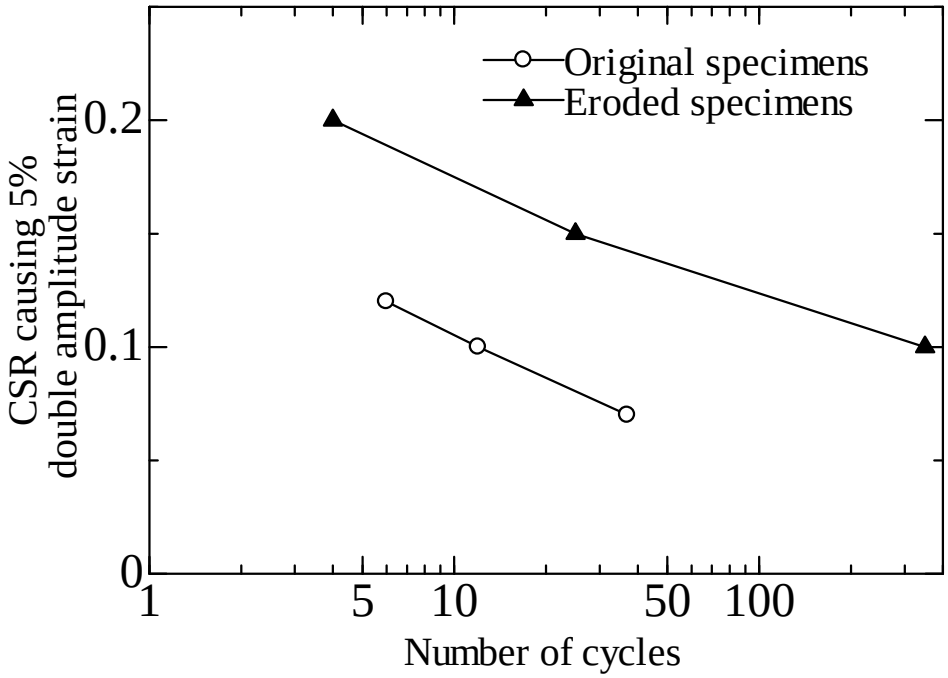

Figure 6.34 Cyclic strength of original specimens and eroded specimens

6.7 Conclusions

The mechanical consequences of internal erosion on a series of non-cohesive soils are presented in this chapter. Isotropic compression, undrained and drained monotonic compression, and undrained cyclic tests are performed on the eroded specimens to reveal their mechanical behavior.

In the isotropic compression test, compared with the original specimens without erosion, the NCL of the eroded specimens significantly moves upward and become steepening at larger mean effective stress. A unique gradient of NCL may not exist, whereas the gradient of swelling line seems to be identical and can be determined. The coefficient of compressibility of the eroded specimens is lower within the mean effective stress of 50kPa ~ 100kPa and becomes larger at larger mean effective stress compared with the original specimen without erosion. Departing from clean sand, an exceptional mechanical behavior of eroded soil is observed. The volumetric strain at failure derived from drained tests reduces with the increasing of effective confining pressure. A temporary drop in soil stiffness at the initial stage of shearing with respect to the axial strain ranging from 0% ~ 1% is observed. In terms of undrained tests, generally, the deviator stress of the eroded specimens reaches a marked peak at low axial strain, approximately 1%, followed by the temporary strain softening and then becoming dilative as the phase transformation point is arrived. The increasing effective confining pressure results in the rising of stress ratio (q_{ss}/q_{peak}), indicating an increasing stability. The mobilized friction angle shows the trend of increasing with the increasing of effective confining pressure. Compression test results have revealed the probable existence of a distinctive packing of soil grains after internal erosion. The “surviving” fines after internal erosion may actively participate in the force chains, acting like reinforcement. The reinforced post-erosion soil packing renders the eroded specimen much stiffer and less compressible. With the subsequent compression the reinforcement will be deteriorated and the eroded specimen may behave like typical fines-containing sand.

The changes in soil strength after internal erosion are assessed by four criteria: ASTM failure criterion, Ishihara’s residual strength criterion, Mohr-Coulomb criterion and Lade’s instability criterion. In terms of ASTM criterion, the drained strength of eroded specimens is less than that of original specimens by 20% in average, irrespective of the initial effective confining pressure. The variations in undrained strength appear to relate with the initial effective confining pressure. Compared with the original specimens, under lower confining pressure, a larger undrained strength is observed for the eroded specimens while it becomes smaller under larger confining pressure. The residual strength of eroded specimens is larger than that of the original specimens. An interesting point is that the eroded specimens seem to gain the strength even under zero confining pressure, similar to “cohesion”. Under an effective confining pressure of 200kPa, the normalized residual strength is similar for both specimens, indicating the probable deterioration of the strengthened soil packing. To further quantitatively reveal the changes in void ratio during internal erosion, an “erosion line” in $v \sim \log p'$ space may be helpful to indicate the post-erosion soil fabric by giving the initial void ratio and stress state. The critical friction angle of eroded specimen and original specimen,

derived from drained monotonic tests, is 35.27° and 36.87°, respectively. At the same normal stress, the shear strength decreases by 5.7%. A larger instability region is observed for the eroded specimens. The comparison of secant stiffness within the initial axial strain of 1% between the eroded specimens and the original specimens has noted that the initial secant stiffness is larger for the post-erosion specimens. With subsequent compression, the eroded specimens show a sudden drop in stiffness, which is considered as a sign of the deterioration of the temporary reinforcement.

In the undrained cyclic tests, the original specimens display typical behavior of “flow deformation”, whereas the eroded specimens show dilative response as soon as the phrase transformation line is touched and then asymptotically moves towards CSL associated with dilatancy. Mostly the stress ~ strain curves and effective stress paths follow the pattern of behavior established by the monotonic compression. The cyclic strength, defined as the CSR causing 5% double amplitude strain in 20 cycles increases by two times after internal erosion.

CHAPTER 7

CONCLUSIONS

The phenomenon of internal erosion in cohesionless soils exhibits itself as the gradual migration of fine grains through the voids of the coarse matrix, transported by volumes of seepage water. The chronic process of internal erosion always accompanies with the significant loss of soil grains and changes in hydraulic conductivity. The coarse grains may rearrange their inter-position into a new equilibrium and consequently, eroded soil will become loose. The stress ~ strain relationship of the internally eroded soil might be greatly altered compared with the original soil. There is a high possibility that the strength of the post-erosion soil decreases due to the destructive function of internal erosion. Full comprehension of the characteristics of internal erosion and its mechanical influence on soil behavior is beneficial for the assessment of the stability of potentially eroded earthen structures, such as levees.

In this research, common fixed wall seepage test has been conducted to preliminarily understand the erosion mechanism of the tested soil specimens. Parametric study is conducted to examine the effects of soil properties (i.e., relative density, initial fines content) and hydraulic conditions on the erosion mechanism. The soil strength reduction after erosion in the fixed-wall seepage test is elaborated by interpreting the cone tip resistance profile of the tested specimens after erosion. On the basis of the fixed wall seepage test, an automated triaxial seepage testing system has been developed by installing several new components, including a flow pump, a sedimentation tank and a revised pedestal. The hydromechanical behavior of tested specimen during the progress of internal erosion are studied by assessing the changes of the key parameters, such as hydraulic gradient, hydraulic conductivity, soil deformation and cumulative eroded soil mass at various stress states. The effects of stress state and initial fines content are experimentally investigated. The changes in stress ~ strain relationship after internal erosion is directly assessed by conducting undrained and drained monotonic compression test on the internally eroded soil specimen. Internal erosion induced changes in cyclic strength is studied by performing undrained cyclic test on the eroded soil specimens and original specimens without erosion, respectively, under the same effective confining pressures.

7.1 Main conclusions

In Chapter 3, the influence of internal erosion on soil strength has been experimentally studied through a series of one-dimensional upward seepage tests at a constant water head and cone penetration tests. By giving an upward seepage flow to the gap-graded soil specimens, the characteristics of hydraulic behavior of tested soil are understood. The mechanical consequences of internal erosion are examined by cone penetration tests on internally eroded specimens. Before the internal erosion, the relationship between the average hydraulic gradient and Darcy velocity is basically linear. After the onset of erosion, the slope of the relationship is no longer linear, indicating that the hydraulic conductivity of soils drastically increases with the progress of the internal

erosion. The hydraulic gradient for internal erosion is found to be about one fifth to one third of the Terzaghi's critical hydraulic gradient for soil stability. The lower the fines content, the larger the hydraulic gradient required to cause internal erosion. Those specimens containing the same mass ratio of fines as the larger relative density require a larger critical hydraulic gradient to initiate the internal erosion. The loss of fines proportionally increases with the imposed hydraulic gradient. The internal erosion causes a reduction in cone tip resistance, the extent of which may be related to the imposed hydraulic gradient. A larger imposed hydraulic gradient, indicating a greater loss of fines, would lead to further cone resistance reduction. Drastic changes in the strength can be seen with hydraulic gradients over 0.5. The internal erosion causes the angle of shearing resistance of a soil specimen to decrease within a certain hydraulic gradient range.

Chapter 4 introduces the newly developed triaxial internal erosion apparatus, capable of directly investigating not only the hydraulic characteristics of soils at the onset and the progress of internal erosion under preferred stress state but also the mechanical behaviors of those internally eroded soils. By installing a sedimentation tank, back pressure could be maintained in the tested specimens during erosion test to ensure a relatively high saturation degree. A measurement system of the cumulative eroded soil mass is installed in the tank to continuously record the eroded soil mass. Erosion tests are performed by constant-flow-rate control manner with the measurement of the induced pressure difference between the top and bottom of the tested specimens. Volumetric strain of the soil specimen could be assessed by measuring the axial and radial deformation. The mechanical consequences of internal erosion could be evaluated by directly performing undrained and drained compression tests or undrained cyclic tests on the eroded soil.

Erosion mechanisms for saturated sand with different initial fines contents under different effective confining pressures at triaxial condition are presented in Chapter 5. Seepage tests are performed by the constant-flow-rate control in triaxial apparatus. The back pressure is applied to ensure the fully saturated soil state. Cumulative eroded soil mass is continuously recorded by a consecutive monitoring system. Hydraulic gradient dramatically drops during internal erosion with the dislodgement of large amounts of fines. Correspondingly, hydraulic conductivity, derived from Darcy's law, keeps increasing at this stage. Afterwards, the soil packing would gradually reach a new equilibrium when the hydraulic gradient and cumulative eroded soil mass become constant. A moderate decrease of hydraulic conductivity is detected after a significantly long period of test time, which might be caused by the clogging of fines inside tested specimens. Erosion of fines would result in the increase of contractive volumetric strain. The post-erosion grain size distribution analysis indicates that the fines loss is larger in the upper layer. The saturation degree drops after seepage test with the B-value higher than 0.93. Assigned the seepage flow with the same velocity, the specimens under the larger effective confining pressure show less increments in hydraulic conductivity within the test range. The percentage of cumulative fines loss and volumetric strain induced by internal erosion is the least in the specimens under the effective confining pressure of 200kPa and the largest in the specimens under the effective confining pressure of 50kPa. Comparing the seepage test results of the specimens with 35%, 25%

and 15% initial fines content, respectively, the largest change of hydraulic conductivity occurs in the specimen with 35% initial fines content. Fines loss is larger for the specimens with larger initial fines content and correspondingly, the internal erosion induced volumetric strain is larger. The change of void ratio is closely associated with the volumetric strain during erosion. In this series of seepage tests, the tested specimens show contractive behavior and the post-erosion void ratio increases.

Chapter 6 discusses the mechanical consequences of internal erosion on a series of non-cohesive soils. Isotropic compression, undrained and drained monotonic compression, and undrained cyclic tests are performed on the eroded specimens to reveal their mechanical behavior. In the isotropic compression test, compared with the original specimens without erosion, the NCL of the eroded specimens significantly moves upward and become steepening under larger effective confining pressure. A unique gradient of NCL may not exist, whereas the gradient of swelling line seems to be identical and can be determined. The coefficient of compressibility is lower within the mean effective stress of 50kPa ~ 100kPa and becomes larger at larger mean effective stress compared with the original specimen without erosion. Departing from clean sand, an eccentric mechanical behavior of eroded soil is observed. The volumetric strain at failure derived from drained tests reduces with the increasing of effective confining pressure. A temporary drop in soil stiffness at the initial stage of shearing with respect to the axial strain ranging from 0% ~ 1% is observed. In terms of undrained tests, the mobilized friction angle shows trend of increasing with the increasing of effective confining pressure. Compression test results have revealed the probable existence of a distinctive packing of soil grains after internal erosion. The “surviving” fines after internal erosion may actively participate in the force chains, acting like reinforcement. The reinforced post-erosion soil packing renders the eroded specimen much stiffer and less compressible. With the subsequent compression the reinforcement will be deteriorated and the eroded specimen may behave like typical fines-containing sand. The changes in soil strength after internal erosion are assessed by four criteria: ASTM failure criterion, Ishihara’s residual strength criterion, Mohr-Coulomb criterion and Lade’s instability criterion. Generally, the soil strength decreases after internal erosion. The comparison of secant stiffness at the initial axial strain of 1% between the eroded specimens and original specimens has noted that the initial secant stiffness is larger for the post-erosion specimens. With subsequent compression, the eroded specimens show a sudden drop in stiffness, which is considered as a sign of the deterioration of the temporary reinforcement. In the undrained cyclic tests, the stress ~ strain curves and effective stress paths mostly follow the pattern of behavior established by the monotonic test: the original specimens display typical behavior of “flow deformation”, whereas the eroded specimens show dilative response as soon as the phrase transformation line is touched and then asymptotically moves towards CSL associated with dilatancy. The cyclic strength, defined as the CSR causing 5% double amplitude strain in 20 cycles increases by two times after internal erosion.

7.2 Recommendations for future study

Experimental evidences derived from soil strength tests have indicated the existence of a distinctive microstructure for eroded specimens. Specifically, internal erosion triggers

the transformation of the function of fines from “lubrication” to “jamming”. Therefore, an microscopic observation of the soil fabric after erosion might be of great help to further interpret the mechanical behavior of eroded specimens.

It is recognized that the soil history and stress state exerts an influence on the onset and progress of internal erosion. In this study, to fully reveal the changes of soil behavior by erosion, an isotropic stress state is selected. However, Chang and Zhang (2011b) concluded that internal erosion will intensify at anisotropic state. Therefore, conduction of seepage test at different stress states would be helpful to determine the critical effects of internal erosion on soil.

Bibliography

Ahmadi, M.M., Byrne, P.M. and Campanella, R.G. (2005): Cone tip resistance in sand: modeling, verification, and applications, *Can. Geotech. J.*, Vol.42, No.4, 977~993

Al-Awkati, Z.A. (1975), On problems of soil bearing capacity at depth, *PhD thesis, Department of Civil Engineering, Duke University, Durham, NC, USA*

Anisimov, V.V. and Ter-Martirosyan, A.G. (2009), Effect of mechanical suffosion on additional settlements of foundation beds, *Soil Mechanics and Foundation Engineering*, Vol.46, No.4, 129~135

Arulanandan, K. and Perry, E.B. (1983), Erosion in relation to filter design criteria in earth dams, *Journal of Geotechnical Engineering, ASCE*, Vol.109, No.5, 682~698

ASTM D2487-11 (2012), Standard Practice for Classification of Soils for Engineering Purposes (Unified Soil Classification System), *Annual Book of ASTM Standards, Vol.04.08, ASTM International, West Conshohocken*

ASTM D4647-06e1 (2012), Standard Test Methods for Identification and Classification of Dispersive Clay Soils by the Pinhole Test, *Annual Book of ASTM Standards, Vol.04.08, ASTM International, West Conshohocken*

ASTM D4767-11 (2012), Standard Test Method for Consolidated Undrained Triaxial Compression Test for Cohesive Soils, *Annual Book of ASTM Standards, Vol.04.08, ASTM International, West Conshohocken*

ASTM D7181-11 (2012), Method for Consolidated Drained Triaxial Compression Test for Soils, *Annual Book of ASTM Standards, Vol.04.09, ASTM International, West Conshohocken*

ASTM D6913-04 (2012), Standard Test Methods for Particle-Size Distribution (Gradation) of Soils Using Sieve Analysis, *Annual Book of ASTM Standards, Vol.04.09, ASTM International, West Conshohocken*

ASTM D4245 (2006), Standard Test Methods for Minimum Index Density and Unit Weight of Soils and Calculation of Relative Density, *Annual book of ASTM Standards, Vol.04.08, ASTM International, West Conshohocken, PA*

ASTM D4221-11 (2012), Standard Test Method for Dispersive Characteristics of Clay Soil by Double Hydrometer, *Annual Book of ASTM Standards, Vol.04.08, ASTM International, West Conshohocken*

Atkinson, J. (2007), *The Mechanics of Soils and Foundations, 2nd Ed., Taylor & Francis Group, London*

Bear, J. (1972), *Dynamics of fluids in porous media, American Elsevier Pub. Co., New York, USA*

Been, K., Crooks, J.H.A., Becker, D.E. and Jefferies, M.G. (1986), The cone penetration test in sands: part I, state parameter interpretation, *Géotechnique*, Vol.36, No.2, 239~249

Been, K., Jefferies, M.G., Crooks, J.H.A. and Rothenburg, L. (1987), The cone penetration test in sands: part II, general inference of state, *Géotechnique*, Vol.37, No.3, 285~299

Bendahmane, F., Marot, D. and Alexis, A. (2008), Experimental parametric study of suffusion and backward erosion, *Journal of Geotechnical and Geoenvironmental Engineering*, Vol.134, No.1, 57~67

Bonelli, S., Brivois, O., Borghi, R., and Benahmed, N. (2006), On the modelling of piping erosion, *Comptes Rendus Mécanique*, Vol.344, Issues.8~9, 555~559

Bonelli, S. and Marot, D. (2008), On the modelling of internal soil erosion, *The 12th International Conference of International Association for Computer Methods and Advances in Geomechanics (IACMAG), Goa, India*.

Bonelli, S. (2012), *Erosion of Geomaterials, ISTE Ltd and John Wiley & Sons, Inc.*

Bradshaw, A.S. and Baxter, C.D. (2007), Sample preparation of silts for liquefaction testing, *Geotechnical Testing Journal*, Vol. 30, No. 4, 324~332

Briaud, J.L., Ting, F. C. K., Chen, H. C., Cao, Y., Han, S. W. and Kwak, K. W. (2001), Erosion function apparatus for scour rate predictions, *Journal of Geotechnical and Geoenvironmental Engineering*, Vol.127, No.2, 105~113

Burenkova, V.V. (1993), Assessment of suffosion in non-cohesive and graded soils. *Proceedings of the First International Conference of "Geo-Filters", Karlsruhe, Germany, Oct. 1992, Filters in Geotechnical and Hydraulic Engineering, Brauns, Heibaum and Schuler, Eds., Balkema, Rotterdam, Netherlands*, 357~360

Carrera, A., Coop, M. and Lancellotta, R. (2011), Influence of grading on the mechanical behaviour of Stava tailings, *Géotechnique*, Vol.61, No.11, 935~946

Chang, D.S. and Zhang, L.M. (2011a), Internal stability criteria for soils. *Rock and Soil Mechanics*, Vol.32, Supp.1, 253~259 (in Chinese)

Chang, D.S. and Zhang, L.M. (2011b), A stress-controlled erosion apparatus for studying internal erosion in soils. *Geotechnical Testing Journal*, Vol.34, No.6, 579~589

Chang, D.S. and Zhang, L.M. (2012), Critical hydraulic gradients of internal erosion under complex stress states, *Journal of Geotechnical and Geoenvironmental Engineering*, Vol.139, No.9, 1454~1467

Chang, C.S. and Meidani, M. (2012), Deformation and failure behavior of soils under erosion, *Poster of NSF CMMI Engineering Research and Innovation Conference, Boston, MA, USA*, CMMI-0928433

Chang, D.S. and Zhang, L.M. (2013), Extended internal instability criteria for soils under seepage, *Soils and Foundations*, Vol.53, No.4, 569~583

Chapuis, R.P. (1992), Similarity of internal stability criteria for granular soils, *Can. Geotech. J.*, Vol.29, 711~713

Chapuis, R.P., Contant, A. and Baass, K.A. (1996), Migration of fines in 0-20mm crushed base during placement, compaction and seepage under laboratory conditions, *Can. Geotech. J.*, Vol.33, 168~176

Cividini, A. and Gioda, G. (2004), Finite-element approach to the erosion and transport of fine particles in granular soils, *International Journal of Geomechanics*, Vol.4, No.3, 191~198

Cividini, A., Bonomi, S., Vignati, G.C. and Gioda, G. (2009), Seepage-induced erosion in granular soil and consequent settlements, *International Journal of Geomechanics*, Vol.9, No.4, 187~194

Crosta, G. and di Prisco, C. (1999), On slope instability induced by seepage erosion, *Can. Geotech. J.*, Vol.36, 1056~1073

Cubrinovski, M. and Ishihara, K. (2002), Maximum and minimum void ratio characteristic of sands, *Soils and Foundations*, Vol.42, No.6, 65~78

Daniel, D.E., Trautwein, S. J., Boynton, S.S and Foreman, D.E. (1984), Permeability testing with flexible-wall permeameters, *Geotechnical Testing Journal*, Vol.7, No.3, 113~122

Daniel, D.E. (1994), State-of-the-art: laboratory hydraulic conductivity tests for saturated soils, *Hydraulic Conductivity and Waste Contaminant Transport in Soil, ASTM STP 1142, Daniel, D.E. and Trautwein, S.J., Eds., American Society for Testing and Materials, Philadelphia*, 30~71

de Mello, V.F.B. (1975), some lessons from unexpected, real and fictitious problems in earth dam engineering in Brazil, *Proceedings of 6th Regional Conference for Africa on Soil Mechanics and Foundation Engineering, Durban, South Africa, Robertson, A.M.G. and Caldwell, J.A., Eds.*, Vol.2, 285~304

Decker, R.S. and Dunnigan, L.P. (1977), Development and use of the soil conservation service dispersion test, *Dispersive clays, related piping, and erosion in geotechnical projects: a symposium presented at the seventy-ninth annual meeting, ASTM, Chicago, Ill., 27th June~2nd July 1976, Sherard, J.L. and Decker, R.S., Eds., ASTM International, West Conshohocken, PA*, 94~109

Duncan, J.M. and Chang, C.Y. (1970), Nonlinear analysis of stress and strain in soils, *Journal of the Soil Mechanics and Foundations Division, ASCE*, Vol. 96, No. 5, 1629-1653

Durgunoglu, H.T. and Mitchell, J.K. (1975), Static penetration resistance of soils: I-ANALYSIS, *Proceedings of ASCE Specialty Conference on In-situ Measurement of Soil Parameters, Raleigh, USA*, Vol. 1

Emerson, W. W. (1964), The slaking of soil crumbs as influenced by clay mineral composition, *Australian Journal of Soil Research*, Vol.2, 211~217

Evans, J.C. and Fang, H. Y. (1988), Triaxial permeability and strength testing of contaminated soils, *Advanced Triaxial Testing of Soil and Rock, ASTM STP 977, Donaghe, R.T., Chaney, R.C. and Silver, M.L., Eds., American Society for Testing and Materials, Philadelphia*, 387~404

Fannin, R.J. and Moffat, R. (2006), Observations on internal stability of cohesionless soils, *Géotechnique*, Vol.56, No.7, 497~500

Fell, R., MacGregor, P., Stapledon, D. and Bell, G. (2005), *Geotechnical Engineering of dams, CRC Press, Taylor & Francis Group, London, UK*

Fell, R. and Fry, J.-J. (2013), State of the Art on the Likelihood of Internal Erosion of Dams and Levees by Means of Testing (Chapter 1), *Erosion in Geomechanics Applied to Dams and Levees*, Bonelli, S., Ed., Wiley/ISTE, 1~99

Ferreira, P.M.V. and Bica, A.V.D. (2006), Problems in identifying the effects of structure and critical state in a soil with a transitional behaviour, *Géotechnique*, Vol.56, No.7, 445~454

Foster, M. and Fell, R. (2001), Assessing embankment dam filters that do not satisfy design criteria, *Journal of Geotechnical and Geoenvironmental Engineering*, Vol.127, No.5, 398~407

Frost, J.D. and Park, J.Y. (2003), A critical assessment of the moist tamping technique, *Geotechnical Testing Journal*, Vol. 26, No. 1, 57~69

Fry, J.-J. (2012), Introduction to the Process of Internal Erosion in Hydraulic Structures: Embankment Dams and Dikes (Chapter 1), *Erosion of Geomaterials*, Bonelli, S., Ed., Wiley/ISTE, 1~36

Fujisawa, K., Murakami, A. and Nishimura, S. (2010), Numerical analysis of the erosion and the transport of fine particles within soils leading to the piping phenomenon, *Soils and Foundations*, Vol.50, No.4, 471~482

Ghafghazi, M. and Shuttle, D. (2008), Interpretation of sand state from cone penetration resistance, *Géotechnique*, Vol.58, No.8, 623~634

Goldin, A.L. and Rumyantsev, O. A. (2009), On the history of development of the seepage and seepage strength of soils issue in Russia and at Vedeneev VNIIG, *International Workshop on Internal Erosion in Dams and Foundations, St. Petersburg, Russia, April, 2009.*

Haghighi, I., Chevalier, C., Duc, M., Guédon, S. and Reiffsteck, P. (2013), Improvement of Hole Erosion Test and results on reference soils, *Journal of Geotechnical and Geoenvironmental Engineering*, Vol.139, No.2, 330~339

Hagerty, D.J. (1991a), Piping/sapping erosion 1: basic considerations, *Journal of Hydraulic Engineering*, Vol.117, No.8, 991~1008

Hagerty, D.J. (1991b), Piping/sapping erosion 2: identification-diagnosis, *Journal of Hydraulic Engineering*, Vol.117, No.8, 1009~1025

Hanson, G.J. and Simon, A. (2001), Erodibility of cohesive streambeds in the loess area of the midwestern USA, *Hydrological Processes*, Vol.15, No.1, 23~38

Head, K.H. (1998), *Manual of Soil Laboratory Testing, Volume 3: Effective Stress Tests, 2nd Edition, John Wiley & Sons*

Hicher, P.-Y. (2013), Modelling the impact of particle removal on granular material behaviour, *Géotechnique*, Vol.63, No.2, 118~128

Honjo, Y., Haque, M.A. and Tsai, K.A. (1996), Self-filtration behavior of Broadly and gap graded cohesionless soils, *Proceedings of Geofilters '96, Lafleur, J. and Rollin, A., Eds., Montreal, Canada, Bitech Publishers, Richmond, Canada*, 227~236

Huang, Y.T., Huang, A.B., Kuo, Y.C. and Tsai, M.D. (2004), A laboratory study on the undrained strength of silty sand from Central Western Taiwan, *Soil Dynamics and Earthquake Engineering*, Vol.24, 733~743

Høeg, K., Dyvik, R. and Sandbækken, G. (2000), Strength of undisturbed versus reconstituted silt and silty sand specimens, *Journal of Geotechnical and Geoenvironmental Engineering*, Vol.126,No.7, 606~617

Ichiyama, T. (2011), Seepage analysis of landslide dam considering internal erosion, *Extended abstract of Master's thesis, Department of Civil Engineering, Tohoku University* (in Japanese)

Indraratna, B. and Vafai, F. (1997), Analytical model for particle migration within base soil-filter system, *Journal of Geotechnical and Geoenvironmental Engineering*, Vol.123, No.2, 100~109

Indraratna, B. and Radampola, S. (2002), Analysis of critical hydraulic gradient for particle movement in filtration, *Journal of Geotechnical and Geoenvironmental Engineering*, Vol.128, No.4, 347~350

Indraratna, B. and Raut, A.K. (2006), Enhanced criterion for base soil retention in embankment dam filters, *Journal of Geotechnical and Geoenvironmental Engineering*, Vol.132, No.12, 1621~1627

Indraratna, B., Raut, A.K. and Khabbaz, H. (2007), Constriction-based retention criterion for granular filter design, *Journal of Geotechnical and Geoenvironmental Engineering*, Vol.133, No.3, 266~276

Indraratna, B., Athukorala, R. and Vinod, J. (2013), Estimating the rate of erosion of a silty sand treated with lignosulfonate, *Journal of Geotechnical and Geoenvironmental Engineering*, Vol.139, No.5, 701~714

Ishihara, K. and Towhata, I. (1982), Dynamic response analysis of level ground based on the effective stress method, *Soil Mechanics-Transient and Cyclic Loads, New York: Wiley*

Ishihara, K. (1993): Liquefaction and flow failure during earthquakes, *Géotechnique*, Vol.43, No.3, 351~415

Ishihara, K. (1996), *Soil behavior in earthquake geotechnics (Oxford engineering science series: 46), Clarendon press, Oxford, UK*, 268~272

Janbu, N. and Senneset, K. (1974), Effective stress interpretation of in situ static penetration tests, *Proceedings of the European Symposium on Penetration Testing, ESOPT I, Stockholm, Sweden*, Vol. 2.2, 181~193

JGS 0561-2000 (2000), Method for Consolidated Constant Pressure Direct Box Shear Test on Soils, *Standard of Japanese Geotechnical Society for Laboratory Shear Test, Japanese Geotechnical Society*, 104~109

JGS 0524-2000 (2000), Method for Consolidated-Drained Triaxial Compression Test on Soils, *Standards of Japanese Geotechnical Society for Laboratory Shear Test, Japanese Geotechnical Society*, 23~27

JGS 0525-2000 (2000), Method for K_0 Consolidated-Undrained Triaxial Compression

Test on Soils with Pore Water Pressure Measurement, *Standards of Japanese Geotechnical Society for Laboratory Shear Test, Japanese Geotechnical Society*, 28~34

JGS 1435-2003 (2003), Electric Cone Penetration Test, *Site investigation method and explanation, Japanese Geotechnical Society* (in Japanese)

Jiang, M.J., Konrad, J.M. and Leroueil, S. (2003), An efficient technique for generating homogeneous specimens for DEM studies, *Computers and Geotechnics*, Vol.30, 579~597

JIS A1204-1990 (2000), Test Method for Particle Size Distribution of Soils, *Soil testing: fundamentals and procedures, Japanese Geotechnical Society* (in Japanese)

Jones, J.A.A. (1981), *The nature of soil piping: a review of research, Geo Books in Norwich, England*

Julian, J.P. and Torres, R. (2006), Hydraulic erosion of cohesive riverbanks, *Geomorphology*, Vol.76, No.1~2, 193~206

Kenney, T.C. and Lau, D. (1985), Internal stability of granular filters. *Can. Geotech. J*, Vol.22, 215~225

Kenney, T.C. and Lau, D. (1986), Internal stability of granular filters: Reply. *Can. Geotech. J.*, Vol.23, 420~423

Kezdi, A. (1979), *Soil Physics: Selected Topics (Developments in Geotechnical Engineering), Elsevier Science Ltd*.

Khilar, K.C., Fogler, H.S. and Gray, D.H. (1985), Model for piping-plugging in earthen structures, *Journal of Geotechnical Engineering (ASCE)*, Vol.111, No.7, 833~846

Kovacs, G. (1981), *Seepage hydraulics, Elsevier Scientific Publishing Company, Amsterdam, Netherlands*

Kuerbis, R., Negussey, D. and Vaid, Y.P. (1988), Effect of gradation and fines content on the undrained response of sand, *Hydraulic Fill Structures (Geotechnical Special Publication No.21), Van Zyl, D.J.A. and Vick, S.G. Ed., Geotechnical Engineering Division of ASCE, New York, NY, USA*, 330~345

Kuerbis, R. (1989), The effect of gradation and fines content on the undrained loading response of sand, *Master Thesis, Department of Civil Engineering, University of British Columbia, Vancouver, Canada*

Kulhawy, F.H. and Mayne, P.W. (1990), Manual on estimating soil properties for foundation design, *Final report for Electric Power Research Institute*

Kuwano, R., Connolly, T.M. and Jardine, R.J. (2000), Anisotropic stiffness measurements in a stress-path triaxial cell, *Geotechnical Testing Journal*, Vol.23, No.2, 141~157

Ladd, R.S. (1978), Preparing test specimens using undercompaction, *Geotechnical Testing Journal*, Vol.1, No.1, 16~23

Ladd, R.S. (1978), Preparing test specimens using undercompaction, *Geotechnical Testing Journal*, Vol.1, No.1, 16~23

Lade, P.V. and Pradel, D. (1990), Instability and plastic flow of soils. I: experimental observations, *Journal of Engineering Mechanics*, Vol.116, No.11, 2532~2550

Lade, P.V. and Yamamuro, J.A. (1997), Effects of nonplastic fines on static liquefaction of sands, *Can. Geotech. J.*, Vol.34, 918~928

Lade, P.V., Liggio, C.D., Jr., and Yamamuro, J.A. (1998), Effects of non-plastic fines on minimum and maximum void ratios of sand, *Geotechnical Testing Journal*, Vol.21, No.4, 336~347

Lafleur, J. (1984), Filter testing of broadly graded cohesionless tills, *Can. Geotech. J.* Vol.21, 634~643

Lafleur, J., Mlynarek, J. and Rollin, A.L. (1989), Filtration of Broadly graded cohesionless soils, *Journal of Geotechnical Engineering, ASCE*, Vol.115, No.12, 1747~1768

Li, M. and Fannin, R.J. (2008), Comparison of two criteria for internal stability of granular soil, *Can. Geotech. J.*, Vol.45, 1303~1309

Li, M. and Fannin, R.J. (2012), A theoretical envelope for internal instability of cohesionless soil, *Géotechnique*, Vol.62, No.1, 77~80

Liu, Y.Z. (2003), Critical hydraulic gradient for piping in noncohesive soils, *Journal of Zhengzhou University (Engineering Science)*, Vol.24, No.4, 67~71 (in Chinese)

Locke, M., Indraratna, B. and Adikari, G. (2001), Time-dependent particle transport through granular filters, *Journal of Geotechnical and Geoenvironmental Engineering*, Vol.127, No.6, 521~529

Locke, M. and Indraratna, B. (2002), Filtration of broadly graded soils: the reduced PSD method, *Géotechnique*, Vol.52, No.4, 285~287

Lourenço, S.D.N., Sassa, K. and Fukuoka, H. (2006), Failure process and hydrologic response of a two layer physical model: Implications for rainfall-induced landslides, Geomorphology, Vol.73, Issue 1~2, 115~130

Lubochkov, E.A. (1962), The self-filtering behavior of non-cohesive soils, *Izvestia VNIIG*, No.71

Lubochkov, E.A. (1965), Graphical and analytical methods for the determination of the properties of non-cohesive soils characterizing suffusion, *Izvestia VNIIG*, No.78

Luo, Y., Qiao, L., Liu, X., Zhan, M. and Sheng, J. (2013), Hydro-mechanical experiments on suffusion under long-term large hydraulic heads, *Natural Hazards*, Vol.65, 1361~1377

Lupini, J.F., Skinner, A.E. and Vaughan, P.R. (1981), The drained residual strength of cohesive soils, *Géotechnique*, Vol.31, No.2, 181~213

Marot, D., Bendahmane, F., Rosquoet, F. and Alexis, A. (2009), Internal flow effects on isotropic confined sand-clay mixtures, *Soil & Sediment Contamination*, Vol.18, 294~306

Marot, D., Bendahmane, F. and Konrad, J.M. (2011), Multichannel optical sensor to quantify particle stability under seepage flow, *Can. Geotech. J.*, Vol.48, 1772~1787

Marot, D., Bendahmane, F. and Nguyen, H.H. (2012), Influence of angularity of coarse fraction grains on internal erosion process, Proceedings of the 6th international conference on scour and erosion, Paris, France, Paper No.75

Marot, D. and Benamar, A. (2012), Suffusion, Transport and Filtration of Fine Particles in Granular Soil (Chapter 2), *Erosion of Geomaterials*, Bonelli, S., Ed., Wiley/ISTE, 39~75

Mao, C.X. (2005), Study on piping and filters: Part I of piping, *Rock and Soil Mechanics*, Vol.26, No.2, 209~215 (in Chinese)

McDougall, J. and Pyrah, I.C. (2004), Phase relations for decomposable soils, *Géotechnique*, Vol.54, No.7, 487~493

McDougall, J., Kelly, D. and Barreto, D. (2013), Particle loss and volume change on dissolution: experimental results and analysis of particle size and amount effects, *Acta Geotechnica*, Vol. 8, 619~627

Mitchell, J.K. (1976), *Fundamentals of soil behavior, New York: Wiley*

Mitchener, H. and Torfs, H. (1996), Erosion of mud/sand mixtures, *Coastal Engineering*, Vol.29, No.1~2, 1~25

Miura, K., Maeda, K., Furukawa, M. and Toki, S. (1997), Physical characteristics of sands with different primary properties, *Soils and Foundations*, Vol.37, No.3, 53~64

Moffat, R.A. and Fannin, R.J. (2006), A large permeameter for study of internal stability in cohesionless soils, *Geotechnical Testing Journal*, Vol.29, No.4, 273~279

Moffat, R.A., Fannin, R.J. and Garner, S.J. (2011), Spatial and temporal progression of internal erosion in cohesionless soil, *Can. Geotech. J.*, No.48, 399~412

Moffat, R.A. and Fannin, R.J. (2011), A hydromechanical relation governing internal stability of cohesionless soil, *Can. Geotech. J.*, No.48, 413~424

Monkul, M.M. and Yamamuro, J.A. (2011), Influence of silt size and content on liquefaction behavior of sands, *Can. Geotech. J.*, Vol.48, 931~942

Moore, W.L. and Masch, F.D. (1962), Experiments on the scour resistance of cohesive sediments, *Journal of geophysical research*, Vol.67, No. 4, 1437~1446

Moraci, N., Mandaglio, M.C. and Lelo, D. (2012), A new theoretical method to evaluate the internal stability of granular soils, *Can. Geotech. J.*, Vol.49, 45~58

Muir Wood, D. (2006), Geomaterials with changing grading: A route towards modeling, *Geomechanics and Geotechnics of Particulate Media, Hyodo, Murata and Nakata Eds., Taylor & Francis Group, London, UK*, 313~318

Muir Wood, D. (2007), The magic of sands-The 20th Bjerrum Lecture presented in Oslo, 25 November 2005, *Can. Geotech. J.*, Vol.44, 1329~1350

Muir Wood, D. and Maeda, K. (2008), Changing grading of soil: effect on critical states, *Acta Geotechnica*, Vol.3, 3~14

Muir Wood, D., Maeda, K. and Nukudani, E. (2010), Modeling mechanical consequences of erosion. *Géotechnique*, Vol.60, No.6, 447~457

Murthy, T.G., Loukidis, D., Carraro, J.A.H., Prezzi, M. and Salgado, R. (2007), Undrained monotonic response of clean and silty sands, *Géotechnique*, Vol.57, No.3, 273~288

Ni, Q., Tan, T.S., Dasari G.R. and Hight, D.W. (2004), Contribution of fines to the compressive strength of mixed soils, *Géotechnique*, Vol.54, No.9, 561~569

Nocilla, A., Coop, M. R. and Colleselli, F. (2006), The mechanics of an Italian silt: an example of "transitional" behaviour, *Géotechnique*, Vol.56, No.4, 261~271

Ouyang, M. (2013), Influence of initial fines content on mechanical behavior of soil subjected to internal erosion, *extended abstract of Master thesis, Tokyo Institute of Technology*, Tokyo, Japan

Papadopoulou, A. and Tika T. (2008), The effect of fines on critical state and liquefaction resistance characteristics of non-plastic silty sands, *Soils and Foundations*, Vol.48, No.5, 713~725

Papamichos, E., Vardoulakis, I., Tronvoll, J. and Skjærstein, A. (2001), Volumetric sand production model and experiment, *International Journal for Numerical and analytical Methods in Geomechanics*, Vol.25, 789~808

Papamichos, E. and Vardoulakis, I. (2005), Sand erosion with a porosity diffusion law, *Computers and Geotechnics*, Vol.32, 47~58

Pare, J., Ares, R., Cabot, L. and Garzon, M. (1982), Large scale permeability and filter tests at LG3, *Proceedings of 14th International Conference of Large Dam, Rio de Janeiro, Brazil*, 103~122

Perzlmaier, S. (2007), Hydraulic criteria for internal erosion in cohesionless soil, *Internal Erosion of Dams and Their Foundations: Selected and Reviewed Papers from the Workshop on Internal Erosion and Piping of Dams and their Foundations, Aussois, France, 2005, Fell, R. and Fry, J.J. Eds., Taylor & Francis*, 179~190

Pitman, T.D., Robertson, P.K. and Sego, D.C. (1994), Influence of fines on the collapse of loose sands, *Can. Geotech. J*. Vol.31, No.5, 728~739

Rahman, Md.M., Lo, S.R. and Baki, Md.A.L. (2011), Equivalent granular state parameter and undrained behaviour of sand-fines mixtures, *Acta Geotechnica*, Vol.6, 183~194

Reboul, N., Vincens, E. and Cambou, B. (2010), A computational procedure to assess the distribution of constriction sizes for an assembly of spheres, *Computers and Geotechnics*, Vol.37, 195~206

Reddi, L.N. and Inyang, H.I. (2000), *Geoenvironmental Engineering: Principles and Applications, 1st Ed., Marcel Dekker, New York, USA*

Reddi, L.N., Lee, I. M. and Bonala, M.V.S. (2000), Comparison of internal and surface erosion using flow pump tests on a sand-kaolinite mixure, *Geotechnical Testing Journal*, Vol.23, No.1, 116~122

Richards, K.S. and Reddy, K.R. (2007), Critical appraisal of piping phenomena in earth dams, *Bull Eng. Geo. Environ.*, Vol.66, 381~402

Richards, K.S. and Reddy, K.R. (2010), True triaxial piping test apparatus for evaluation of piping potential in earth structures, *Geotechnical Testing Journal*, Vol.33, No.1, 83~95

Richards, K.S. and Reddy, K.R. (2012), Experimental investigation of initiation of backward erosion piping in soils, *Géotechnique*, Vol.62, No.10, 933~942

Robertson, P.K. and Campanella, R.G. (1983), Interpretation of cone penetration test. Part I: sand, *Can. Geotech. J.* Vol.20, 718~733

Salgado, R., Bandini, P. and Karim, A. (2000), Shear strength and stiffness of silty sand, *Journal of Geotechnical and Geoenvironmental Engineering*, Vol.126, No.5, 451~462

Sanchez, R.L., Strutynsky, A.I. and Silver, M.L. (1983), Evaluation of the erosion potential of embankment core materials using the laboratory triaxial erosion test procedure, Technical Report GL-83-4, Geotechnical Laboratory, U.S. Army Engineer Waterways Experiment Station, Vicksburg, Mississippi, USA

Scheuermann, A., Steeb, H. and Kiefer, J. (2010), Internal erosion of granular materials-identification of erodible fine particles as a basis for numerical calculations, *Proceedings of 9th HSTAM International Congress on Mechanics, Vardoulakis Mini-symposia, Limassol, Cyprus*, 275~282

Scholtès, L., Hicher, P.Y. and Sibille, L. (2010), Multiscale approaches to describe mechanical responses induced by particle removal in granular materials. *Comptes Rendus Mecanique*, Vol.338, 627~638

Schuler, U. and Brauns, J. (1993), Behaviour of coarse and well-graded filters, *Proceedings of the First International Conference of "Geo-Filters", Karlsruhe, Germany, Oct. 1992, Filters in Geotechnical and Hydraulic Engineering, Brauns, Heibaum and Schuler, Eds., Balkema, Rotterdam, Netherlands*, 3~18

Schuler, U. (1995), How to deal with the problem of suffosion, *Research and Development in the Field of Dams, SNCLD, Crans-Montana, Switzerland*, 145~159

Sherard, J.L., Dunnigan, L.P., Decker, R.S. and Steele, E.F. (1976), Pinhole test for identifying dispersive soils, *Journal of the Geotechnical Engineering Division, Proceedings of the American Society of Civil Engineers*, Vol.102, No.GT1 11846, 69~85

Sherard, J.L. (1979), Sinkholes in dams of coarse, broadly graded soils. *Transactions, 13th Congress on Large Dams, New Delhi, India*, Vol.2, 25~35

Sherard, J.L. (1984), Basic properties of sand and gravel filters, *Journal of Geotechnical Engineering, ASCE*, Vol.110, No.6, 397~414

Sherard, J.L. and Dunnigan, L.P. (1984), Filters for silts and clays, *Journal of Geotechnical Engineering, ASCE*, Vol.110, No.6, 397~414

Shwiyhat, N. and Xiao, M. (2010), Effect of suffusion on mechanical characteristics of sand, *Proceedings of the fifth international conference on scour and erosion, Burns, S.E., Bhatia, S.K., Avila, C.M.C. and Hunt, B.E., Eds., San Francisco, California, USA, American Society of Civil Engineers*, 378~386

Silveira, A. (1965), An analysis of the problem of washing through in protective filters, *Proceedings of 6th International Conference on Soil Mechanics and Foundation Engineering, Montreal, Canada*, Vol.2, 551~555

Silveira, A., de Lorena Peixoto, Jr J. and Nogueira, J. (1975), On void size distribution of granular materials, *Proceedings of 5th Pan-American Conference on Soil Mechanics and Foundation Engineering, Buenos Aires, Argentina*, Vol.3, 161~176.

Sjah, J. and Vincens, E. (2012), Determination of the constriction size distribution of granular filters by filtration tests, *International Journal for Numerical and Analytical Methods in Geomechanics*, DOI: 10.1002/nag.2076

Skempton, A.W. and Brogan, J.M. (1994), Experiments on piping in sandy gravels. *Géotechnique*, Vol.44, No.3, 449~460

Skempton, A.W. and Brogan, J.M. (1995), Discussion: Experiments on piping in sandy gravels, *Géotechnique*, Vol.45, No.3, 565~567

Smerdon, E.T. and Beasley, R.P. (1961), Critical tractive forces in cohesive soils, *Agricultural Engineering*, Vol.42, No.1, 26~29

Srivastava, A. and Sivakumar Babu, G.L. (2011), Analytical solutions for protective filters based on soil-retention and permeability criteria with respect to the phenomenon of soil boiling, *Can. Geotech. J.*, Vol.48, 956~969

Stavropoulou, M., Papanastasiou, P. and Vardoulakis, I. (1998), Coupled wellbore erosion and stability analysis, *International Journal for Numerical and Analytical Methods in Geomechanics*, Vol.22, 749~769

Sterpi, D. (2003), Effects of the erosion and transport of fine particles due to seepage flow, *International Journal of Geomechanics*, Vol.3, No.1, 111~122

Sugita, H., Sasaki, T. and Nakajima, S. (2008), Damage investigation of road embankment caused by the 2007 Noto Peninsula, Japan Earthquake, *Public Works Research Institute Report*

Sun, B.C. (1989), Internal stability of clayey to silty sands, *PhD thesis, University of Michigan, USA*

Terzaghi, K. (1943), *Theoretical Soil Mechanics, John Wiley and Sons, New York*

Terzaghi, K. and Peck, R.B. (1948), *Soil Mechanics in Engineering practice. 1st.Edition. John Wiley and Sons, New York.*

Terzaghi, K. (1956), Varieties of submarine slope failures, *Proceedings of 8th Texas Conference on Soil Mechanics and Foundation Enginnering, University of Texas at Austin, Bureau of Engineering Special Research Publication*, No.29, 41

Terzaghi, K., Peck, R.B. and Mesri, G. (1996), Soil Mechanics in Engineering practice. 3rd.Edition. John Wiley and Sons, INC.

Thevanayagam, S. (1998), Effect of fines and confining stress on undrained shear strength of silty sands, *Journal of Geotechnical and Geoenvironmental Engineering*, Vol.124, No.6, 479~491

Thevanayagam, S. and Mohan, S. (2000), Intergranular state variables and stress-strain behavior of silty sands, Géotechnique, Vol.50, No.1, 1~23

Thevanayagam, S., Shenthan, T., Mohan, S. and Liang, J. (2002), Undrained fragility of clean sands, silty sands, and sandy silts, *Journal of Geotechnical and Geoenvironmental Engineering*, Vol.128, No.10, 849~858

Thevanayagam, S. (2007), Intergrain contact density indices for granular mixes - I : Framework, *Earthquake Engineering and Engineering Vibration*, Vol.6, No.2, 123~134

Thoman, R.W. and Niezgoda, S.L. (2008), Determining erodibility, critical shear stress, and allowable discharge estimates for cohesive channels: case study in the Power River Basin of Wyoming, *Journal of Hydraulic Engineering*, Vol.134, No.12, 1677~1687

Tomlinson, S.S. and Vaid, Y.P. (2000), Seepage forces and confining pressure effects on piping erosion, *Can. Geotech. J.*, Vol.37, 1~13

Tanaka, T. and Toyokuni, E. (1991), Seepage-failure experiments on multi-layered sand columns-Effects of flow conditions and residual effective stress on seepage-failure phenomena, *Soils and Foundations*, Vol.31, No.4, 13~36

Uno, T. (2009), The state of the knowledge on seepage failure phenomena, *Geotechnical Engineering Magazine, Japanese Geotechnical Society*, Vol.57, No.9, 1~5. (in Japanese)

U.S. Army Corps of Engineers (1953), Filter experiments and design criteria. *Technical Memorandum No. 3~360, Waterways Experiment Station, Vicksburg.*

Vaid, Y.P. and Chern, J.C. (1985), Cyclic and monotonic undrained response of saturated sands, *Proceedings of Advances in the Art of Testing Soils Under Cyclic Conditions, Khosla, V., Eds., ASCE*, 120~147

Vallejo, L.E. (2001), Interpretation of the limits in shear strength in binary granular mixtures, *Can. Geotech. J.*, Vol.38, 1097~1104

Vardoulakis, I., Stavropoulou, M. and Papanastasiou, P. (1996), Hydro-mechanical aspects of the sand production problem, *Transport in porous media*, Vol.22, 225~244

Vardoulakis, I., Papanastasiou, P. and Stavropoulou, M. (2001), Sand erosion in axial flow conditions, *Transport in porous media*, Vol.45, 267~281

Vardoulakis, I. (2004a), Fluidisation in artesian flow conditions: Hydromechanically stable granular media, *Géotechnique*, Vol.54, No.2, 117~130

Vardoulakis, I. (2004b), Fluidisation in artesian flow conditions: Hydromechanically unstable granular media, *Géotechnique*, Vol.54, No.3, 165~177

Vesic, A.S. (1972), Expansion of cavities in infinite soil masses, *ASCE Journal of the Soil Mechanics and Foundations Division*, 96(SM3), 265~290

Vincens, E., Reboul, N. and Cambou, B. (2012), The Process of Filtration in Granular Materials (Chapter 3), *Erosion of Geomaterials*, Bonelli, S., Ed., Wiley/ISTE, 81~111

Voivret, C., Radjai, F., Delene, J.Y. and EI Youssoufi, M.S. (2009), Multiscale force networks in highly polydisperse granular media, *Physical review letters*, Vol.102, No.17, 178001

Wan, C.F. and Fell, R. (2004a), Laboratory tests on the rate of piping erosion of soils in embankment dams, *Geotechnical Testing Journal*, Vol.27, No.3, 295~303

Wan, C.F. and Fell, R. (2004b), Investigation of rate of erosion of soils in embankment dams, *Journal of Geotechnical and Geoenvironmental Engineering*, Vol.130, No.4, 373~380

Wan, R.G. and Wang, J. (2004), Analysis of sand production in unconsolidated oil sand using a coupled erosional-stress-deformation model, *Journal of Canadian Petroleum Technology*, Vol.43, No.2, 47~52

Wan, C.F. (2006), Experimental investigations of piping erosion and suffusion of soils in embankment dams and their foundations, *PhD Thesis, School of Civil and Environmental Engineering, University of New South Wales, Australia*

Wan, C.F. and Fell, R. (2008), Assessing the potential of internal instability and suffusion in embankment dams and their foundations, *Journal of Geotechnical and Geoenvironmental Engineering*, Vol.134, No.3, 401~407

Wang, J. and Wan, R.G. (2004), Computation of sand fluidization phenomena using stabilized finite elements, *Finite Elements in Analysis and Design*, Vol.40, 1681~1699

Wu, L.J. (1980), Computation of the critical hydraulic gradient for piping of granular soil, *Hydro-Science and Engineering*, Vol.4, 90~95 (in Chinese)

Xiao, M., Gomez, J., Adams, B., Shwiyhat, N. and Sinco, E. (2010), Experimental study on subsurface erosion of peats, *Proceedings of GeoFlorida 2010: Advances in Analysis, Modeling, & Design, Fratta, D.O., Puppala, A.J. and Muhunthan, B., Eds., West Palm Beach, Florida, USA,* Paper ID 93

Xiao, M. and Shwiyhat, N. (2012), Experiment investigation of the effects of suffusion on physical and geomechanic characteristics of sandy soils, *Geotechnical Testing Journal*, Vol.53, No.6, 1~11

Yamamuro, J.A. and Lade, P.V. (1997), Static liquefaction of very loose sands, *Can. Geotech. J.*, Vol.34, 905~917

Yamamuro, J.A. and Covert, K.M. (2001), Monotonic and cyclic liquefaction of very loose sands with high silt content, *Journal of Geotechnical and Geoenvironmental Engineering*, Vol.127, No.4, 314~324

Yang, Z.X., Li, X.S. and Yang, J. (2008), Quantifying and modeling fabric anisotropy of granular soils, *Géotechnique*, Vol. 58, No. 4, 237~248

Yang, S.L., Sandven, R. and Grande, L. (2006), Steady-state lines of sand-silt mixtures, *Can. Geotech. J.*, Vol.43, 1213~1219

Zhang, G. (2007), Experimental research on piping and DEM simulation, *PhD Thesis, Department of Civil Engineering, Tongji University, Shanghai, China* (in Chinese)

Zlatovic S. and Ishihara, K. (1995), On the influence of non-plastic fines on residual strength, *Proceedings of 1st International Conference on Earthquake Geotechnical Engineering, IS-TOKYO 95', Ishihara, K., Ed., Balkema, Tokyo, Japan,* Vol. 1, 239~244

水道管の破損などによる道路の陥没が相次ぐ (2009),日経コンストラクション (Nikkei Construction), 2009.7 (in Japanese)

APPENDIX A

ASSESSMENT OF SIZE EFFECT IN CPT

A.1 Grain size effect

Due to the comparatively large grain size of silica No. 3, the grain size effect, characterized by the ratio of cone diameter to mean grain size, should be considered. Gui and Bolton (1998) introduced the new concept of "effective diameter", which is the sum of the cone diameter and the mean particle size, to erase the grain size effect (Fig. A1). The effective diameter was considered in the interpretation of the test data in this study. The mean particle size was obtained from the grain size distribution curve before and after the seepage test.

A.2 Chamber size effect

Chamber size and imposed boundary conditions are influential on cone resistance. Detailed discussions can be found in Been, *et al.* (1986, 1987), Mayne (1991), Schnaid and Houlsby (1991); among others. Even though many studies have been conducted on this issue, it appears that there are no universally accepted explanations. Generally, the chamber size effect is less for loose sand, while for medium and dense sand, the size effect depends on the chamber-to-cone diameter ratio, stress state and so on.

To assess the size effect, CPT tests were conducted using a 300mm-in-diameter container with a diameter ratio of 30 as well as a seepage cell with a diameter ratio of 10. The dry silica No. 3 specimen was prepared in the above-mentioned two containers by the air pluviation method. Three relative densities corresponding to loose (D_r = 30%), medium (D_r = 70%) and dense (D_r = 100%) states are considered. In terms of Bearing Capacity Number N_q, the effect of the container diameter is plotted in Fig. A2. As expected, the size effect becomes much more obvious with a larger relative density. Due to the comparatively small relative densities of the tested specimens in Table 3.8, this effect is not considered in the interpretation of the test data in this study.

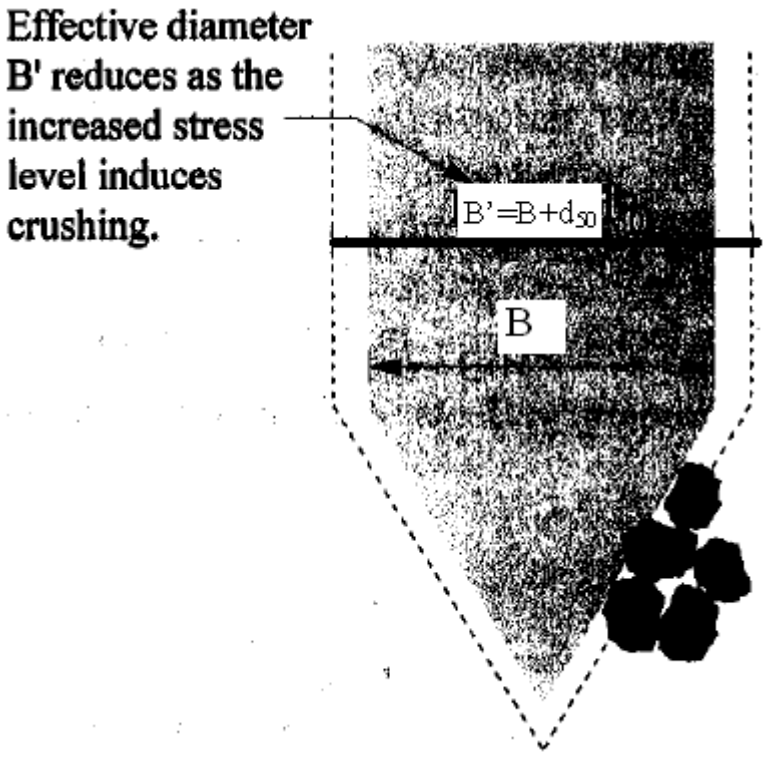

Figure A1 Concept of effective diameter (after Gui and Bolton, 1998)

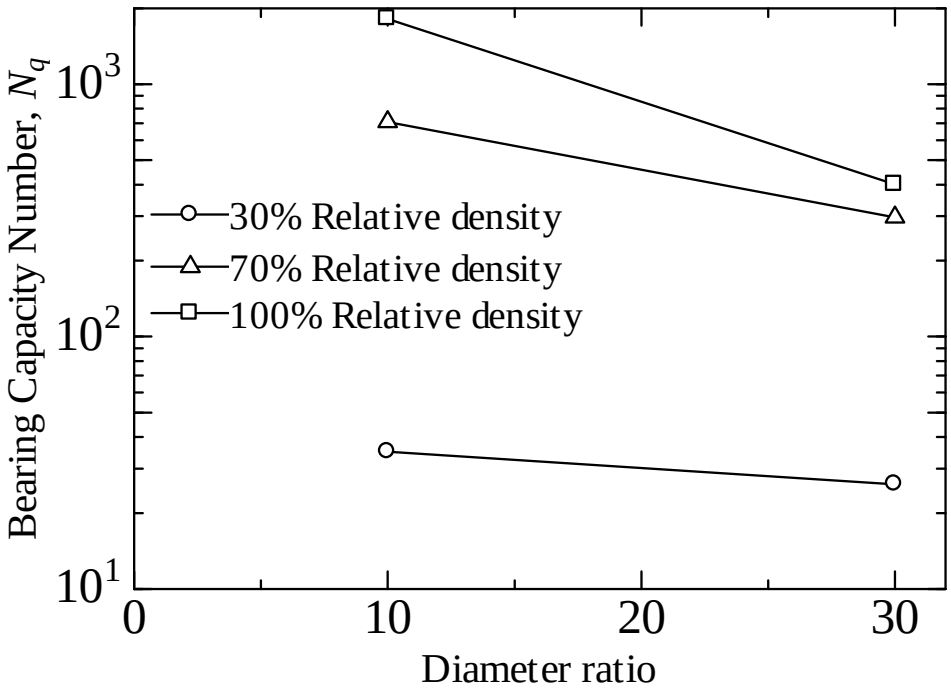

Figure A2 Relation between bearing capacity number and diameter ratio

REFERENCES

Been, K., Crooks, J.H.A., Becker, D.E. and Jefferies, M.G. (1986), The cone penetration test in sands: part I, state parameter interpretation, *Géotechnique*, Vol.36, No.2, 239~249

Been, K., Jefferies, M.G., Crooks, J.H.A. and Rothenburg, L. (1987), The cone penetration test in sands: part II, general inference of state, *Géotechnique*, Vol.37, No.3, 285~299

Gui, M.W. and Bolton, M.D. (1998), Geometry and scale effects in CPT and pile design, *Proceedings of 1st International Conference on Site Characterization, ISC'98, Atlanta, Georgia, USA*, Vol.1

Mayne, P.W. (1991), Determination of OCR in Clays by Piezocone Tests using cavity expansion and critical state concepts, *Soils and Foundations*, Vol.31, No.2, 65~76.

Schnaid, F. and Houlsby, G.T. (1991), An assessment of chamber size effects in the calibration of in situ tests in sand, *Géotechnique*, Vol.41, No.3, 437~445